NUREG/CR-3157

Design of Reinforced Concrete Containment Wall Elements Under Combined Action of Shear and Tension

Massachusetts Inst. of Tech.
Cambridge

Prepared for

Nuclear Regulatory Commission
Washington, DC

Mar 83

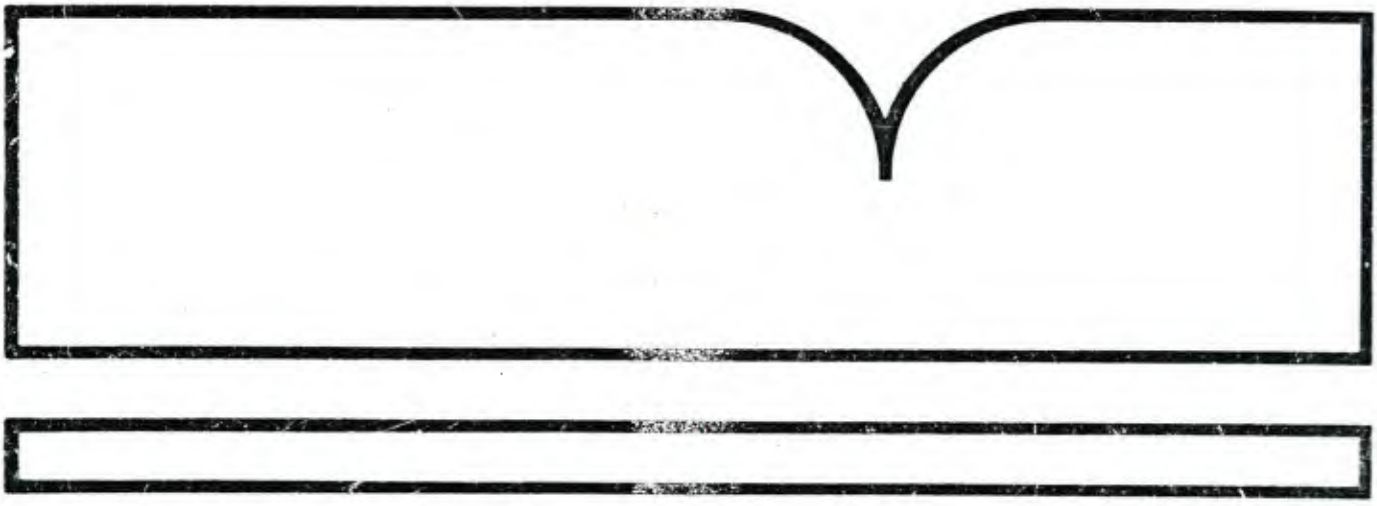

NUREG/CR-3157

Design of Reinforced Concrete Containment Wall Elements Under Combined Action of Shear and Tension

Prepared by J. Calvo, O. Buyukozturk, J. J. Connor

Department of Civil Engineering
Massachusetts Institute of Technology

Prepared for
U.S. Nuclear Regulatory Commission

NRC FORM 335 (7-77) U.S. NUCLEAR REGULATORY COMMISSION

BIBLIOGRAPHIC DATA SHEET

1 REPORT NUMBER (Assigned by DDC)
NUREG/CR-3157

4. TITLE AND SUBTITLE (Add Volume No., if appropriate)
Design of Reinforced Concrete Containment Wall Elements Under Combined Action of Shear and Tension

2 (Leave blank)

3 RECIPIENT'S ACCESSION NO

7. AUTHOR(S)
Jorge Calvo, Oral Buyukozturk, and Jerome Connor

5 DATE REPORT COMPLETED
MONTH June YEAR 1982

9. PERFORMING ORGANIZATION NAME AND MAILING ADDRESS (Include Zip Code)
Massachusetts Institute of Technology
Department of Civil Engineering
Cambridge, MA 02139

DATE REPORT ISSUED
MONTH March YEAR 1983

6 (Leave blank)

8 (Leave blank)

12. SPONSORING ORGANIZATION NAME AND MAILING ADDRESS (Include Zip Code)
Division of Engineering Technology
Office of Nuclear Regulatory Research
U.S. Nuclear Regulatory Commission
Washington, D.C. 20555

10 PROJECT/TASK/WORK UNIT NO

11. CONTRACT NO
FIN B6618

13. TYPE OF REPORT
Technical Report

PERIOD COVERED (Inclusive dates)

15. SUPPLEMENTARY NOTES

14 (Leave blank)

16. ABSTRACT (200 words or less)

Behavioral models are developed for reinforced concrete containment wall panels having orthogonal reinforcement and for those having both orthogonal and diagonal reinforcement. An initial axial tension which causes cracking in the concrete, is applied to the orthogonal reinforcement to simulate the normal membrane stresses induced by an accidental internal pressure load. This load is followed by the application of cyclic membrane shear histories representing the tangential shear stresses generated in the event of an earthquake. Using these two models, the experimentally measured strengths of various specimens are evaluated in view of important behavioral parameters. Then, an equation in terms of the governing parameters is proposed to predict the ultimate strength of these panels. Finally, a practical design procedure is developed and recommended as a replacement for the design criteria specified by the current Code. Applications of the proposed design procedure are shown and the results obtained are evaluated.

17. KEY WORDS AND DOCUMENT ANALYSIS 17a. DESCRIPTORS
Containment Structure, Shear transfer, Cyclic loading, Axial force, Design procedure, shear walls

17b. IDENTIFIERS/OPEN-ENDED TERMS
Structural shear walls, reinforced concrete

18. AVAILABILITY STATEMENT
Unlimited

19. SECURITY CLASS (This report) Unclassified

21. NO OF PAGES 223

20. SECURITY CLASS (This page) Unclassified

22. PRICE $

NRC FORM 335 (7-77)

* U.S. GOVERNMENT PRINTING OFFICE: 1983-381-207/2004

NUREG/CR-3157
RD

Design of Reinforced Concrete Containment Wall Elements Under Combined Action of Shear and Tension

Manuscript Completed: June 1982
Date Published: February 1983

Prepared by
J. Calvo, O. Buyukozturk, J. J. Connor

Department of Civil Engineering
Massachusetts Institute of Technology
Cambridge, MA 02139

Prepared for
Division of Engineering Technology
Office of Nuclear Regulatory Research
U.S. Nuclear Regulatory Commission
Washington, D.C. 20555
NRC FIN B6618

U. S. Nuclear Regulatory Commission

Previous Reports in Concrete Structure Research Series

Analysis of Shear Transfer in Reinforced Concrete with Application to Containment Wall Specimens, P. Leombruni, O. Buyukozturk, J.J. Connor, Massachusetts Institute of Technology, NUREG/CR-1085, October 1979.

Safety Analysis of Nuclear Concrete Containment Structures, P. Petrina, R. Sexsmith, R.N. White, Cornell University, NUREG/CR-1097, December 1979.

Shear Transfer in Large Scale Reinforced Concrete Containment Elements Report No. 1, R.G. Oesterle, H.G. Russell, Construction Technology Laboratories, Portland Cement Association, NUREG/CR-1374, April 1980.

Strength and Stiffness of Tensioned Reinforced Concrete Panels Subjected to Membrane Shear, Two-Way Reinforcing, P.C. Perdikaris, R.N. White, P. Gergely, Cornell University, NUREG/CR-1602, July 1980.

Strength and Stiffness of Reinforced Concrete Panels Subjected to Membrane Shear, Two-Way and Four-Way Reinforcing, C.H. Conley, R.N. White, P. Gergely, Cornell University, NUREG/CR-2049, April 1981.

Shear Transfer in Large Scale Reinforced Concrete Containment Elements Report No. 2, R.G. Oesterle, H.G. Russell, Construction Technology Laboratories, Portland Cement Association, NUREG/CR-2450, December 1981.

Behavioral Model for Reinforced Concrete Panels Under Cyclic Shear, Tsi-Ming Tseng, J. Calvo, O. Buyukozturk, J. Connor, Massachusetts Institute of Technology, NUREG/CR-2451, December 1981.

Strength and Stiffness of Uniaxially Tensioned Reinforced Concrete Panels Subjected to Membrane Shear, S.I. Hilmy, R.N. White, P. Gergely, Cornell University, NUREG/CR-2788, June 1982.

Behavior of Reinforced Concrete Slabs Subjected to Combined Punching Shear and Biaxial Tension, W.C. Jau, R.N. White, P. Gergely, Cornell University, NUREG/CR-2920, September 1982.

ABSTRACT

Behavioral models are developed for reinforced concrete containment wall panels having orthogonal reinforcement and for those having both orthogonal and diagonal reinforcement. An initial axial tension which causes cracking in the concrete, is applied to the orthogonal reinforcement to simulate the normal membrane stresses induced by an accidental internal pressure load. This load is followed by the application of cyclic membrane shear histories representing the tangential shear stresses generated in the event of an earthquake. Using these two models, the experimentally measured strengths of various specimens are evaluated in view of important behavioral parameters. Then, an equation in terms of the governing parameters is proposed to predict the ultimate strength of these panels. Finally, a practical design procedure is developed and recommended as a replacement for the design criteria specified by the current Code. Applications of the proposed design procedure are shown and the results obtained are evaluated.

TABLE OF CONTENTS

TABLE OF CONTENTS (cont'd)

LIST OF TABLES

LIST OF FIGURES

LIST OF FIGURES (cont'd)

LIST OF FIGURES (cont'd)

LIST OF FIGURES (cont'd)

LIST OF FIGURES (cont'd)

FOREWORD

The U.S. Nuclear Regulatory Commission has established a research program on reinforced concrete related to licensing of containments and other safety-related Category I structures. Participants of this program are Construction Technology Laboratories, a division of the Portland Cement Association (PCA); Cornell University; and Massachusetts Institute of Technology (MIT). The Portland Cement Association and Cornell University contribute to this program with experimental testing of structural elements. The Portland Cement Association is testing large-scale elements. Cornell University is testing intermediate size elements. Massachusetts Institute of Technology contributes with analytical interpretation, primarily for PCA's test program.

This report is the third report on research performed by the Massachusetts Institute of Technology.

U.S. Nuclear Regulatory Commission

CHAPTER 1

INTRODUCTION

1.1 General

The containment structure is an important component of a nuclear reactor structural system. It prevents the release of radioactive material to the environment in the event of a component failure inside the containment. For this reason much emphasis has been placed on the assessment of the level of containment safety that is provided by the currently prescribed analysis and design procedures.

The utilization of reinforced concrete for the containment structure has confronted the designer with many challenges. Problems arise in several areas. There has been some increase in the magnitude of pressure-induced internal forces. More significantly, increasing attention to earthquake design has led to higher seismic forces which are now a major design consideration. Also, significant difficulty arises in assessing concrete behavior under the induced multi-dimensional stress states. Unfortunately, analytical closed form solutions for prediction of the stress and deformation fields of

homogeneous continua encounter numerous difficulties when applied to reinforced concrete structures. Among these are the incorporation of the nonhomogeneous behavior caused by the presence of the reinforcement, concrete cracking, nonlinear concrete behavior in multiaxial stress states, and shear transfer across cracked sections.

Because of the importance of these structures, a high degree of reliability has been sought in the proposed solutions. Unfortunately, this has sometimes led to impractical and uneconomical design procedures. An example of this is in the design of the reinforcement to carry the shear stress induced by the seismic loads. The lack of knowledge of the concrete behavior under these applied membrane stresses has led to the use of diagonal reinforcement in addition to the orthogonal reinforcement. This steel is both expensive and difficult to place. It also leads to congestion which may inhibit the proper placement of the concrete.

1.2 Program Objectives

The overall objective of this ongoing research program is to provide a fundamental understanding of the structural behavior of concrete containment vessels for nuclear power facilities, and to evaluate the adequacy of existing codes and standards governing the design of these structures. Particular emphasis is placed on the effect of normal and tangential shear membrane stresses induced as a result of the applied internal pressure and earthquake loading.

The initial objective of this overall program has been to provide an understanding of the behavior of these structures at the element level (Figure 1.1). The technical approach to meet this objective involves: (1) experimental study of the behavior of concrete containment wall panels subjected to biaxial tension and shear forces, (2) development of analytical techniques for modeling and evaluating this behavior, and (3) development of economical and practical design criteria. The Portland Cement Association and Cornell University contributed to this program with experimental testing of structural elements. The Portland Cement Association tested large-scale elements and Cornell University tested intermediate size elements. Analytical interpretation and numerical modeling were carried out by the Massachusetts Institute of Technology.

In Chapter Two, a numerical model is developed for predicting the behavior of orthogonally reinforced concrete wall panels. The loading conditions consist of initially applying an axial stress to the reinforcement followed by the application of either a monotonic or cyclic tangential shear load history. The model was developed based on the experimental results of the large scale specimens tested at Portland Cement Association (PCA) [4]. To further validate the model, the behavior of a series of small scale specimens tested by Cornell University was simulated [2,6]. Based on the experimental and analytical results, the key parameters affecting the behavior of these panels are identified. They include the material properties, the specimen geometry, and detailing. Finally, a lower bound measure for the specimen strength is proposed as a function of a stress parameter

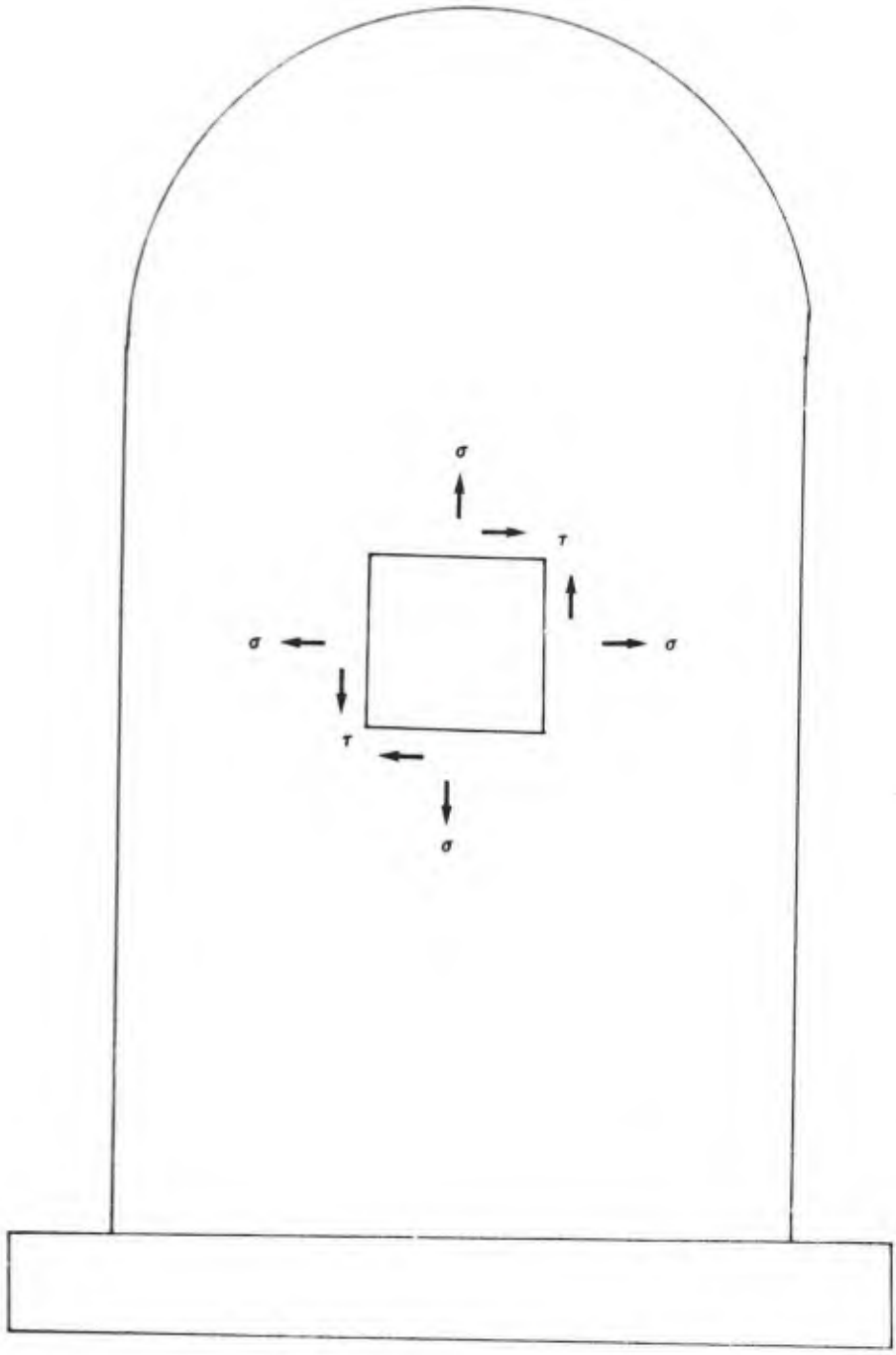

FIGURE 1.1: TYPICAL CONTAINMENT VESSEL AND ELEMENT MEMBRANE STRESSES

which includes the most important factors.

In Chapter Three, the contribution made to the specimen strength by the addition of diagonal reinforcement is studied. A numerical model for the diagonally reinforced specimens is developed based on the currently available experimental data [2]. Finally, a simplified approach is proposed to incorporate the contribution to the overall strength made by the addition of diagonal reinforcement.

In Chapter Four the provisions of current design codes for nuclear containment vessels are reviewed. The experimental program on which they were based is also evaluated. Using the newly avalilable experimental and analytical results an improved analysis and design procedure is proposed. Finally, in Chapter Five, conclusions and further research needs are cited.

CHAPTER 2

BEHAVIORAL MODEL FOR ORTHOGONALLY REINFORCED CONCRETE PANELS UNDER CYCLIC SHEAR

2.1 Introduction

In the first part of this Chapter the proposed model for orthogonally reinforced concrete wall panels under axial tension and a tangential cyclic shear load history is described. A more detailed description is given in Reference 1. In the containment wall the axial force may occur due to initial pressurization or as a result of an accidental internal pressure; tangential shear may occur as a result of the seismic excitation from an earthquake.

In the second part of this Chapter, the behavior of the most recent series of wall panels tested at Cornell University [2] is simulated. The results from the analysis of these panels along with the results of the previous simulation of all the other applicable Cornell [6] and PCA [7] specimens is presented. Based on these results, an evaluation of the proposed model is made.

Finally, in the last part of this Chapter an overall assessment of the behavior of orthogonally reinforced concrete wall panels is presented. The controlling parameters in terms of material properties, specimen geometry, and characteristics of the applied loading history are identified.

2.2 Description of Orthogonal Shear Transfer Model

The proposed shear transfer model is applicable to orthogonally reinforced wall panels. The model is based on three assumptions. First, the wall panels are assumed to be precracked prior to applying the cyclic shear load history. This is a reasonable assumption since in reality the containment structure is actually precracked due to the prescribed internal pressure that is applied to it during the initial structural integrity tests performed before the reactor is put into operation. These cracks may later widen and increase in number during a loss of coolant accident. Second, the resulting crack pattern is assumed to be identical to the reinforcement pattern, i.e., the initial crack spacing is equal to the reinforcement spacing. This has been experimentally observed [1] and may be explained by the stress concentrations in the concrete surrounding the reinforcing bars. Finally, it is assumed that the initial axial tension is taken up entirely by the reinforcement. Again this assumption was verified with the experimental results from the PCA tests described in Reference 1.

With these assumptions a model having the following characteristics was developed. The first cycle of loading is assumed to have a constant stiffness. For every cycle thereafter, a bilinear stiffness is used to model the response. The unloading stiffness for all cycles is assumed to be infinite. The behavior under subsequent load reversals is assumed to be the mirror image response of the positive loading. Figure 2.1 shows the resulting stress-strain history.

The low stiffness portion exhibited at the lower shear stress levels of every cycle is referred to as the "free slip" region, and its stiffness is denoted by K_f. The stiffer portion that follows at the higher shear stress levels is called the "contact" region and its stiffness is denoted by K_c. K_1 is the stiffness of the first cycle. For the corresponding strains or slips, δ_f is used to denote the maximum strain attained during the free slip portion of loading, and δ_m is the maximum strain or slip reached during a given cycle.

The proposed model incorporates the contribution to the overall stiffness of both the shear transfer mode at the orthogonal cracks and the dowel action of the reinforcing bars that cross these cracks. However, the experimental studies [3] conducted to date indicate that the dowel action stiffness is small.

2.2.1 First Cycle Stiffness

A constant stiffness is assumed for the first cycle. As long as the shear stress level that is reached during this cycle does not exceed a value of approximately 100 psi, the constant stiffness

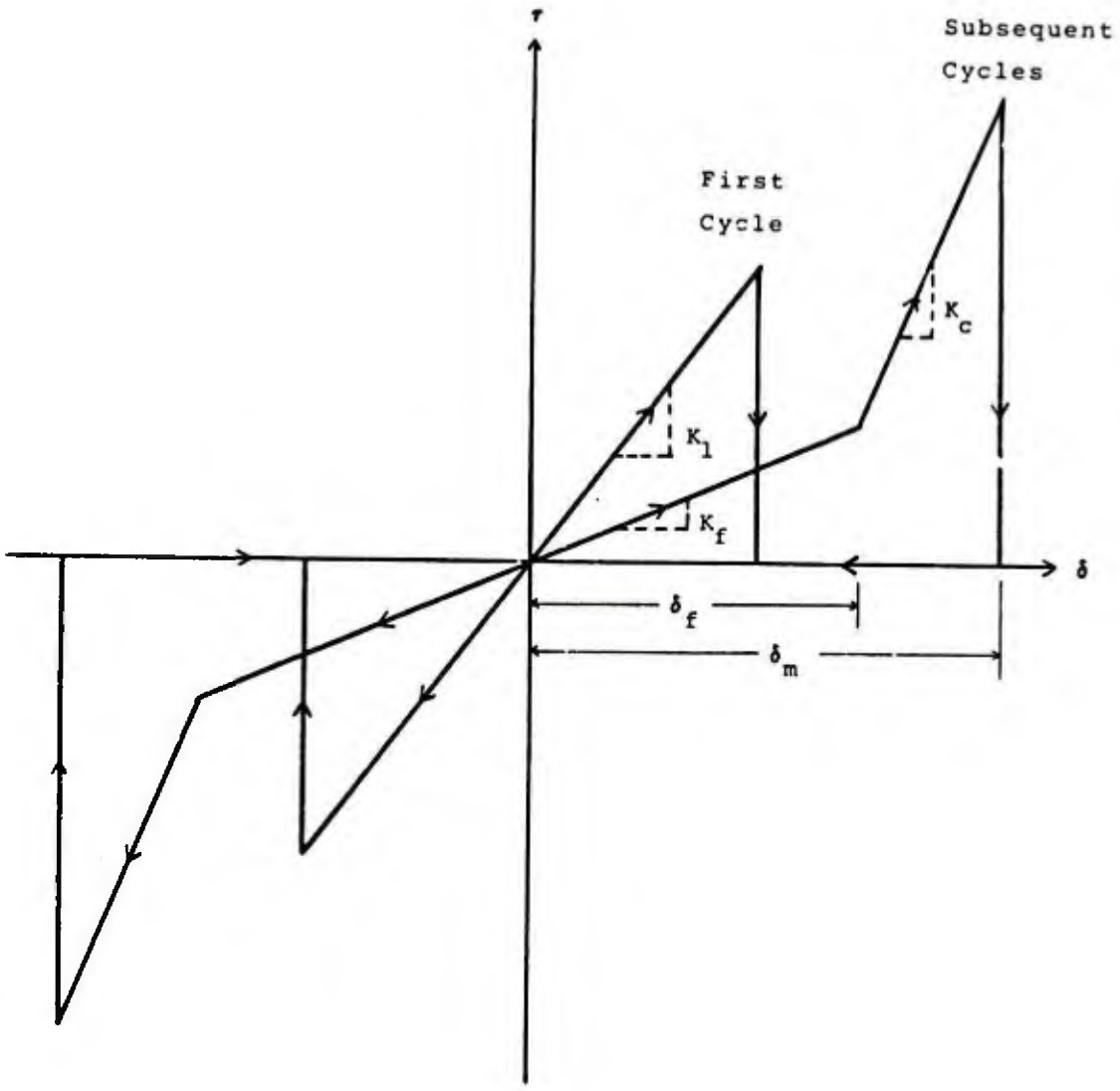

FIGURE 2.1: PROPOSED CYCLIC SHEAR MODEL

assumption is valid. For shear stresses up to this level it has been experimentally observed [1] that the specimen behavior is fairly linear. The overall stiffness of the element comes from the individual contributions of the dowel stiffness of the reinforcing bars and the interface shear transfer stiffness which is merely the frictional resistance between the crack planes that exists as they move relative to each other. The interface shear transfer mode is the largest contributor to the overall stiffness. There is an interaction between the two modes since it is the reinforcing bars which provide the stresses normal to the crack planes where the shear transfer mode is developed. Unfortunately, the available experimental data is not sufficient to model this interaction. Thus, direct superposition of the individual effects of these two modes is generally considered. A summary of the proposed procedures to evaluate the first cycle stiffness is given in Reference 3.

2.2.2 Free Slip Stiffness Degradation

At every cycle of loading after the first, there is a low stiffness portion referred to as the "free slip" region. This behavior is not observed during the first cycle for two reasons. First, because the load level attained in the first cycle is generally low. Second, the aggregate particles have random shape and orientation. As a result, the initial crack surfaces produced by the applied axial tension are not perfectly flat or parallel to each other throughout their length. In fact, at certain locations the crack faces may even be normal to each other. However, in the subsequent

cycles, as these local imperfections along the crack plane are worn out, there occurs an increasing amount of free slip.

The function proposed to describe the experimentally [4] observed behavior for the degradation of the free slip stiffness as a function of cycle number is:

$$R_f = \frac{K_f}{K_1} = \frac{1}{N} \tag{2.1}$$

where:

R_f = free slip stiffness ratio

K_f = free slip stiffness for cycle N

K_1 = first cycle stiffness

N = cycle number

Therefore:

$$K_f = \frac{K_1}{N} \tag{2.2}$$

A plot of this function is given in Figure 2.2. Two important features are displayed. First, within the first ten to fifteen cycles the free slip stiffness has been reduced to less than 10% of its initial value. In the subsequent cycles the stiffness continues to decrease but very slowly. This is illustrated by R_f being asymptotic about the value of 0. The higher values of free slip stiffness

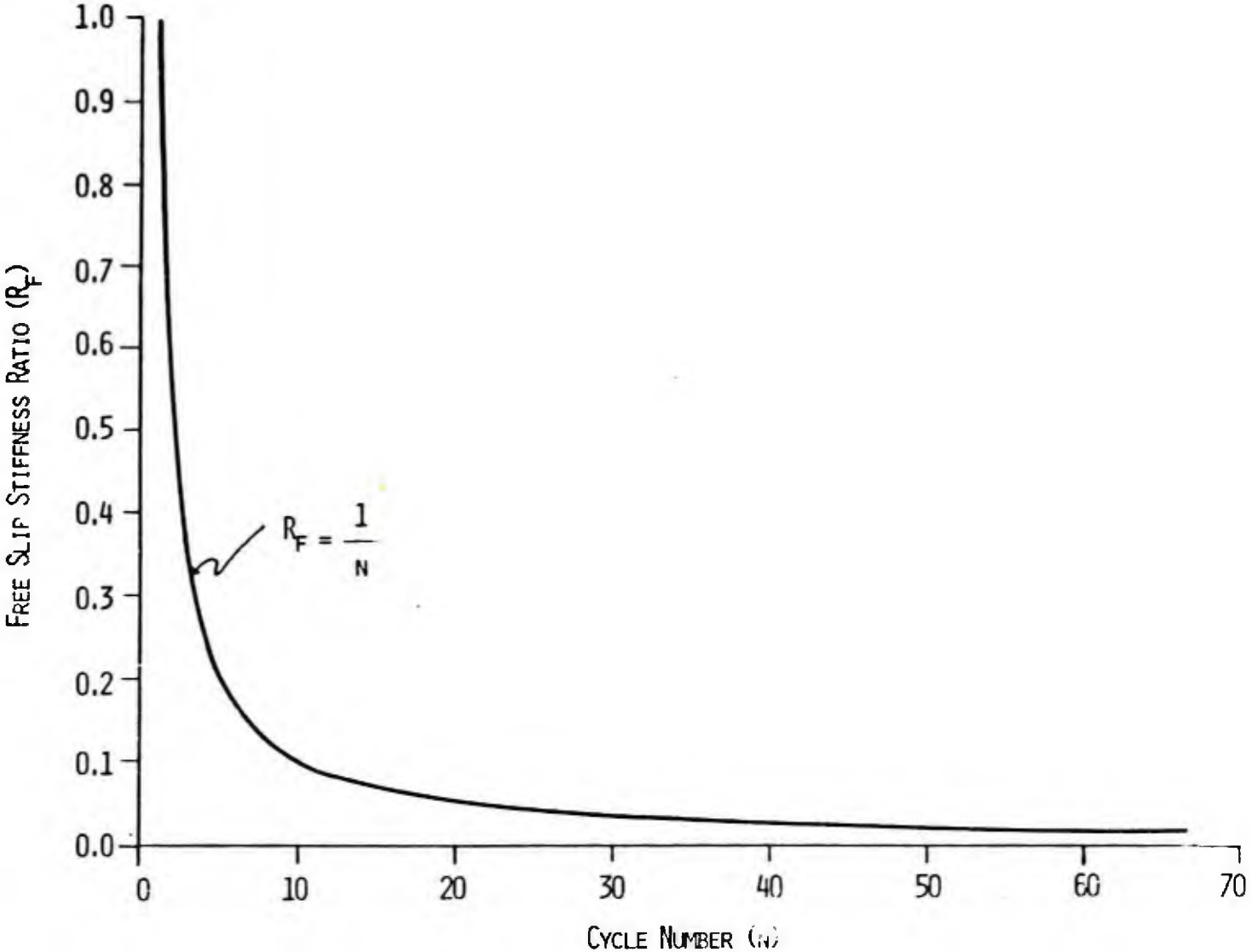

FIGURE 2.2: DEGRADTION FUNCTION FOR FREE SLIP STIFFNESS

displayed during the initial cycles of loading are due to the roughness induced by the localized imperfections in the initial crack planes. However, this initial roughness is quickly worn out and the lower stiffness exhibited at the latter cycles is merely due to the inherent roughness of the concrete surface. At this point the behavior truly becomes one of almost "free" slip at the low stress levels.

2.2.3 Contact Stiffness Degradation

The free slip portion of the load slip curve is followed by the contact region. As illustrated in Figure 2.3, this stiffness initially increases with each successive cycle and then later in the loading history decreases with subsequent cycles. The proposed function that best describes the experimentally observed behavior has the following form [4]:

$$R_c = \frac{K_c}{K_1} = \alpha_1 N^{\alpha_2} \exp(-\alpha_3 N) + 1 \qquad (2.3)$$

where:

R_c = contact stiffness ratio

K_c = contact stiffness

K_1 = first cycle stiffness

N = cycle number

$\alpha_3, \alpha_2, \alpha_1$ = empirical constants

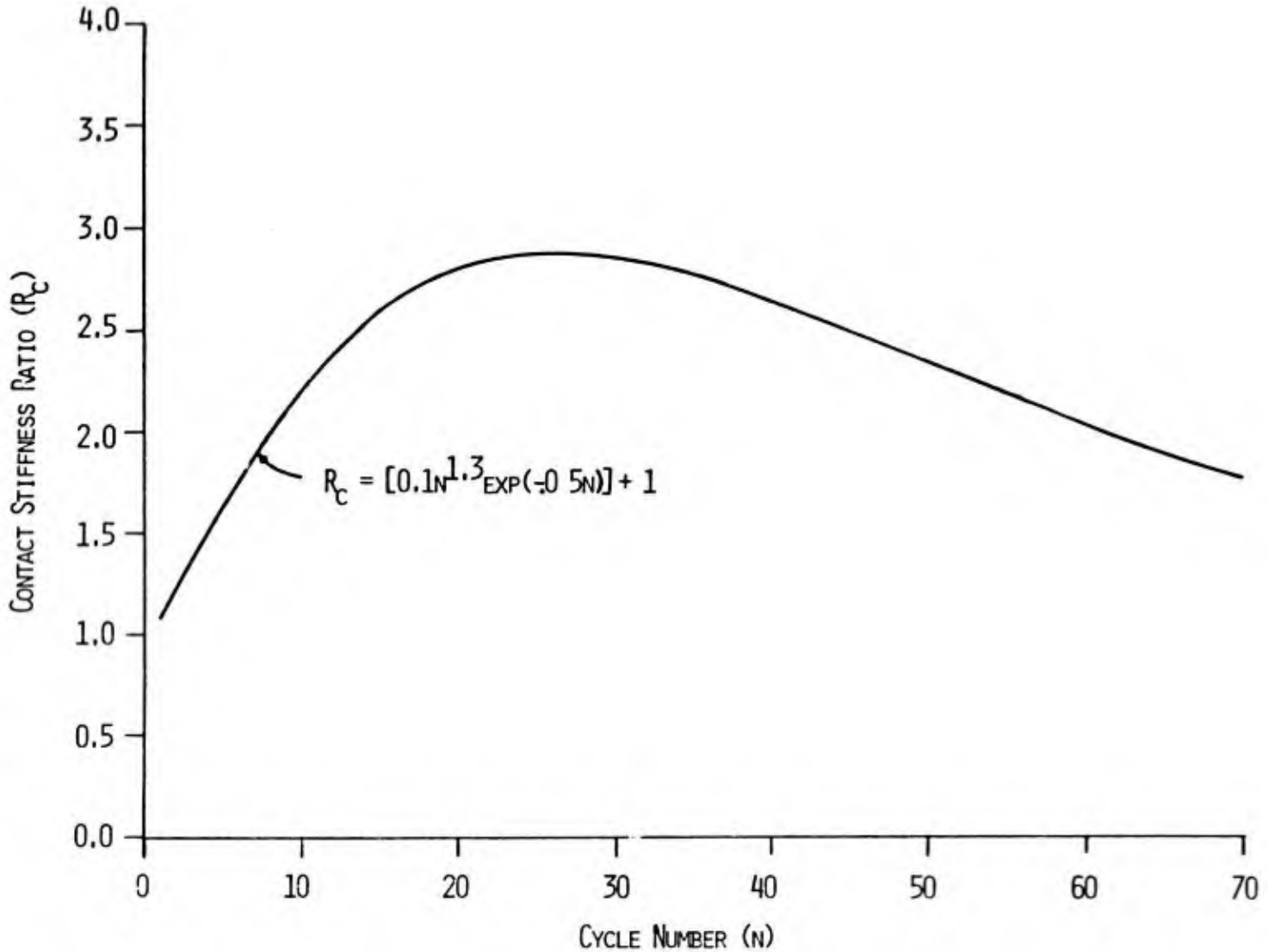

Figure 2.3: Degradation Function for Contact Stiffness

The following values for the empirical constants were found to best fit the experimental results:

$$\alpha_1 = 0.1$$

$$\alpha_2 = 1.3$$

$$\alpha_3 = 0.05$$

The reason for the initial increase and subsequent decrease of the contact stiffness is not yet clear. One possible explanation for the decrease may be due to the deleterious effect caused by the increasing number and propagation of diagonal cracks that appear in the latter stages of loading. Another possible cause might be the local crushing of the crack faces. While some of the mortar particles produced by this local crushing fall from the crack, others become trapped in the crack and wedge it open. They act like a "ball bearing" as the crack faces move relative to one another, inducing a wedging action that causes the separation at all load levels to increase. Still another possible cause may be due to the yielding of some of the reinforcement many cycles before the specimen actually fails. This yielding causes a reduction in both the dowel stiffness and the shear transfer mode stiffness due to the resulting increase in crack widths.

2.2.4 Unloading Stiffness

It has been experimentally observed that in the initiation of unloading from the peak to some fraction of the maximum load the crack surface remains essentially locked. This locking diminishes gradually

as the cycle number increases. At a shear load of about 10 to 50% of the maximum load there occurs an abrupt decrease in shear stiffness. Unfortunately, this behavior is relatively random in nature. Since it is less important to the overall performance of shear resistance under completely reversing loading conditions, the change in stiffness is neglected and a vertical line corresponding to infinite stiffness is used to approximate the unloading stiffness K_u. The shear slip or shear strain is assumed to pass through the origin for reversing loads, immediately after the shear stress reaches a value of zero.

2.2.5 Free Slip to Maximum Slip Relationship

In developing the model it was found that it is best to relate the free slip of the current cycle to the maximum slip ever attained in all the previous cycles. It was observed [4] that within the first five cycles the ratio of free slip to maximum slip increases to a value of around 0.8 and then remains constant at this value throughout the rest of the loading history. Based on this observation, the following equation is proposed to describe this behavior.

$$R_s = \frac{\delta_f}{\delta_m} = \alpha_4\{1 - \exp[\alpha_5(N-1)]\} \qquad (2.4)$$

where:

R_s = free slip to maximum slip ratio

δ_f = maximum free slip for cycle N

δ_m = maximum slip before cycle N

N = cycle number

α_4, α_5 = empirical constants

The values α_4=0.78 and α_5=-1.25 were found to provide the best fit with the experimental data. Figure 2.4 illustrates the variation of R_s with the number of cycles. Note that since R_s is a ratio, either slips or strains may be used in the model.

2.2.6 Failure Criteria

Failure of any structure is often defined in terms of its ultimate load level carrying capacity. However, in other cases failure may also be defined in terms of serviceability considerations as related to certain deflection levels. In the present Code [5] governing the design of reinforced concrete nuclear containment vessels the ultimate load is defined as that load at which the reinforcing bars reach a stress level of $0.9f_y$, where f_y is the yield stress of the reinforcement. In this model, the numerical capability for predicting the steel strains as well as the overall specimen shear strains throughout the loading history is presented. Failure may then be defined as either a limit deflection or stress level in the reinforcement.

The reinforcing bars are strained due to both the initial axial tension, and the subsequent shear load history. Assuming that the reinforcement takes up the entire initial axial force, the

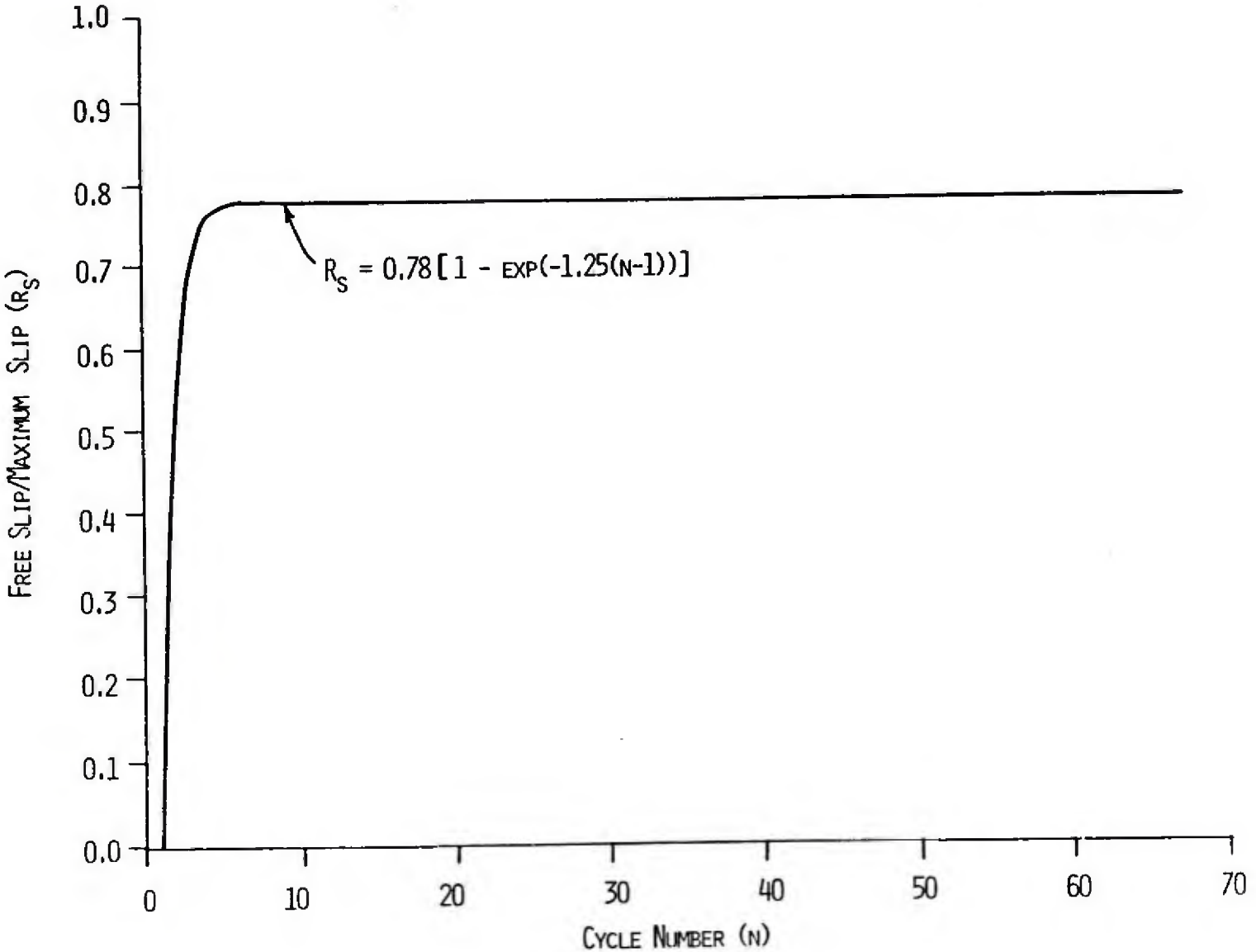

FIGURE 2.4: FREE SLIP TO MAXIMUM SLIP RELATIONSHIP

initial steel strain is determined from:

$$\varepsilon_o = \frac{f_p}{E_s} \tag{2.5}$$

where:

ε_o = initial strain due to pretensioning

f_p = initial axial stress

E_s = Young's Modulus for reinforcement

Using this equation, the calculated values of ε_o were found to be within 10% of the experimental values [1].

The total steel strain at any point during the loading history may then be found by superimposing the strain due to axial force and the strain due to the shear stresses.

$$\varepsilon_t = \varepsilon_o + \varepsilon_s \tag{2.6}$$

where:

ε_t = total steel strain

ε_s = steel strain due to shear stress applied to the panel

For the relationship between ε_s and the specimen shear strain, an empirical equation of the following form is proposed.

$$\varepsilon_s = \alpha_6 \gamma \tag{2.7}$$

where:

α_6 = empirical constant

γ = overall specimen shear strain

The value of the empirical constant α_6 depends on the initial axial stress applied to the reinforcing bars. The following linear interpolation based on the experimental results [4] is proposed:

$$\alpha_6 = 0.170 - 0.00167(f_s) \qquad (2.8)$$

where:

f_s = initial axial stress applied to reinforcement (ksi)

α_6 = empirical constant

This proposed equation for converting the specimen shear strains to additional steel strains is intended to predict the overall average behavior of all the reinforcing bars. It was observed in the tests [4] that the steel strains in the bars located in the outer region of the specimens were much higher than the strains in the bars located in the central portion.

2.2.7 Implementation of the Proposed Model

The previously described model provides a numerical capability for predicting specimen shear strains and steel strains at any point during the applied axial tension and cyclic shear load history. A flowchart for the computer program that incorporates the model is shown in Figure 2.5. The required inputs to the program are: the

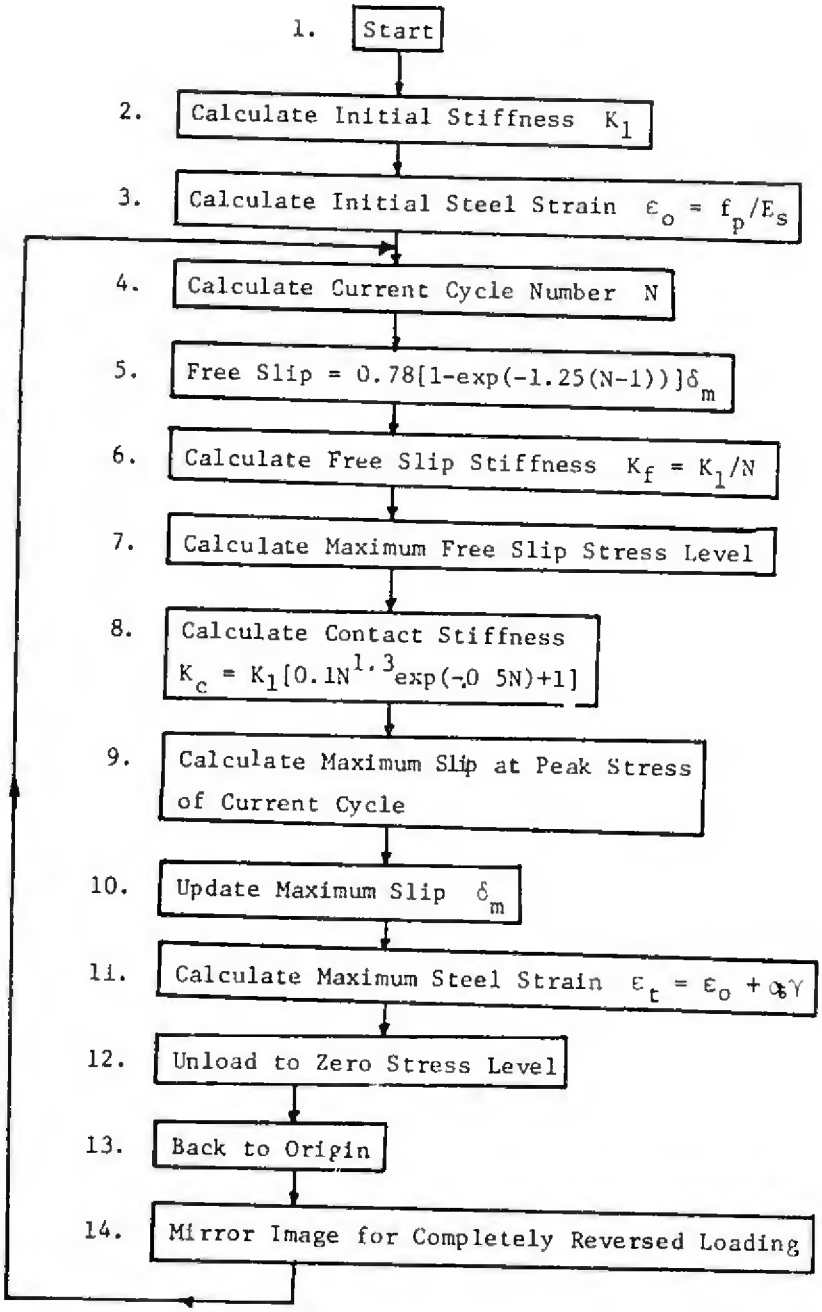

FIGURE 2.5: FLOWCHART FOR CYCLIC SHEAR MODEL

initial stiffness, the number of cycles of loading, the maximum shear stress achieved in each cycle, and the initial axial force applied to the reinforcement. The actual Fortran program along with a detailed users manual is given in Appendix A.

2.3 Simulation of Experimental Specimens

In the following section the experimental results of the PCA [4,7] and Cornell [2,6] programs are briefly presented. These two experimental programs represent major efforts in the testing of small and large scale orthogonally reinforced concrete wall panels under an initial axial tension and a subsequent tangential cyclic shear history. The behavioral model presented in the previous sections was used to simulate the behavior of the applicable specimens tested in these two experimental programs. This allows an evaluation of the proposed model as well as an assessment of the characteristics of the behavior of these types of panels.

2.3.1 PCA Experimental Program [4,7]

This program included the testing of 5 large scale specimens. The overall specimen geometry was 5' x 5' x 2'. The orthogonal reinforcement consisted of 8-#18 bars @ 12" in one direction and 8-#14 bars @ 12" in the orthogonal direction, giving steel ratios of 0.013 and 0.022 in the x and y directions respectively. The first three specimens tested were monotonically loaded to failure. The other two specimens, the RB5 and RB6, were loaded with an initial axial tension and a subsequent cyclic shear load history.

In these tests, the specimen shear strain history was measured on both the top and bottom faces on each specimen, to attempt to correct some of the experimental errors. The history of various typical cracks in the specimens was followed. Steel strain histories of various bars and at several points along their lengths were measured throughout the shear load history. These data were essential in defining and validating an appropriate failure criteria and its corresponding empirical constants. Finally, by using different values of initial axial pretension, 36 ksi in the RB5 specimen and 54 ksi in the RB6 specimen, an attempt was made to evaluate the effect of this parameter on both the degradation of the stiffness and the transformation of specimen shear strains to steel strains to define the eventual failure of the specimen.

The experimental program suffered from various weaknesses. First, recall that only two specimens were tested under cyclic shear load histories. Unfortunately, these tests were not repeated to investigate their validity. Secondly, the same reinforcement ratio and bar sizes were used in both specimens, so the effect of the variation of these parameters on the behavior cannot be evaluated from these results. In terms of the applied loads, only two initial axial load levels corresponding to $0.6f_y$ and $0.9f_y$ were selected. As was shown in the model, the relationship between the specimen shear strain and the induced steel strain in the reinforcement which may indicate the bond failure and slip occuring at the concrete-reinforcement interface is highly dependent on the initial axial force applied to the bars. Thus, for lower initial axial tensions of say $0.3f_y$, it is

necessary to extrapolate linearly from the results obtained to establish the appropriate relationship. Even the assumed linear interpolation for values of initial tension between $0.6f_y$ and $0.9f_y$ may not prove to be entirely valid as more experimental data become available. The cyclic shear load history used in the experiments consisted of a series of steps of 5 to 10 cycles at a constant stress level and then a jump to a higher stress level. In a sense, this corresponds to a series of uniform cyclic shear load histories. The real earthquake input is actually a non-uniform cyclic history with a random nature.

2.3.2 Cornell Experimental Program [2,6]

In this program a total of 47 small scale specimens were tested. All the specimens had the same overall geometry illustrated in Figure 2.6. Two types of specimens with different reinforcement ratios were tested in two phases. In the first group of 16 specimens, #6 bars were used to obtain a $\rho_x = 0.0122$ and a $\rho_y = 0.0244$. Of these sixteen specimens, four were monotonically loaded with a shear load up to failure after the application of the initial axial tension. The rest of the specimens were loaded with a uniform step type of cyclic shear load history as illustrated in Figure 2.7. The initial axial tensions applied to the orthogonal reinforcement were 0.0, 0.3, 0.6, and $0.9f_y$. In the second phase of the program the reinforcement ratios were decreased to 0.0055 and 0.0110 in the x and y directions respectively. In this phase, # 4 as well as #6 bars were used to attain the desired steel ratios. Two specimens with diagonal reinforcement in both

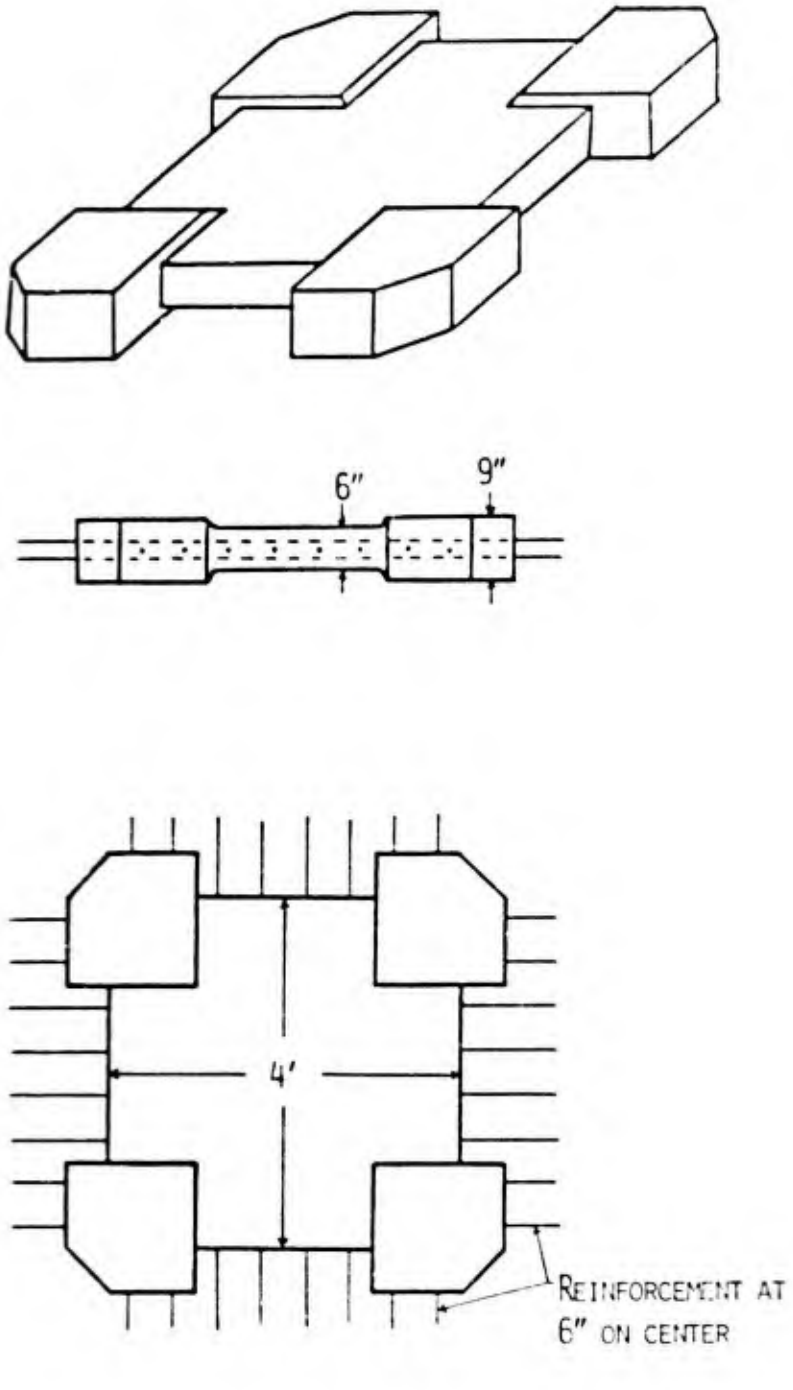

FIGURE 2.6: CORNELL SPECIMEN GEOMETRY (6)

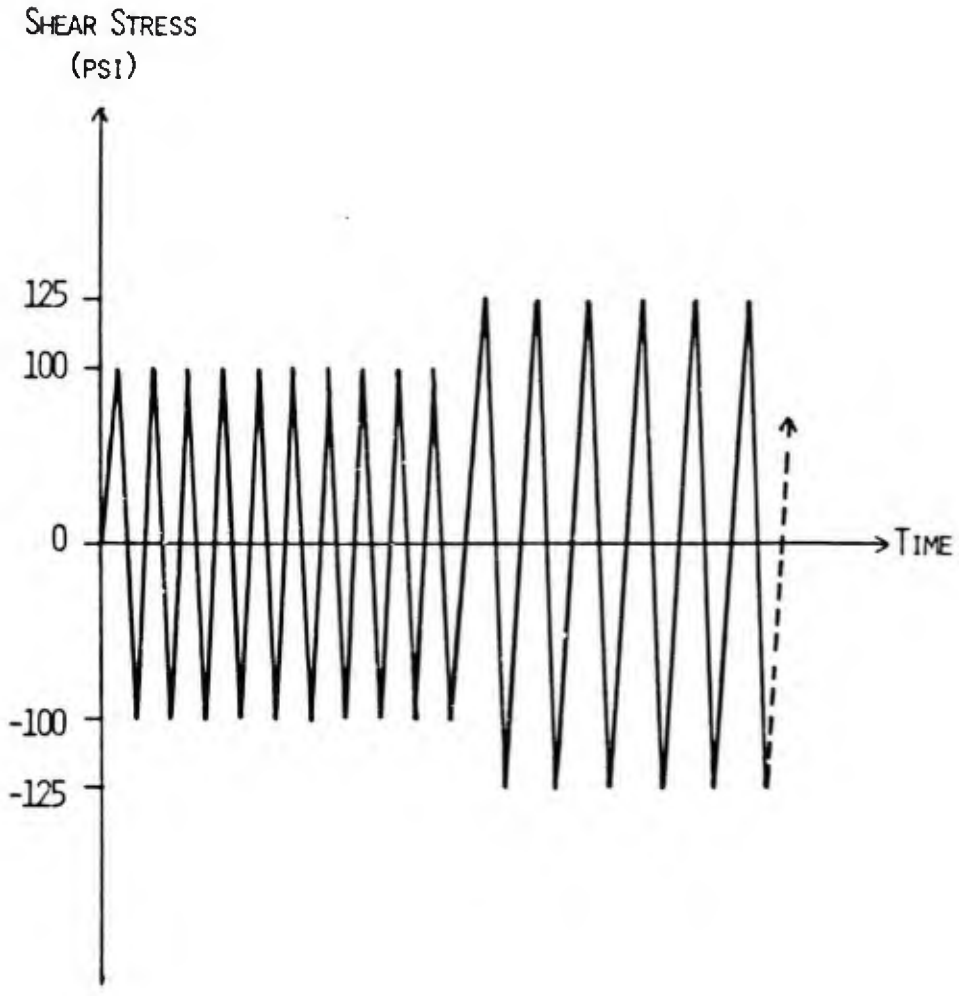

FIGURE 2.7: CYCLIC SHEAR LOAD HISTORY (6)

directions at 45° to the orthogonal reinforcement were also tested. These specimens are described in detail in the next chapter. In addition, a few of the specimens were loaded to failure with various types of monotonic shear loads. The use of two different steel ratios in the two phases of the program helped in the assessment of the effect of this key parameter on the degradation of the specimens. Furthermore, the use of various bar sizes to attain the same steel ratio is also very useful in evaluating the effect this parameter has in the transfer of forces from the concrete to the reinforcement. Note that this is the only experimental program in which diagonal reinforcement in addition to the orthogonal reinforcement was used in initially precracked panels followed by a shear load history.

On the other hand, the Cornell program also had some disadvantages. A major disadvantage lies in the small scale of the specimens. Since the behavior of these specimens is very complex in nature it becomes necessary to utilize a semi-rational empirical approach to arrive at a useful solution. Therefore, it is essential that the panels being tested resemble as closely as possible the actual containment wall panels in overall geometry, reinforcement pattern, and material properties so that the results obtained will be applicable to the actual structures. A second disadvantage is in the method of application of the shear loads. To apply a uniform shear stress along the sides of a panel is very difficult; therefore, in most of these experimental programs equivalent compression/tension stresses ($\sigma = \tau$) are applied at 45° to the normal axis, as shown in Figure 2.8. In Figure 2.9 the actual loading scheme of the Cornell

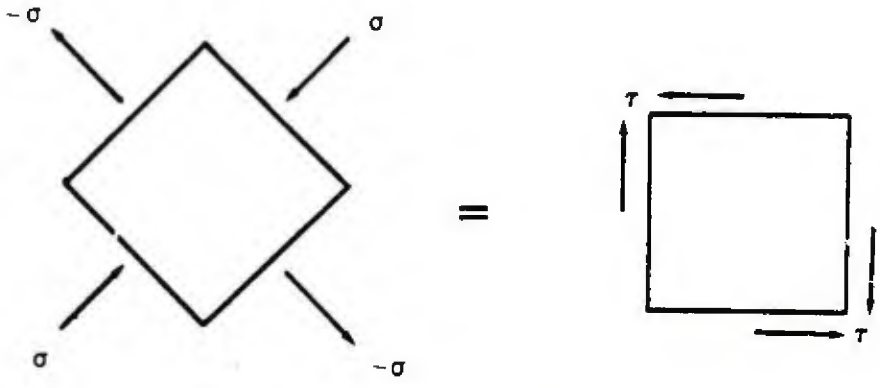

FIGURE 2.8: EQUIVALENT SHEAR STRESS APPLICATION

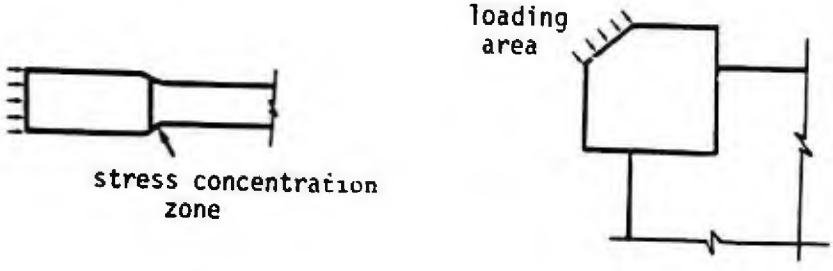

FIGURE 2.9: STRESS CONCENTRATION IN CORNELL LOADING SCHEME

specimens is shown. As can be seen there are two problems. First, the normal forces are applied through the smaller built-up corners of the specimen. Thus, these forces which simulate the shear stresses are not applied uniformly along the entire side of the specimen. This leads to a considerable stress concentration in the corner regions. The second problem in the loading scheme lies in the difference in specimen thickness between the built-up corners and the rest of the specimen. Since the load is applied through these thicker corners the net result is that another source of stress concentration is created at the interface between these two regions. The overall effect of these two problems is to cause the specimens to consistently fail in the region near these built-up corners (Figure 2.10) instead of in the central 4 sq. ft. portion of the specimen. It is in this central portion where all the deformation measurements are being taken and the failure should occur due to symmetry considerations. Because reinforced concrete is an inhomogeneous, anisotropic material and since it contains many included local imperfections one would not expect all the specimens to fail somewhere in the central portion. However, the fact that all the specimens seem to consistently fail in the outer corners indicates that the induced stress concentration plays a major role in the final failure mode and ultimate strength of the specimens. Therefore, the experimental values of ultimate strength must be interpreted accordingly. This problem of stress concentration may be partly avoided by following a loading scheme such as the one used by the Japanese investigators [8]. In this loading scheme (Figure 2.11), again the tension/compression principle to

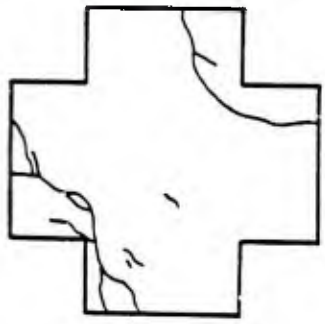

(a) Specimen 0.3A

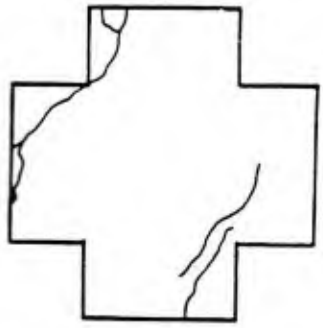

(b) Specimen 0.3B

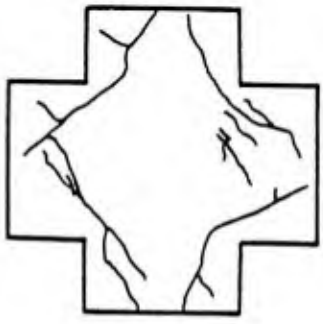

(c) Specimen 0.6C

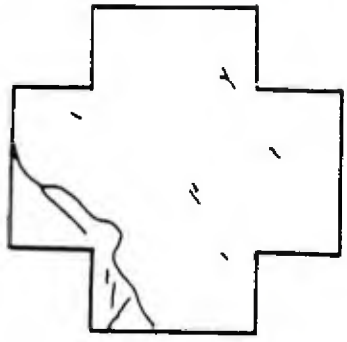

(d) Specimen 2-0.3B

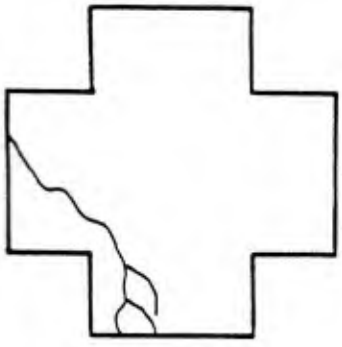

(e) Specimen 2-0.6B

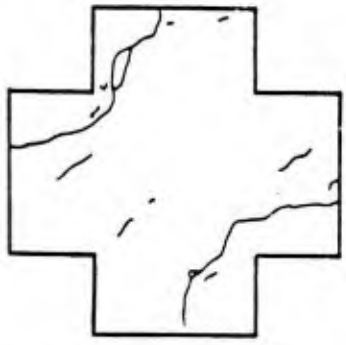

(f) Specimen 2-0.9A

FIGURE 2.10: FAILURE PLANES OF CORNELL SPECIMENS (2,6)

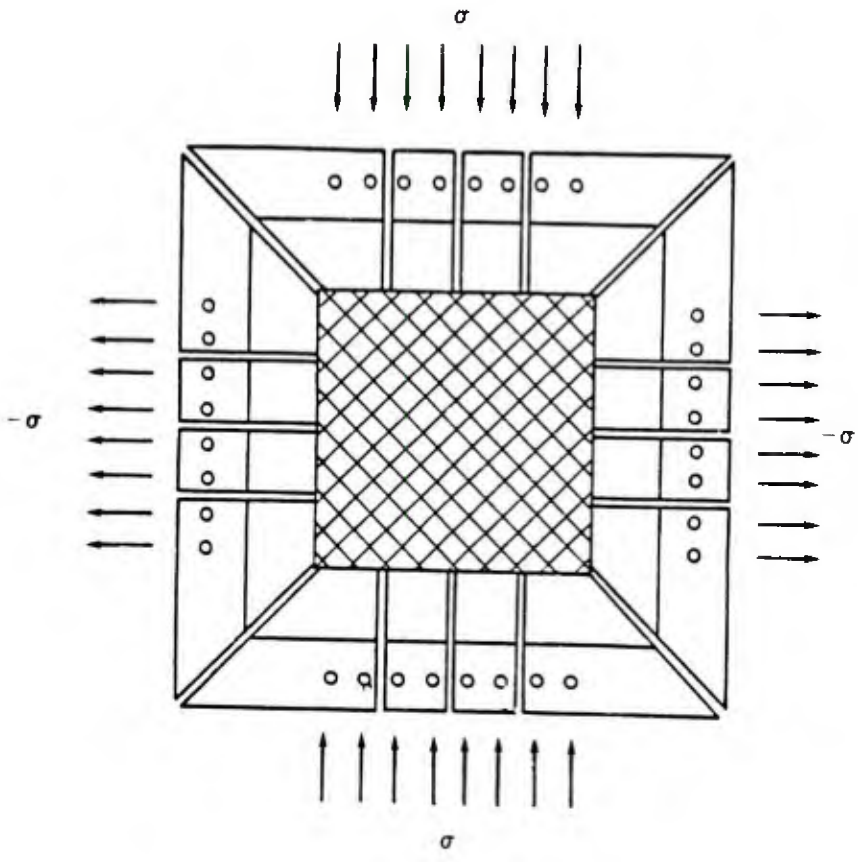

FIGURE 2.11: JAPANESE SPECIMEN AND LOADING SCHEME (8)

simulate the equivalent shear stresses is employed. However, the orthogonal reinforcement is placed at 45° to the global x and y axis of the specimen and then a uniform compression or tension force is applied along the entire side of the specimen.

2.3.3 Evaluation of Specimen Shear Strain History

The overall specimen shear strain, measured as illustrated in Figure 3.7, defines the deformation of the specimens throughout the entire loading history. It also indirectly measures the amount of strain induced in the reinforcement. The complete predicted stress-strain histories up to the predicted failure cycle for the specimens whose behavior was simulated is illustrated in Figures A.3-A.28 (Appendix A). These include the figures for the experimental and predicted maximum shear strain reached in each cycle. The predicted behavior is represented by a smoother curve because the maximum shear strain achieved in every cycle is known. For the experimental results the values for only a few of the cycles were known, so these points were connected by straight lines. Also note the stiffening behavior that occurs in those cycles in which the applied shear stress is increased. This results from increases in the specimen shear strains which lead to increases in the steel strains, which in turn induce higher resistive frictional stresses between the crack planes. As seen in the figures of maximum specimen shear strain vs. cycle number (A.3-A.28), the specimen shear strain remains constant after the initial three or four cycles at a given load level. This implies that any further cycling at this load level would not

cause any further degradation or deformation in the specimen. So the panel exhibits a convergent type of behavior. However, at the higher shear stress levels near failure, the reinforcement begins to yield and the behavior becomes divergent. The implication from this is that there exists a lower bound stress level at which the specimen would not fail regardless of the number of cycles that were applied. Also at higher stress levels, failure could be defined as a particular number of cycles corresponding to a given stress level as is done in fatigue analysis. In the future, as much more experimental data become available it will be possible to construct these stress level vs. number of cycles to failure diagrams.

The predicted and experimental specimen shear strains during the failure cycle for each specimen are listed in Table 2.1. The strain in the final cycle is important not only in defining the failure of the specimen, as it is converted to an equivalent steel strain, but it is also a good measure of how well the model has kept up in predicting the overall specimen deformation. For the RB5 and RB6 specimens the predicted and experimental responses are almost identical. This is not surprising since the proposed model was based on the experimental results of these tests. On the other hand, for the 0.3 specimens the predicted behavior is too soft, while for the 0.6 specimens the behavior is in excellent agreement with the experimental results. Yet for the 0.9 specimens, once again the behavior does not match as closely with the experimental results. This time the predicted behavior is too stiff. Note that although these specimens were smaller their steel ratios were very close to those of the PCA

Table 2.1: Experimental vs. Predicted Shear Strain at Failure Cycle

Specimen	Cycle No.	Shear Strain (rad x 10^{-3})		
		Experimental	Predicted	% Difference
RB5	48	5.38	5.31	1%
RB6	67	6.96	7.25	4%
0.3A	51	4.43	5.85	32%
0.3B	51	3.81	6.55	72%
0.6A	40	8.99	9.24	3%
0.6B	31	6.19	6.37	3%
0.9A	31	9.08	8.25	9%
0.9B	30	20.04	11.17	44%
2-0.3B	41	7.40	4.28	42%
2-0.6A	26	13.08	6.47	50%
2-0.6B	32	12.63	7.20	43%
2-0.9A	30	20.65	8.10	61%
2-0.9B	30	16.80	8.10	52%

Note: For the specimens whose experimental shear strain at failure was not available, the shear strain of the latest cycle recorded is used.

specimens. For the 2-0.3B to 2-0.9B series of specimens the predicted behavior was consistently stiffer in all cases. Recall, however, that these specimens had about half the steel ratio as the previous PCA or Cornell specimens. Overall the behavior of the specimens which had a closer steel ratio to the PCA specimens was more accurately predicted. Since the experimental first cycle stiffnesses were used as inputs the discrepancies between the observed and predicted results cannot be attributed to this factor. The differences between the experimental and predicted values may be regarded within acceptable limits in light of the variation that exists even between the values obtained from the various specimens which had the same reinforcement pattern and initial pretension force. Note also that the values being compared were at or near the failure cycle, where the specimen behavior tends to become highly unstable, as can be seen in the figures in the appendix.

2.3.4 Evaluation of Failure Criteria

In the proposed model, failure is defined as the load level at which the orthogonal bars yield. However, since a cyclic shear load history is under consideration, failure for the specimens consists of the ultimate shear strength and the corresponding cycle number. In Table 2.2 the experimental and predicted failures of the various specimens are listed. In cases where the specimens did not fail at the end of the experimental shear load history the specimen was further loaded with a series of consistent loads. By consistent loads what is meant is the further cycling of the specimen for a total of ten cycles at a given stress level and then increasing the shear

Table 2.2: Experimental vs. Predicted Specimen Ultimate Strength and Cycle Number

Specimen	Failure Shear Stress (psi)			Failure Cycle No.	
	Experimental	Predicted	%Difference	Experimental	Predicted
RB5	210	230	9%	48	64
RB6	218	218	0%	67	65
0.3B	375	450	20%	54	68
0.3A	375	475	20%	56	74
0.6A	325	275	15%	41	33
0.6B	275	325	18%	40	41
0.9A	225	125	44%	38	11
0.9B	275	125	54%	31	1
2-0.3B	300	475	58%	41	80
2-0.6A	250	300	20%	26	40
2-0.6B	250	275	10%	32	46
2-0.9A	200	125	38%	31	3
2-0.9B	200	125	38%	31	3

stress by a certain amount.

The predicted behavior follows the same trend as it did in terms of the specimen shear strains. It is slightly stiff or unconservative for the 0.3 level of pretension; it is most accurate for the 0.6 specimen; and it is considerably conservative in predicting the strength at the 0.9 level of pretension. This indicates that the relationship between the specimen shear strain and the additional strain induced in the reinforcement is dependent on the initial axial tension (f_s). The amount of bond failure and slip between the reinforcement and concrete determines when the reinforcment yields and the specimen fails. This relationship seems to be slightly dependent on the scale of the specimen, since the proposed model was more accurate in predicting the ultimate strength of the PCA specimens.

It is interesting to note that the RB5 specimen actually had a slightly lower shear strength than the RB6 specimen. Considering that the two specimens had the same overall geometry, material properties and detailing, the one with the lower initial axial tension would be expected to have a higher shear strength if they were both loaded with the same cyclic shear load history. The reason that the RB5 specimen with an initial axial tension of 36 ksi vs. the 54 ksi applied to the RB6 specimen failed at a lower stress might be that slightly different load histories were applied to these specimens. The RB5 specimen was loaded with higher shear stresses throughout the loading history except during the last ten or so cycles. This resulted in a lower ultimate shear strength. This is very important because it

illustrates various points. The specimen shear strength presented for all these specimens does not necessarily represent a conservative measure of their shear strength. As a matter of fact the 0.6A specimen, whose overall behavior was very well predicted by the proposed model, was also loaded with a simulated load history (Figure A.2 in Appendix A). This load history had the same fundamental characteristics, in terms of number of load levels and cycles, as the experimental load history. The specimen failed at a shear stress of 240 psi (cycle 40), a 26% reduction in shear strength over the predicted value. This is a crucial point if the experimental values are to be used to propose some type of conservative analysis and design procedure.

2.4 Summary and Conclusions

In the beginning of this chapter the behavioral model for orthogonally reinforced nuclear containment wall panels was presented in detail. The model is intended for application in cases where the panels are initially precracked by the application of axial tension to the reinforcing bars and a subsequent cyclic shear load history is applied. In the second part of this chapter the model presented was used to simulate the behavior of the currently available experimental panels. Based on the results of these simulations the following observations may be made regarding the behavior of orthogonally reinforced wall panels.

(a) The first cycle response is basically linear as long as the maximum stress level reached during this cycle does not exceed a value of around 100 psi.

(b) The response for every successive cycle after the first is clearly bilinear and characterized by a low stiffness region at the lower stress levels and a much higher stiffness region at the higher stress levels.

(c) The lower stiffness portion corresponds to basically the free slip that occurs between the crack faces as they move relative to each other in response to the applied shear stress. This free slip occurs due to the initial orthogonal cracks that result from the application of the initial axial force to the reinforcement.

(d) At the higher shear stresses, as the specimen further deforms, high normal stresses develop between the crack faces as a result of the straining of the reinforcement. In order for the specimen to further deform, these high frictional forces must be overcome. The final result is the stiffer behavior displayed in the higher shear stress portion of loading.

(e) The higher the initial axial force, the lower the ultimate strength of the specimen for any given consistent cyclic shear load history.

(f) The main factor affecting the degradation of the stiffness of the specimen is the number of cycles of loading. Factors such as the specimen size, reinforcement ratio, and material properties only slightly influence the degradation, and can thus be appropriately incorporated into the overall behavior through the evaluation of the first cycle stiffness.

(g) The relationship between the specimen shear strain and the additional steel strain induced in the reinforcement is mainly dependent on the initial axial tension. Physically this relationship measures the amount of bond failure and slip that occurs at the reinforcement-concrete interface. Factors such as the specimen scale and bar sizes also affect, to some extent,this relationship.

(h) The failure of the specimen, and in turn its shear capacity are controlled by the yielding of the reinforcement. Therefore in order to accurately predict the ultimate shear strength capacity of the specimens, it is necessary to have an accurate knowledge of the reinforcement material properties.

(i) The experimental shear strength of these panels does not necessarily represent a conservative measure of their true lowest shear strength under any arbitrary cyclic shear load history. As was seen from the 0.6A specimen, reductions of up to around 25% in strength can be predicted by applying other consistent cyclic shear load histories.

CHAPTER 3

BEHAVIORAL MODEL FOR ORTHOGONALLY AND DIAGONALLY REINFORCED CONCRETE WALL PANELS

3.1 Introduction

In this chapter a constitutive element model for reinforced concrete wall panels having both orthogonal and diagonal reinforcement is presented. Again, the two load conditions considered are the initial axial force applied to the orthogonal reinforcement ,and a uniform cyclic shear load history applied to the panel.

The model was developed based on the results of the latest series of wall panels tested by Cornell University [2]. The specimens have the same geometry as the Cornell panels described in the previous chapter (Figure 2.6) except that these specimens have two meshes of diagonal reinforcement running in both directions in addition to the orthogonal reinforcement. With the addition of the diagonal reinforcement at 45° to the orthogonal reinforcement, the effective steel ratios become $\rho_x = 0.0076$ and $\rho_y = 0.013$. Each mesh of diagonal reinforcement consists of two layers of Grade 60 No. 3 bars. Since

the bars are placed at 12" on center, the effective steel ratio in the diagonal direction for these bars alone is $\rho_d = 0.0031$.

In the second part of this chapter the proposed model is employed to simulate the behavior of the two applicable Cornell specimens. This makes possible the assessment of the overall validity of the model and the physical interpretation of the predicted and observed behavior.

3.2 Assumptions

Intrinsic to the numerical model presented in the following sections are the following assumptions.

(a) The orthogonal reinforcement bars are assumed to be fully unbonded after the application of the initial axial force. This assumption is realistic since the concrete surrounding the reinforcement is highly stressed, thus leading to the breakdown of the bond. This behavior has been experimentally confirmed [1].

(b) The orthogonal crack pattern due to the initial axial tension is assumed to be identical to the reinforcement pattern. The two Cornell specimens had orthogonal cracks at an average spacing of 7.1" [1] and the orthogonal bars were placed at 6.5" spacings (Figure 3.1). This crack pattern results from

a) 4-0.6-A Specimen

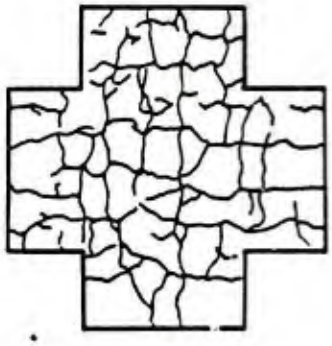

b) 4-0.9-A Specimen

FIGURE 3.1: INITIAL CRACK PATTERN OF CORNELL SPECIMENS (2)

the higher stress intensity in the concrete surrounding the reinforcement.

(c) The diagonal bars are assumed to be only partially bonded to the concrete after the application of the initial axial force. If a perfect bond existed, then it can be shown that these bars should undergo an initial strain equal to the orthogonal bars. The experimentally observed behavior, however, shows that they do not. For the Cornell specimens this occurs because only the orthogonal bars were directly tensioned. The strain in the diagonal bars was induced only as a secondary effect governed by the amount of slip that occurred between these bars and the concrete.

(d) In modeling the behavior, a bilinear loading curve is assumed for every cycle after the first. As can be seen from Figures B.1 - B.30 (Appendix B), there is no clearly defined point which separates the two assumed regions. Actually, there is typically a very smooth transition zone between the low and high stiffness regions. However, the simple bilinear model is sufficient to properly simulate the actual behavior.

(e) For the unloading curve, an infinite stiffness is assumed.

(f) For a given cycle, a positive shear loading is assumed to produce the mirror image behavior of the corresponding negative shear loading. This implies that at the end of one complete cycle, a positive and a negative loading, there

should be no residual strain in the specimen. In reality, however, there is always some residual strain which is either always positive or negative for all the cycles of a given test. Tables 3.1 and 3.2 illustrate the residual strains for the Cornell specimens. In one case the residual strain is always positive while for the other specimen it is always negative. Although it appears that the residual strain increases with every cycle, this may only be true because the maximum strain in these tests was increasing with every cycle of loading. This phenomenon is quite random in nature since it is probably due to either aggregate interlock or some other localized discontinuities. In the proposed model, its effect is neglected since the residual strain is about an order of magnitude smaller than the specimen failure shear strain.

(g) The degradation of both the free slip and contact stiffness may be expressed in the following form:

$$D = F(f_s, V_a, M, N)$$

where:

f_s = initial axial tension applied to orthogonal reinforcement

V_a = stress amplitudes applied in cyclic shear history

M = material properties of concrete and steel

N = number of cycles

Table 3.1: Residual Strains for 4-0.6A Specimen

Cycle Number	Residual Strain (rad x 10^{-4})
1	7.0
2	7.5
10	9.5
11	11.0
12	11.5
20	12.0
21	13.0
22	13.5
30	14.0
31	14.5
32	14.5
40	15.5
41	14.0
42	14.0
50	11.5
51	11.5
52	10.0

Table 3.2: Residual Strains for 4-0.9A Specimen

Cycle Number	Residual Strain (rad x 10^{-4})
1	-7.5
2	-7.5
10	-5.0
11	-5.5
12	-6.0
20	-8.5
21	-8.5
22	-8.5
30	-7.5
31	-9.5
32	-9.5
40	-9.0
41	-9.0
42	-11.5

i. The degradation is assumed to be fairly independent of f_s and V_a. As will be seen in the following sections, based on the experimental results, this assumption appears to be extremely valid.

ii. The material properties used in most reactors are fairly typical and uniform (e.g. f'_c = 4000 psi, f_y = 60 ksi). Therefore, it is not necessary to study in great detail the effect of variations in the material properties on the overall behavior.

iii. Based on the above assumptions it is evident that the most significant factor in the degradation process is the number of cycles of loading (N).

The resulting model based on the assumptions enumerated above is as illustrated in Figure 2.2. In the following sections the specific functions for the various aspects of the model are developed.

3.3 Evaluation of First Cycle Stiffness

A linear stiffness is assumed to model the behavior during the first cycle of loading. Many methods have been proposed to evaluate the stiffness of panels having only orthogonal reinforcement. For panels having both orthogonal and diagonal reinforcement, it is proposed to evaluate the first cycle stiffness by using the principle of superposition. The total stiffness is then the sum of the stiffness for an equivalent orthogonally reinforced concrete wall panel plus the shear stiffness provided by the diagonal bars. The

resulting first cycle stiffness is expressed as:

$$K_1 = K_{1o} + K_d \tag{3.1}$$

where:

K_1 = first cycle stiffness

K_{1o} = first cycle stiffness considering only the orthogonal reinforcement

K_d = shear stiffness provided by diagonal reinforcement

The K_{1o} term can be evaluated by the procedures recommended in Chapter 2. It corresponds identically to the K_1 term of the orthogonal model. The K_d term is the shear stiffness provided by the diagonal reinforcement in the form of axial straining due to the applied shear.

$$K_d = \frac{E_s \rho_d}{2} \tag{3.2}$$

where:

E_s = Young's Modulus for the steel reinforcement

ρ_d = steel ratio of the diagonal bars in the diagonal direction

This procedure is slightly conservative because it neglects the contribution of the diagonal bars to both the dowel stiffness and the orthogonal shear transfer mode. However, these contributions are negligible when compared to the total stiffness. In Table 3.3 the

Table 3.3: Experimental vs. Predicted First Cycle Stiffness

Specimen	Calculated Stiffness (K_1)			Experimental Stiffness (K_1) (psi/rad)
	K_{1o}	K_d	K_1	
f_s=0.6	66345	40300	106645	109790
f_s=0.9	34239	40300	74629	51941

experimental stiffnesses for the Cornell specimens are compared to the predicted values using the procedure just described. The K_1 values are actually the average first cycle stiffness of the 2-0.6A, 2-0.6B, 2-0.9A, and 2-0.9B Cornell specimens [2] that were described in Chapter 2. The experimental K_1 stiffness is obtained from the observed behavior of the 4-0.9A and 4-0.9B specimens. The f_s is the initial axial force as a fraction of the yield stress. For the f_s = 0.6 specimens the experimental and predicted values are in very close agreement. The predicted value, as expected, is slightly smaller. However, for the f_s = 0.9 specimens there is a larger discrepancy between the two values. Since there was only one test (the 4-0.9A specimen) on which the experimental value is based, the accuracy and reliability of this value are uncertain. However the experimental and predicted values are both close enough to be within acceptable limits.

3.4 Degradation Function for Free Slip Stiffness

The so called "free slip" portion of the stress-strain curve physically corresponds to that low shear stress level portion of loading which in turn induces fairly low normal stresses between the crack planes. In Figure 3.2 the experimental points obtained from the Cornell tests [2] as well as the proposed function are illustrated. As before, the non-dimensional parameter (R_f), which is the ratio of

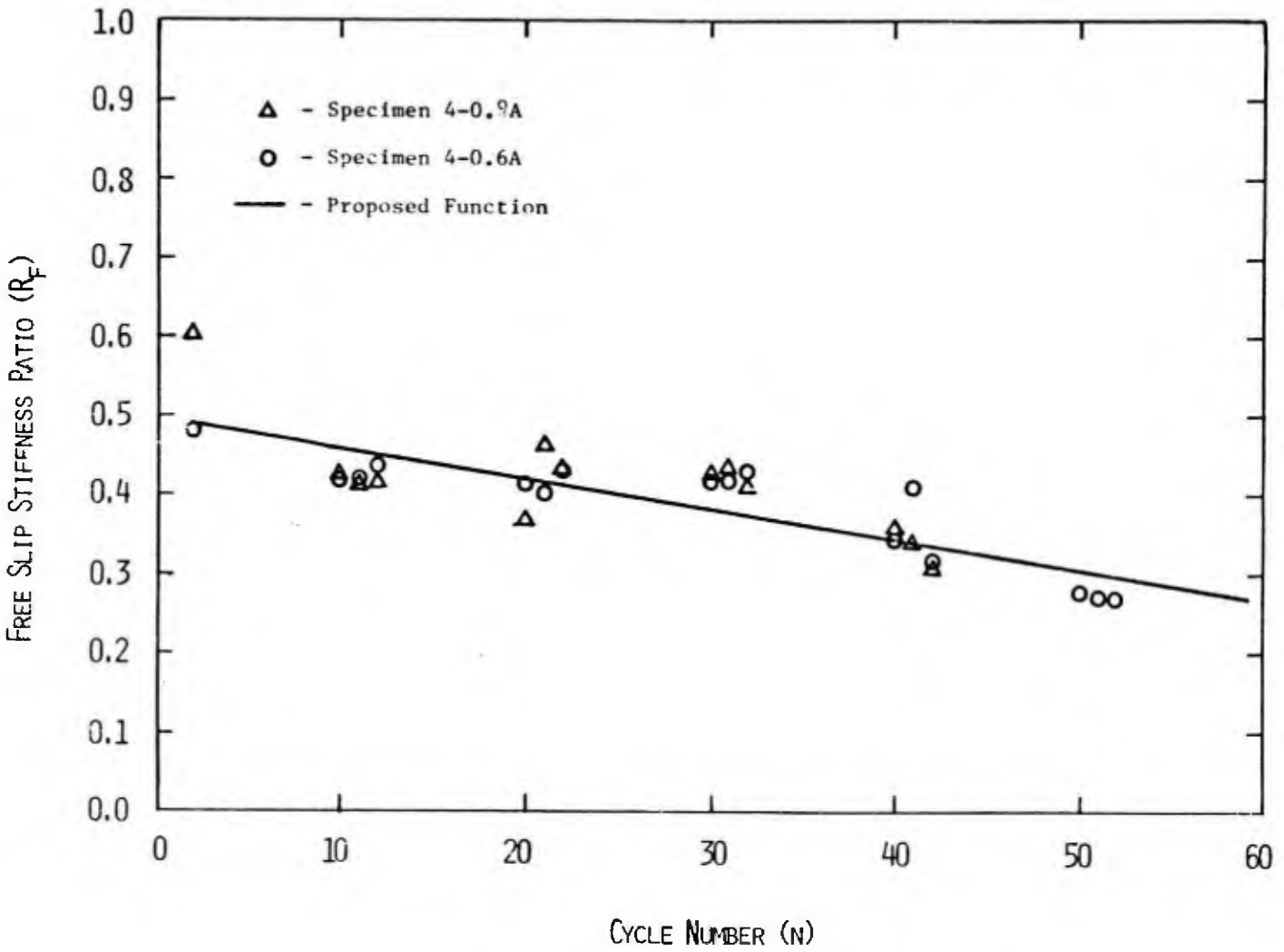

FIGURE 3.2: DEGRADATION FUNCTION FOR FREE SLIP STIFFNESS

the free slip stiffness (K_f) to the first cycle stiffness (K_1) for a given cycle, was selected to study the degradation in this stiffness. The figure illustrates that there is basically a linear decrease of R_f with respect to the cycle number. Therefore, the following function is proposed to describe this behavior:

$$R_f = \frac{K_f}{K_1} = \xi_1 N + \xi_2 \tag{3.3}$$

where:

R_f = free slip stiffness ratio

K_f = free slip stiffness

K_1 = first cycle stiffness

N = cycle number (N=2,3,4 . . .)

ξ_1, ξ_2 = empirical constants

Performing a linear regression analysis gives values of -0.0039 and 0.50 for ξ_1 and ξ_2 respectively.

Observe that the values of R_f for any given cycle are almost always identical for both test specimens. This indicates that the degradation of the free slip stiffness may be independent of both the initial axial tension and the stress amplitudes of the cyclic shear histories. Note also that the line of best fit is almost horizontal indicating that the free slip stiffness does not undergo a considerable amount of degradation and could almost be considered constant. This is physically intuitive since one contribution to this

stiffness is due to the inherent roughness of the concrete crack surfaces. The slightly higher values displayed during the initial cycles of loading are the result of the localized roughness that is present in the initial crack planes. However, these local imperfections do not considerably increase this stiffness and are quickly worn out during the initial cycles of loading.

One other important aspect to note is that at the failure cycle the value of R_f is about 0.3. According to the orthogonal model presented in Chapter Two, the stiffness due to the concrete roughness alone is very small, predicting an R_f value of at most 0.05 at the failure cycle. The free slip stiffness being measured in this model has two components. The first and by far the largest contribution comes from the shear stiffness provided by the diagonal bars as they undergo an axial strain due to the applied shear load. The second, and much smaller contribution, comes from the inherent roughness of the crack faces. The initial shear stiffness provided by the diagonal steel ($K_d = E\rho_d/2$) alone gives a value of $R_f = 0.5$, which is the initial value given by the proposed function. Thus the lower value of R_f at failure is the result of the combined effect of the very slight degradation in the concrete roughness, and the yielding of the diagonal bars. The free slip stiffness in this case is then basically governed by the amount of diagonal steel.

3.5 Degradation of Contact Stiffness

As the specimen deforms under the application of the shear load, the normal stresses between the crack planes increase, thus causing the behavior to become much stiffer. This stiffer behavior displayed at the higher stress levels is referred to as the "contact region". The corresponding stiffness (K_c) is considerably larger than the free slip stiffness displayed at the lower stress levels. The major contributions to this stiffness are provided by the shear stiffness of the diagonal bars as they strain axially due to the shear deformation of the specimen, and the shear transfer interface mode, which is the result of the high frictional forces induced at the orthogonal crack planes as they slide relative to each other. Although the orthogonal reinforcement contributes very little to the overall stiffness in the form of dowel stiffness, its presence is essential to induce the normal stresses that are needed to develop the interface shear transfer mode.

As with the free slip stiffness, a non-dimensional parameter R_c equal to the ratio of the contact stiffness (K_c) to the first cycle stiffness (K_1) for a given cycle, was selected to study the major factors contributing to the degradation process.

As shown in Figure 3.3, the contact stiffness ratio (R_c) is basically a constant for the first twenty cycles, and then gradually decreases with each subsequent cycle of loading. Physically, this indicates that the major degrading mechanism sets in only after about the 20th cycle. Based on this observation the following bilinear

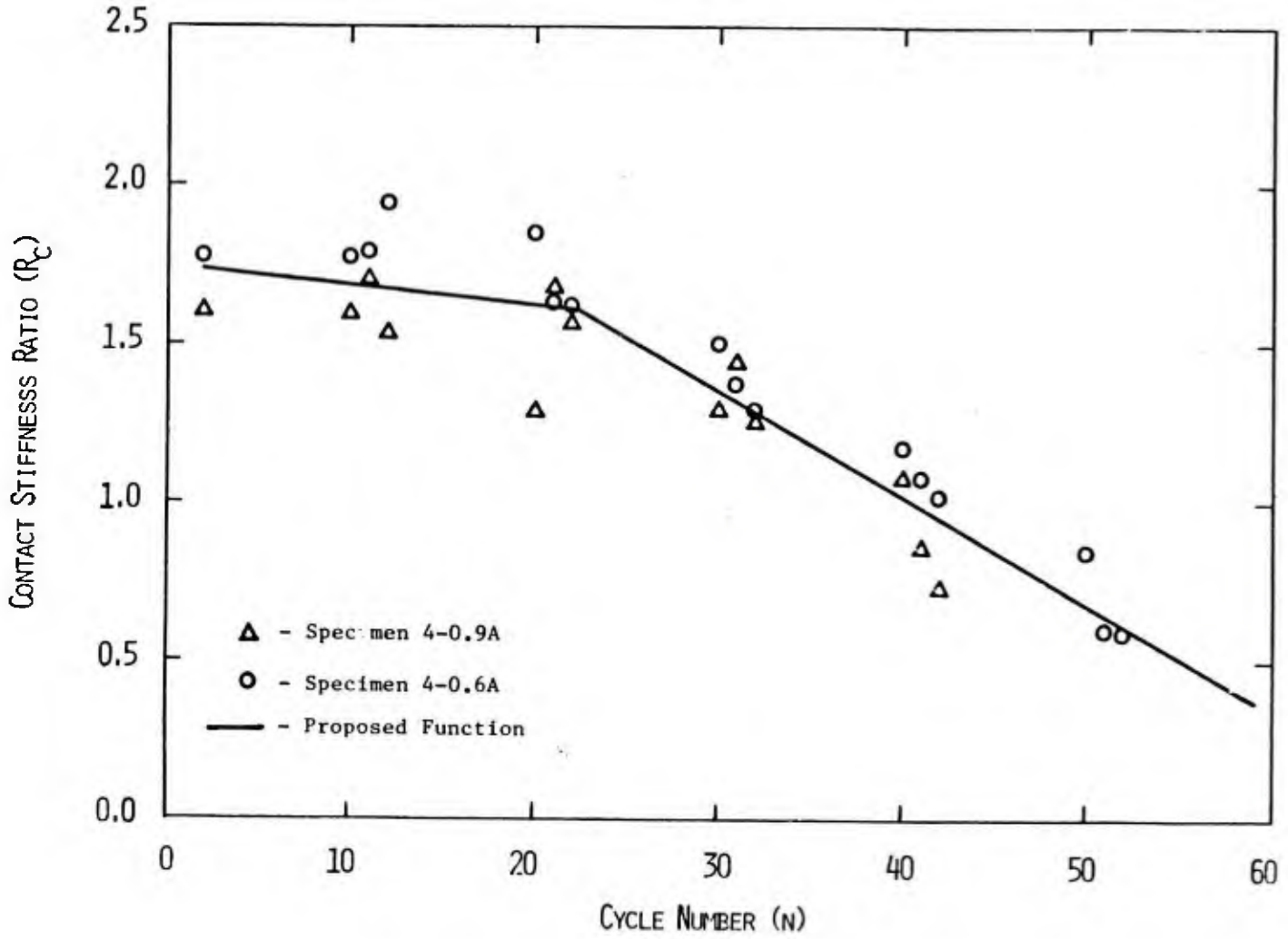

Figure 3.3: Degradation Function for Contact Stiffness

function is proposed to describe this behavior.

$$R_c = \frac{K_c}{K_1} = \xi_3 N + \xi_4 \qquad (3.4)$$

for $2 \leq N \leq 22$

$$R_c = \frac{K_c}{K_1} = \xi_5 N + \xi_6 \qquad (3.5)$$

for $N > 22$

where:

R_c = contact stiffness ratio

K_c = contact stiffness

K_1 = first cycle stiffness

N = cycle number

$\xi_3, \xi_4, \xi_5, \xi_6$ = empirical constants

By performing a linear regression analysis on the experimental points the following values were obtained for the empirical constants:

$$\xi_3 = -0.0060$$

$$\xi_4 = 1.75$$

$$\xi_5 = -0.034$$

$$\xi_6 = 2.38$$

Note that the value of R_c for any given cycle is generally higher for the 4-0.6A specimen than for the 4-0.9A specimen. This indicates that the lower the initial axial tension, the less severe the degradation of the contact stiffness. Such behavior occurs because

the contact stiffness is highly dependent on the concrete-reinforcement bond, and the amount of bond failure increases for increasing values of initial tension. However, since the difference between the experimental results of the two tests is really quite small, the assumption that R_c is relatively independent of the initial axial stress and the stress amplitudes of the cyclic shear load histories is appropriate.

The sharp increase in the degradation process after the 20th cycle is due to various factors. At about this cycle both the orthogonal and diagonal steel may begin to yield, at least in certain regions along the length of the bars. This results in a reduction in the dowel stiffness provided by the bars. However, this is a minor effect since the dowel stiffness only makes a small contribution to the overall stiffness. Another effect of the yielding of the orthogonal steel bars is that it leads to a considerable reduction in the interface shear transfer mechanism, as this mode of shear transfer is highly dependent on the strains occurring in the bars that cross the crack planes. Since the interface shear transfer mode makes a major contribution to the overall stiffness, this reduction is significant in lowering the contact stiffness in the later cycles. Another important cause is the yielding of the diagonal bars. These bars also contribute significantly to the overall stiffness as they resist the shear load through their axial strain. When these effects are coupled with the appearance and propagation of the diagonal cracks it is not surprising that this large reduction of the contact stiffness occurs.

3.6 Evaluation of Unloading Stiffness

The unloading stiffness is not critical to the proper evaluation of the behavior and failure of these wall panels under fully reversing loads. As a result, an infinite stiffness is assumed for the unloading curve. As more experimental data become available it will be possible to define a more sophisticated scheme for this portion of the stress-strain curve.

3.7 Free Slip to Maximum Slip Relationship

In the model the words slip or strain may be used interchangeably. It is through the free slip (δ_f) to maximum slip (δ_m) relationship that the intersection point between the free slip region and the contact region is defined. Note that the free slip corresponds to the current cycle (N), whereas the maximum slip corresponds to the previous cycle (N-1).

As can be seen from Figure 3.4, the ratio of free slip to maximum slip may be adequately modeled by a linear function.

$$\frac{\delta_f}{\delta_m} = \xi_7 N + \xi_8 \qquad (3.6)$$

where:

δ_f = free slip (strain)

δ_m = maximum slip (strain)

N = cycle number

ξ_7, ξ_8 = empirical constants

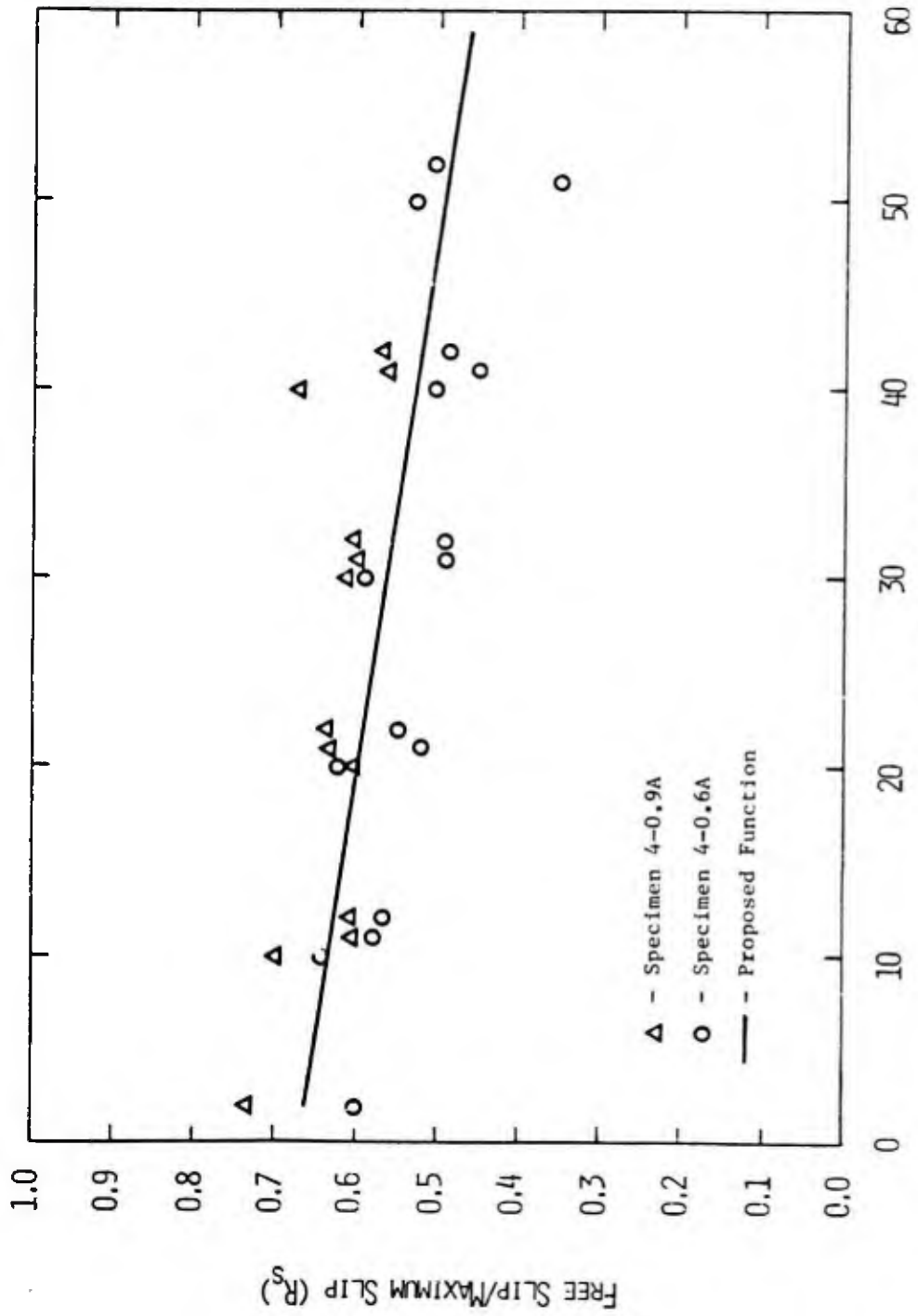

Figure 3.4: Free Slip to Maximum Slip Relationship

The respective best fit linear regression values for ξ_8 and ξ_7 are 0.67 and -0.0035. There is a very slight decrease in this ratio (δ_f/δ_m) with increasing cycle number. The values are consistently higher by a small amount for the 4-0.9A specimen than for the 4-0.6A specimen. Although the ratio of free slip to maximum slip is higher for higher initial axial tensions, the difference is very slight. This difference occurs because the higher the initial axial tension, the larger the initial and subsequent crack widths. This creates a softer system in which more free slip occurs before the contact region of loading is reached.

3.8 Failure Criteria

As with any structural system, failure in these wall panels is due to the cumulative effect of various factors. In this case, as the initial axial load is applied the concrete is cracked into the orthogonal pattern illustrated in Figure 3.1. This causes a load transfer from the concrete to the reinforcement, resulting in an increase in the strains of both the orthogonal and diagonal bars. With the application of the cyclic shear load history, diagonal cracks begin to appear as the concrete undergoes further degradation. Simultaneously, the steel strains also increase. Ultimately, however, it is the eventual yielding of the diagonal reinforcement that finally

causes failure as the specimen loses its load carrying capacity. Thus it is the load level and cycle at which the diagonal steel yields that defines failure. Figure 3.5 shows the average diagonal steel strain for various bars as the 4-0.6A specimen was monotonically loaded up to failure. This is the average steel strain of various bars measured at several points along their lengths. Note that for a given load level there can be considerable variations in strain, not only from one bar to another but also along the length of a given bar. As illustrated in Figure 3.5, by extrapolating beyond the experimental results, the predicted failure shear stress is 366 psi. For the cyclic 4-0.6A test specimen the actual failure stress was 375 psi. Therefore, the proposed failure criteria is consistent with the experimental results.

The first step in providing a quantitative procedure to evaluate failure is the assessment of the steel strains induced in the diagonal bars due to the initial axial tension applied to the orthogonal reinforcement. Theoretically, if a perfect bond existed between the concrete and the reinforcing bars, the following relationship can be developed relating the strains of the orthogonal and diagonal reinforcement (Figure 3.6).

$$\varepsilon_o = \frac{\Delta h}{h} = \frac{2\delta_o}{h} \qquad (3.7)$$

where:

ε_o = strains in orthogonal bars due to initial axial tension

h = initial specimen length or width

δ_o = specimen elongation due to initial axial tension

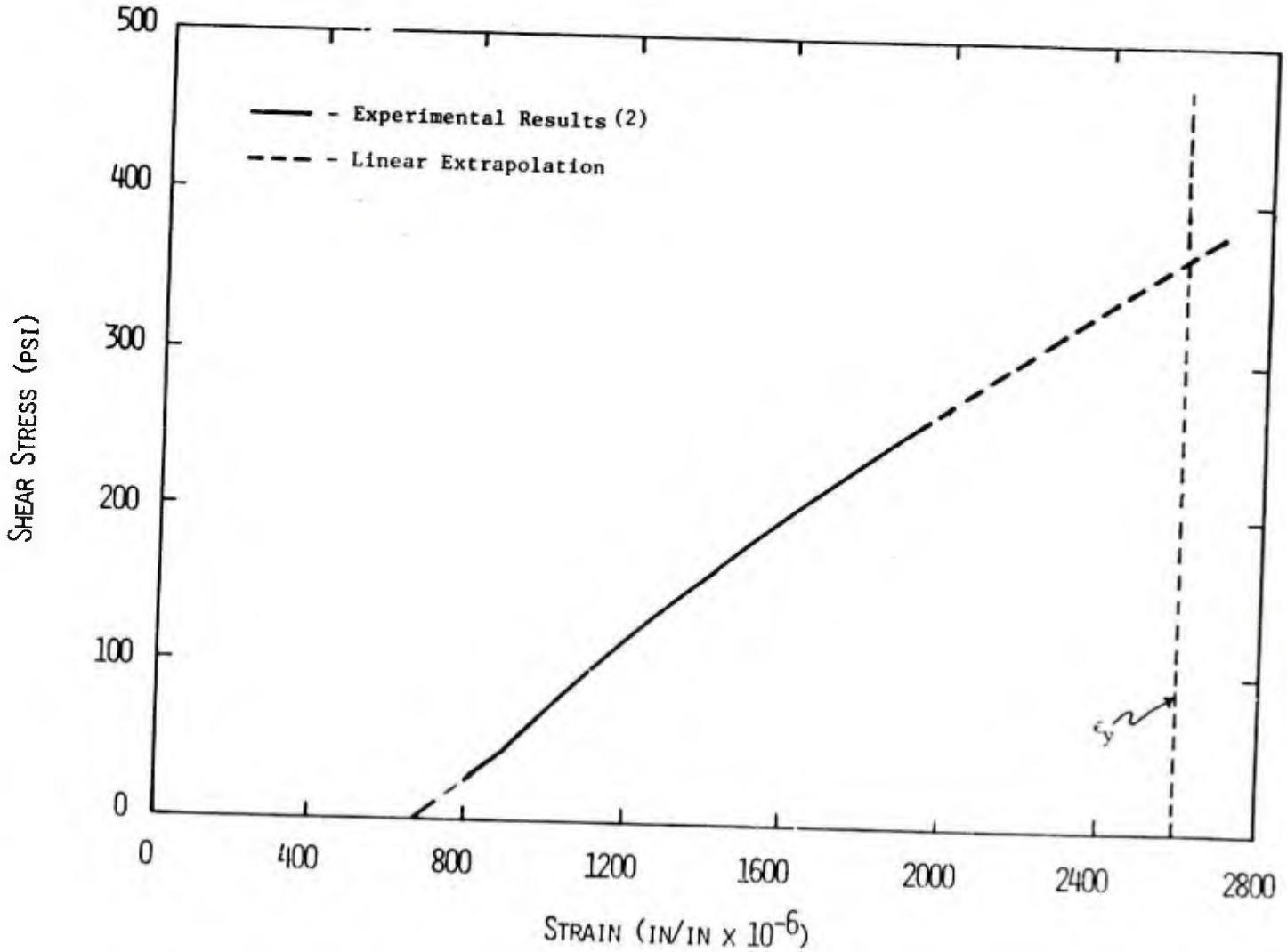

Figure 3.5: Diagonal Steel Strains Under Applied Shear for 4-0.6A Specimen

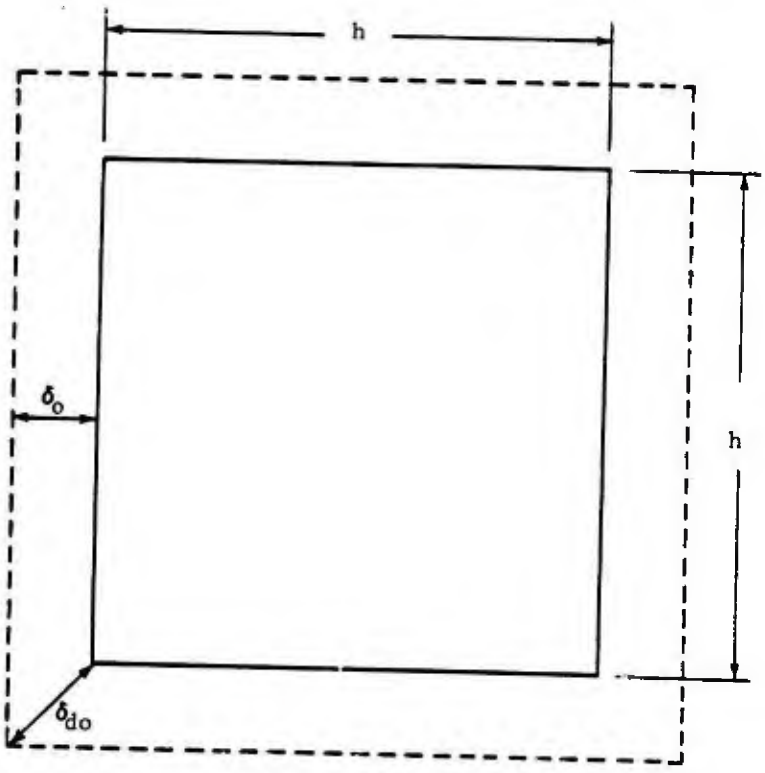

FIGURE 3.6: IDEALIZED SPECIMEN DEFORMATION

$$\varepsilon_{do} = \frac{2\delta_{do}}{h\sqrt{2}} = \frac{2\sqrt{2}\delta_{o}}{h\sqrt{2}} = \frac{2\delta_{o}}{h} \qquad (3.8)$$

where:

ε_{do} = strain in diagonal bars due to initial axial tension

δ_{do} = specimen diagonal elongation due to initial axial tension

Finally, by equating eqs. 3.7 and 3.8

$$\varepsilon_{o} = \varepsilon_{d0} \qquad (3.9)$$

In reality, however, a considerable degree of slip between the reinforcement and the concrete occurs, so the relationship arrived at in eq. 3.9 is not valid. As the orthogonal reinforcement is tensioned a large degree of bond failure occurs. Furthermore, since the diagonal bars are not directly tensioned they undergo considerably lower initial strains than expected. Only for the 4-0.6A specimen were the initial strains measured. Based on this very limited amount of experimental data the following equation is proposed:

$$\varepsilon_{do} = \frac{\varepsilon_{o}}{\xi_{9}} \qquad (3.10)$$

The value of the empirical constant (ξ_9) was found to be 2.5 for the 4-0.6A specimen. This constant is probably dependent on the initial axial tension (f_s). However, since there is no experimental data that allows for some quantitative or even qualitative evaluation on how ξ_9 depends on f_s, the same value is used for all cases.

The next step in defining the failure criteria is to evaluate the additional steel strains induced in the diagonal steel as the cyclic shear load history is applied. The equations which allow the prediction of the specimen shear strain (γ) throughout the loading history have already been established. Since failure is reached when the diagonal bars yield:

$$\gamma_f = \xi_{10}(\varepsilon_y - \varepsilon_{do}) \tag{3.11}$$

where:

γ_f = specimen shear strain at failure

ε_y = yield strain of diagonal reinforcement

ε_{do} = strain in diagonal bars due to initial axial tension

As with the ξ_9 constant, a theoretical value for ξ_{10} can also be obtained. As seen in Figure 3.7, by assuming small deflections and a perfect bond between the diagonal reinforcement and the concrete, the average shear strain may be expressed as:

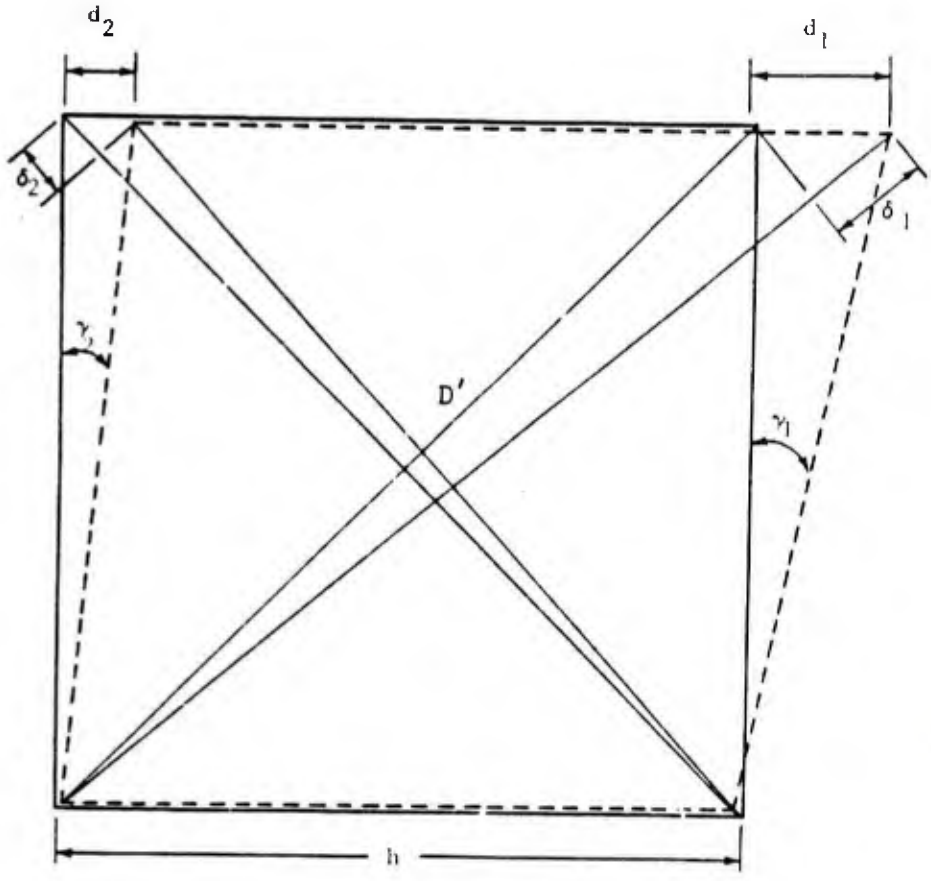

FIGURE 3.7: SPECIMEN SHEAR STRAIN MEASUREMENTS (2)

$$\gamma_{ave} = \frac{(\delta_1 + \delta_2)\sqrt{2}}{2h} \tag{3.12}$$

But,

$$\delta_{ave} = \frac{(\delta_1 + \delta_2)}{2} \tag{3.13}$$

Then,

$$\gamma_{ave} = \frac{\delta_{ave}\sqrt{2}}{h} \tag{3.14}$$

and

$$\varepsilon_{ave} = \frac{\delta_{ave}}{D'} = \frac{\delta_{ave}}{h\sqrt{2}} \tag{3.15}$$

$$\delta_{ave} = \varepsilon_{ave}\, h\sqrt{2} \tag{3.16}$$

Finally, substituting equation 3.16 into 3.17 yields,

$$\gamma_{ave} = \frac{(\varepsilon_{ave} h\sqrt{2})(\sqrt{2})}{h} \tag{3.17}$$

which reduces to,

$$\gamma_{ave} = 2\varepsilon_{ave} \tag{3.18}$$

This means that the steel strain in the diagonal reinforcement (ε_{ave}) should be half the specimen shear strain. So the theoretical value of ξ_{10} is 2. But since some partial bond failure occurs at the concrete-reinforcement interface, this results in a variable value for ξ_{10} which is dependent on the initial axial force applied to the orthogonal reinforcement. The values of ξ_{10} for both the monotonic and cyclic Cornell specimens are given in Table 3.4, where f_s is the initial axial stress applied to the orthogonal reinforcement as a fraction of f_y.

Table 3.4: Empirical Values for ξ_{10}

f_s	ξ_{10}	
	Monotonic	Cyclic
0.3	25.80	----
0.6	33.22	3.60
0.9	25.34	6.37

The final value of ξ_{10} is a function of two competing effects. On one hand, the higher the value of f_s, the larger the initial crack widths. Physically, this translates to a "looser" system leading to higher values of shear strain at failure. The resulting effect is an increasing value of ξ_{10} for increasing values of f_s. On the other hand, the higher the value of f_s, the higher the initial strain in the orthogonal reinforcement. Therefore, the amount of additional strain that the diagonal bars can undergo before they reach yield and the specimen fails is smaller. The effect of this factor is to reduce the value of ξ_{10} for higher values of f_s.

As can be seen from Table 3.5, for the monotonic tests, there is an increase in the value of ξ_{10} as the initial axial tension is increased from $0.3f_y$ to $0.6f_y$. Therefore, for this range of f_s it is the first effect, the loosening due to larger initial cracks, that is the governing factor. However, when f_s is increased to $0.9f_y$, the value of ξ_{10} decreased. At these higher initial stresses it is the second effect that controls. Note, however, that inherent in this entire argument is the assumption that the initial strain induced in the diagonal reinforcement is directly proportional to the initial axial strain of the orthogonal reinforcement. The proportionality constant is assumed to be independent of f_s.

For the cyclic tests the value of ξ_{10} was determined for the two values of f_s corresponding to the two specimens that were tested. For these specimens the value increased when f_s was increased from 0.6 to 0.9, instead of decreasing as in the monotonic tests. This indicates

that for cyclic loading, at least for these values of initial tension, it is the first factor that governs. Also note that for a given value of f_s the monotonic values for ξ_{10} are much higher than the corresponding cyclic values. For f_s=0.6, the monotonic value is actually an order of magnitude higher, and for f_s=0.9 the monotonic value is about four times greater. To explain the cause of this it is necessary to examine the failure stresses and strains for the various specimens listed in Table 3.5.

Table 3.5: Failure Stresses and Strains

f_s	Monotonic		Cyclic	
	Stress (psi)	Strain (rad x 10^{-3})	Stress (psi)	Strain (rad x 10^{-3})
0.3	550	7.74	--	--
0.6	450	19.93	375	7.20
0.9	350	25.34	300	10.60

As expected, the monotonic specimens had a higher shear stress capacity. Since at higher shear stresses the behavior of the concrete is highly non-linear and displays a much lower stiffness, the slightly higher capacity of the monotonic specimens leads to considerably larger shear strains at failure. It is these larger shear strains which result in the much higher values of ξ_{10} for the monotonic specimens.

Since it is the primary intent of this model to evaluate the degradation and ultimate shear strength of these specimens under cyclic shear load histories, the following equation is proposed to evaluate the value of ξ_{10} based on the experimental results of the cyclic tests:

$$\xi_{10} = 9.23(f_s/f_y) - 1.94 \qquad (3.19)$$

where:

ξ_{10} = empirical constant relating specimen shear strains and and axial strain in the diagonal reinforcement

f_s = initial axial stress applied to orthogonal reinforcement

f_y = yield stress of orthogonal reinforcement

With the above equation, the development of the behavioral model is complete. In the next section the implementation of the proposed model is outlined.

3.9 Implementation of Model

A simple computer program was written incorporating all the individual aspects of the proposed model. It allows for the prediction of the entire specimen shear strain history for an arbitrary initial axial force and a cyclic shear load history. The flowchart for this computer program is given in Figure 3.8. The required inputs include: the cyclic shear load history and the material properties of the reinforcement and of the concrete (the

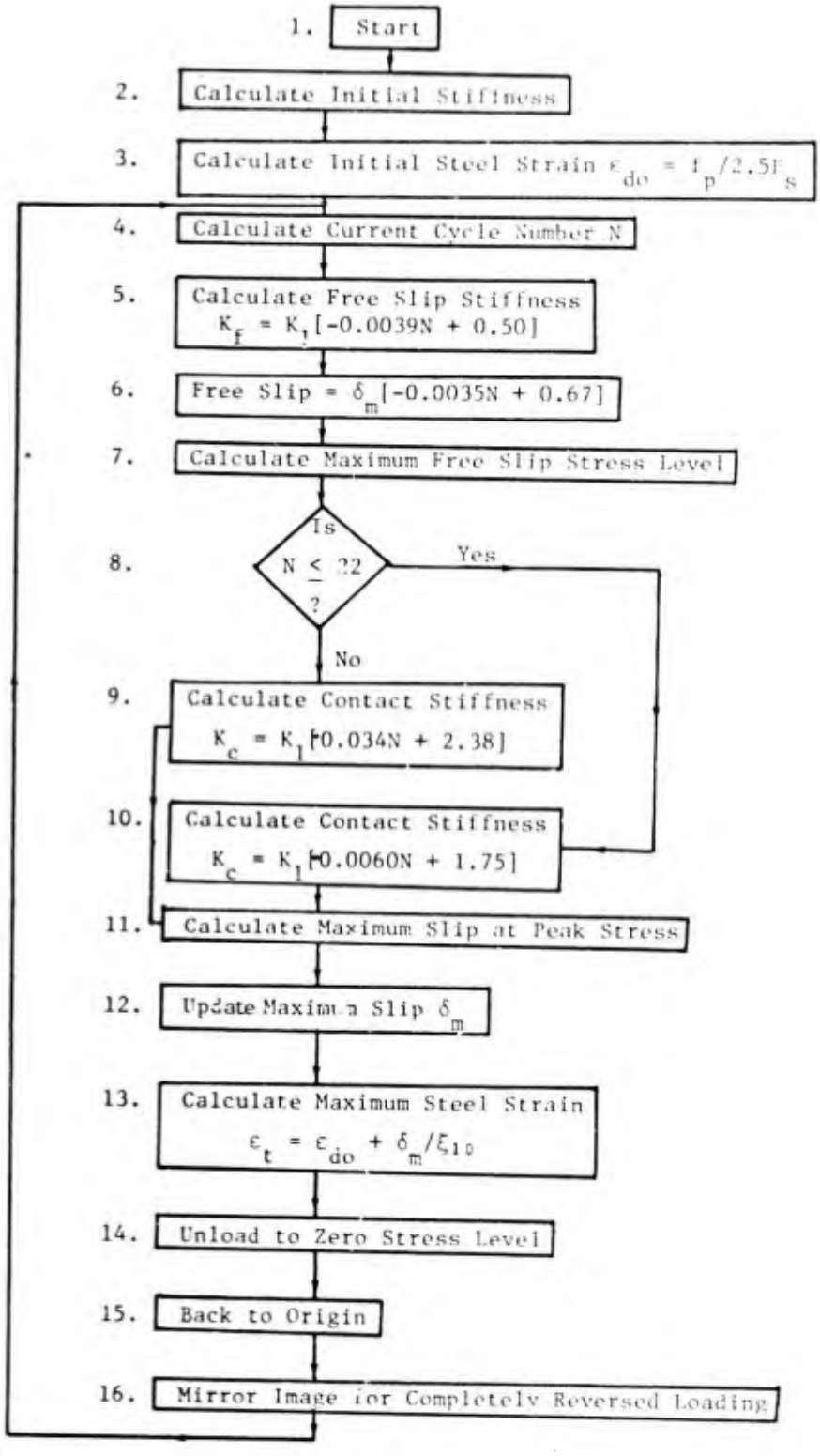

FIGURE 3.8: FLOWCHART FOR ORTHOGONAL + DIAGONAL CYCLIC SHEAR MODEL

program does provide default values).

The first cycle stiffness may be calculated as prescribed in Section 3.3. With these inputs the program generates the entire specimen shear strain history along with the failure cycle number and shear stress. A complete listing of the actual computer program along with a detailed users manual is given in Appendix B. This program serves as the actual numerical tool by which the behavior of orthogonally and diagonally reinforced concrete wall panels under an initial axial tension and a cyclic shear load history may be evaluated. In the following section, the behavior of the two applicable Cornell specimens [2] is simulated.

3.10 Simulation of Behavior of Cornell Specimens

To evaluate the overall consistency of the proposed model, the behavior of the 4-0.6A and 4-0.9A specimens, on which the model was based, was simulated. Unfortunately, at this time further verification of the model is not possible since there are presently no other experimental programs on orthogonally and diagonally reinforced wall panels that have undergone an initial axial tension with a subsequent tangential cyclic shear load history.

3.10.1 Specimen 4-0.6A

The overall geometry and reinforcement ratios as well as the material properties for this specimen were described in detail in Section 3.1. For the first cycle stiffness the experimentally observed value is 109790 psi/rad. The experimental tangential shear history is listed in Table 3.6.

Using these values as inputs into the program, the predicted response is illustrated in Figure 3.9. This figure illustrates the specimen stress- strain history throughout the entire loading history. In Figure 3.10, both the experimental and predicted maximum specimen shear strains achieved during a given cycle are illustrated. Note that the experimental and predicted curves almost coincide identically. The model predicts that the specimen will fail at a stress level of 375 psi on the 52nd cycle of loading. The actual specimen did in fact fail at a stress level of 375 psi, but on the 59th cycle. So the model is very consistent with the experimentally observed behavior.

3.10.2 Specimen 4-0.9A

The particular details regarding the configuration of this specimen have also been described at the beginning of this chapter. The only fundamental difference between this specimen and the previous one is that in this case the initial axial stress applied to the orthogonal reinforcement was $0.9f_y$ instead of $0.6f_y$. This led to an experimentally measured first cycle stiffness of 51941 psi/rad. The

Table 3.6: Cyclic Shear Load History for 4-0.6A Specimen

Cycle Number	Maximum Shear Stress (psi)
1-10	150
11-20	200
21-30	250
31-40	300
41-50	350
51-59	375

Table 3.7: Cyclic Shear Load History for 4-0.9A Specimen

Cycle Number	Maximum Shear Stress (psi)
1-10	125
11-20	175
21-30	225
31-40	275
41-46	300

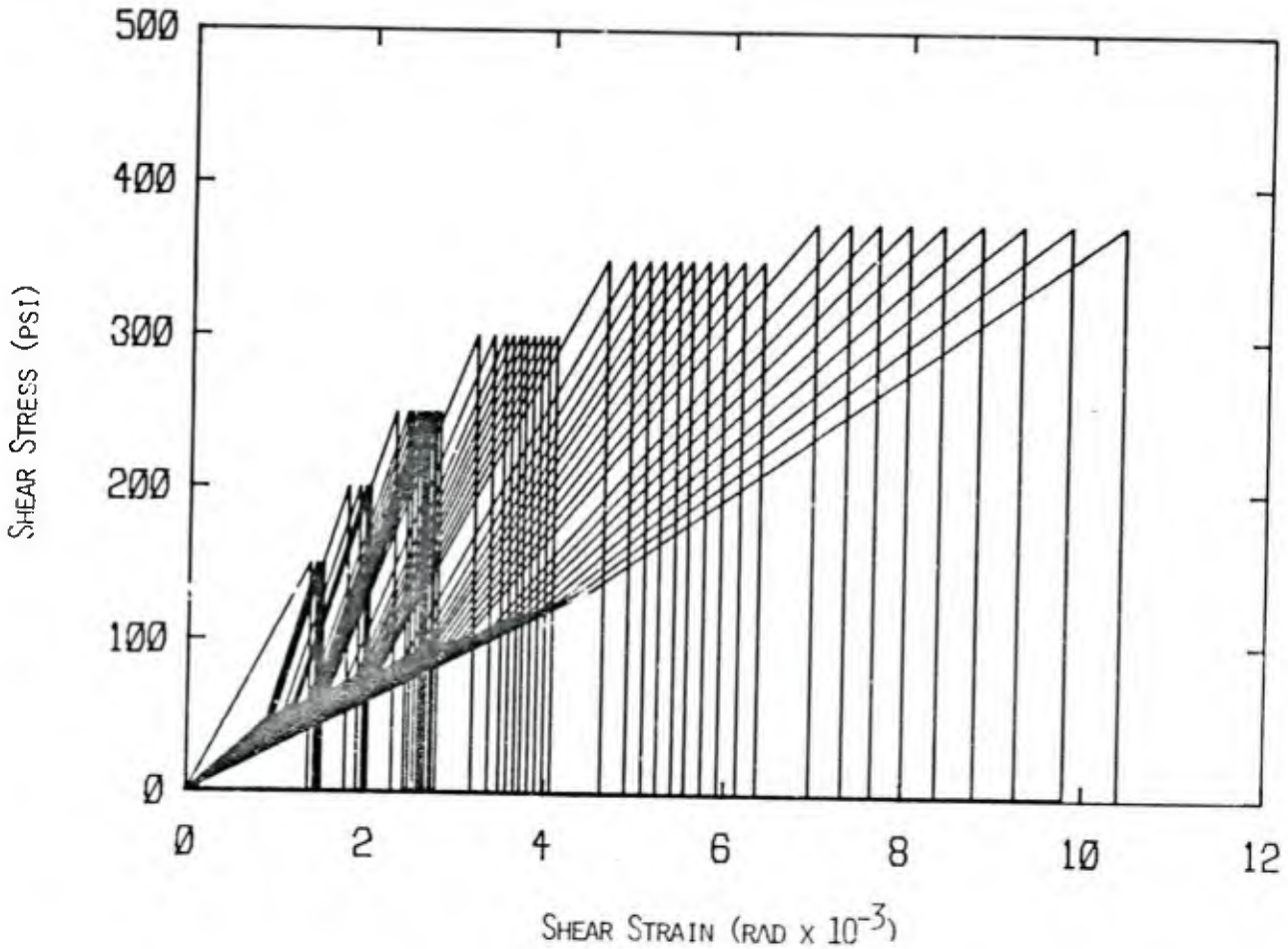

FIGURE 3.9: STRESS-STRAIN HISTORY FOR 4-0.6A SPECIMEN

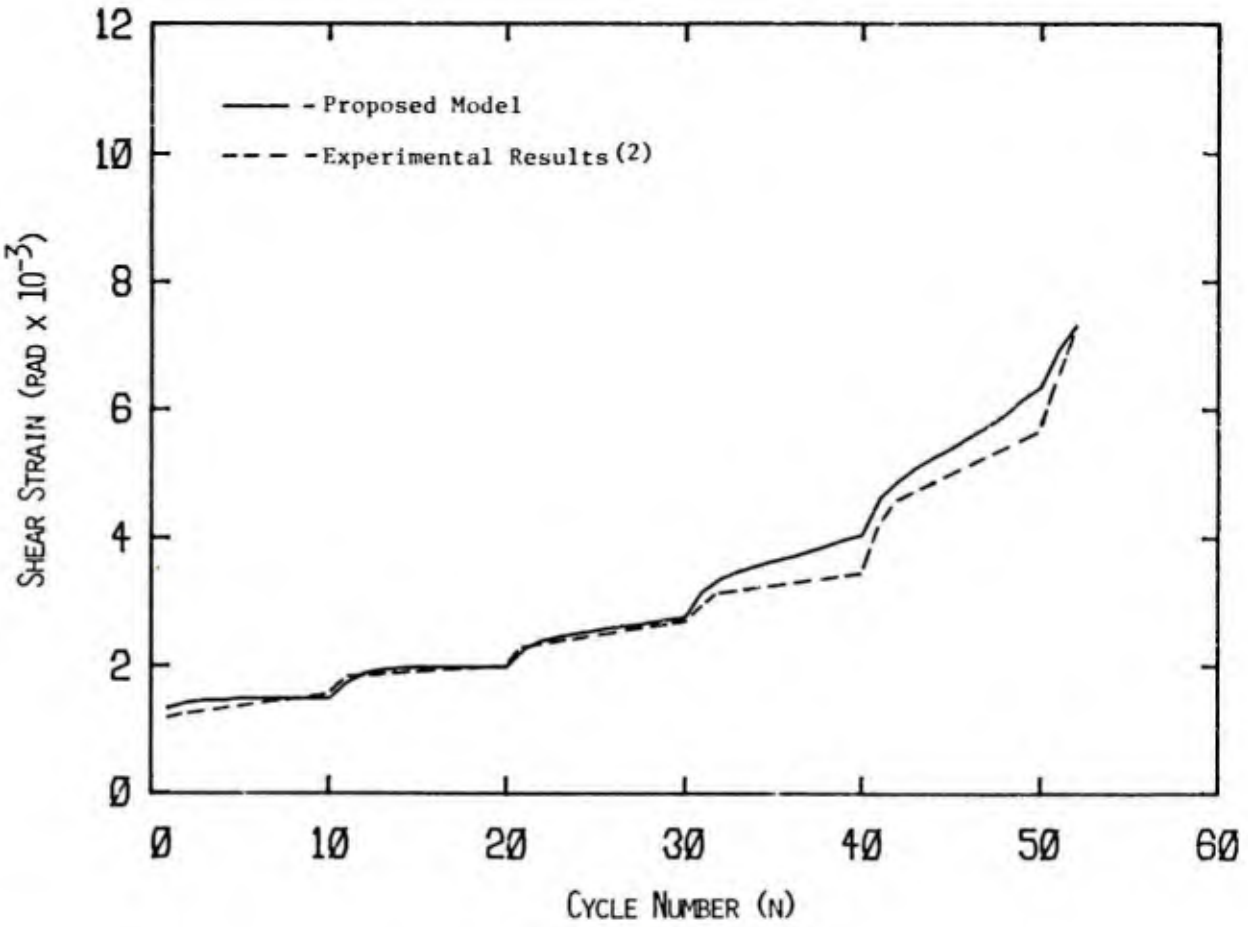

FIGURE 3.10: SHEAR STRAIN VS. CYCLE NUMBER FOR 4-0.6-A SPECIMEN

cyclic shear load history (Table 3.7) was very similar to the one applied to the 4-0.6A specimen.

The resulting predicted specimen shear strain history is shown in Figure 3.11. Comparison with the experimental values (Figure 3.12) indicates that again the model is consistent. This is not surprising, however, since the model was partly based on the results from this test. The model accurately predicts the specimen capacity at 300 psi as was experimentally observed. The actual specimen failed on cycle 46, while the model predicted failure on cycle 47. This slight difference is insignificant.

The simulation of these two specimens serves to indicate that the proposed model is consistent, both in the prediction of the specimen shear strain history and in the stress level and cycle number corresponding to failure, with the experimental data base upon which it was derived and calibrated.

Also note the stiffening behavior that occurred in both specimens (Figures 3.10 and 3.12) during the cycles where the applied shear stress was increased. This behavior, which was also observed in the orthogonally reinforced specimens, is due to the increase in normal stresses that are induced as a result of the higher shear stresses. This in turn leads to higher resistive frictional stresses which must be overcome for the specimen to deform further. The net result is the stiffer behavior.

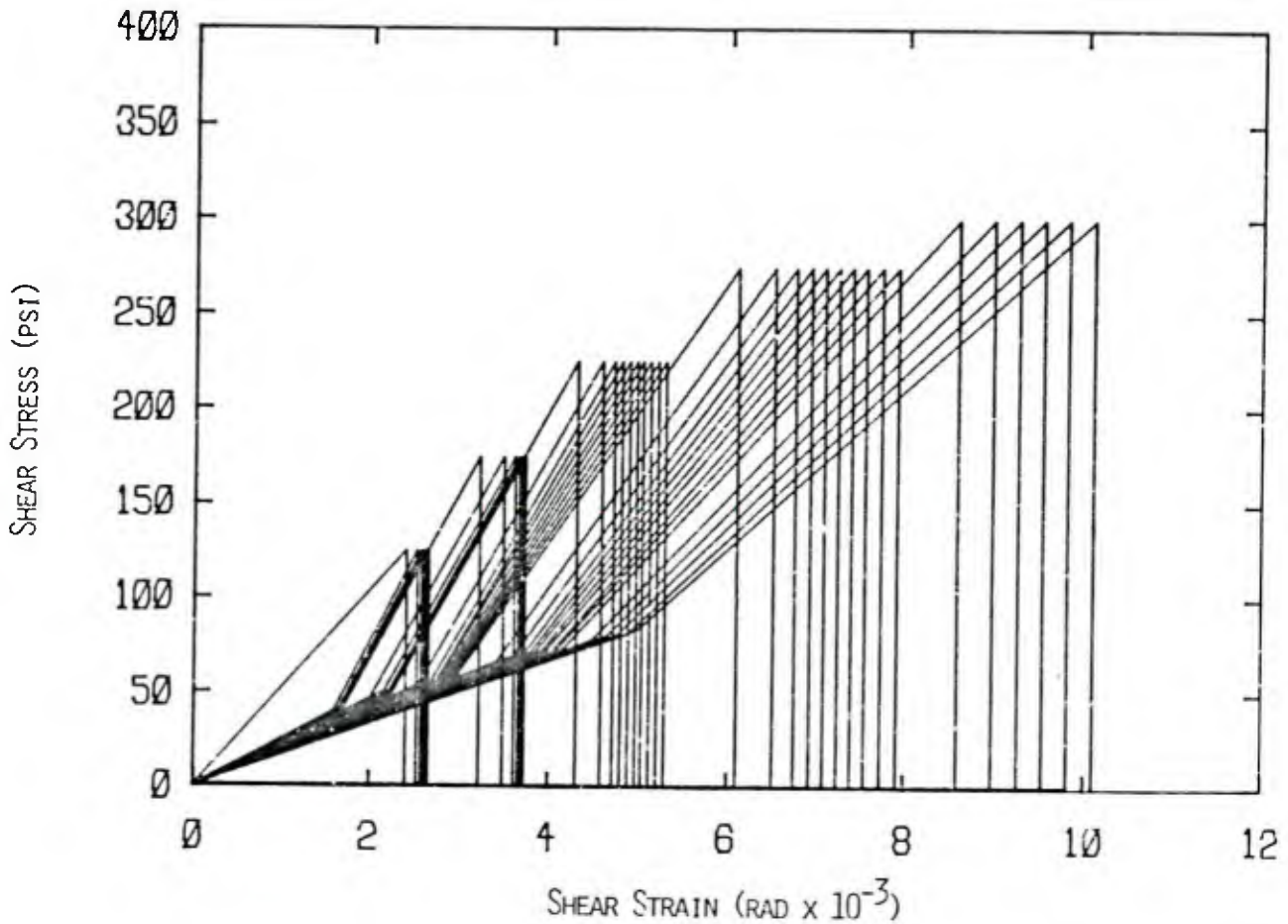

FIGURE 3.11: STRESS-STRAIN HISTORY FOR 4-0.9A SPECIMEN

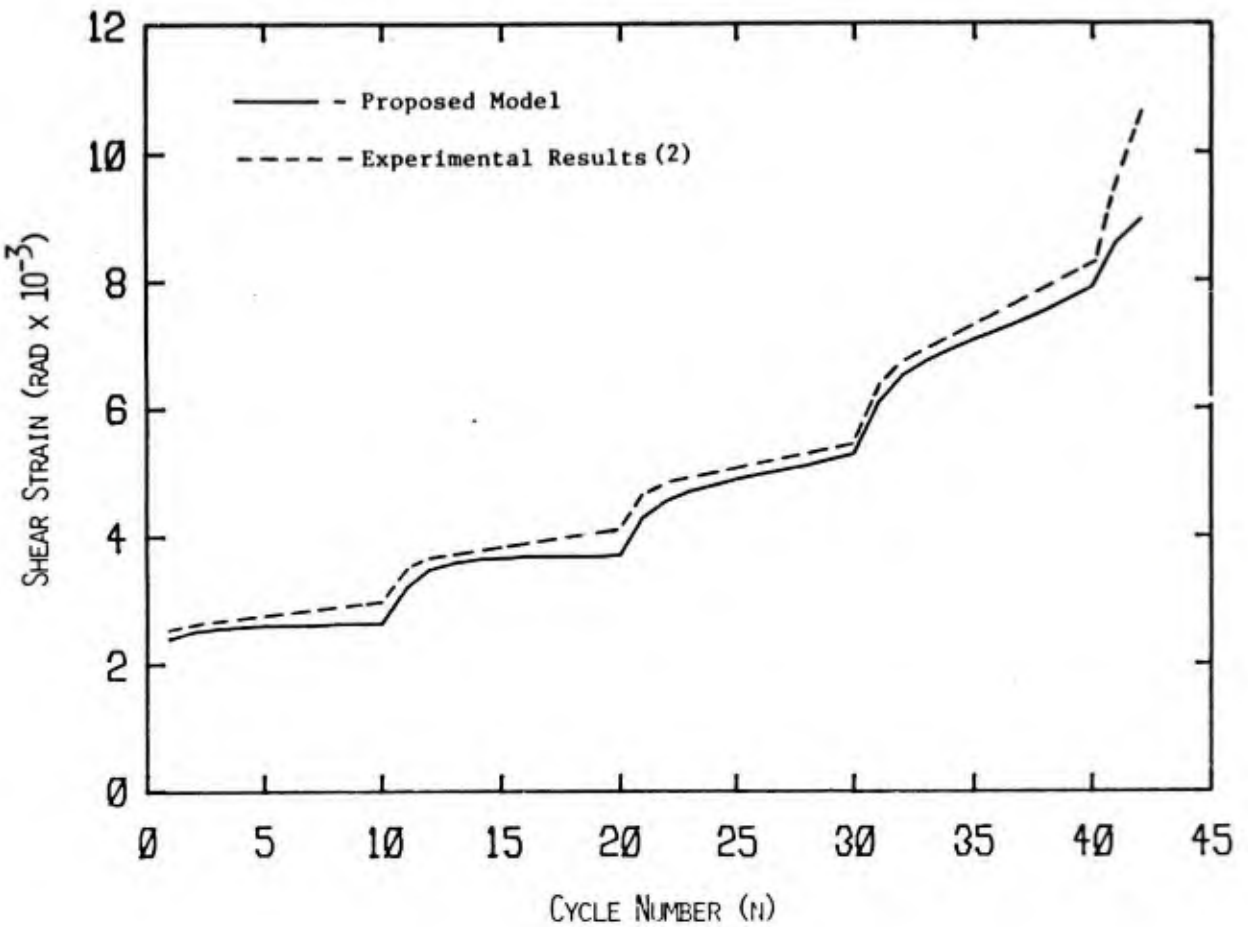

Figure 3.12: Shear Strain vs. Cycle Number for 4-0.9-A Specimen

3.11 Additional Simulations of the Experimental Specimens

Since the proposed model has been shown to predict the behavior of the two Cornell specimens having both orthogonal and diagonal reinforcement, it is possible to use this model to further simulate the behavior of these panels under other cyclic loading histories. It will then be possible to assess the true conservative strength of these panels. To do this the specimens were loaded with a series of consistent load histories. Consistent load histories are those having: the same number of cycles of loading at each stress amplitude, the same number of steps or levels of stress amplitude, and approximately the same number of cycles to failure as the original experimental cyclic shear load history. The experimental initial stiffness and material properties used in the original simulations of the specimens were also used in these further simulations.

Specimen 4-0.6A was loaded with a total of five of these consistent load histories. The specific inputs into the program are shown in Figure B.3 (Appendix B). In Table 3.9 the results of the experimental load history along with the five additional histories are presented. Recall that under the experimental load history the specimen failed at a shear stress of 375 psi on the 59th cycle. Observe that under the fifth load history the specimen failed at a shear stress of 250 psi on the 60th cycle. This represents a 33% reduction of shear strength over the experimentally predicted capacity.

Table 3.8: Results for Simulated Behavior for 4-0.6A Specimen

Load History	Failure	
	Stress (psi)	Cycle
Cornell	375	59
1	350	59
2	320	56
3	300	57
4	280	58
5	250	60

Table 3.9: Results for Simulated Behavior for 4-0.9A Specimen

Load History	Failure	
	Stress (psi)	Cycle
Cornell	300	46
6	275	50
7	270	50
8	275	50

The 4-0.9A specimen, which also had diagonal reinforcement in addition to orthogonal reinforcement, was also loaded with a series of consistent load histories (Figure B.3) whose results are presented in Table 3.9. Note that for this specimen the maximum shear stress reduction when compared to the experimental value was obtained by load history No. 7. The failure of the specimens on the 50th cycle at a shear stress of 270 psi represents a 10% reduction from the predicted strength.

These simulated reductions in strength are significant for various reasons. The applied load histories are at least as significant as the experimental load histories in simulating an actual seismic input since they both have the same basic characteristics. And since any proposed analysis and design procedure must rely on a lower bound measure of the experimental results it is important to ascertain if these results are truly conservative for any possible loading history imposed on the structure. These further simulations have indicated that reductions of up to 33% of the experimentally obtained values would be a more truly conservative measure of the actual strength.

3.12 Simplified Approach for Evaluation of Ultimate Strength

The behavioral model and the present state of the art regarding the ultimate shear strength of concrete wall panels having both orthogonal and diagonal reinforcement is based on the experimental results of only two panels, the 4-0.6A and 4-0.9A Cornell specimens [2]. This obviously does not provide for a high level of confidence

in the experimental or predicted behavior. On the other hand, the behavior of the panels having only orthogonal reinforcement counts with a broader experimental data base. Therefore both the observed and predicted strengths are much more accurate and reliable.

In light of this the following procedure is proposed to evaluate more realistically and conservatively the behavior of the specimens having both orthogonal and diagonal reinforcement. Using the principle of superposition, the ultimate strength of these specimens may be calculated by merely adding the strength provided by an equivalent orthogonally reinforced specimen to the additional strength provided by the diagonal reinforcement. Therefore, the total strength of the specimen may be expressed as:

$$V_p = V_o + V_d \tag{3.20}$$

where:

$$V_d = \rho_d f_{yd}(1 - f_{yd}/f_d) \tag{3.21}$$

$$f_d = \frac{f_s}{2.5} \tag{3.22}$$

where:

V_p = proposed shear strength of specimen having both orthogonal and diagonal reinforcment

V_o = experimental shear strength of specimen having only orthogonal reinforcement

V_d = additional shear strength provided by diagonal reinforcement

ρ_d = steel ratio of diagonal reinforcement alone, measured in in the diagonal (45°) direction

f_{yd} = yield stress of diagonal reinforcement

f_d = initial axial stress induced in diagonal reinforcement by axial tension applied to orthogonal reinforcement

The equation for the contribution of the diagonal reinforcement (Equation 3.21) is simply the static equilibrium condition along a diagonal crack. The accuracy of this procedure may be verified using the available Cornell experimental results. The strengths for various specimens having only orthogonal reinforcement and under various initial axial tensions is known. These are the experimental values for V_o. Since the material properties for the diagonal reinforcement are known, the V_d values may be easily calculated. These two values may then be summed to obtain V_p. This predicted value of the specimen shear strength may be compared with the experimental strength (V_u) of the specimens having both orthogonal and diagonal reinforcement. This procedure was followed for the available specimens, and as can be seen in Table 3.10, the experimental (V_u) and predicted strength (V_p) are very close. The largest difference between the two values is only 11%. Note that for the monotonic tests the proposed procedure is generally conservative. However, for the cyclic tests this procedure is always unconservative by around 10%. This possibly results from the use of the empirical constant in calculating f_s. However, this proposed procedure for evaluating the ultimate strength of specimens

Table 3.10: Experimental and Predicted Ultimate Strengths

for Orthogonally and Diagonally Reinforced Specimens

Orthogonal		Orthogonal + Diagonal		Proposed Diagonal		% Difference
Specimen	V_o (psi)	Specimen	Vu (psi)	V_d (psi)	$V_p = V_o + V_d$ (psi)	V_u vs. V_p
2-0.0-M	375	4-0.0-M	550	208	583	6%
2-0.6-M	250	4-0.6-M	450	158	408	9%
2-0.9-M	190	4-0.9-M	350	133	323	8%
2-0.6-A	250	4-0.6-A	375	158	408	9%
2-0.6-B	250	4-0.6-A	375	158	408	9%
2-0.9-A	200	4-0,9-A	300	133	333	11%
2-0.9-B	200	4-0.9-A	300	133	333	11%

Notes: M - monotonic loading
A,B - cyclic loadings
f_{yd} = 67 ksi

having both orthogonal and diagonal reinforcement is quite accurate overall.

3.13 Summary and Conclusions

The model developed in this chapter serves two purposes. First, it serves as the numerical tool for quantifying the various aspects of the behavior of these wall panels. Second, it is now possible to make the following qualitative observations.

(a) The first cycle stiffness may be appropriately evaluated by superimposing the stiffness of an equivalent orthogonally reinforced panel to the axial stiffness provided by the diagonal reinforcement.

(b) The stress-strain history for all cycles of loading beyond the first may be appropriately modeled using a bilinear curve. The transition zone between the low and high stiffness regions is much smoother and less well-defined than it was for the specimens having only orthogonal reinforcement.

(c) The "free slip" stiffness does not undergo a major amount of degradation as the cyclic shear load is applied. The major contribution to this stiffness comes from the diagonal reinforcement in the form of axial straining in response to the applied shear load.

(d) The "contact" stiffness undergoes only negligible degradation for about the first twenty cycles of loading. However, during the subsequent cycles this stiffness degrades considerably. This latter degradation is probably due to extensive yielding that occurs in the reinforcement, combined with the increasing number and propagation of diagonal cracks that appear in the concrete.

(e) The degradation of both the "free slip" and "contact" stiffnesses is fairly independent of both the initial axial tension applied to the orthogonal reinforcement and the stress amplitudes of the cyclic shear load histories. The major factor in determining the level of degradation is the number of cycles of loading.

(f) The failure criteria of yielding of the diagonal reinforcement seems reasonable not only because this is what was experimentally observed but also because the resulting model based on this premise of failure yields consistent results in terms of specimen shear capacities and the failure cycle number.

(g) The experimental shear strengths of these panels may be reduced by up to 33% by applying other consistent cyclic shear load histories.

The proposed model provides some insight into the basic characteristics of the behavior of these types of panels. It also predicts the behavior of the two Cornell specimens. This is to be expected, since the model was based on the experimental results of these two wall panels. Yet it must be pointed out that since the proposed model identifies the key parameters, it could just as well predict the behavior of other panels. The experimental and predicted results might not be in as close agreement as for the two Cornell tests, but the predicted results would probably still be within acceptable limits. This issue will only be answered as more experimental data become available. Then it will be possible to validate and further calibrate the proposed model to predict the behavior of an actual nuclear containment wall panel.

CHAPTER 4

ANALYSIS AND DESIGN CRITERIA FOR NUCLEAR CONTAINMENT STRUCTURES

4.1 Introduction

In the previous two chapters an in-depth evaluation of the latest experimental results from the testing of containment wall specimens was made. Based on this assessment the currently prescribed analysis and design procedures are reviewed in this Chapter. and the results obtained are utilized to formulate a more realistic and accurate analysis and design procedure.

In the first part of this Chapter the experimental program on which the current ASME Pressure Vessel and Boiler Code [5] provisions are based is briefly reviewed. Next, a description of the provisions of this Code is given. In the second part of this chapter a new analysis and design procedure is proposed. It is based on the latest series of results and analyses presented in the previous two chapters. Finally, a design example for an actual containment structure is performed and the results compared with those of the current design

provisions.

4.2 ASME Pressure Vessel and Boiler Code Provisions

This Code currently governs the design of nuclear containment vessels under combined internal pressure and seismic loads. In order to evaluate the provisions that are prescribed in this Code, it is first necessary to examine the experimental program upon which they are based.

4.2.1 White and Holley Study [9]

This experimental study represents one of the first programs undertaken to make a quantitative evaluation of the amount of membrane shear stress that may be transferred along the crack planes of reinforced concrete panels. The main source of shear resistance of these cracked panels comes from the interface shear transfer mode which is due to the frictional resistance that develops between the crack planes.

In this program a total of 16 specimens were tested. The overall geometry and external reinforcement rods are shown in Figure 4.1. The effective cross sectional area of each specimen was 280 in^2 for the first six specimens and 240 in^2 for the last ten specimens. The loading consisted of fully reversing shear in the range of 120 to 160 psi for a maximum of 55 cycles and subsequently to a terminal shear stress of up to 300 psi. The three parameters that were measured include: the slip along the crack plane, the change in crack width during the shear loading, and the magnitude of the clamping force in

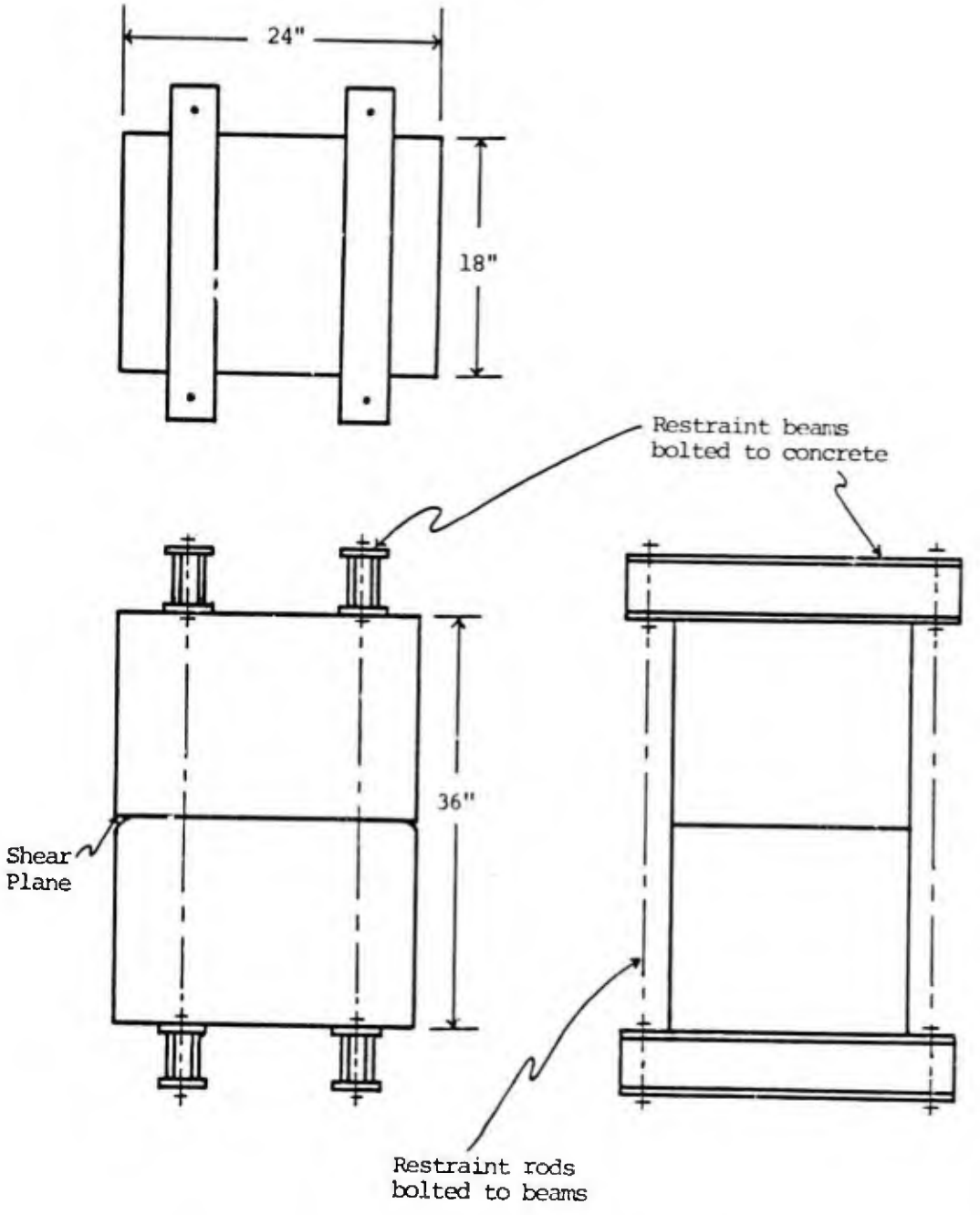

FIGURE 4.1: TEST SPECIMEN GEOMETRY (9)

the external rods which served as reinforcement. Based on the results from these tests the experimenters observed the following characteristics of the behavior.

(a) Both the amount of slip and crack width increased due to the applied cyclic shear load.

(b) Generally, the amount of force induced in the clamping rods was fairly low, ranging from around 30 to 50% of the applied cyclic shear stress.

(c) All the specimens are believed to have a higher shear capacity than measured in the experiments.

(d) For most of the specimens the increase in crack width after 25 cycles of loading was less than or equal to 0.010 in.

(e) The major damage to the shear surface occurred during the final load application up to a high shear stress level and not during the normal cyclic loading.

(f) There was always a residual slip even after the specimens were fully unloaded to a zero shear stress level.

(g) The larger the aggregate size the smaller the amount of slip that occurred at an equivalent load.

(h) The slip decreased with increasing size of the clamping rods.

(i) The smaller the initial crack width the less amount of slip that occurred.

(j) The specimens having a variable crack width throughout the crack plane underwent less slip than those specimens having a uniform crack width. However, both types of specimens degraded in the same fashion regardless of the uniformity of the initial crack width.

(k) The specimens usually exhibited the same characteristic load-slip curve during all cyles, with an unloading stiffness much higher than the loading stiffness.

(l) Even though the specimens were loaded through complex load histories, it was found that there was great symmetry between the magnitude of positive and negative slips.

Based on these observations and the numerical results obtained, the following recommendations were made for design. A unit shear stress function, which is just the shear strength, as a function of the clamping steel ratio (ρ) as illustrated in Figure 4.2 was proposed. Also note that a bar clamping capacity of 1.5 times the applied shear must be provided in both the x and y directions to guarantee that the minimum clamping capacity along a plane in any arbitrary direction will be at least 1.0 times the shear that is to be transmitted along that plane. How these functions are to be converted into a detailed design procedure is discussed in detail in the next section.

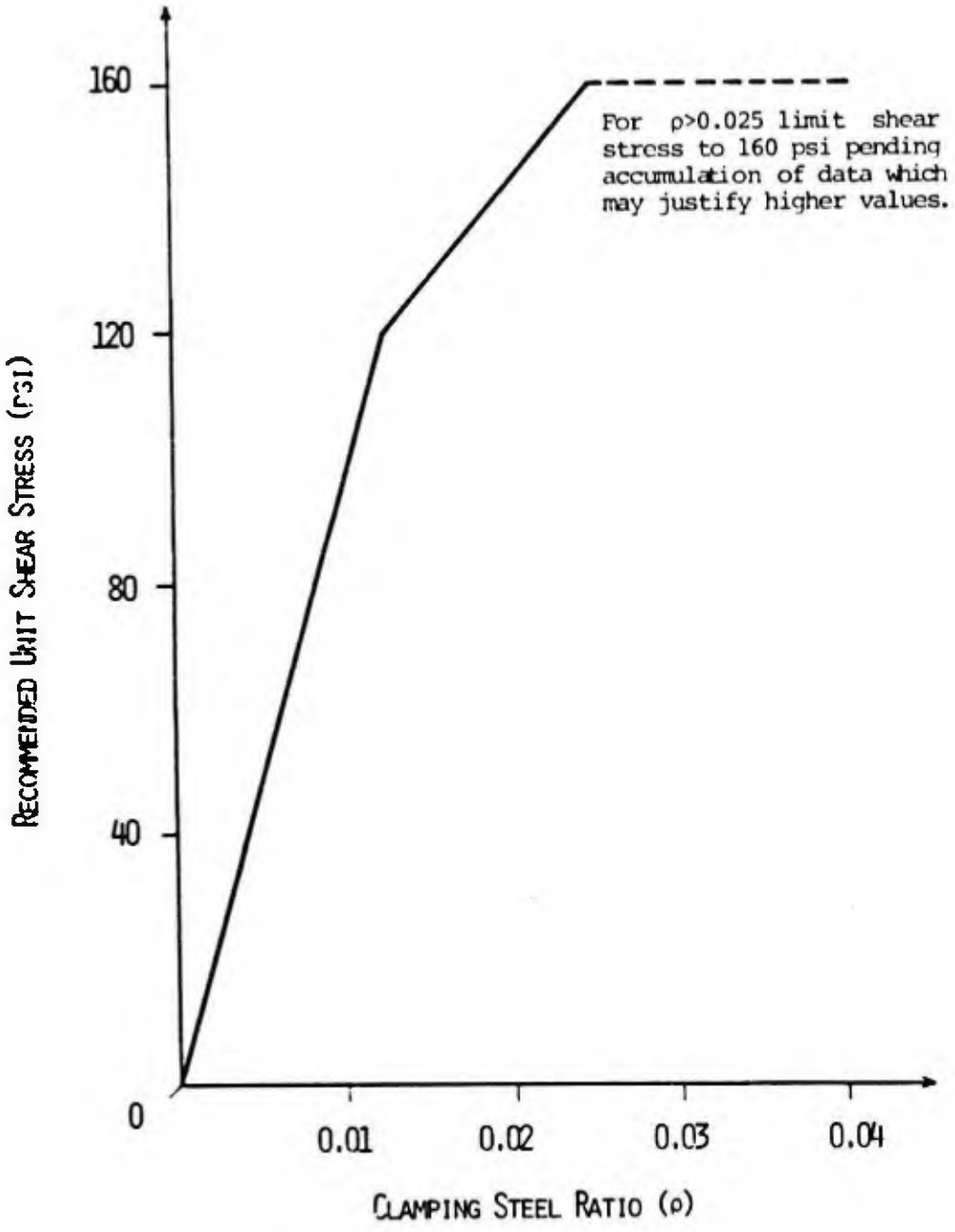

FIGURE 4.2: RECOMMENDED UNIT SHEAR STRESS (9)

The White and Holley study laid the foundation to quantitatively define the amount of shear force that may be transmitted along the crack faces. However, their program also had various limitations. First, the specimens tested were small scale (18" x 24" x 36"), so extrapolation of the results to large scale cracked panels which make up the actual containment vessel may not be entirely valid. Second, the reinforcement in these specimens, which consisted of restraint rods, was placed outside instead of being embedded inside the concrete. Because of this, the contribution of the reinforcing bars through their dowel stiffness was neglected. Also, the bond failure and concrete crushing that was induced at the concrete-reinforcement interface was not incorporated. The selection of 160 psi as the maximum allowable shear stress is quite arbitrary except for the fact that it might guarantee small displacements. This fact has been borne out by the recent experimental studies [2,6] in which shear stresses of up to 485 psi were developed in initially cracked wall panels. Furthermore, the only parameter considered in the proposed function is the clamping ratio which corresponds to the reinforcement ratio of the actual panels. The effect of all the other parameters is neglected by the proposed function. These include: the material properties of both the steel and the concrete, the initial axial tension in the reinforcement, the steel ratio, and the number of cycles of loading. Furthermore, the reinforcement used in the experiments was placed perpendicular to the crack plane. This would correspond to the orthogonal reinforcement in the actual containment panel. The effect of diagonal reinforcement was not studied. The specimens tested

initially had only one horizontal crack. The actual containment panel and the panels tested in the recent Cornell and PCA tests include an orthogonal crack pattern.

4.2.2 ASME Pressure Vessel and Boiler Code [5]

The following provisions are those prescribed by the Code for the designing of reinforced concrete vessels under an internal pressure and a tangential shear resulting from an earthquake. The resultant membrane forces on a typical panel from the wall of a nuclear containment are illustrated in Figure 4.3.

The pertinent sections of this Code, Sections CC-3421.5 and CC-3521.1.1, govern the design for meridian, hoop, and inclined reinforcing for the required membrane forces. The tangential shear stress that may be taken up by the concrete is:

$$V_c = 12000\rho \qquad \text{for } \rho \leq 0.01 \tag{4.1}$$

$$V_c = 93 + 2700\rho \leq 160 \text{ psi} \qquad \text{for } 0.01 < \rho \leq 0.25 \tag{4.2}$$

where:

ρ = lesser of the reinforcement ratios in the meridional and circumferential directions

V_c = maximum tangential shear stress that may be carried by the concrete (psi)

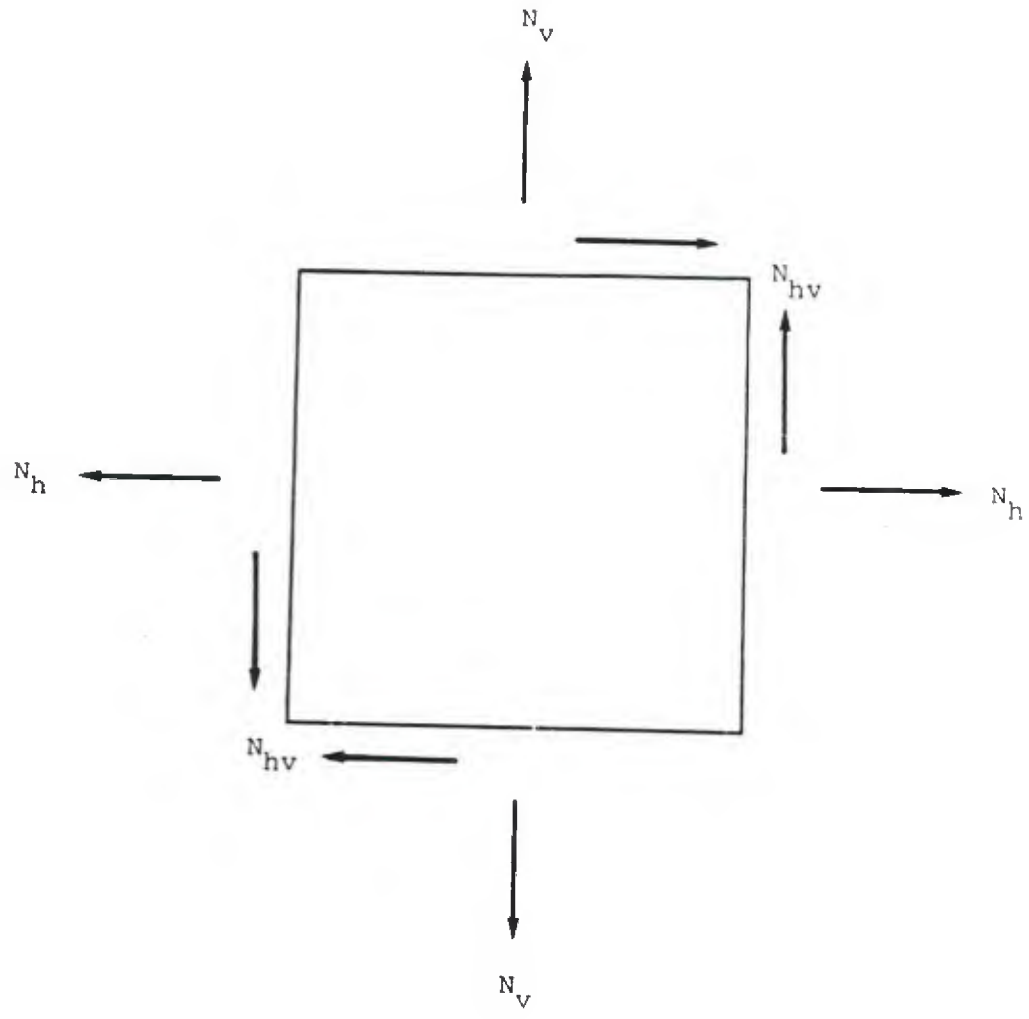

FIGURE 4.3: MEMBRANE STRESSES FOR NUCLEAR CONTAINMENT PANEL

In order to calculate the required reinforcement areas, two cases must be considered.

Case 1: $N_{hv} \leq N_{hv}^{c}$ (applied shear less than concrete capacity)

In this case inclined reinforcing is not required and the horizontal and vertical reinforcement areas are to be proportioned as follows:

$$A_{sh} = \frac{N_h + N_{hv}}{0.9f_y} \tag{4.3}$$

$$A_{sv} = \frac{N_v + N_{hv}}{0.9f_y} \tag{4.4}$$

Case 2: $N_{hv} > N_{hv}^{c}$ (applied shear greater than concrete capacity)

In this case in addition to the horizontal and vertical areas as calculated for Case 1, the Code requires that diagonal reinforcement (at 45°) be placed in both directions to take up the excess shear. The area of the diagonal reinforcement is calculated as:

$$A_{si} = \frac{N_{hv} - N_{hv}^{c}}{0.9f_y} \tag{4.5}$$

where:

A_{sh} = area of reinforcing steel in the horizontal direction (in^2/ft).

A_{sv} = area of reinforcing steel in the vertical direction (in^2/ft).

A_{si} = area of reinforcing steel in the inclined direction (in^2/ft).

N_h = total membrane stress resultant in the horizontal direction at the section under consideration (K/ft). The component from earthquake loading is based on the square root of the sum of the squares of the components of the two horizontal and vertical earthquakes and is always positive.

N_v = total membrane stress resultant in the vertical direction at the section under consideration (K/ft). The component from earthquake loading is based on the square root of the sum of the squares of the components of the two horizontal and vertical earthquakes and is always positive.

N_{hv} = the maximum tangential shear resultant at the section under consideration (always positive, K/ft).

N_{hv}^{c} = the tangential shear force carried by concrete equal to $V_c b_t$ where b_t is the thickness of the concrete section.

f_y = yield stress for the reinforcement (ksi).

These provisions are in some respects inconsistent in both nomenclature and principle. The Code defines V_c as the maximum allowable tangential shear stress that may be carried by concrete. Actually, V_c is the maximum allowable tangential shear stress that may be carried by orthogonally reinforced concrete. This is important because V_c is really the shear capacity which is provided through the interface shear transfer mode which can only occur if the orthogonal reinforcement is present to create the necessary frictional resistance forces between the crack planes.

The Code, based on the White and Holley proposal, also limits the shear stress that may be carried by panels having only orthogonal reinforcement (V_c) to 160 psi. As was pointed out earlier, this value is conservative and must be modified to a more realistic, higher value due to the results obtained in the recent experimental programs [2,6].

In proportioning the meridional and circumferential reinforcement, the current Code provisions (Equations 4.3 and 4.4) are the static equilibrium conditions assuming that failure occurs along a 45° diagonal crack (Figure 4.4). So the concrete provides no direct contribution to the ultimate strength but plays a role in the transfer

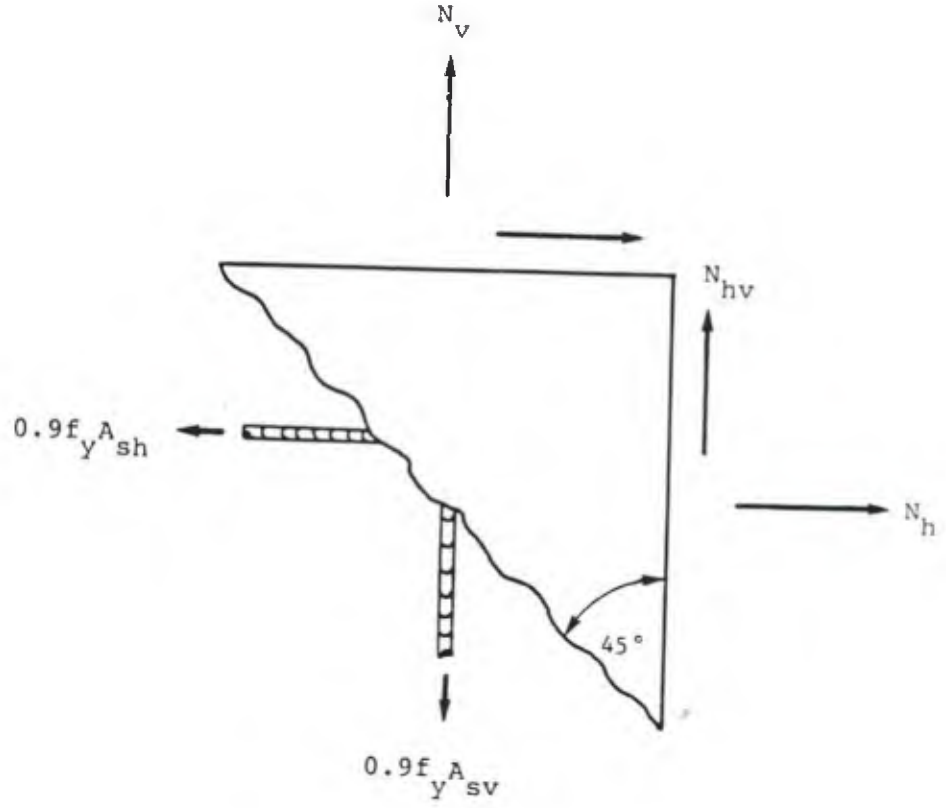

$$\Sigma F_x: \quad 0.9A_{sh}f_y = N_h + N_{hv}$$

$$\Sigma F_y: \quad 0.9A_{sv}f_y = N_v + N_{hv}$$

FIGURE 4.4: EQUILIBRIUM CONDITIONS ALONG A DIAGONAL CRACK

of the applied membrane shear stresses to the reinforcement.

The provisions for the contribution made by the diagonal reinforcement (Equation 4.5) involve the superposition of the strength provided by the orthogonal reinforcement to the strength provided by the diagonal reinforcement. As was illustrated in Table 3.11, this procedure is quite accurate in light of the recent experimental results [2,6].

4.3 Parametric Study

With the proposed behavioral models it is possible to make a sensitivity analysis of various parameters which play an important role in the ultimate shear strength of the specimens. These parameters include the first cycle stiffness, the steel ratio, and variations in the shear stress histories.

4.3.1 Evaluation of First Cycle Stiffness

The first cycle stiffness is an important parameter because it incorporates the contribution of various other parameters. It is through the first cycle stiffness that the other parameters such as the steel ratio and detailing of the specimen are included. In Table 4.1 the experimental and predicted values for the first cycle stiffness of various specimens [2,4,6] are illustrated. The predicted values were calculated based on the procedures prescribed in Reference 3. The variations between the experimental and predicted values range from 56% to 278%. It is clear that the currently available methods are not satisfactory. However, there are also discrepancies within

Table 4.1: Experimental and Predicted First Cycle Stiffness

Specimen	First Cycle Stiffness (ksi/rad)		
	Experimental	Predicted	% Difference
RB5	57.143	89.131	56%
0.3B	93.750	354.885	278%
0.6B	55.894	155.700	179%
2-0.9B	32.550	112.884	247%

the experimental stiffnesses. Two specimens with the same overall geometry, reinforcement pattern, and initial axial tension would be expected to display very similar first cycle stiffnesses. But as illustrated from the values given in Table 2.1, differences ranging from 4% up to 120% exist between compatible specimens tested by Cornell University [2,6].

Using the behavioral model developed in Chapter 2 the sensitivity of the predicted ultimate shear strength to variations in the first cycle stiffness was studied. Four representative specimens with initial axial stress ranging from $0.0f_y$ to $0.9f_y$ were evaluated, where f_y is the orthogonal reinforcement yield stress. Values of first cycle stiffness corresponding to 25% to 200% of the experimental first cycle stiffness were used as inputs into the model. The ultimate strengths obtained using these values were then compared to the ultimate strength predicted by the model using the experimental first cycle stiffness and cyclic shear load history. As illustrated in Table 4.2, the variations in ultimate shear strength are generally of the same proportion as the variations of first cycle stiffness. In other words, a 50% reduction in the first cycle stiffness led to around a 50% reduction in ultimate shear strength. Conversely, a 25% increase in the first cycle stiffness led to around a 25% increase in the ultimate shear strength.

Table 4.2: Sensitivity of Predicted Ultimate Shear Strengths to Variations in First Cycle Stiffness

Specimen	First Cycle Stiffness (ksi/rad)	% of Experimental First Cycle Stiffness	Shear Strength (psi)	% of Predicted Shear Strength
2-0.9B	24.412	75%	125	100%
	40.678	125%	125	100%
	48.825	150%	150	120%
	56.962	175%	200	160%
	65.100	200%	200	160%
0.6A	23.707	50%	125	45%
	35.561	75%	275	82%
	59.268	125%	325	118%
	71.121	150%	325	118%
	82.975	175%	375	136%
	94.828	200%	375	136%
0.3B	23.348	25%	175	39%
	46.875	50%	325	72%
	70.313	75%	375	83%
	117.188	125%	475	106%
	140.625	150%	525	117%
	164.630	175%	575	128%
0.0B	25.510	25%	225	43%
	51.021	50%	375	71%
	76.531	75%	425	81%
	127.551	125%	575	109%

4.3.2 Effect of Shear Stress Histories on Strength

There are two issues regarding the behavior of a nuclear containment wall panel. First, the normal membrane stresses induced by the internal pressure can be assumed to be taken up entirely by the orthogonal reinforcement in the form of axial strain. This assumption has been validated by the experimental results [4,7]. The second issue regards the strength of these panels for the membrane shear stresses induced by the seismic load. Based on the current experimental data the researchers at Cornell [2,6] have proposed the following function as a lower bound measure for the experimental results (Figure 4.5).

$$V_u = [2.7 + 0.006\rho(f_y - f_s)]\sqrt{f'_c} \qquad (4.6)$$

$$\text{for } \rho(f_y - f_s) > 40 \text{ psi}$$

For values of $\rho(f_y - f_s)$ less than 40 psi, it is assumed that the strength (V_u) decreases linearly, becoming zero for $\rho = 0$ or $f_s = f_y$.

where:

V_u = ultimate shear strength of specimens (psi)

ρ = lower value of steel ratios

f_y = reinforcement yield stress (psi)

f'_c = concrete compressive strength (psi)

f_s = initial axial stress in orthogonal reinforcement

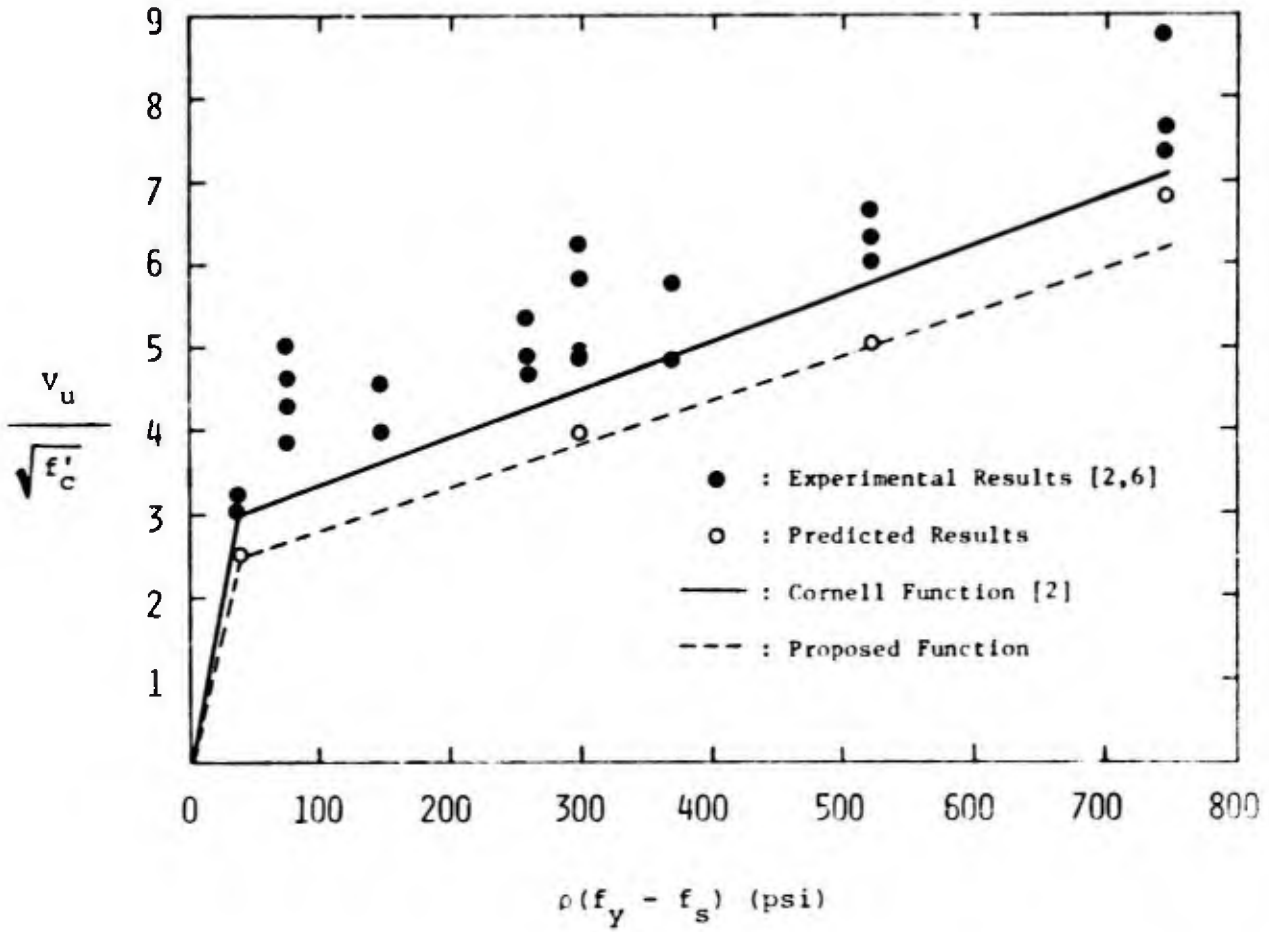

FIGURE 4.5: ULTIMATE SHEAR STRENGTH FOR ORTHOGONALLY REINFORCED PANELS

Although this equation is the lower bound for all the specimens, the specimens having both orthogonal and diagonal reinforcement displayed a considerably higher shear strength [2,6] for a given value of the stress parameter $\rho(f_y - f_s)$. This is not surprising since diagonal reinforcement is more effective in carrying the membrane shear stresses than is the orthogonal reinforcement.

Using the behavioral model for orthogonally reinforced panels presented in Chapter 2, an analysis of the sensitivity of the predicted ultimate shear strengths to variations in the stress amplitudes of the cyclic shear load histories was performed. The analysis was performed on four specimens which were close to the lower bound function (Equation 4.6) proposed by Cornell [2]. The results listed in Table 4.3 illustrate that reductions of up to 32% below the predicted ultimate shear strengths occurred by varying the stress amplitudes of the cyclic shear histories. These reductions occur because the simulated load histories were started at lower stress amplitudes then the experimental cyclic shear histories. The stress amplitude was the only factor that was varied. In all other respects these simulated load histories were similar to the experimentally applied load histories. Based on these lower predicted shear strengths the following lower bound function is proposed to predict the ultimate shear strength of orthogonally reinforced specimens (Figure 4.6).

$$V_o = [0.063\rho_o(f_{yo} - f_s)]\sqrt{f'_c} \qquad (4.7)$$

$$\text{for } 0 \leq \rho_o(f_{yo}-f_s) \leq 40 \text{ psi}$$

Table 4.3: Sensitivity of Predicted Ultimate Shear Strengths to Variations in Cyclic Shear Load Histories

Specimen	Predicted V_u (psi)	Lowest Predicted V_u (psi)	% Reduction
2-0.9B	125	100	20%
0.6A	325	220	32%
0.3B	450	380	16%
0.0B	525	490	7%

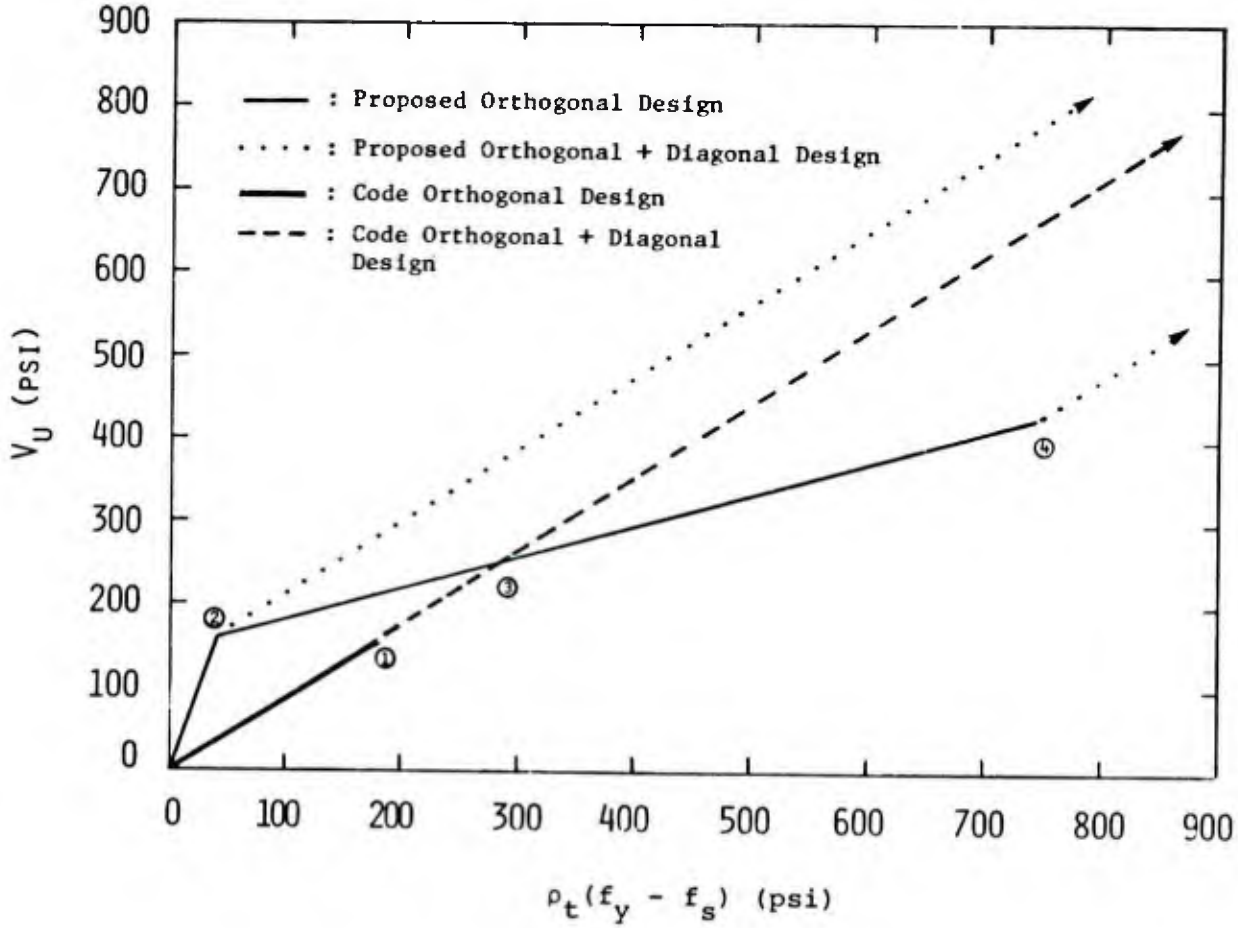

FIGURE 4.6: COMPARISON OF CURRENT CODE AND PROPOSED DESIGN PROCEDURE

$$V_o = [2.28 + 0.006\rho_o(f_{yo} - f_s)]\sqrt{f'_c} \leq 6.8\sqrt{f'_c} \qquad (4.8)$$

$$\text{for } 740 \geq \rho_o(f_{yo}-f_s) > 40 \text{ psi}$$

where:

V_o = tangential shear stress of orthogonally reinforced panels (psi)

ρ_o = smaller of steel ratios running in the orthogonal directions (psi)

f_{yo} = orthogonal reinforcement yield stress (psi)

f_s = initial pretension stress in orthogonal reinforcement (psi)

f'_c = concrete compressive strength (psi)

There are several important characteristics in this scheme for evaluating the ultimate shear strength of orthogonally reinforced panels. First, because the proposed function is a lower bound, it tends to be conservative. Second, the proposed function incorporates various important parameters. The material properties of both the concrete and the steel are incorporated through f_y and f'_c. More importantly, the amount of reinforcement and the initial pretension force, two key parameters, are incorporated through ρ_o and f_s. Third, the entire $\rho_o(f_y - f_s)$ parameter is the static equilibrium of forces for the reinforcement alone along a diagonal crack in the concrete. Thus the proposed equation has a corresponding physical interpretation. The empirical constants that were attached to this

parameter were necessary to incorporate the contrib.tion of the interface shear transfer mode and the degrading effect that the cyclic load has on the reinforcement and bond. The proposed function provides a lower bound for the ultimate shear strength based on the experimental and simulated cyclic shear histories. However, if the specific cyclic shear load history to be applied to a given containment structure was known, it could be used as the input into the proposed model for orthogonally reinforced specimens (Chapter 2) to evaluate directly the ultimate shear strength for that given history.

To evaluate the additional strength provided by the addition of diagonal reinforcement the procedure described in Section 3.12 may be used. The procedure involves the superposition of the strength provided by the orthogonal reinforcement to the contribution made by the diagonal reinforcement. This term (Equation 3.21) with the appropriate reduction in allowable stress to $0.9f_y$ is then:

$$V_d = 0.9\rho_d(f_{yd} - f_s) \tag{4.9}$$

where:

V_d = contribution to shear strength provided by the diagonal reinforcement (psi)

ρ_d = steel ratio of diagonal reinforcement alone, measured along the diagonal direction

f_{yd} = initial pretension stress in diagonal reinforcement (psi)

f_s = initial pretension force in the diagonal reinforcement (assumed equal to the initial force in the orthogonal reinforcement)

Finally, the ultimate shear strength (V_u) is merely the sum of the two individual terms.

$$V_u = V_o + V_d \tag{4.10}$$

The V_o term is evaluated by Equations 4.7 and 4.8 and the V_d term is evaluated by Equation 4.10.

4.4 Proposed Analysis and Design Criteria

In the following sections a detailed analysis and design procedure for reinforced concrete nuclear containment structures under simultaneous internal pressure and seismic loads is presented. The intent of this proposed procedure is to incorporate the extensive experimental as well as analytical findings that have been developed in the past ten years.

4.4.1 Ultimate Strength Analysis and Design Procedure

The following analysis and design procedure is recommended as a revision to the presently prescribed procedures of the ASME Pressure Vessel and Boiler Code, Section III, Division 2, Code for Concrete Reactor Vessels and Containments (Sections CC-3421.5.1 and CC-3521.1.1). These procedures apply to the analysis and design of tangential shear in combination with normal membrane stresses. The

proposed revisions would have the corresponding sections of the Code read as follows.

Proposed Revision for Section CC-3421.5.1 (Allowable Stress for Factored Load: Reinforced Concrete):

(a) The amount of tangential shear stress that may be carried by reinforced concrete having only orthogonal reinforcement (V_o) is equal to (Equations 4.7 and 4.8):

$$V_o = [0.063\rho_o(f_{yo} - f_s)]\sqrt{f'_c}$$
$$\text{for } 0 \leq \rho_o(f_{yo}-f_s) \leq 40 \text{ psi}$$

$$V_o = [2.28 + 0.006\rho_o(f_{yo} - f_s)]\sqrt{f'_c} \leq 6.8\sqrt{f'_c}$$
$$\text{for } 740 \geq \rho_o(f_{yo}-f_s) > 40 \text{ psi}$$

where V_o is given in psi, ρ_o is the lesser of the reinforcement steel ratios in the meridional and circumferential directions, f_y is the yield stress of said reinforcement, f_s is the initial axial force carried by such reinforcement as a result of normal membrane stresses (psi), and f'_c is the compressive strength of the concrete (psi).

When the applied shear stress is greater then $6.8\sqrt{f'_c}$, diagonal reinforcement in the form of 45° inclined bars in both directions shall be added to carry the excess shear. The increase in shear strength provided by the diagonal reinforcement (V_d) is equal to $0.9\rho_d(f_{yd} - f_s)$, where V_d is given in psi, ρ_d is

the steel ratio provided by the diagonal bars alone as measured in the diagonal direction, and f_{yd} is the yield stress of the diagonal reinforcement (psi). The total shear stress capacity of reinforced concrete having both orthogonal and diagonal reinforcement (V_u) is equal to $V_o + V_d$, where V_u is given in psi and V_o and V_d are as previously defined.

Proposed Revision for Section CC-3521.1 (Design for Shear Reinforcement: Tangential Shear):

(a) In those cases in which the applied factored shear stress resultant, N_{hv}, is less than the shear stress resultant that may be developed by orthogonal reinforcement alone, $N^c_{hv} = (6.8\sqrt{f'_c})b_t$ the meridional and hoop reinforcement shall be proportioned as follows:

$$A_{sh} = \left[\frac{N_h + (16/\sqrt{f'_c})N_{hv}}{0.9f_{yo}} \right] \qquad (4.11)^*$$

for $0 \leq N_{hv}/b_t \leq 2.5\sqrt{f'_c}$

$$A_{sh} = \left[\frac{N_h + (170/\sqrt{f'_c})N_{hv} - 380(b_t)}{0.9f_{yo}} \right] \qquad (4.12)^*$$

for $2.5\sqrt{f'_c} < N_{hv}/b_t \leq 6.8\sqrt{f'_c}$

$$A_{sv} = \left[\frac{N_v + (16/\sqrt{f'_c})N_{hv}}{0.9f_{yo}} \right] \qquad (4.13)^*$$

for $0 \leq N_{hv}/b_t \leq 2.5\sqrt{f'_c}$

$$A_{sv} = \left[\frac{N_v + (170/\sqrt{f'_c})N_{hv} - 380(b_t)}{0.9f_{yo}} \right] \qquad (4.14)^*$$

$$\text{for } 2.5\sqrt{f'_c} < N_{hv}/b_t \leq 6.8\sqrt{f'_c}$$

*Note: For derivation of these equations refer to Appendix C.

In those cases in which the applied factored shear stress resultant exceeds the shear stress resultant that may be carried by orthogonal reinforcement alone ($N_{hv} > N^c_{hv}$), in addition to the orthogonal reinforcement, diagonal reinforcement in the form of 45° inclined bars shall be used in the following proportion:

$$A_{si} = \left[\frac{N_{hv} - N^c_{hv}}{0.9f_{yd}} \right] \qquad (4.15)$$

where:

$$N^c_{hv} = (6.8\sqrt{f'_c})b_t$$

As an alternative procedure only part of the applied shear stress resultant (η) need be developed by the use of orthogonal reinforcement, even if the applied shear stress resultant is less than $(6.8\sqrt{f'_c})b_t$. The remaining portion of shear stress is then developed through the use of additional diagonal reinforcement. This reinforcement is to be proportioned as follows:

$$A_{sh} = \left[\frac{N_h + [16(\eta)\sqrt{f'_c}]N_{hv}}{0.9f_{yo}} \right] \qquad (4.16)$$

$$\text{for } 0 \leq N_{hv}/b_t \leq 2.5\sqrt{f'_c}$$

$$A_{sh} = \left[\frac{N_h + [170(\eta)/\sqrt{f'_c}]N_{hv} - 380b_t}{0.9f_{yo}} \right] \qquad (4.17)$$

$$\text{for } 2.5\sqrt{f'_c} < N_{hv}/b_t \leq 6.8\sqrt{f'_c}$$

$$A_{sv} = \left[\frac{N_v + [16(\eta)/\sqrt{f'_c}]N_{hv}}{0.9f_{yo}} \right] \qquad (4.18)$$

$$\text{for } 0 \leq N_{hv}/b_t \leq 2.5\sqrt{f'_c}$$

$$A_{sv} = \left[\frac{N_v + [170(\eta)/\sqrt{f'_c}]N_{hv} - 380b_t}{0.9f_{yo}} \right] \qquad (4.19)$$

$$\text{for } 2.5\sqrt{f'_c} < N_{hv}/b_t \leq 6.8\sqrt{f'_c}$$

$$A_{si} = \left[\frac{(1 - \eta)N_{hv}}{0.9f_{yd}} \right] \qquad (4.20)$$

where:

A_{sh} = reinforcing steel area in horizontal direction (in^2/in)

A_{sv} = reinforcing steel area in vertical direction (in^2/in)

A_{si} = steel area of diagonal reinforcement alone, measured along the diagonal (45°) direction (in^2/in)

b_t = thickness (in)

N_h = total applied horizontal stress resultant (lbs/in)

N_v = total applied vertical stress resultant (lbs/in)

N_{hv} = total applied shear stress resultant (lbs/in)

η = portion of applied shear stress resultant to be carried by the orthogonal reinforcement ($0 \leq \eta \leq 1$)

f'_c = concrete compressive strength (psi)

f_{yo} = yield stress of orthogonal reinforcement (psi)

f_{yd} = yield stress of diagonal reinforcment (psi)

Note that the proposed formulas (eqs. 4.11-4.20) are of the same form as the ASME Code equations (eqs. 4.3-4.5) but with a modified coefficient for N_{hv}.

4.4.2 Comparison of Current Code and Proposed Design Procedure

The current Code [5] and the proposed procedure are compared in Figure 4.6. In this figure, the predicted ultimate shear strength is plotted as a function of the stress parameter $\rho_t(f_y - f_s)$. As before, f_s is the initial axial stress in the orthogonal reinforcement due to the normal stresses, and f_y is the yield stress of the reinforcement. ρ_t represents the total steel ratio which may be expressed as:

$$\rho_t = \rho_o + \rho_d \tag{4.21}$$

where:

ρ_t = total steel ratio

ρ_o = minimum orthogonal steel ratio based on orthogonal reinforcement alone

ρ_d = diagonal steel ratio based on diagonal reinforcement alone measured along the diagonal (45°) direction

Figure 4.6 is drawn for a compressive strength concrete (f'_c) of 4000 psi. A typical value had to be chosen since the ultimate shear strength in the proposed procedure is dependent on $\sqrt{f'_c}$. This figure illustrates the various characteristics of both procedures. The Code specifies that the maximum strength that can be developed using only orthogonal reinforcement is 160 psi (Point 1). So up to this shear stress level $\rho_t = \rho_o$. For higher shear stresses, diagonal reinforcement in addition to the orthogonal reinforcement must be used. For these cases $\rho_t = \rho_o + \rho_d$. In the proposed model shear

stresses of up to $6.8\sqrt{f'_c} = 430$ psi (Point 4) may be developed using orthogonal reinforcement alone.

From this figure the following conclusions may be drawn:

(a) In light of the proposed procedure, the Code is always safe. This can be seen because up to a shear stress of 160 psi the Code provisions always yield higher steel ratios than the proposed procedure. For higher shear stresses the additional strength provided by the diagonal reinforcement is calculated in the same way in both the current Code and the proposed procedure.

(b) Up to a shear stress level of 250 psi (Point 3) the Code is always conservative (i.e. gives larger steel ratios for an equivalent shear stress) when compared to the proposed design procedure.

(c) For shear stresses above 250 psi (Point 3) whether the Code is conservative compared to the proposed design procedure depends on the relative proportions of orthogonal and diagonal steel selected by the designer to develop the required shear strength.

(d) For the proposed design procedure up to shear stresses of 160 psi (Point 2) the use of orthogonal reinforcement alone provides the most efficient design in terms of steel ratios. For shear stresses between 160 psi (Point 2) and 450 psi (Point 4) a design using both orthogonal and diagonal

reinforcement is more efficient than developing the required strength by using only orthogonal reinforcement.

(e) For any shear stress level a design based on the proposed procedure may be found which will be more efficient in terms of steel ratios than the design prescribed by the current Code.

4.3.3 Sample Design of Containment*

The following design considers membrane forces only. Design for flexure is not shown. All stresses are at 30 ft above the mat. Temperature stresses are not included.

Geometry:

Internal Diameter = 150'
Wall Thickness = 5'-3"
Height to Dome Bend Line = 120'
Hemispherical Dome Thickness = 2'-6"

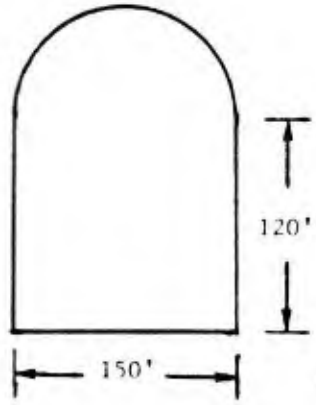

Material Properties:

All concrete: f'_c = 4000 psi
All steel: f_y = 60 ksi

Loads:

Load	Meridional Stress (psi)	Hoop Stress (psi)	Shear Stress (psi)
Dead Load	-238		
Internal Pressure (48 psi)	331	688	
Vertical Earthquake	238		
1st Horizontal Earthquake	681	40	
2nd Horizontal Earthquake			358

*Note: Geometry, material properties, loads and membrane stresses were provided by Stone & Webster Engineering Corporation, Boston, Massachusetts.

Resulting Membrane Stresses:

σ_h = 688 psi; N_h = (688)(12)(63)/1000 = 520 K/ft = 43300 lbs/in

$\sigma_v = [(331-238)+\sqrt{(238)^2+(681)^2}]$ = 814 psi

N_v = 615 K/ft = 22580 lbs/in

σ_{hv} = 358 psi; N_{hv} = (358)(12)(63)/1000 = 271 K/ft = 22580 lbs/in

Case I: Current Code Design Procedure

358 psi > 160 psi

∴ diagonal reinforcement required in addition to orthogonal reinforcement

by iterating, obtain the following orthogonal reinforcement areas:

$$A_{sh} = \frac{520 + 101}{0.9(60)} = 11.5 \text{ in}^2/\text{ft}$$

checking:

$$\rho_h = \frac{11.5}{(12)(63)} = 0.0152$$

thus:

$$V_c = \frac{[93 + 0.0152(2700)](63)(12)}{1000} = 101 \text{ psi} \quad \text{OK}$$

$$A_{sv} = \frac{615 + 106}{0.9(60)} = 13.4 \text{ in}^2/\text{ft}$$

checking:

$$\rho_v = \frac{13.4}{(12)(63)} = 0.0177$$

thus:

$$V_c = \frac{[93 + 0.0177(2700)](63)(12)}{1000} = 106 \text{ psi} \quad \text{OK}$$

additional diagonal reinforcement:

$$A_{si} = \frac{(271 - 101)}{0.9(60)} = 3.2 \text{ in}^2/\text{ft}$$

total steel volume:

$$\text{Vol.} = 12[11.5 + 13.4 + 3.2(2\sqrt{2})] = 407 \text{ in}^3/\text{ft}^3$$

Case II: Proposed Design Procedure Minimizing Steel Ratio

To minimize the steel ratio required to develop the required strength, orthogonal reinforcement is used to develop 160 psi of the applied shear stress. The remaining portion of shear stress is developed with diagonal reinforcement.

therefore:

$$\eta = 160/358 = 0.45$$

orthogonal reinforcement:

160 > 40 psi ∴ Use Equations 4.17 and 4.19

$$A_{sh} = [43300 + 170(0.45)(22580)/\sqrt{4000} - 380(63)]/(0.9)(60000) = 0.86 \text{ in}^2/\text{in}$$

$$A_{sh} = (0.86)(12) = 10.4 \text{ in}^2/\text{ft}$$

$$A_{sv} = [51250 + 170(0.45)(22580)/\sqrt{4000} - 380(63)]/(0.9)(60000) = 1.01 \text{ in}^2/\text{in}$$

$$A_{sv} = (1.01)(12) = 12.2 \text{ in}^2/\text{ft}$$

diagonal reinforcement (Equation 4.20):

$$A_{si} = [(1 - 0.45)(22580)]/(0.9)(60000) = 0.23 \text{ in}^2/\text{in}$$

$$A_{si} = (0.23)(12) = 2.7 \text{ in}^2/\text{ft}$$

total steel volume:

$$\text{Vol.} = 12[10.4 + 12.2 + 2.7(2\sqrt{2})] = 362 \text{ in}^3/\text{ft}^3$$

Case III: Proposed Design Criteria Using Only Orthogonal Reinforcement

358 psi < $6.8\sqrt{f'_c}$; Use Equations 4.12 and 4.14

∴ shear strength may be developed by using only orthogonal reinforcement

orthogonal reinforcement:

$A_{sh} = [43300 + 170(22580)/\sqrt{4000} - 380(63)]/(0.9)(60000) = 1.48 \text{ in}^2/\text{in}$

$A_{sh} = (1.48)(12) = 17.8 \text{ in}^2/\text{ft}$

$A_{sv} = [51250 + 170(22580)/\sqrt{4000} - 380(63)]/(0.9)(60000) = 1.63 \text{ in}^2/\text{in}$

$A_{sv} = (1.63)(12) = 19.6 \text{ in}^2/\text{ft}$

total steel volume:

Vol. = $12[17.8 + 19.6] = 448 \text{ in}^3/\text{ft}^3$

Case IV: Proposed Design Procedure Using Orthogonal and Diagonal reinforcement

select:

$\eta = 250/358 = 0.70$

orthogonal reinforcement:

250 psi > 40 psi ∴ Use Equations 4.17 and 4.19

$A_{sh} = [43300 + 170(0.70)(22580)/\sqrt{4000} - 380(63)]/(0.9)(60000) = 1.15 \text{ in}^2/\text{in}$

$A_{sh} = (1.15)(12) = 13.8 \text{ in}^2/\text{ft}$

$A_{sv} = [51250 + 170(0.70)(22580)/\sqrt{4000} - 380(63)]/(0.9)(60000) = 1.29 \text{ in}^2/\text{in}$

$A_{sv} = (1.29)(12) = 15.5 \text{ in}^2/\text{ft}$

diagonal reinforcement (Equation 4.20):

$$A_{si} = [(1 - 0.70)(22580)]/(0.9)(60000) = 0.12 \text{ in}^2/\text{in}$$

$$A_{si} = (0.12)(12) = 1.5 \text{ in}^2/\text{ft}$$

total steel volume:

$$\text{Vol.} = 12[13.8 + 15.5 + 1.5(2\sqrt{2})] = 403 \text{ in}^3/\text{ft}^3$$

From the results of the sample calculations (Cases I - IV) the following observations can be made. The most efficient design, in terms of minimizing the total steel volumes, using the proposed design procedure (Case II) gives a steel volume of 362 $in.^3/ft^3$. This represents a 12% reduction in the required reinforcement over the $407 in^3/ft^3$ required by the design based on the current Code (CaseI). Also, according to the present Code, costly diagonal reinforcement was necessary to develop the appropriate strength. On the other hand, the proposed design procedure (Case III) permits the development of the required shear strength using only orthogonal reinforcement since the applied shear stress (358 psi) is less than $6.8\sqrt{f'_c}$. However, in this case the steel volume increases to 448 $in.^3/ft.^3$, which represents a 10% increase over the reinforcement required by the Code (Case 1) and a 24% increase over the optimum design (Case II) in terms of steel volumes. However, the orthogonal reinforcement is less difficult and inexpensive to place than the diagonal reinforcement. So there is a tradeoff between these two factors. Finally, Case IV illustrates that there exists a design according to the proposed procedure which requires the same amount of reinforcement as that required by the current Code to develop a given strength. The proposed design (Case IV) required 403 $in.^3/ft.^3$ vs. the 407 $in.^3/ft.^3$ required by the Code (Case I).

CHAPTER 5

CONCLUSIONS AND FURTHER RESEARCH NEEDS

5.1 Conclusions

The behavior of the orthogonally reinforced panels and of the panels having both orthogonal and diagonal reinforcement displayed the following characteristics. The first cycle stiffness was basically linear. For the subsequent cycles, a bilinear stiffness seems to adequately model the observed response. The major factor in the degradation of the specimens appears to be the number of cycles of loading. Factors such as the initial axial force and the stress amplitudes of the cyclic shear load history seem to play a lesser role in the degradation process.

Based on the results obtained, the following conclusions may be drawn. It appears that higher values of tangential shear stress than the presently prescribed maximum value of 160 psi. may be developed by the use of orthogonal reinforcement alone. The proposed design criteria suggests that shear strengths of up to $6.8\sqrt{f'_c}$ may be developed in these orthogonally reinforced panels. This procedure

also gives the designer more flexibility in selecting the proportions of orthogonal and diagonal reinforcement to be used in developing the required shear strength.

The proposed analysis and design procedure has the benefit of the extensive experimental as well as analytical results that have been obtained in the last ten years, when the current Code provisions were instituted. By incorporating these results, the resulting analysis and design procedure is not only more realistic but also may provide a higher level of safety for these critical structures.

5.2 Further Research Needs

Although considerable advances have been made in the understanding of the behavior of typical nuclear containment panels there still remains much work to be done in both the analytical and experimental phases. Further research is primarily required in the following areas.

5.2.1 Further Validation of Behavioral Models

Due to the complexity of the problem it is not possible to formulate a closed form analytical solution. Therefore, both the design and analysis procedures are heavily dependent on empirical results. To obtain realistic results it is necessary to test more wall panel specimens. By broadening the experimental data base it will be possible to more clearly identify the key parameters and their effect on the behavior of the wall panels. The parameters include the material properties, geometric configuration, and load histories.

This way it will be possible to continually validate and calibrate the proposed behavioral models. More sophisticated functions to include the effect of a larger number of parameters may then be incorporated into the proposed models.

5.2.2 Development of Behavioral Model Under Non-Uniform Cyclic Shear Load Histories

The critical loading conditions considered are the accidental internal pressure load inside the containment and the ground motion due to an earthquake. At the element level, the internal pressure which is initially applied to the reactor as part of the required preliminary testing procedure can be appropriately modeled by applying an initial axial force to the reinforcing bars. This produces the initial orthogonal crack pattern which has been observed in both the specimens and in the actual containments.

The ground motion due to an earthquake results in a non-uniform cyclic shear load history. It typically consists of an initial portion during which it continually builds up to a peak and a subsequent decay phase. There is to date no experimental program in which specimens with both an initial axial tension and a subsequent non-uniform cyclic shear load history have been tested. The Cornell [2,6] and PCA [4,7] specimens were loaded with an initial axial stress but with a uniform cyclic shear load history. On the other hand, the Japanese investigators [8] used a non-uniform cyclic shear history but did not apply an initial axial stress to produce the orthogonal crack pattern. When the appropriate experimental data become available, the

proposed model must be refined and extended to apply to these more realistic load conditions.

5.2.3 Punching Shear

Another critical loading condition in certain regions of the containment is punching shear. This type of loading may occur due to structural or mechanical components that are attached to the containment or due to an accidental loading in the form of a missile impact. This load must therefore also be combined with the internal pressure and seismic loads and the effect on the overall behavior studied.

5.2.4 Effect of Steel Liner

The induced forces in the containment are resisted by the concrete, reinforcing steel, and liner plate. The steel liner is an important component of the overall structural system since it maintains the pressure integrity of the containment. Because it is anchored to the concrete wall, there exists a compatibility condition between the displacment of the wall and the liner. Although the reinforced concrete wall may provide the required strength, the deformation long before failure may be large enough to cause severe deformations or even rupture of the liner. Therefore, deformations as well as stresses must be limited. For these reasons the effect of the liner should be incorporated into the overall analysis.

5.2.5 Simulation of the Entire Containment Structure

Most of the effort in both the experimental and analytical phases of the ongoing research has been aimed at solving the problem at the element level. This has led to the extensive testing of the experimental wall panels and the subsequent proposed behavioral models. Eventually, however, both the experimental and analytical efforts must be directed at the modeling of the entire containment structure. The effect of factors such as the overturning moment that have been neglected at the element level may then be assessed. The Japanese [10,11] have conducted some initial tests of scale models of the containment vessel. As more data becomes available, behavioral models for predicting the response of the entire containment structure may be developed.

APPENDIX A

Orthogonal Cyclic Shear Model

In this section the computer program for the orthogonal cyclic shear model is described and a copy of the actual program listing is given. The program requires two cards of input. All input is free format, so it is only necessary to separate each entry within a card by either a comma or or by leaving one or more spaces in between. As output the program gives two plots. The first is the specimen shear stress vs. shear strain history. The second plot gives the maximum strain in the reinforcement vs. cycle number.

CARD 1: 6 Entries

	Variable	Type	Meaning
(1)	T	F	First Cycle Stiffness
(2)	N	I	Number of Cycles
(3)	FP	F	Initial Axial Force
(4)	FY	F	Yield Stress 0.=default value (60ksi)
(5)	E	F	Young's Modulus 0.=default value (30000 ksi)
(6)	JP	I	0=stop program execution when $\epsilon_s \geq \epsilon_y$ 1=continue program execution to final prescribed cycle

Notes:

If a variable is type F, a floating point number must be entered. For type I variables, an integer is required as the input.

(4) If 0. is input for FY, the program uses the default value of 60 Ksi for FY. Otherwise it uses the value given in this entry.

(5) If 0. is input for the value of E, the program uses the default value of 30000 Ksi. Otherwise it uses the given value.

(6) The value given for JP determines whether the program is to stop executing when ϵ_s reaches ϵ_y.

CARD 2: N Entries

	Variable	Type	Meaning
(1)	P(I)	F	Maximum Shear Stress for Cycle I.

Notes:

(1) P(I) is the vector which contains the maximum shear stress level reached in each cycle. There should be as many entries as there are cycles (N).

```
C*************************************************************
C*                      CYCLIC SHEAR MODEL                   *
C*************************************************************
      DIMENSION A(2,400),B(2,100),P(100),ET(100)
C  READ INITIAL STIFFNESS(T), NO. OF CYCLES(N),
C  AND INITIAL PRETENSIONING(FP)
      READ(5,*)T,N,FP,FY,E,JP
C  READ VECTOR OF MAXIMUM SHEAR STRESS APPLIED IN EACH CYCLE
      READ(5,*) (P(I),I=1,N)
C  UNLOADING STIFFNESS(T3)
      T3=1000000000.
C  READ OR DEFAULT CORRESPONDING VALUE OF E AND FY
      IF (FY .EQ. 0.) GO TO 5
      GO TO 6
5     FY=60.
6     IF (E .EQ. 0.) GO TO 7
      GO TO 8
7     E=30000.
C  CALCULATE THE YIELD STRAIN(EY)
8     EY=FY/E*1000.
C  CALCULATE INITIAL STEEL STRAIN(EO) DUE TO PRETENSIONING
      EO=FP/E*1000.
      ET(1)=EO
      B(1,1)=0
      B(2,1)=ET(1)
C  CALCULATE THE FIRST CYCLE RESPONSE
      A(1,1)=0.
      A(2,1)=0.
      A(1,2)=P(1)/T
      A(2,2)=P(1)
      A(1,3)=A(1,2)-P(1)/T3
      A(2,3)=0.
      XS=A(1,2)
      F=0.170-0.00167*FP
      ET(2)=EO+F*A(1,2)
      B(1,2)=1
      B(2,2)=ET(2)
      IF (ET(2) .GE. EY) GOTO 12
      GOTO 15
12    I1=1
      NP=3
      N1=2
      GO TO 20
C   CALCULATE RESPONSE FOR CYCLES 2 TO N
15    DO 10 I=2,N
C   CALCULATE YIELD STRAIN(EY)
      K=(I-1)*4
C   CALCULATE THE FREE SLIP STIFFNESS(T1)
      T1=T*(1./FLOAT(I))
```

```
C    CALCULATE THE CONTACT STIFFNESS(T2)
         T2=T*(0.1*(FLOAT(I)**1.3)*(EXP(-0.05*FLOAT(I)))+1.)
         A(1,K)=0.
         A(2,K)=0.
C    CALCULATE THE FREE SLIP(STRAIN) FOR CYCLE N
         FS=XS*0.78*(1.-EXP(-1.25*(FLOAT(I)-1.)))
         A(1,K+1)=FS
C    CALCULATE THE STRESS CORRESPONDING TO FREE SLIP(STRAIN)
         A(2,K+1)=FS*T1
C    CALCULATE THE MAXIMUM SLIP(STRAIN) FOR CYCLE N
         A(1,K+2)=A(1,K+1)+(P(I)-A(2,K+1))/T2
C    UPDATE THE MAXIMUM SLIP(STRAIN)
         IF(A(1,K+2).GT.XS) XS=A(1,K+2)
C    CALCULATE THE MAXIMUM STRESS FOR CYCLE N
         A(2,K+2)=P(I)
C    CALCULATE THE TOTAL STEEL STRAIN(ET)
         N1=I+1
         ET(N1)=EO+F*A(1,K+2)
         B(1,N1)=I
         B(2,N1)=ET(N1)
         A(1,K+3)=A(1,K+2)-P(I)/T3
         A(2,K+3)=0.
         NP=4*I-1
         IF (JP .EQ. 1) GO TO 10
         IF (ET(N1) .GE. EY) GO TO 20
         I1=I+1
10       CONTINUE
C    CALL SUBROUTINE TO PLOT SHEAR STRESS VS STRAIN(SLIP) HISTORY
20       WRITE(6,*)I1
         CALL QPICTR(A,2,NP,QX(1),QY(2),QLABEL(12))
C    CALL SUBROUTINE TO PLOT STEEL STRAIN VS. CYCLE NUMBER
         CALL QPICTR(B,2,N1,QX(1),QY(2),QLABEL(12))
         STOP
         END
```

FIGURE A.1: COMPUTER PROGRAM FOR ORTHOGONAL MODEL

LIST OF VARIABLES

A(1,K) = initial strain at beginning of cycle (always 0 in this model)

A(1, K+1) = free slip (strain) for current cycle

A(1, K+2) = maximum slip (strain) for current cycle

A(1, K+3) = residual stress for current cycle

A(2,1) = initial stress at beginning for current cycle (always 0 in this model)

A(2, K+1) = stress corresponding to free slip for current cycle

A(2, K+2) = stress corresponding to maximum slip for current cycle

A(2, K+3) = stress corresponding to residual stress (always 0 in this model)

B(1,I) = cycle number

B(2,I) = total steel strain attained for current cycle

E = reinforcement Young's Modulus

ET = total steel strain attained for current cycle

ED = steel strain due to pretensioning

EY = reinforcement yield strain

F = empirical constant dependent on FP

FP = initial pretensioning steel stress

FS = free slip for current cycle

FY = reinforcement yield stress

JP = determines when program execution is to terminate

N = total number of cycles

N1 = counter (current cycle + 1)

P = maximum stress level of each cycle

LIST OF VARIABLES (continued)

T = initial stiffness

T_1 = free slip stiffness for current cycle

T_2 = constant stiffness for current cycle

T_3 = unloading stiffness

X_s = maximum slip (strain) attained in all previous cycles

(a) Input data for RB5 specimen:

```
70.000  64  36. 68.6  27250. 0
47.  47.  47.  47.  47.
121.  121.  121.  121.  121.  121.  121.  121.  121.  121.  121.
169.  169.  169.  169.  169.  169.  169.  169.  169.  169.  169.
212.  212.  212.  212.  212.  212.  212.  212.  212.  212.  212.
210.  210.  210.  210.  210.  210.  210.  210.  210.  210.  210.
230.  230.  230.  230.  230.  230.  230.  230.  230.  230.  230.
```

(b) Input data for RB6 specimen:

```
65.000  70  54.  68.6  27250.  0
47.  47.  47.  47.  47.
115.  115.  115.  115.  115.  115.  115.  115.  115.  115.  115.
140.  140.  140.  140.  140.  140.  140.  140.  140.  140.  140.  140.
139.  139.  139.  139.  139.  139.  139.  139.  139.  139.  139.  139.
163.  163.  163.  163.  163.  163.  163.  163.  163.  163.  163.  163.
189.  189.  189.  189.  189.  189.  189.  189.  189.  189.  189.  189.
218.  218.  218.  218.  218.  218.
```

(c) Input data for 0.3A specimen:

```
105.000  80  18.30  61.  28000. 0
125.  125.  125.  125.  125.  125.  125.  125.  125.  125.
175.  175.  175.  175.  175.  175.  175.  175.  175.  175.
225.  225.  225.  225.  225.  225.  225.  225.  225.  225.
275.  275.  275.  275.  275.  275.  275.  275.  275.  275.
325.  325.  325.  325.  325.  325.  325.  325.  325.  325.
375.  375.  375.  375.  375.  375.  375.  375.  375.  375.
425.  425.  425.  425.  425.  425.  425.  425.  425.  425.
475.  475.  475.  475.  475.  475.  475.  475.  475.  475.
```

(d) Input data for 0.3B specimen:

```
93.750  70  18.30  61.  28000. 0
125.  125.  125.  125.  125.  125.  125.  125.  125.  125.
175.  175.  175.  175.  175.  175.  175.  175.  175.  175.
225.  225.  225.  225.  225.  225.  225.  225.  225.  225.
275.  275.  275.  275.  275.  275.  275.  275.  275.  275.
325.  325.  325.  325.  325.  325.  325.  325.  325.  325.
375.  375.  375.  375.  375.  375.  375.  375.  375.  375.
450.  450.  450.  450.  450.  450.  450.  450.  450.  450.
```

(e) Input data for 0.6A specimen:

```
47.414  42   36.60  61.   28000. 0
125.  125.  125.  125.  125.  125.  125.  125.  125.  125.
175.  175.  175.  175.  175.  175.  175.  175.  175.  175.
225.  225.  225.  225.  225.  225.  225.  225.  225.  225.
275.  275.  275.  275.  275.  275.  275.  275.  275.  275.
325.  325.
```

(f) Input data for 0.6B specimen:

```
55.894  45   36.60  61.   28000. 0
125.  125.  125.  125.  125.  125.  125.  125.  125.  125.
175.  175.  175.  175.  175.  175.  175.  175.  175.  175.
225.  225.  225.  225.  225.  225.  225.  225.  225.  225.
275.  275.  275.  275.  275.  275.  275.  275.  275.  275.
325.  325.  325.  325.  325.
```

(g) Input data for 0.9A specimen:

```
 33.854  35   54.90  61.   28000. 0
 50.   50.   50.   50.   50.   50.   50.   50.   50.   50.
125.  125.  125.  125.  125.  125.  125.  125.  125.  125.
175.  175.  175.  175.  175.  175.  175.  175.  175.  175.
225.  225.  225.  225.  225.
```

(h) Input data for 0.9B specimen:

```
30.093  35   54.90  61.   28000. 0
125.  125.  125.  125.  125.  125.  125.  125.  125.  125.
175.  175.  175.  175.  175.  175.  175.  175.  175.  175.
225.  225.  225.  225.  225.  225.  225.  225.  225.  225.
275.  275.  275.  275.  275.
```

(i) Input data for 2-0.3B specimen:

```
108.333 80   18.0  64.5  28000.  0
125.  125.  125.  125.  125.  125.  125.  125.  125.  125.
175.  175.  175.  175.  175.  175.  175.  175.  175.  175.
225.  225.  225.  225.  225.  225.  225.  225.  225.  225.
275.  275.  275.  275.  275.  275.  275.  275.  275.  275.
325.  325.  325.  325.  325.  325.  325.  325.  325.  325.
375.  375.  375.  375.  375.  375.  375.  375.  375.  375.
425.  425.  425.  425.  425.  425.  425.  425.  425.  425.
475.  475.  475.  475.  475.  475.  475.  475.  475.  475.
```

(j) Input data for 2-0.6A specimen:

```
56.24  40  36.  64.5  28000.  0
150.  150.  150.  150.  150.  150.  150.  150.  150.  150.
200.  200.  200.  200.  200.  200.  200.  200.  200.  200.
250.  250.  250.  250.  250.  250.  250.  250.  250.  250.
300.  300.  300.  300.  300.  300.  300.  300.  300.  300.
```

(k) Input data for 2-0.6B specimen:

```
49.48  50  36.  64.5  28000.  0
125.  125.  125.  125.  125.  125.  125.  125.  125.  125.
175.  175.  175.  175.  175.  175.  175.  175.  175.  175.
225.  225.  225.  225.  225.  225.  225.  225.  225.  225.
250.  250.  250.  250.  250.  250.  250.  250.  250.  250.
275.  275.  275.  275.  275.  275.  275.  275.  275.  275.
```

(l) Input data for 2-0.9A specimen:

```
32.55  35  54.0  64.5  28000.  1
125.  125.  125.  125.  125.  125.  125.  125.  125.  125.
150.  150.  150.  150.  150.  150.  150.  150.  150.  150.
175.  175.  175.  175.  175.  175.  175.  175.  175.  175.
200.  200.  200.  200.  200.
```

(m) Input data for 2-0.9B specimen:

```
32.55  35  54.0  64.5  28000.  1
125.  125.  125.  125.  125.  125.  125.  125.  125.  125.
150.  150.  150.  150.  150.  150.  150.  150.  150.  150.
175.  175.  175.  175.  175.  175.  175.  175.  175.  175.
200.  200.  200.  200.  200.
```

(n) Input data for 0.6A specimen (simulated load):

```
47.414  40  36.60  61.  28000.  0
100.  100.  100.  100.  100.  100.  100.  100.  100.  100.
150.  150.  150.  150.  150.  150.  150.  150.  150.  150.
200.  200.  200.  200.  200.  200.  200.  200.  200.  200.
240.  240.  240.  240.  240.  240.  240.  240.  240.  240.
```

FIGURE A.2: INPUT DATA FOR ORTHOGONAL SPECIMENS

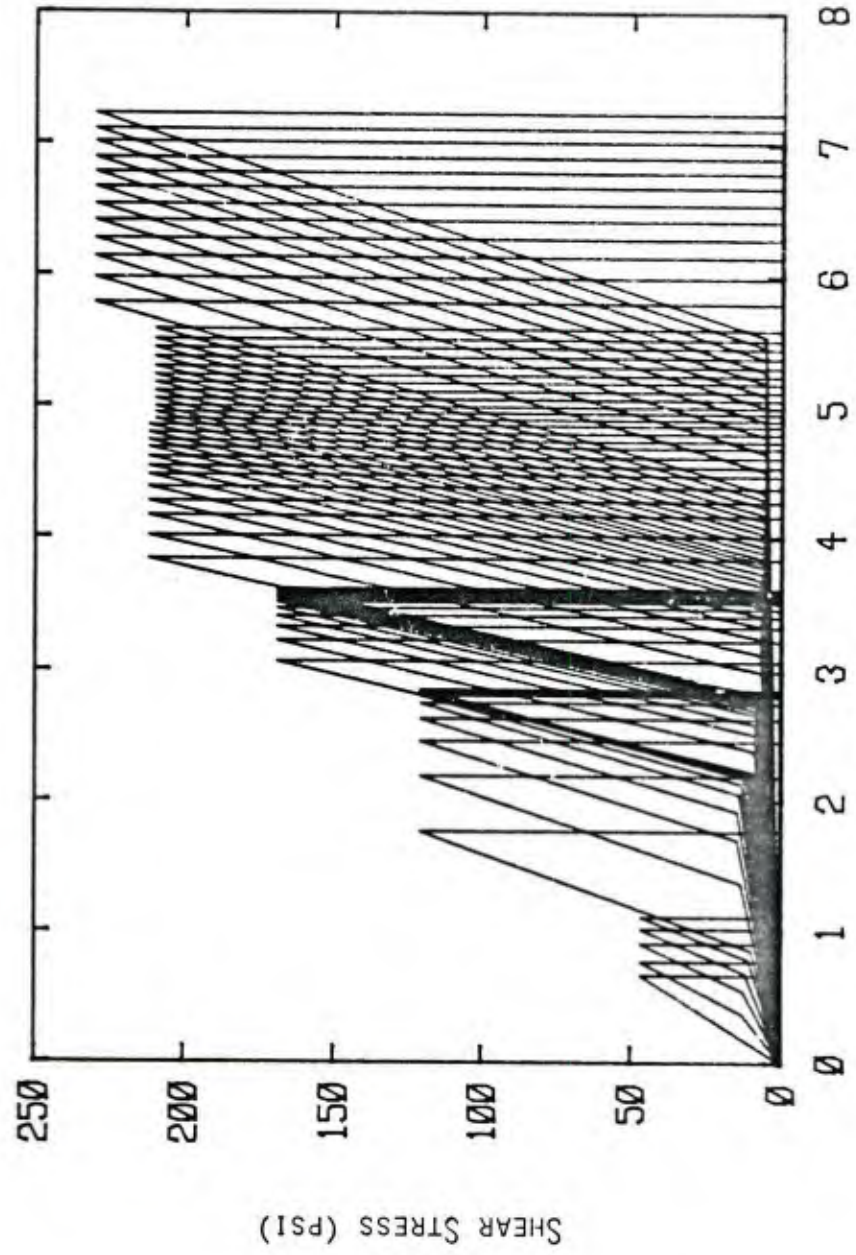

FIGURE A.3: STRESS-STRAIN HISTORY FOR RB5 SPECIMEN

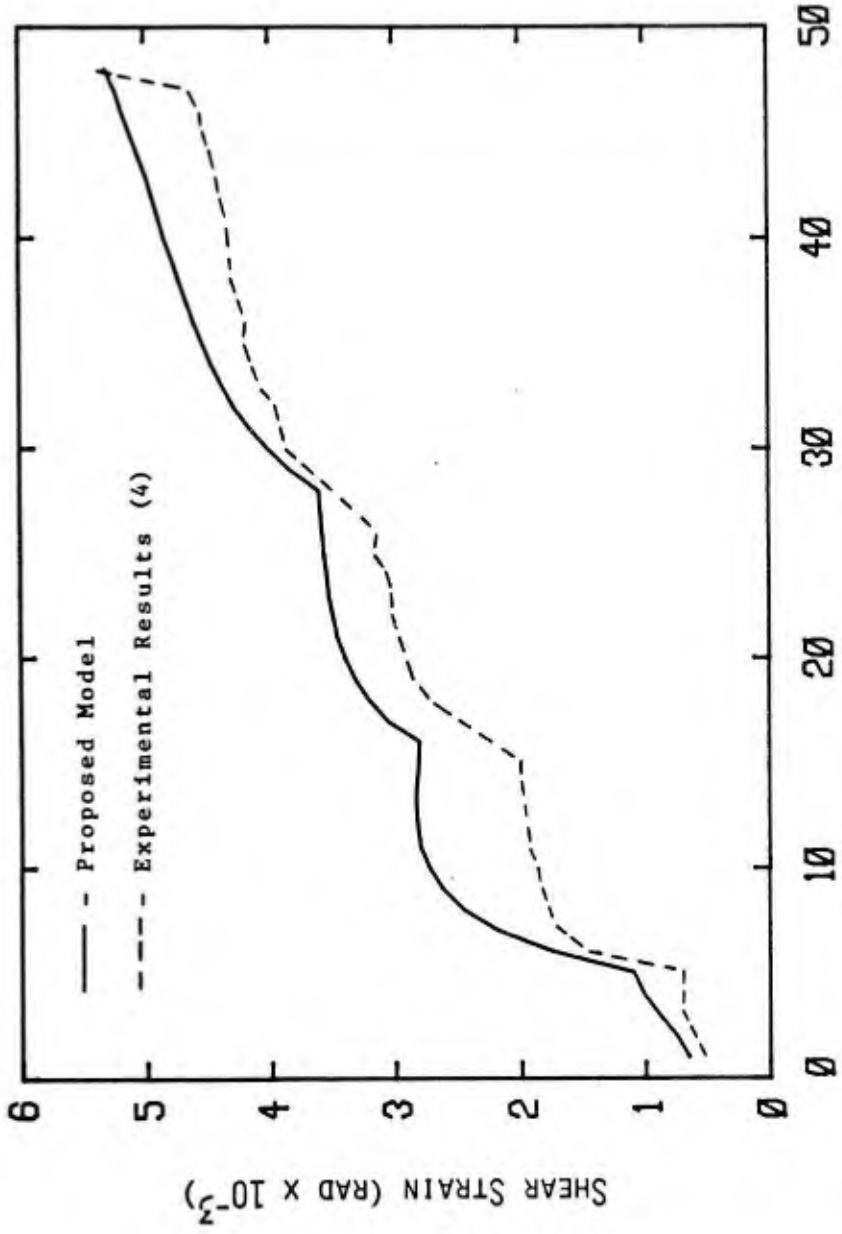

Figure A.4: Shear Strain vs. Cycle Number for RB5 Specimen

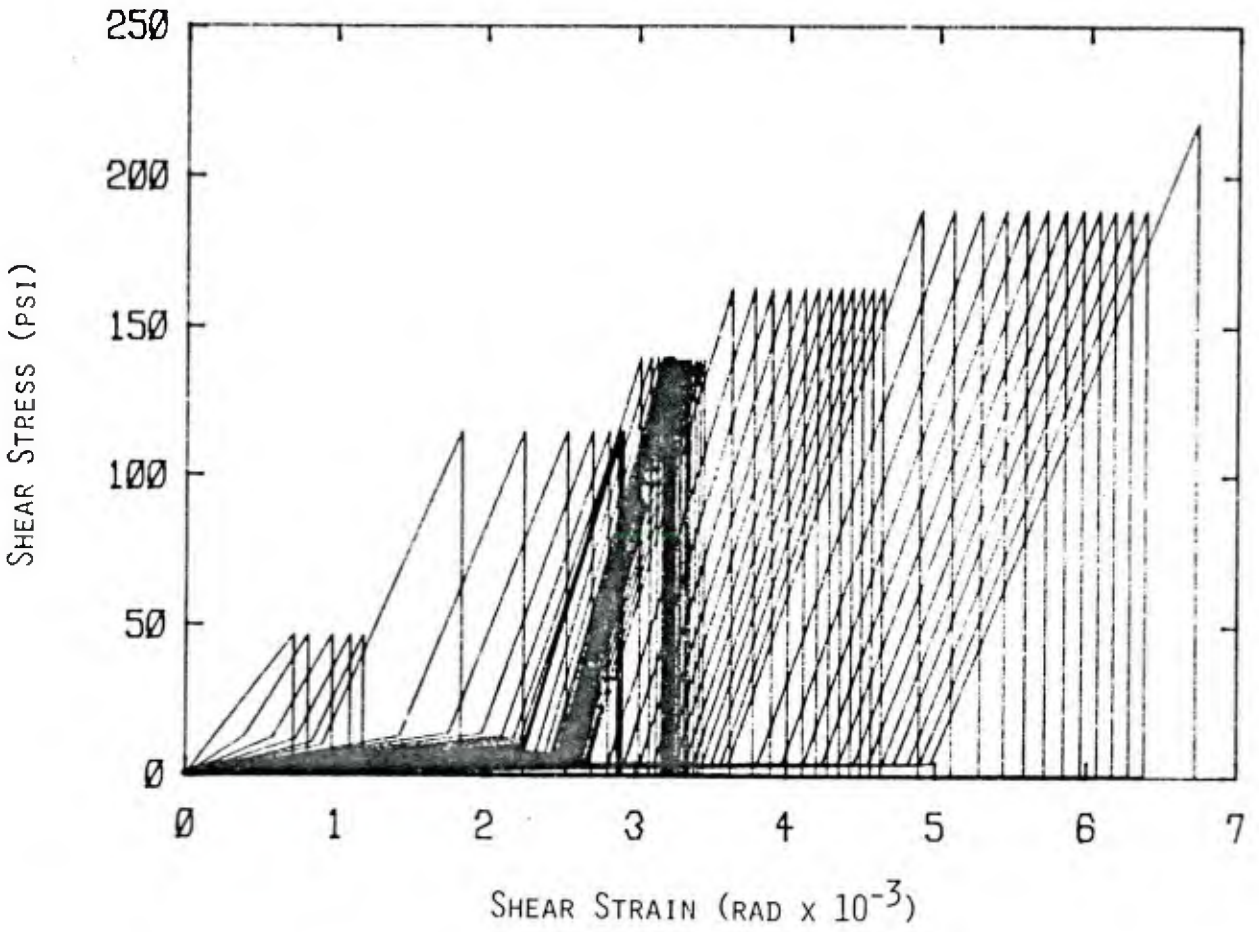

FIGURE A.5: STRESS-STRAIN HISTORY FOR RB6 SPECIMEN

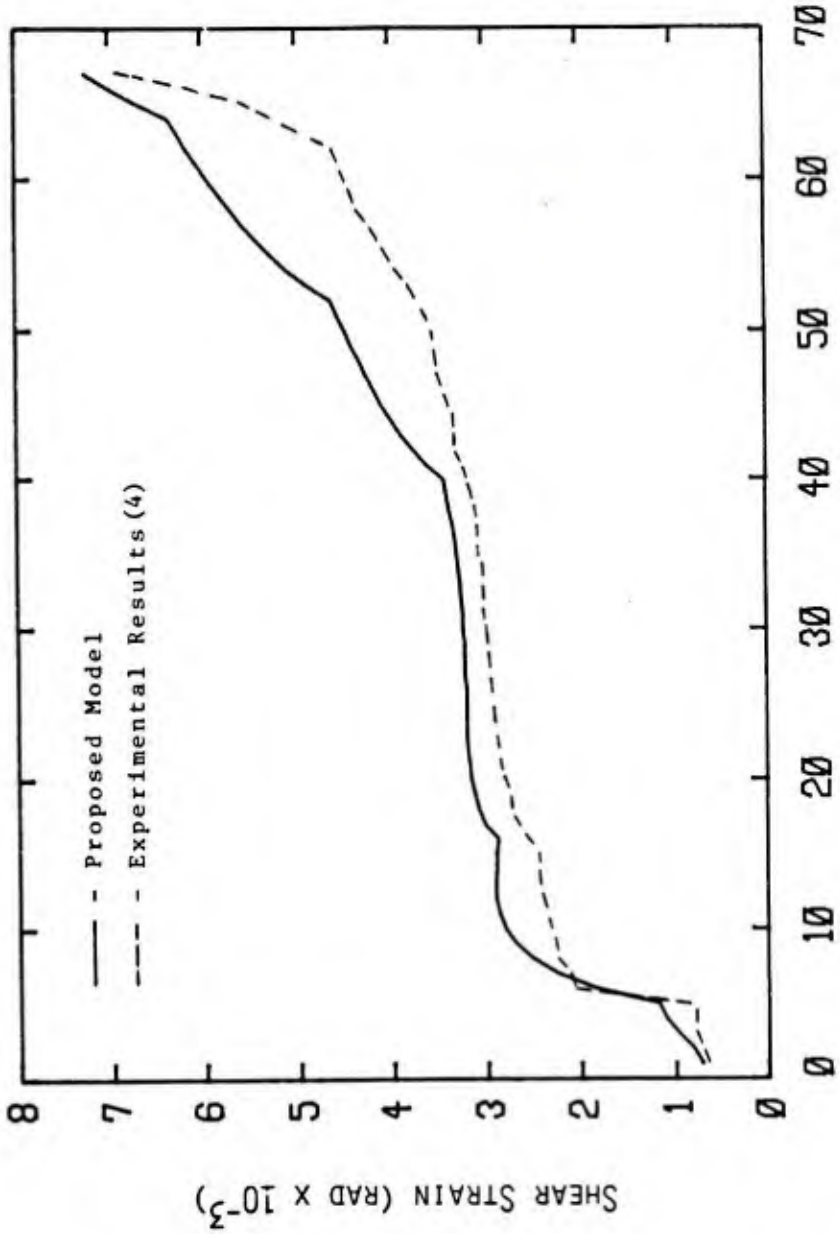

Figure A.6: Shear Strain vs. Cycle Number for RB6 Specimen

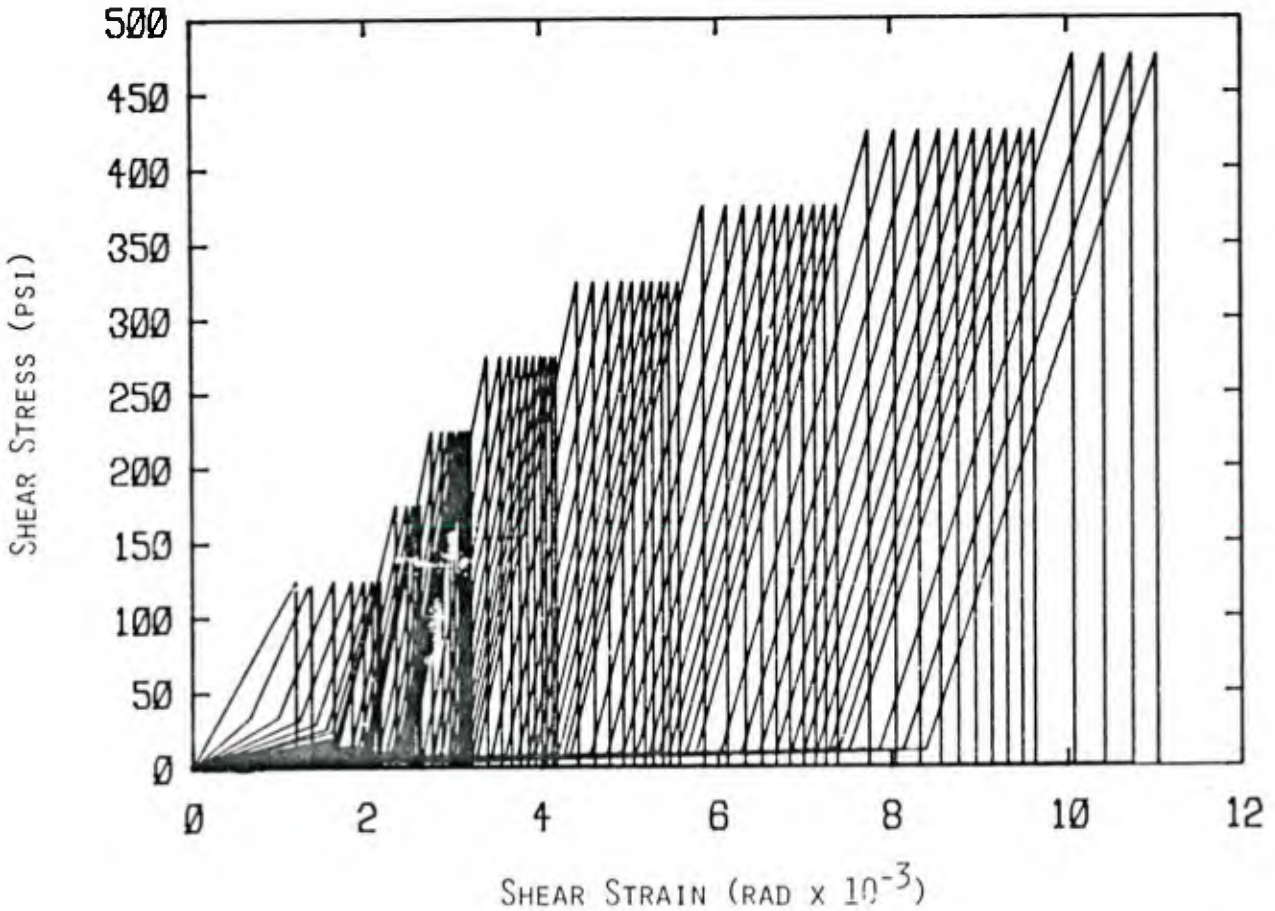

FIGURE A.7: STRESS-STRAIN HISTORY FOR 0.3A SPECIMEN

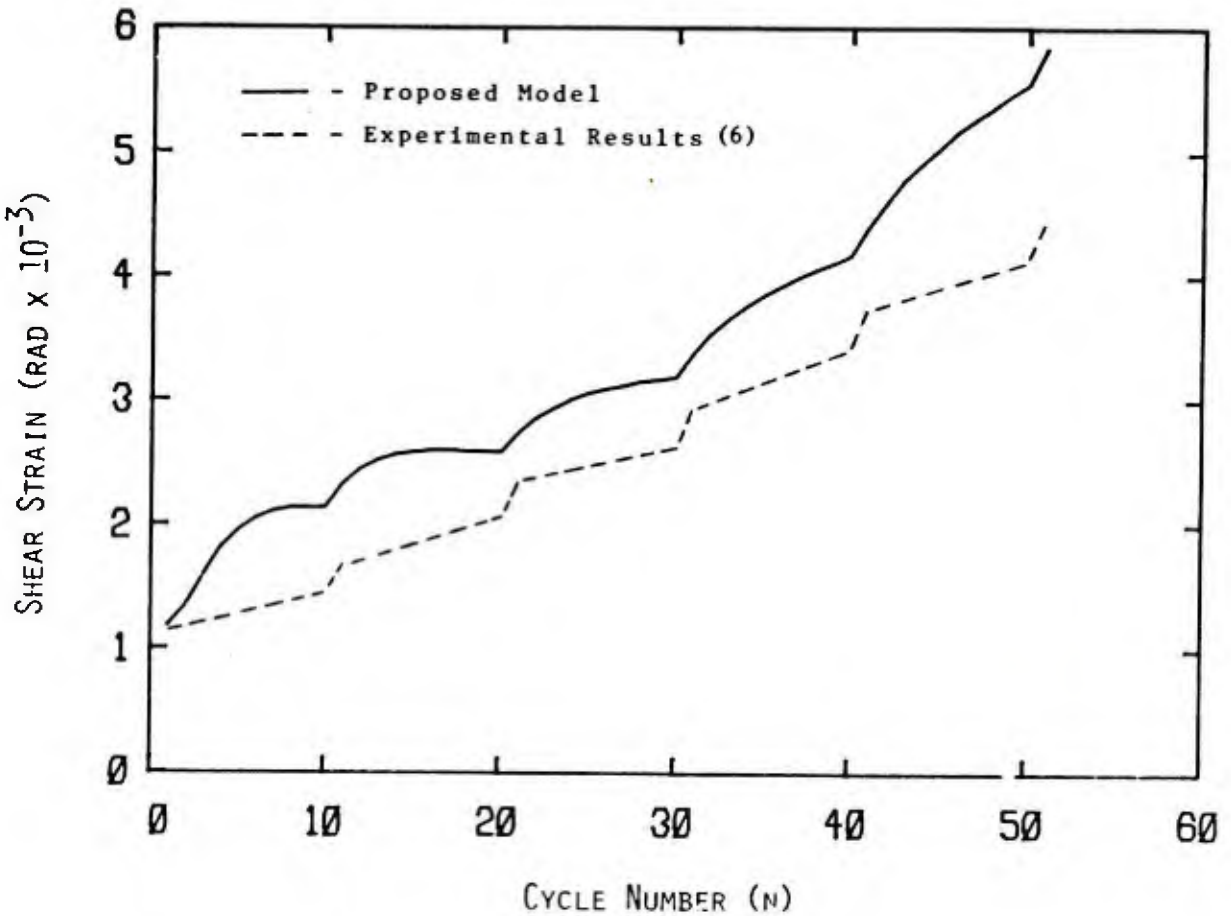

Figure A.8: Shear Strain vs. Cycle Number for 0.3A Specimen

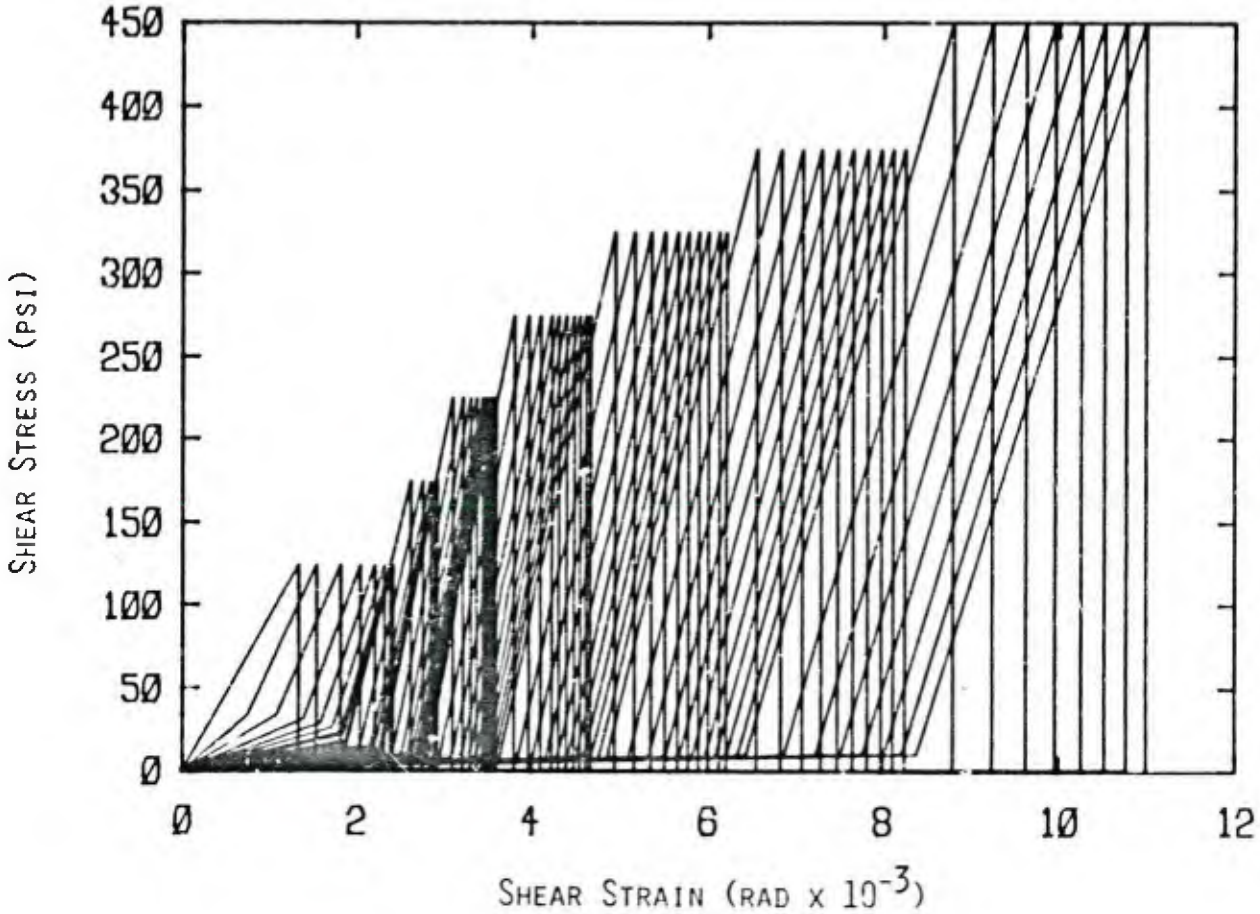

FIGURE A.9: STRESS-STRAIN HISTORY FOR 0.3B SPECIMEN

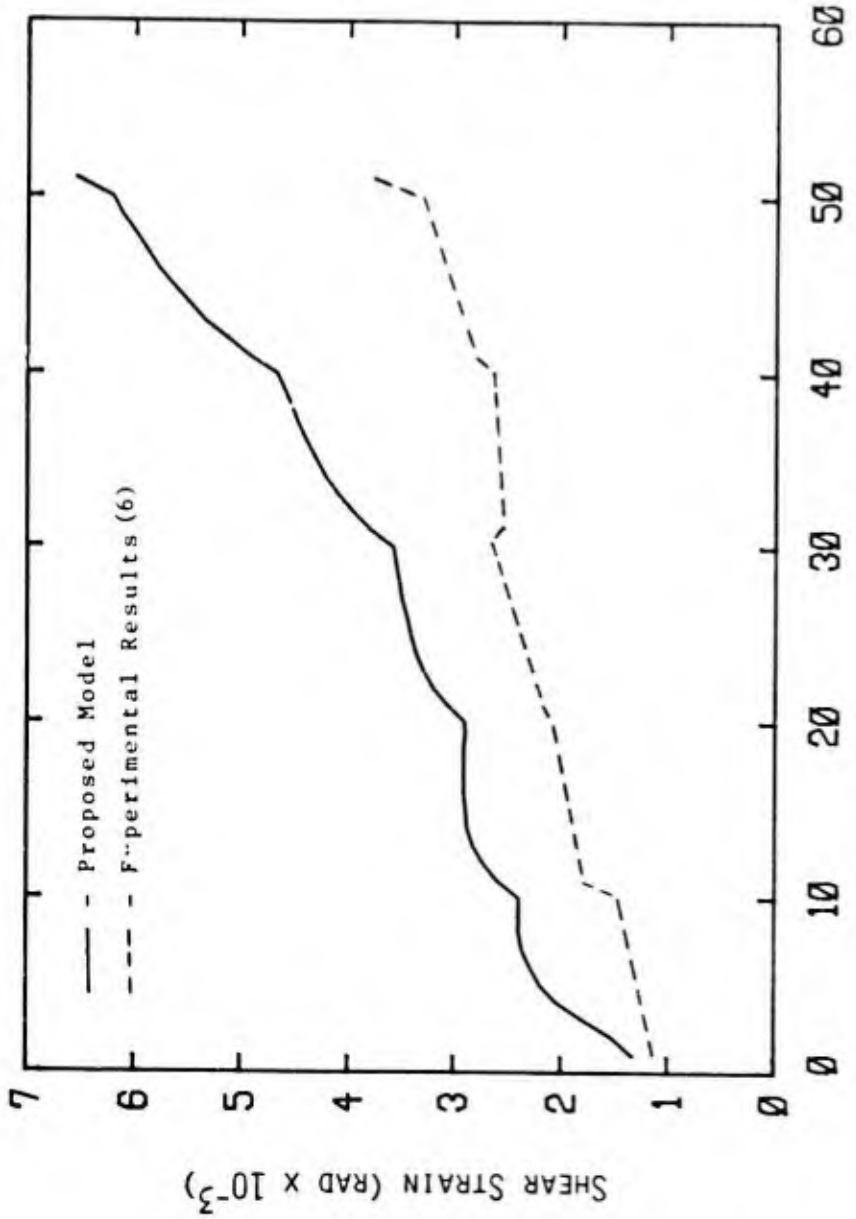

Figure A.10: Shear Strain vs. Cycle Number for 0.3B Specimen

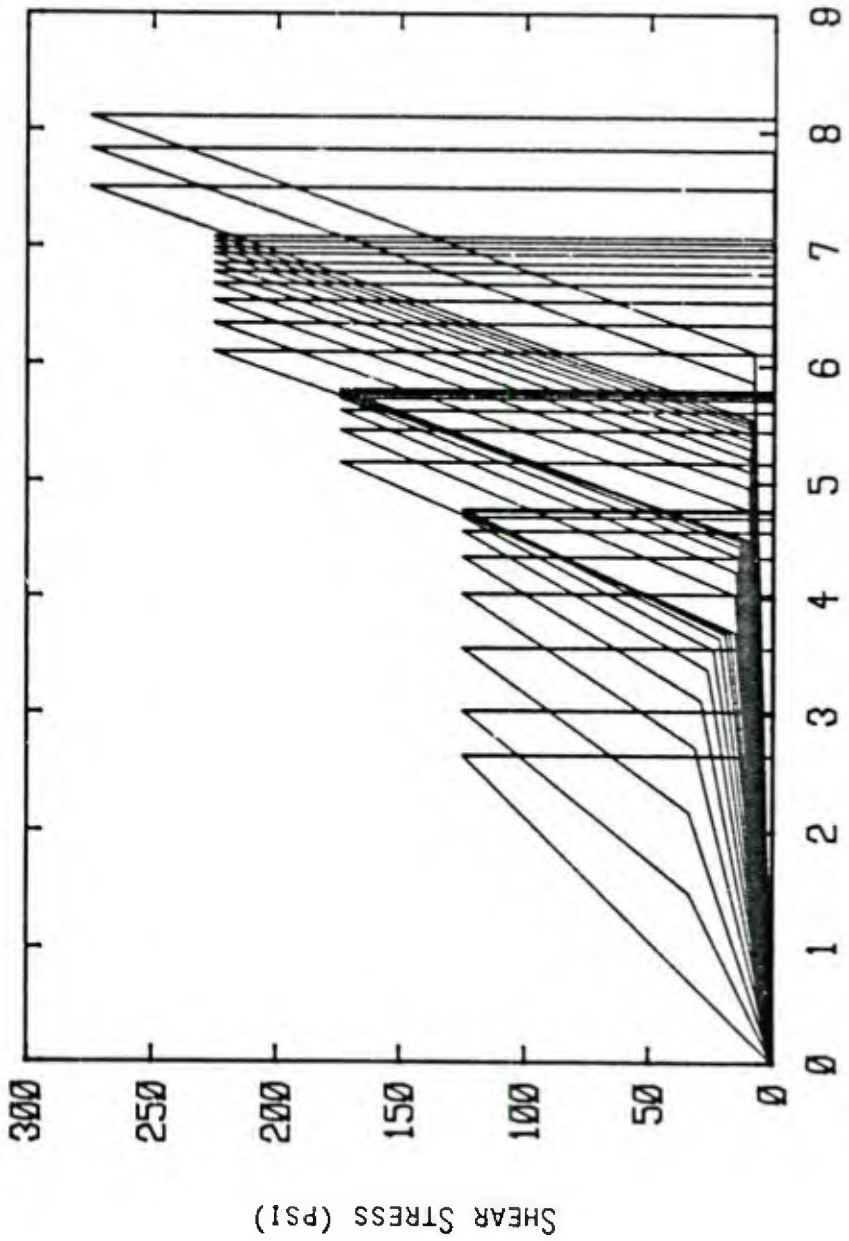

FIGURE A.11: STRESS-STRAIN HISTORY FOR 0.6A SPECIMEN

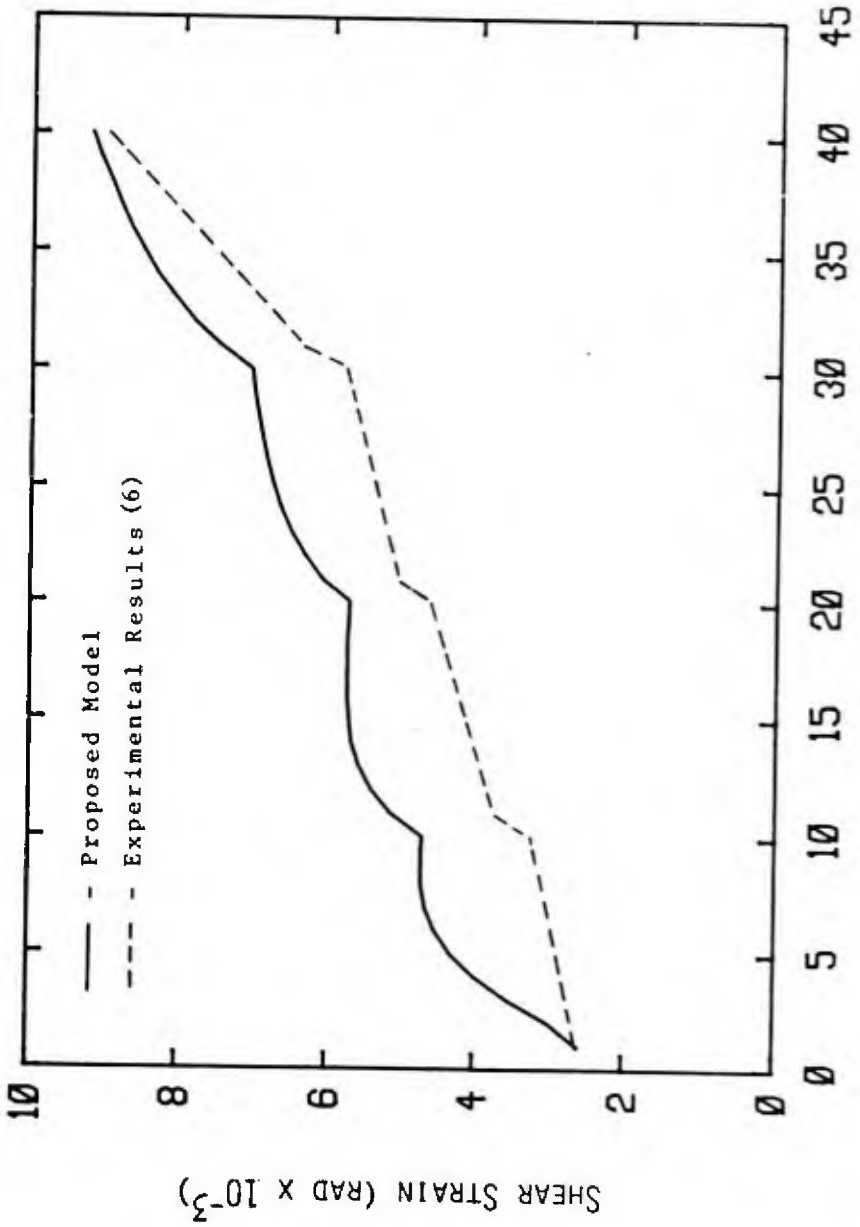

FIGURE A.12: SHEAR STRAIN VS. CYCLE NUMBER FOR 0.6A SPECIMEN

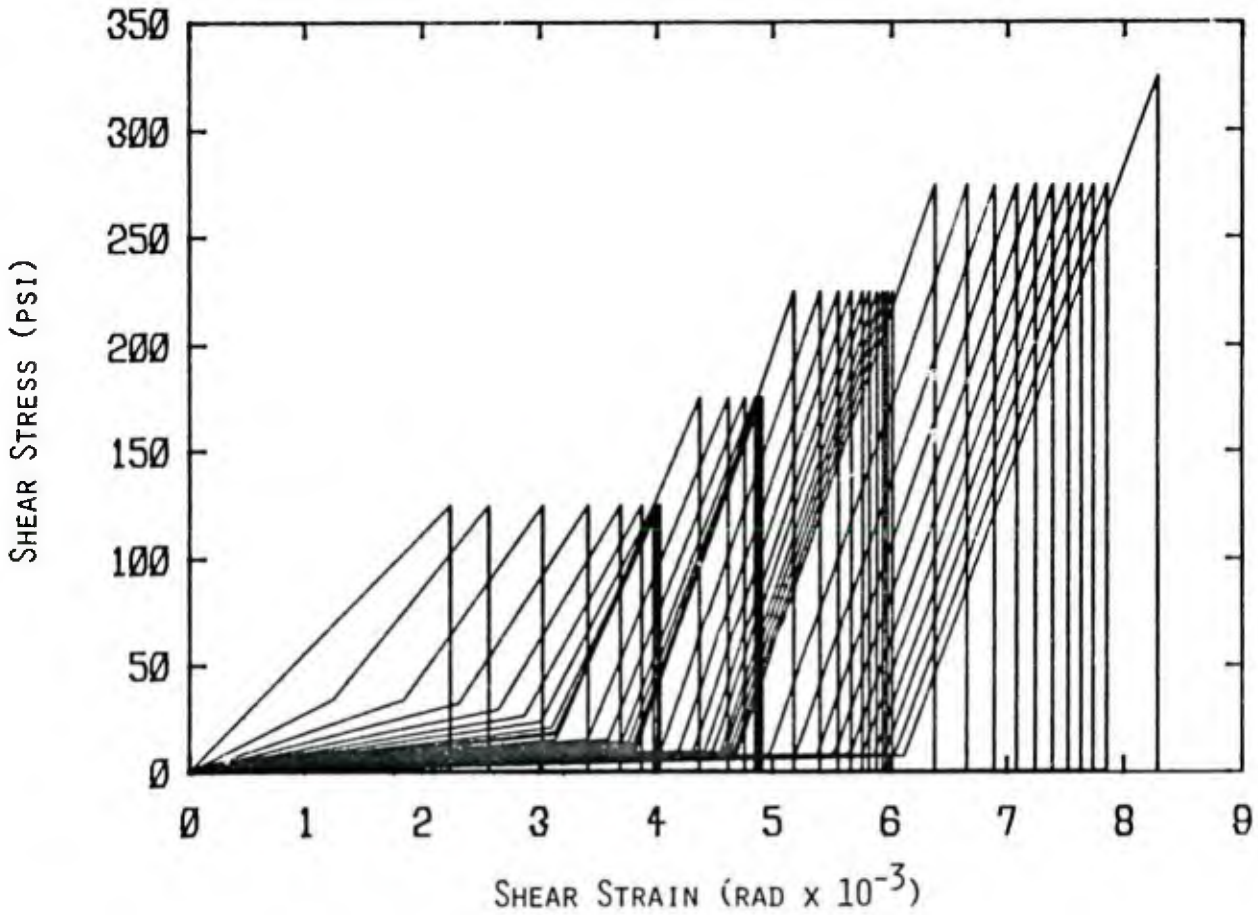

Figure A.13: Stress-Strain History for 0.6B Specimen

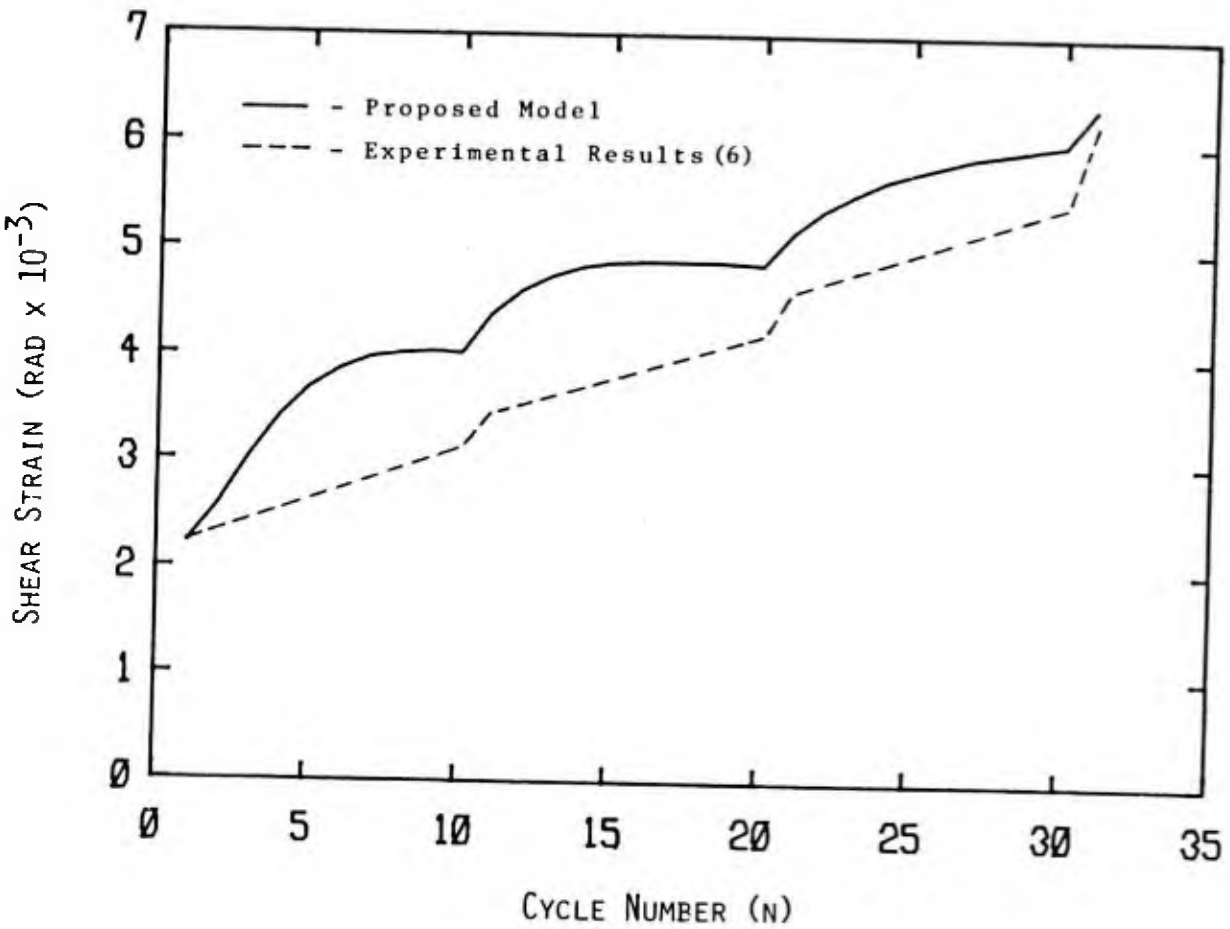

Figure A.14: Shear Strain vs. Cycle Number for 0.6B Specimen

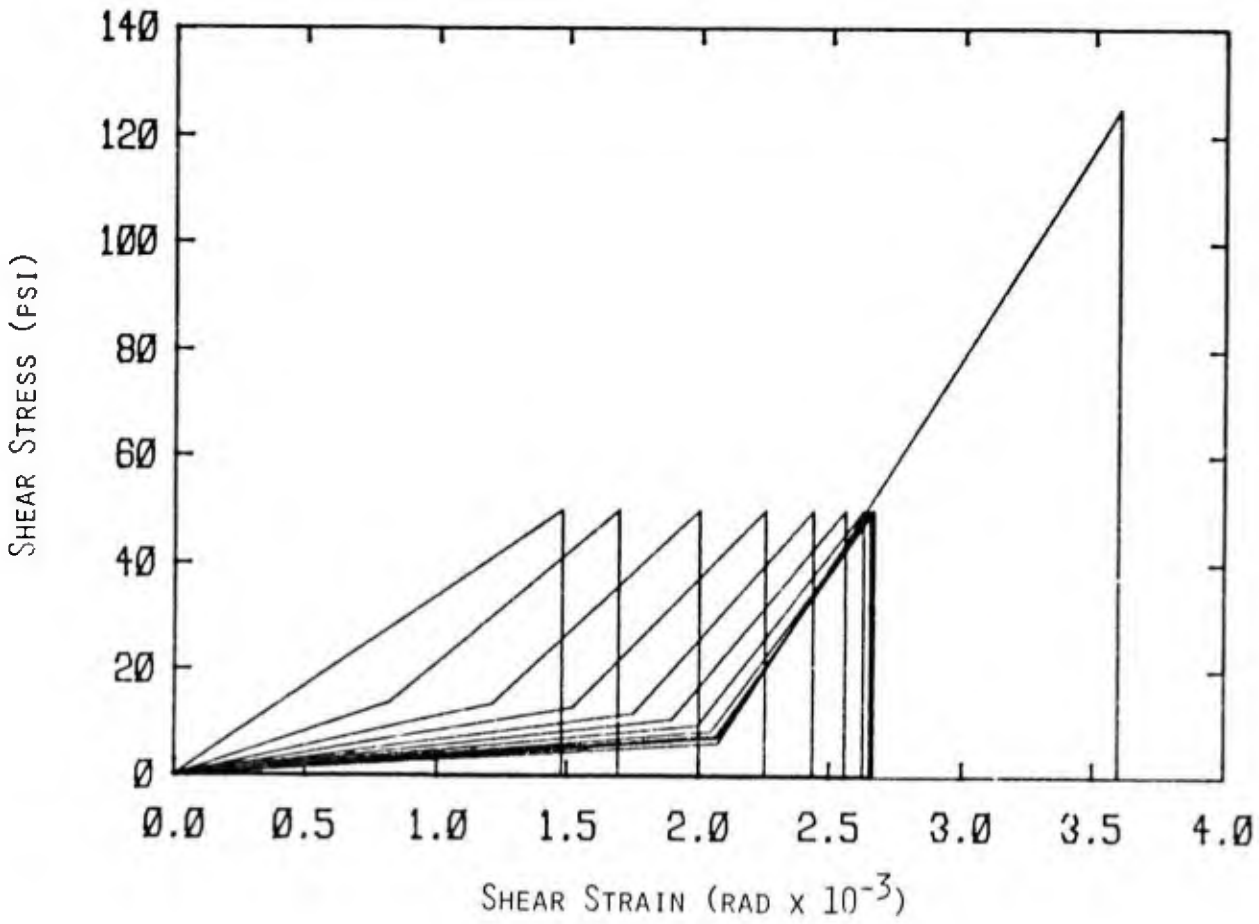

FIGURE A.15: STRESS-STRAIN HISTORY FOR 0.9A SPECIMEN

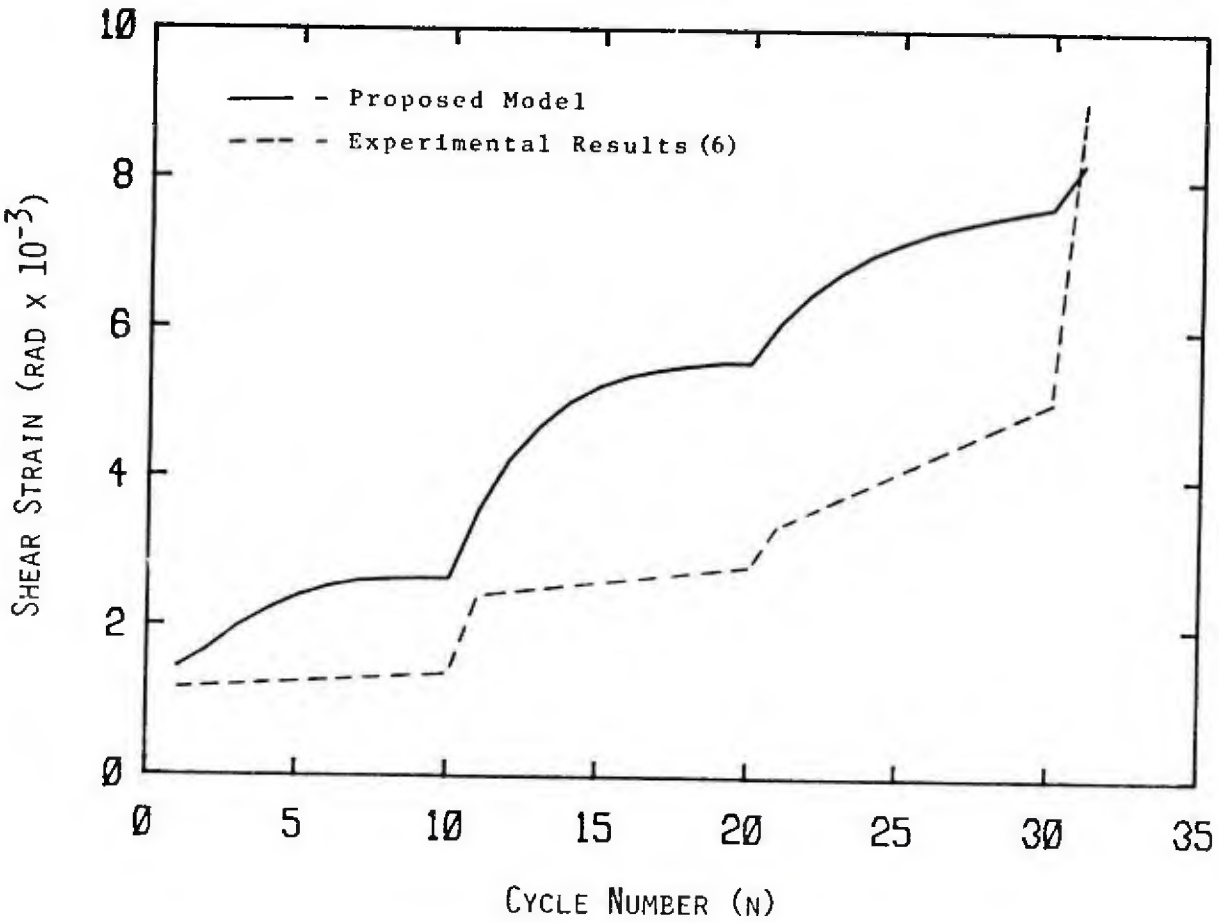

FIGURE A.16: SHEAR STRAIN VS. CYCLE NUMBER FOR 0.9A SPECIMEN

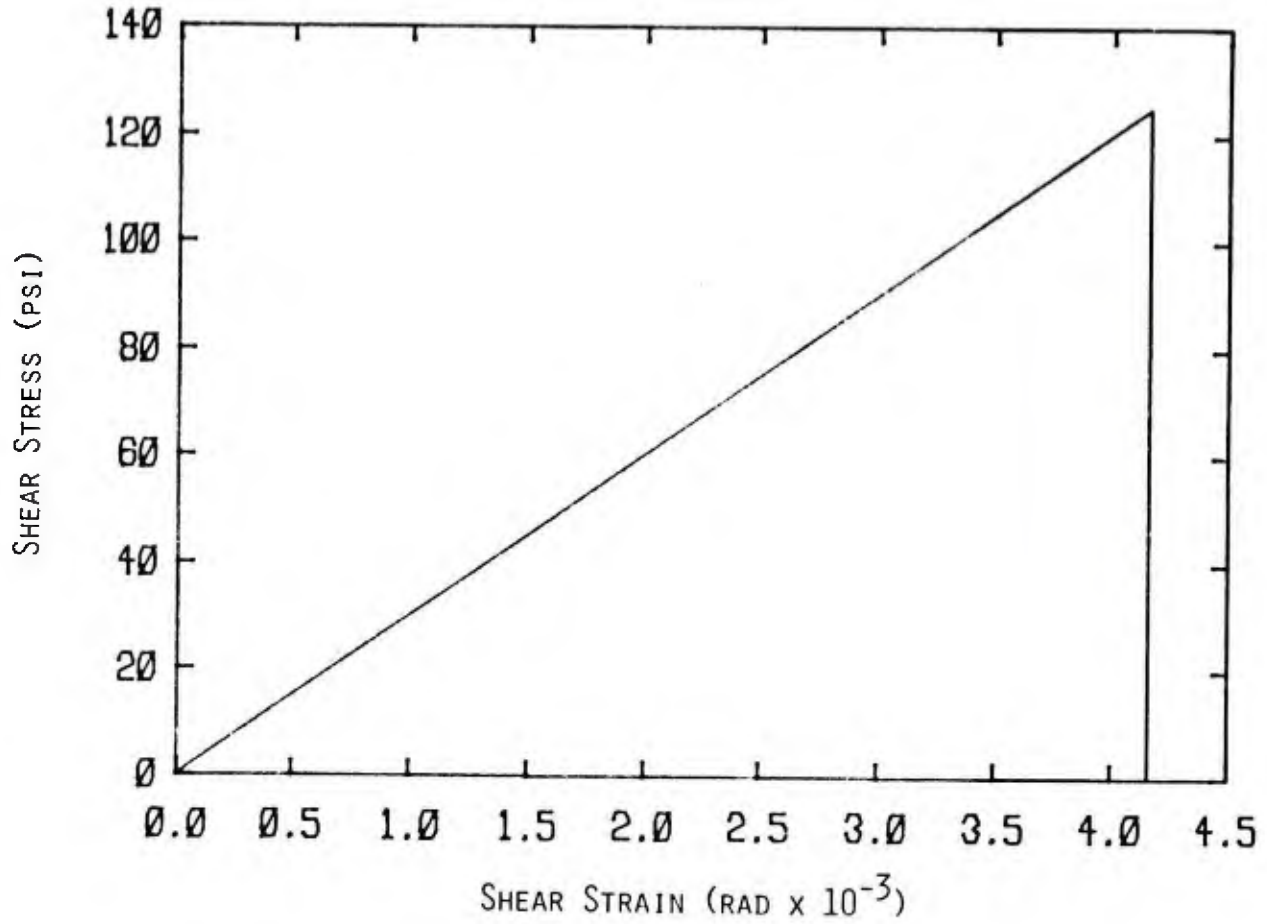

Figure A.17: Stress-Strain History for 0.9B Specimen

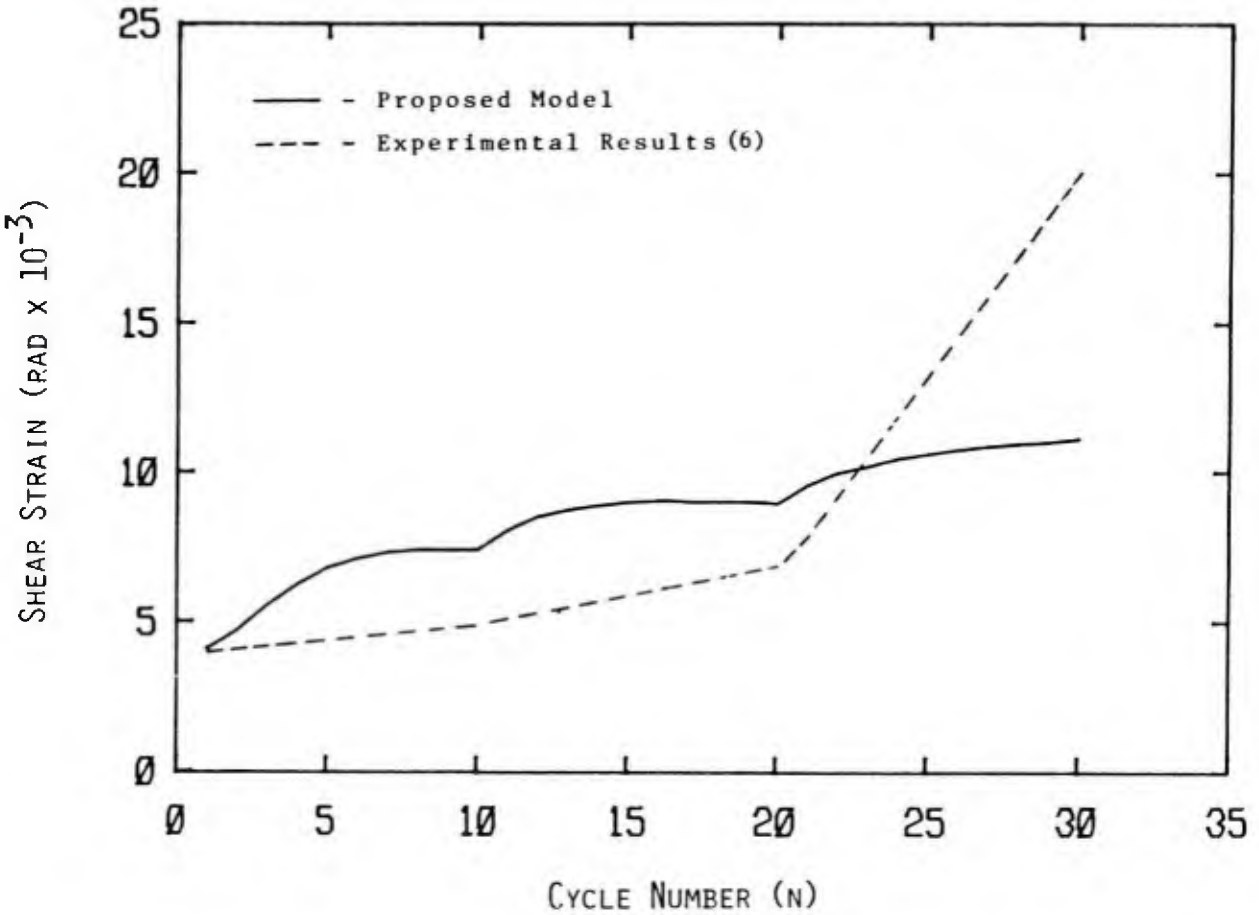

Figure A.18: Shear Strain vs. Cycle Number for 0.9B Specimen

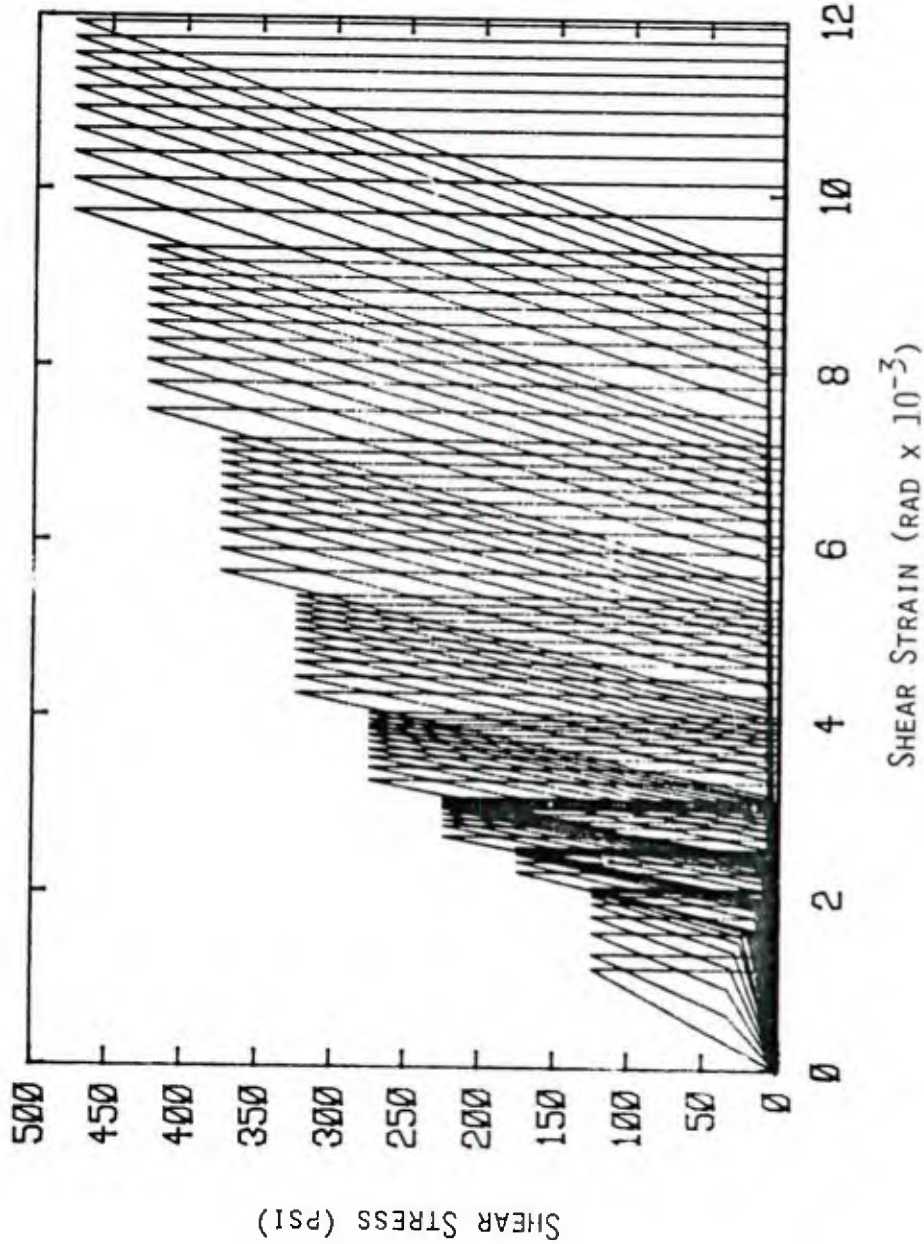

FIGURE A.19: STRESS-STRAIN HISTORY FOR 2-0.3B SPECIMEN

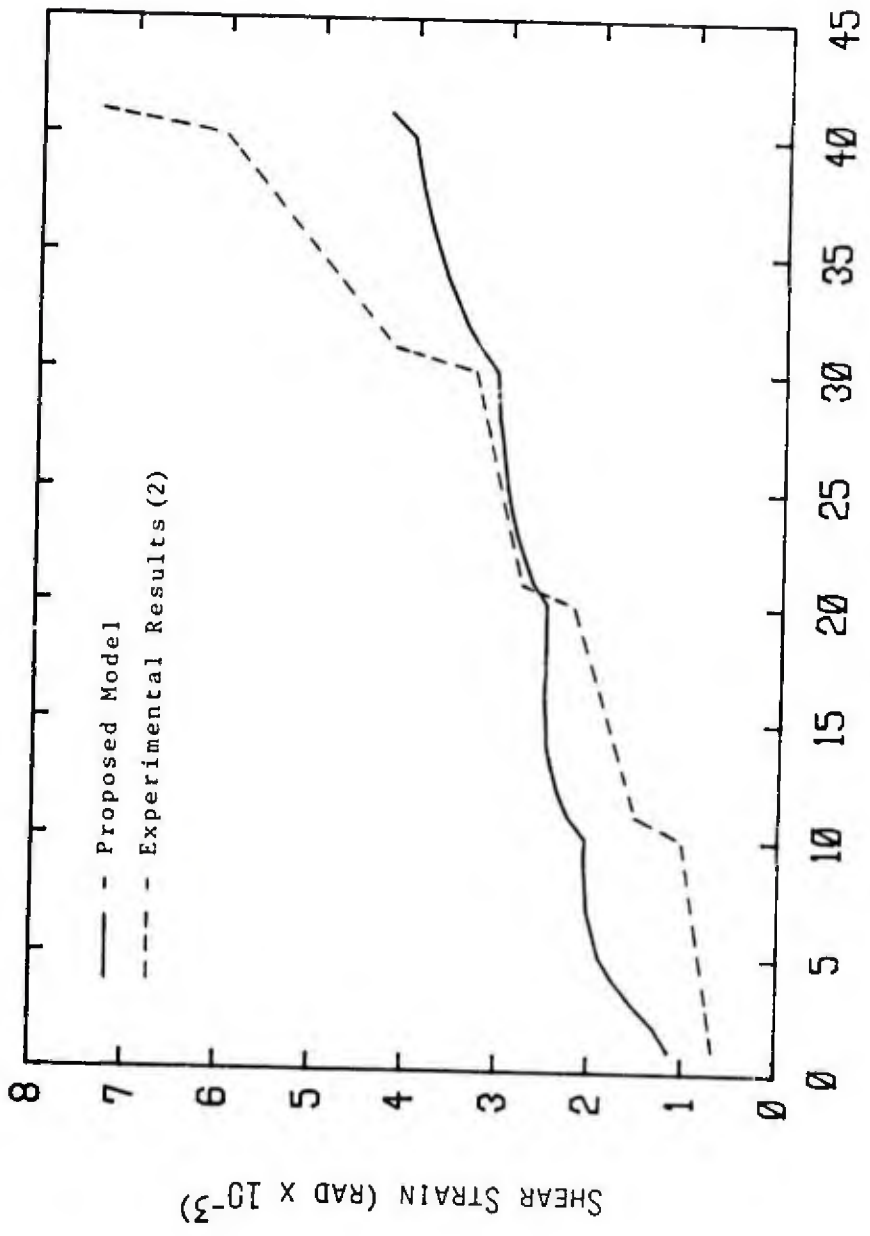

FIGURE A.20: SHEAR STRAIN VS. CYCLE NUMBER FOR 2-0.3B SPECIMEN

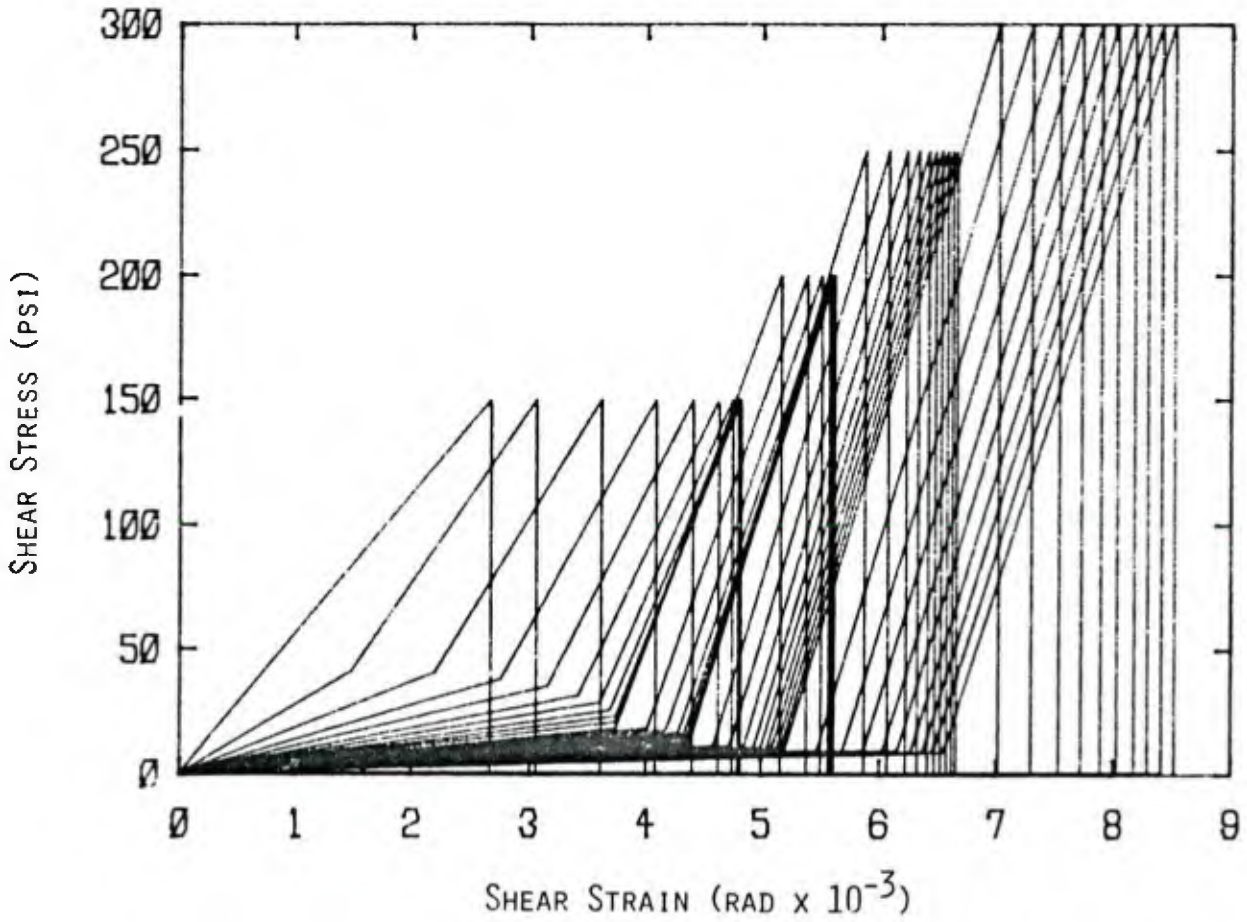

FIGURE A.21: STRESS-STRAIN HISTORY FOR 2-0.6A SPECIMEN

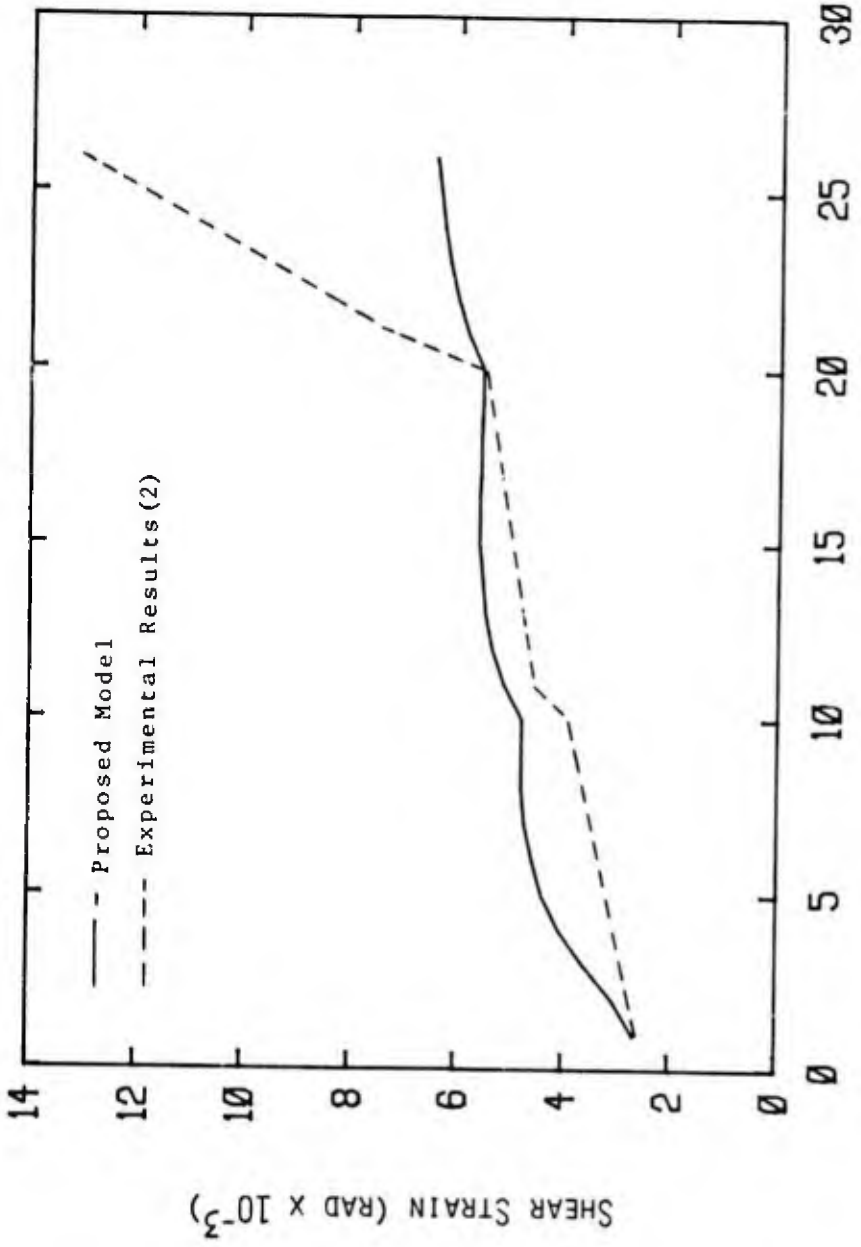

Figure A.22: Shear Strain vs. Cycle Number for 2-0.6A Specimen

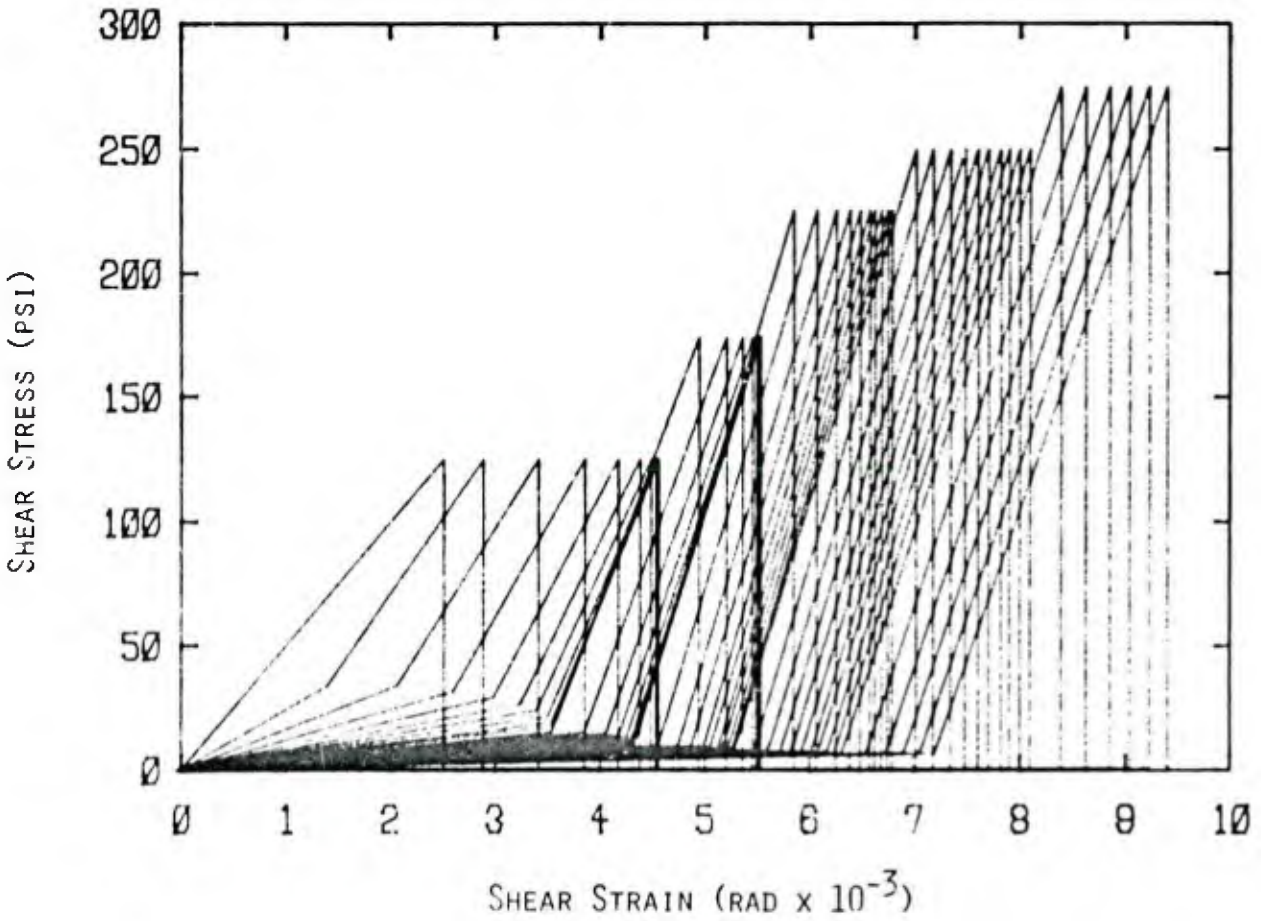

FIGURE A.23: STRESS-STRAIN HISTORY FOR 2-0.6B SPECIMEN

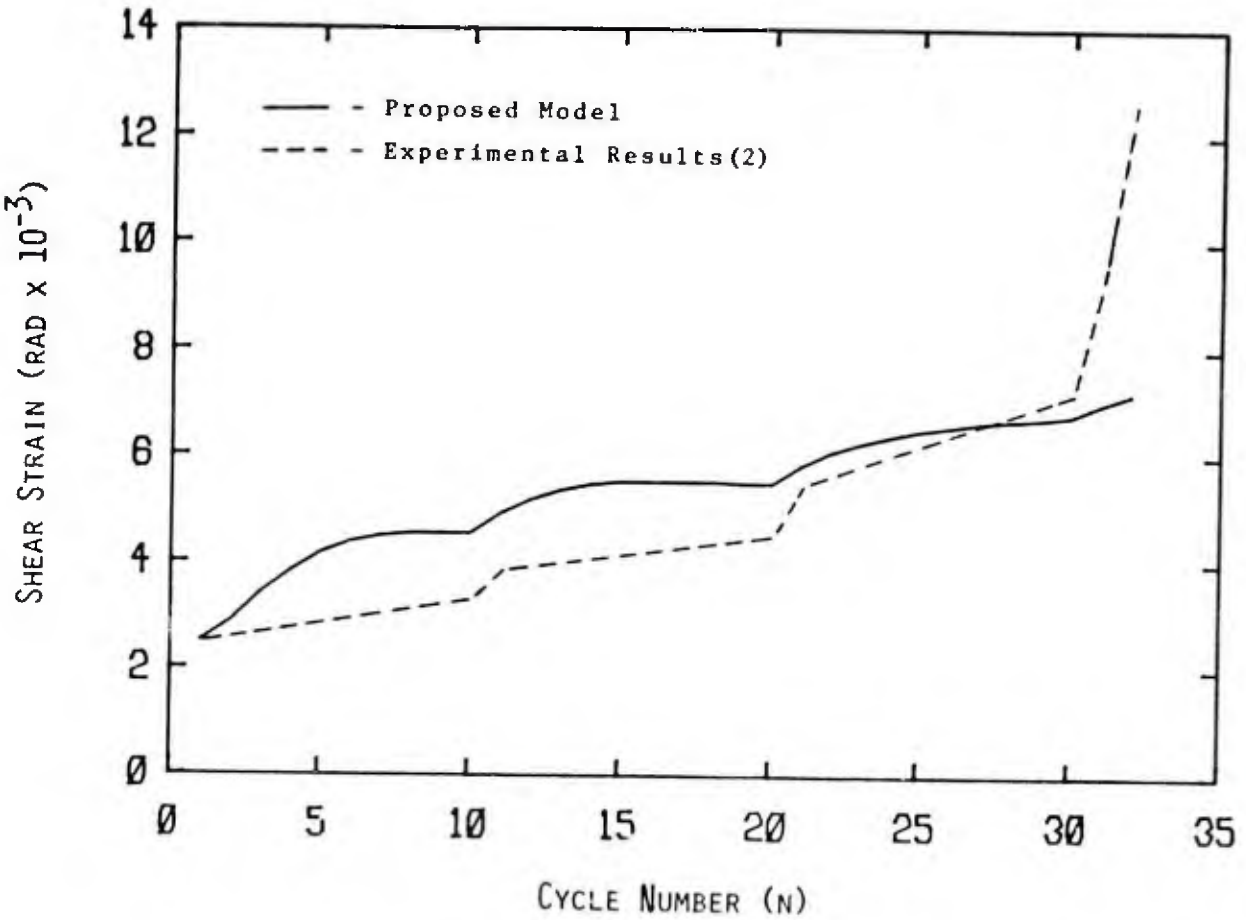

Figure A.24: Shear Strain vs. Cycle Number for 2-0.6B Specimen

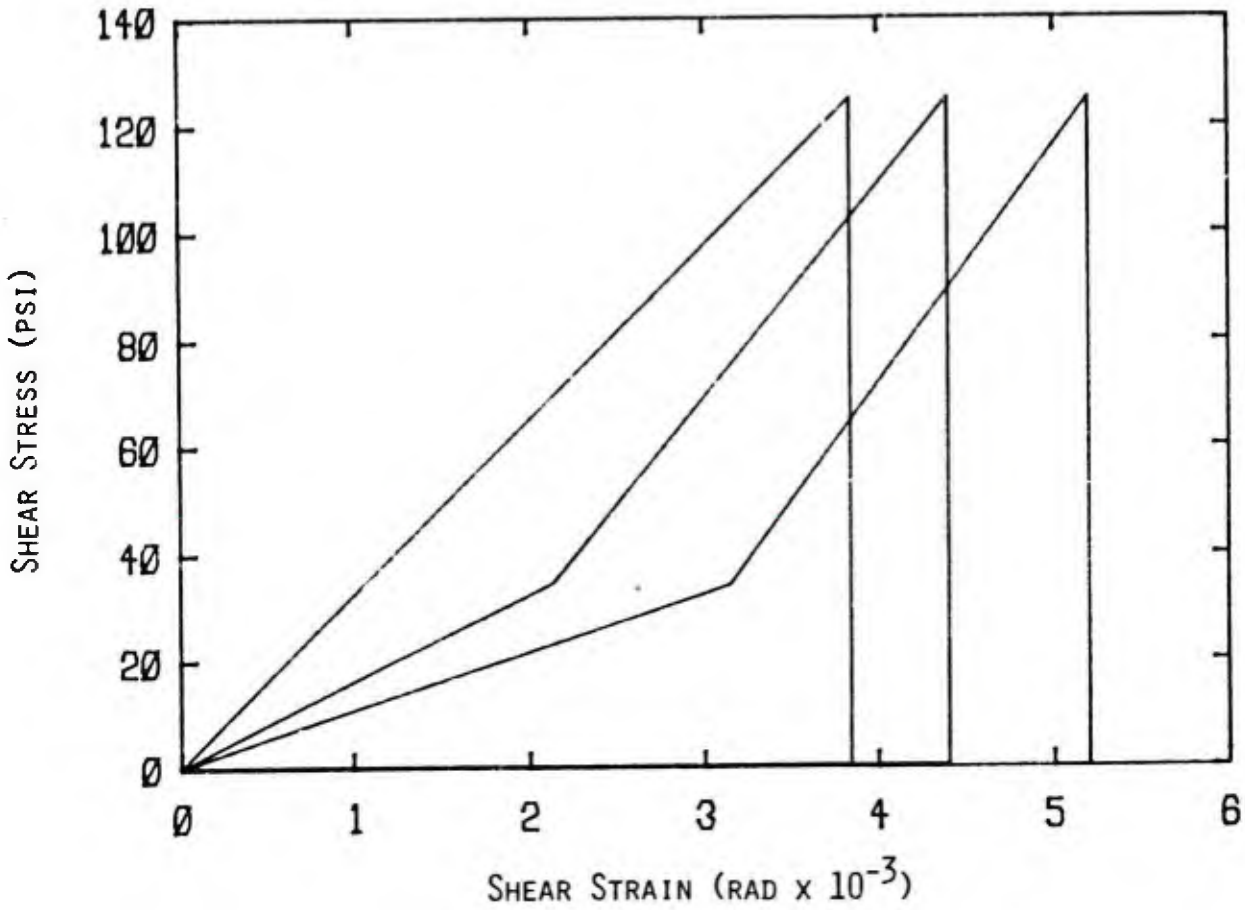

FIGURE A.25: STRESS-STRAIN HISTORY FOR 2-0.9A SPECIMEN

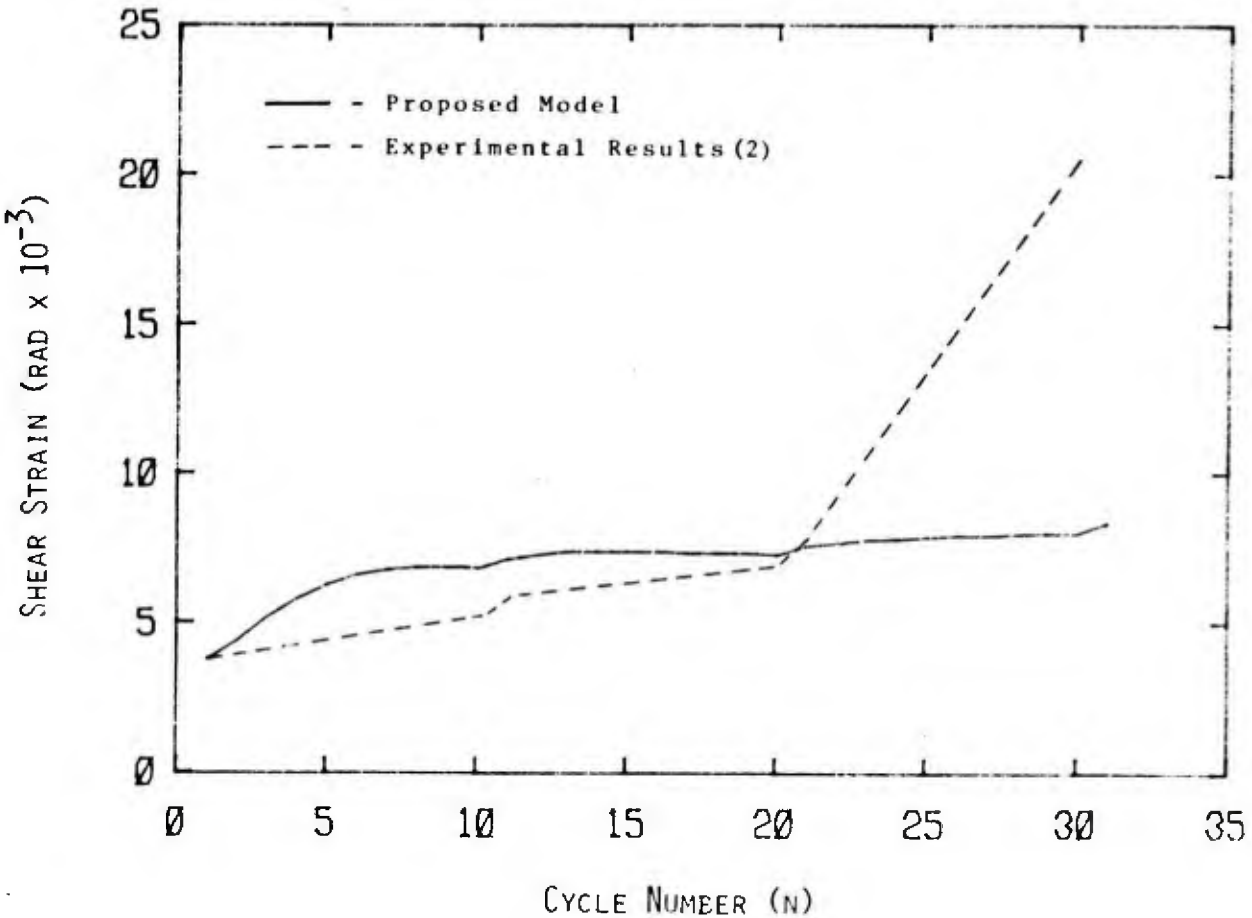

Figure A.26: Shear Strain vs. Cycle Number for 2-0.9A Specimen

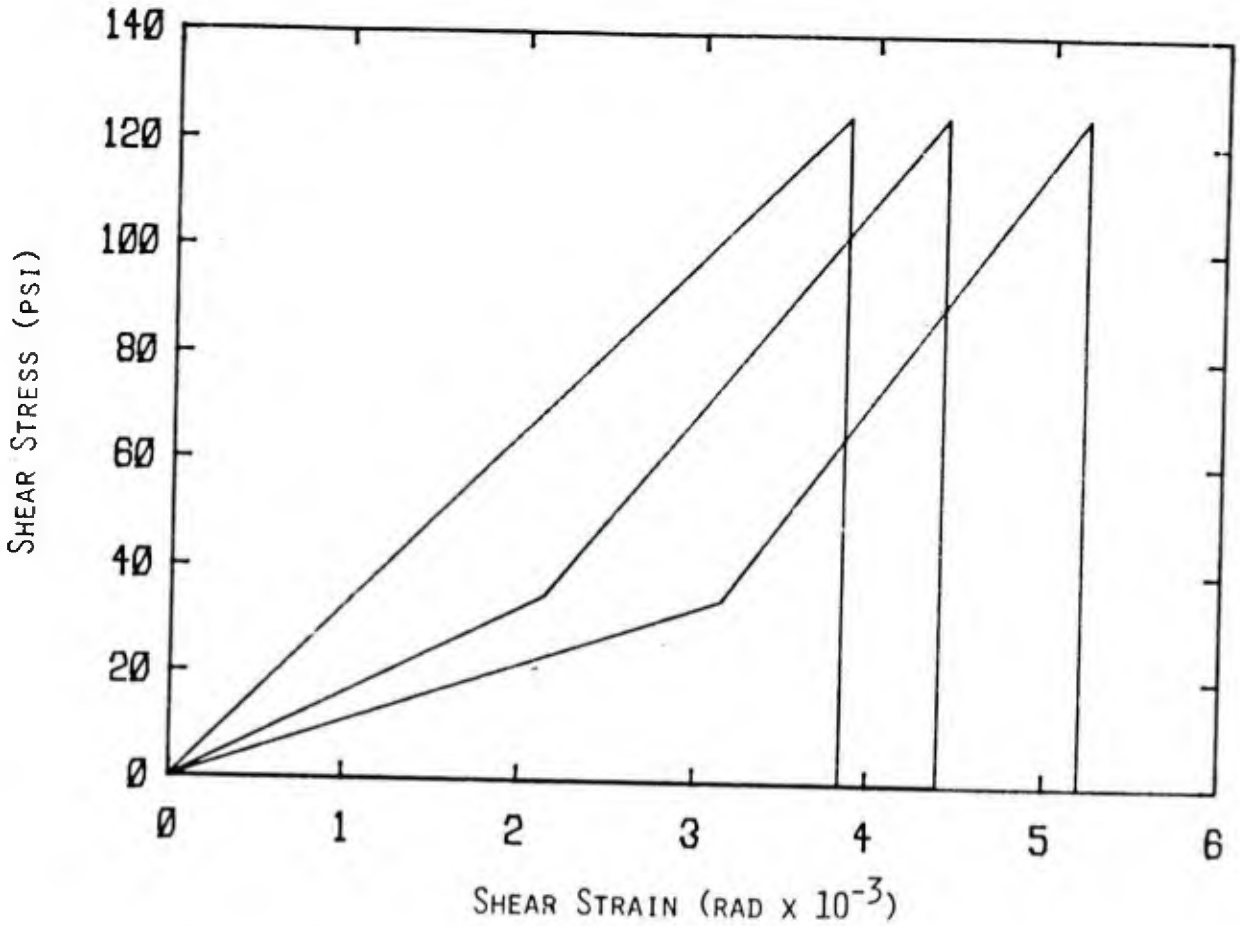

Figure A.27: Stress-Strain History for 2-0.9B Specimen

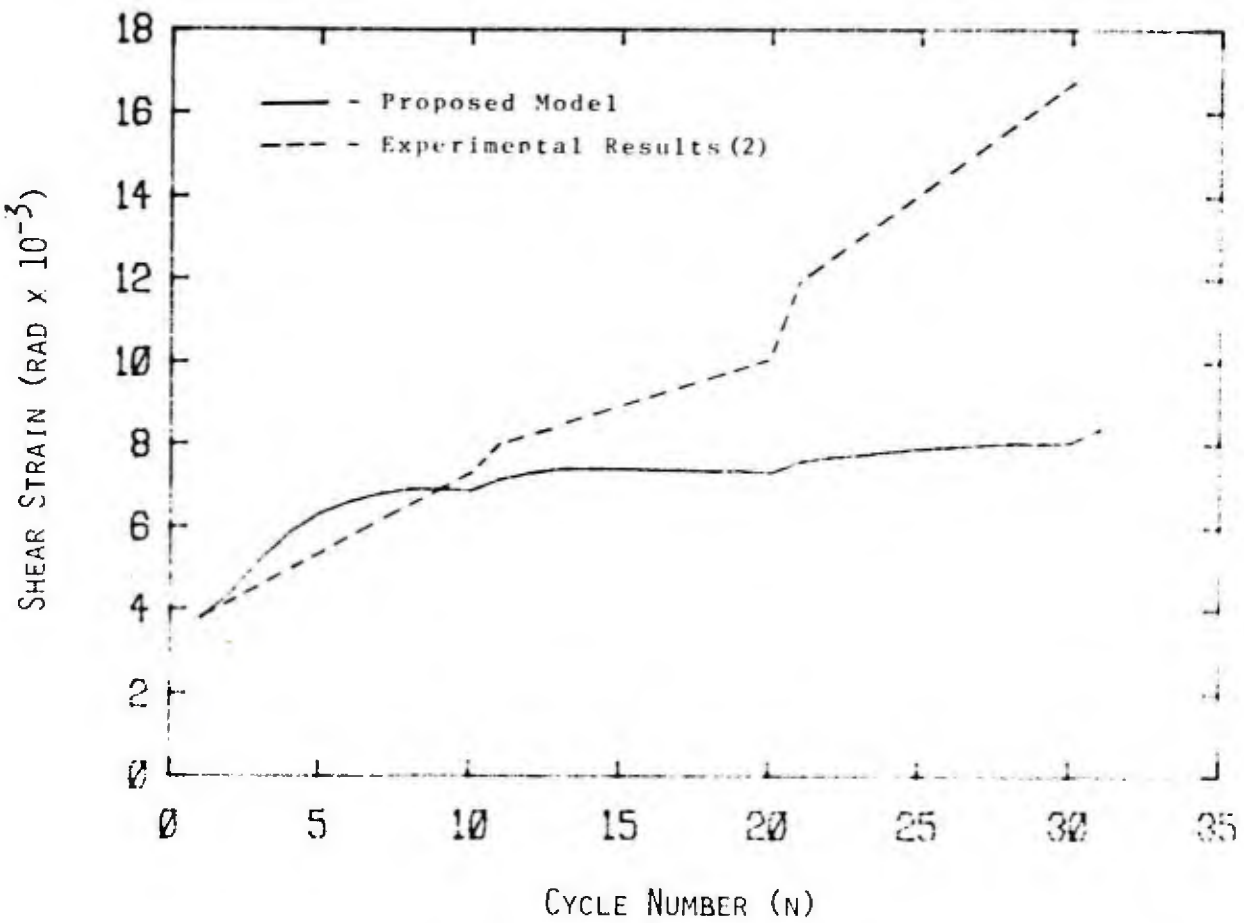

FIGURE A.28: SHEAR STRAIN VS. CYCLE NUMBER FOR 2-0.9B SPECIMEN

APPENDIX B

Orthogonal/ Diagonal Program Users Manual

The required inputs for this program are the same as those for the Orthogonal model program given in Appendix B. In the first card the material properties, the first cycle stiffness, the number of cycles in the shear load history, and the other control information is given. In the following cards the maximum shear stress achieved during each cycle is listed. For more details refer to the users manual given in Appendix B.

FIGURE B.1: ORTHOGONAL/DIAGONAL PROGRAM USERS MANUAL

```
C*************************************************************
C*                      CYCLIC SHEAR MODEL                   *
C*          ORTHOGONAL AND DIAGONAL REINFORCEMENT            *
C*************************************************************
C
      DIMENSION A(2,400),B(2,100),P(100),ET(100),XSCL(4)
C  READ INITIAL STIFFNESS(T), NO. OF CYCLES(N),
C  INITIAL PRETENSIONING(FP), AND MATERIAL PROPERTIES
      READ(5,*)T,N,FP,FY,E,JP
C  READ VECTOR OF MAXIMUM SHEAR STRESS APPLIED IN EACH CYCLE
      READ(5,*) (P(I),I=1,N)
C  UNLOADING STIFFNESS(T3)
      T3=1000000000.
C  READ OR DEFAULT CORRESPONDING VALUE OF E AND FY
      IF (FY .EQ. 0.) GO TO 5
      GO TO 6
5     FY=60.
6     IF (E .EQ. 0.) GO TO 7
      GO TO 8
7     E=30000.
C  CALCULATE THE YIELD STRAIN(EY)
8     EY=FY/E*1000.
C  CALCULATE INITIAL STEEL STRAIN(EO) DUE TO PRETENSIONING
      EO=(FP*1000)/(E*2.5)
      ET(1)=EO
      B(1,1)=0
      B(2,1)=ET(1)
C  CALCULATE THE FIRST CYCLE RESPONSE
      A(1,1)=0.
      A(2,1)=0.
      A(1,2)=P(1)/T
      A(2,2)=P(1)
      A(1,3)=A(1,2)-P(1)/T3
      A(2,3)=0.
      XS=A(1,2)
      F=9.23*(FP/FY)-1.94
      ET(2)=EO+A(1,2)/F
      B(1,2)=1
      B(2,2)=ET(2)
      IF (ET(2) .GE. EY) GO TO 20
C   CALCULATE RESPONSE FOR CYCLES 2 TO N
      DO 10 I=2,N
      K=(I-1)*4
C   CALCULATE THE FREE SLIP STIFFNESS(T1)
      T1=T*(-0.0039*FLOAT(I)+0.50)
```

```
C     CALCULATE THE CONTACT STIFFNESS(T2)
      IF (I .LE. 22) GO TO 15
      T2=T*(-0.034*FLOAT(I)+2.38)
      GO TO 16
15    T2=T*(-0.0060*FLOAT(I)+1.75)
16     A(1,K)=0.
      A(2,K)=0.
C     CALCULATE THE FREE SLIP(STRAIN) FOR CYCLE N
      FS=XS*(-0.0035*FLOAT(I)+0.67)
      A(1,K+1)=FS
C     CALCULATE THE STRESS CORRESPONDING TO FREE SLIP(STRAIN)
      A(2,K+1)=FS*T1
C     CALCULATE THE MAXIMUM SLIP(STRAIN) FOR CYCLE N
      A(1,K+2)=A(1,K+1)+(P(I)-A(2,K+1))/T2
C     UPDATE THE MAXIMUM SLIP(STRAIN)
      IF(A(1,K+2).GT.XS) XS=A(1,K+2)
C     CALCULATE THE MAXIMUM STRESS FOR CYCLE N
      A(2,K+2)=P(I)
C     CALCULATE THE TOTAL STEEL STRAIN(ET)
      N1=I+1
      ET(N1)=EO+A(1,K+2)/F
      B(1,N1)=I
      B(2,N1)=ET(N1)
C     UNLOAD TO ZERO STRESS LEVEL
      A(1,K+3)=A(1,K+2)-P(I)/T3
      A(2,K+3)=0.
      NP=4*I-1
      IF (JP .EQ. 1) GO TO 10
      IF (ET(N1) .GE. EY) GO TO 20
10    CONTINUE
C     CALL SUBROUTINE TO PLOT SHEAR STRESS VS STRAIN(SLIP) HISTORY
20    CALL QPICTR(A,2,NP,QX(1),QY(2),QLABEL(12))
C     CALL SUBROUTINE TO PLOT STEEL STRAIN VS. CYCLE NUMBER
      CALL QPICTR(B,2,N1,QX(1),QY(2),QLABEL(12))
      STOP
      END
```

FIGURE B.2: COMPUTER PROGRAM FOR ORTHOGONAL/DIAGONAL MODEL

(a) Input data for Cornell 4-0.6A specimen:

```
109.790  59  40.2  67.0  26000.  1
150.  150.  150.  150.  150.  150.  150.  150.  150.  150.
200.  200.  200.  200.  200.  200.  200.  200.  200.  200.
250.  250.  250.  250.  250.  250.  250.  250.  250.  250.
300.  300.  300.  300.  300.  300.  300.  300.  300.  300.
350.  350.  350.  350.  350.  350.  350.  350.  350.  350.
375.  375.  375.  375.  375.  375.  375.  375.  375.
```

(b) Input data for load history number 1:

```
109.790  55  40.2  67.0  26000.  1
150.  150.  150.  150.  150   150.  150.  150.  150.  150.
200.  200.  200.  200.  200.  200.  200.  200.  200.  200.
250.  250.  250.  250.  250.  250.  250.  250.  250.  250.
300.  300.  300.  300.  300.  300.  300.  300.  300.  300.
350.  350.  350.  350.  350.  350.  350.  350.  350.  350.
350.  350.  350.  350.  350.
```

(c) Input data for load history number 2:

```
109.790  60  40.2  67.0  26000.  1
100.  100.  100.  100.  100.  100.  100.  100.  100.  100.
150.  150.  150.  150.  150   150.  150.  150.  150.  150.
200.  200.  200.  200.  200.  200.  200.  200.  200.  200.
240.  240.  240.  240.  240.  240.  240.  240.  240.  240.
280.  280.  280.  280.  280.  280.  280.  280.  280.  280.
320.  320.  320.  320.  320.  320.  320.  320.  320.  320.
```

(d) Input data for load history number 3:

```
109.790  60  40.2  67.0  26000.  1
100.  100.  100.  100.  100.  100.  100.  100.  100.  100.
150.  150.  150.  150.  150   150.  150.  150.  150.  150.
190.  190.  190.  190.  190.  190.  190.  190.  190.  190.
230.  230.  230.  230.  230.  230.  230.  230.  230.  230.
270.  270.  270.  270.  270.  270.  270.  270.  270.  270.
300.  300.  300.  300.  300.  300.  300.  300.  300.  300.
```

(e) Input data for load history number 4:

```
109.790   60   40.2   67.0   26000.   1
 50.    50.    50.    50.    50.    50.    50.    50.    50.    50.
100.   100.   100.   100.   100.   100.   100.   100.   100.   100.
150.   150.   150.   150.   150    150.   150.   150.   150.   150.
190.   190.   190.   190.   190.   190.   190.   190.   190.   190.
240.   240.   240.   240.   240.   240.   240.   240.   240.   240.
280.   280.   280.   280.   280.   280.   280.   280.   280.   280.
```

(f) Input data for load history number 5:

```
109.790   60   40.2   67.0   26000.   1
 25.    25.    25.    25.    25.    25.    25.    25.    25.    25.
 50.    50.    50.    50.    50.    50.    50.    50.    50.    50.
100.   100.   100.   100.   100.   100.   100.   100.   100.   100.
150.   150.   150.   150.   150    150.   150.   150.   150.   150.
200.   200.   200.   200.   200.   200.   200.   200.   200.   200.
250.   250.   250.   250.   250.   250.   250.   250.   250.   250.
```

(g) Input data for Cornell 4-0.9A specimen:

```
51.941   46   60.3   67.0   26000.   1
125.   125.   125.   125.   125.   125.   125.   125.   125.   125.
175.   175.   175.   175.   175.   175.   175.   175.   175.   175.
225.   225.   225.   225.   225.   225.   225.   225.   225.   225.
275.   275.   275.   275.   275.   275.   275.   275.   275.   275.
300.   300.   300.   300.   300.   300.   300.   300.   300.   300.
```

(h) Input data for load history number 6:

```
51.941   50   60.3   67.0   26000.   1
100.   100.   100.   100.   100.   100.   100.   100.   100.   100.
150.   150.   150.   150.   150.   150.   150.   150.   150.   150.
200.   200.   200.   200.   200.   200.   200.   200.   200.   200.
235.   235.   235.   235.   235.   235.   235.   235.   235.   235.
270.   270.   270.   270.   270.   270.   270.   270.   270.   270.
```

(i) Input data for load history number 7:

```
51.941   50   60.3   67.0   26000.   1
130.  130.  130.  130.  130.  130.  130.  130.  130.  130.
175.  175.  175.  175.  175.  175.  175.  175.  175.  175.
215.  215.  215.  215.  215.  215.  215.  215.  215.  215.
250.  250.  250.  250.  250.  250.  250.  250.  250.  250.
275.  275.  275.  275.  275.  275.  275.  275.  275.  275.
```

(j) Input data for load history number 8:

```
51.941   50   60.3   67.0   26000.   1
100.  100.  100.  100.  100.  100.  100.  100.  100.  100.
150.  150.  150.  150.  150.  150.  150.  150.  150.  150.
200.  200.  200.  200.  200.  200.  200.  200.  200.  200.
240.  240.  240.  240.  240.  240.  240.  240.  240.  240.
275.  275.  275.  275.  275.  275.  275.  275.  275.  275.
```

FIGURE B.3: INPUT DATA FOR ORTHOGONAL/DIAGONAL SPECIMENS

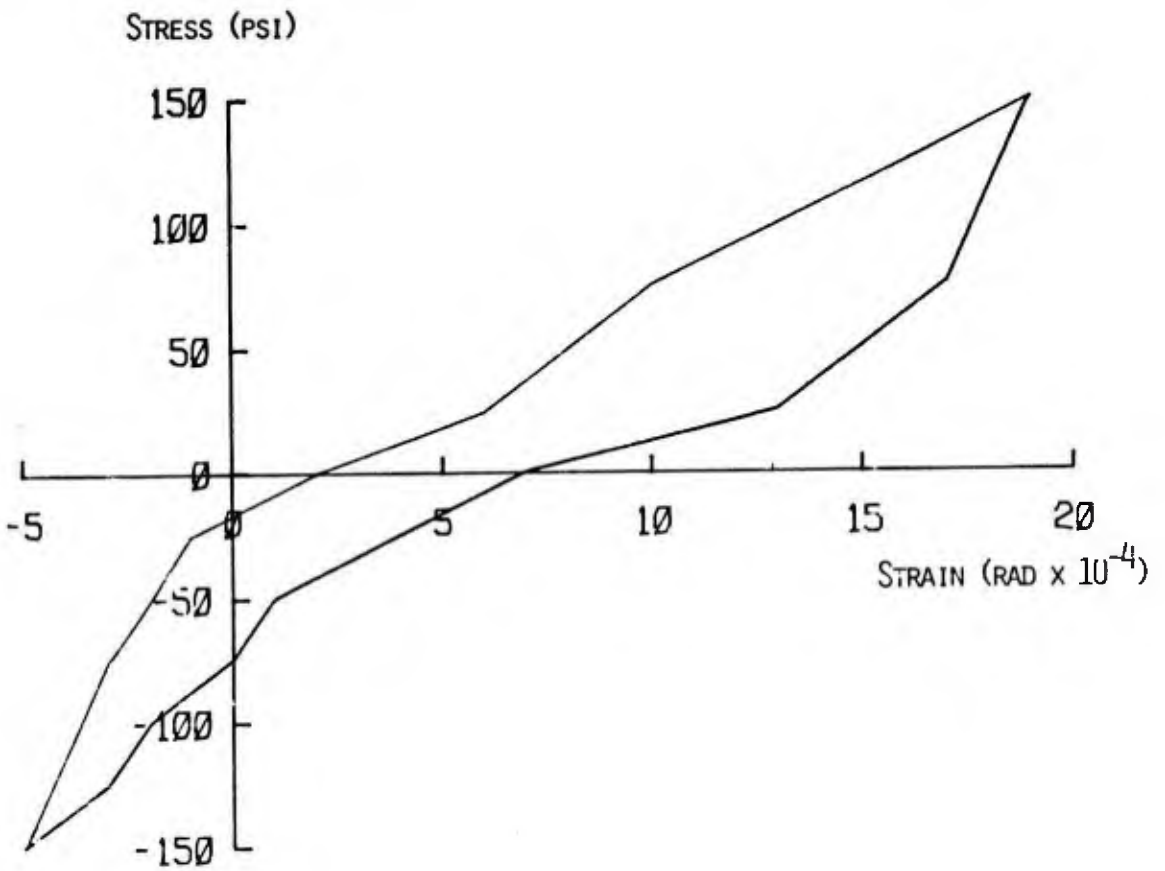

FIGURE B.4: STRESS-STRAIN HISTORY FOR SPECIMEN 4-0.6A FOR CYCLE 1 (2)

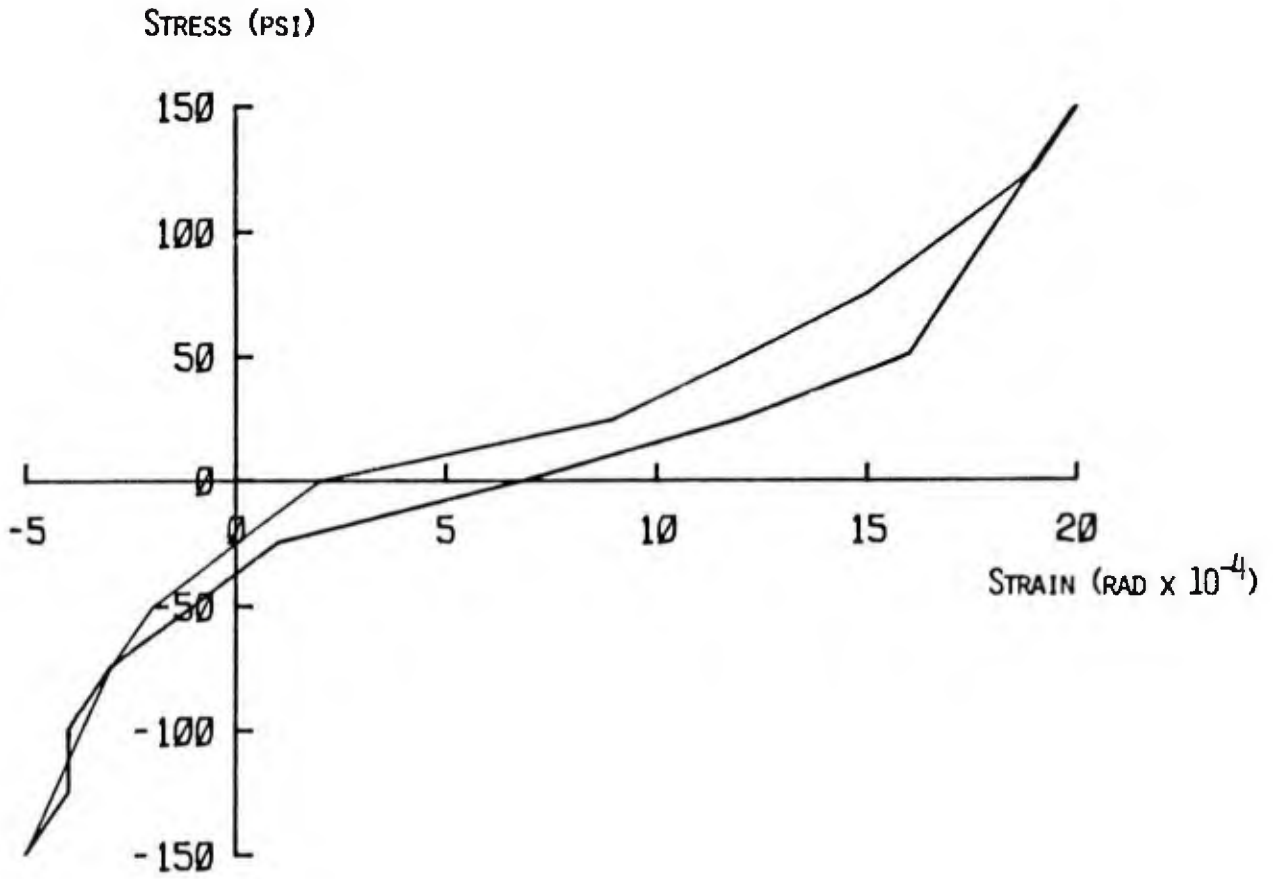

FIGURE B.5: CYCLE 2 STRESS-STRAIN HISTORY FOR 4-0.6A SPECIMEN (2)

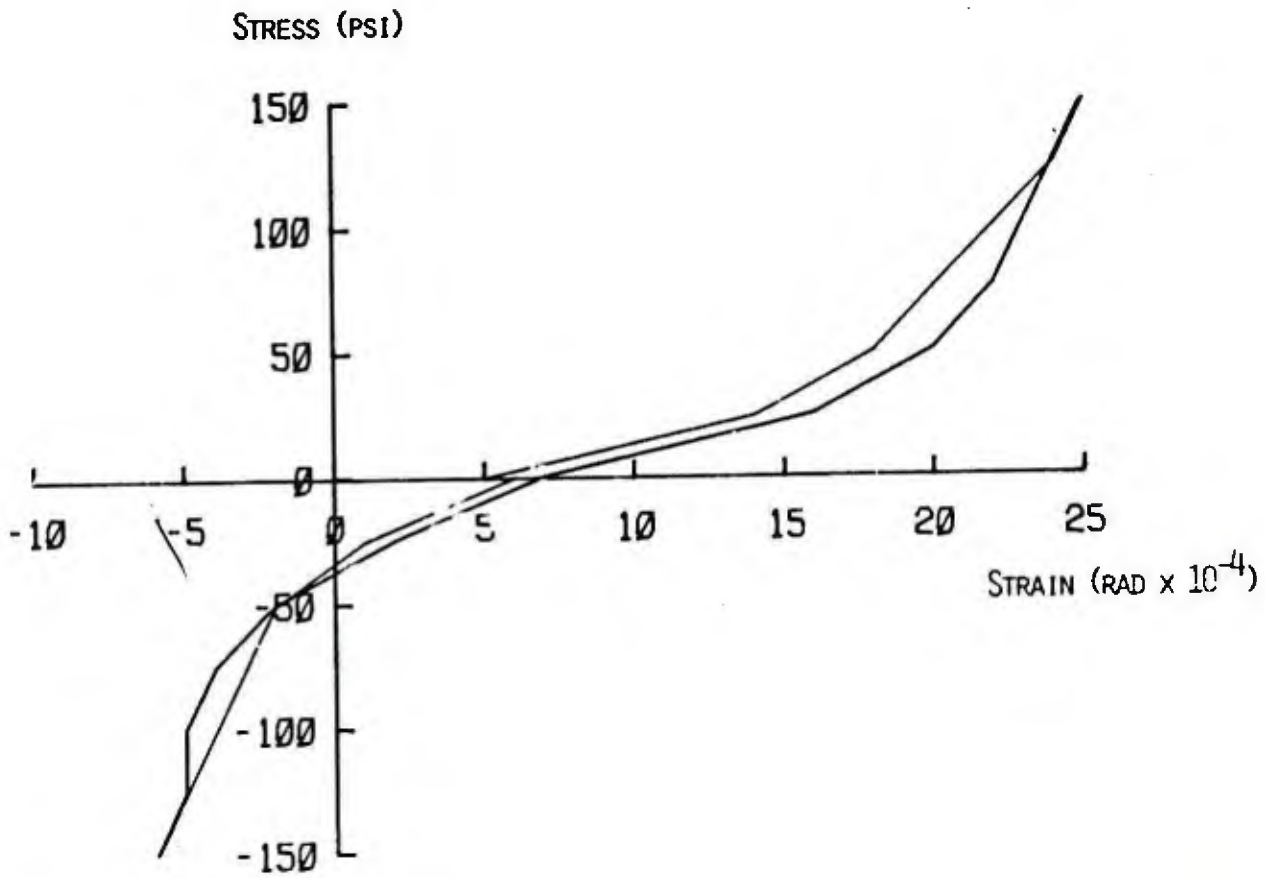

FIGURE B.6: CYCLE 10 STRESS-STRAIN HISTORY FOR 4-0.6A SPECIMEN (2)

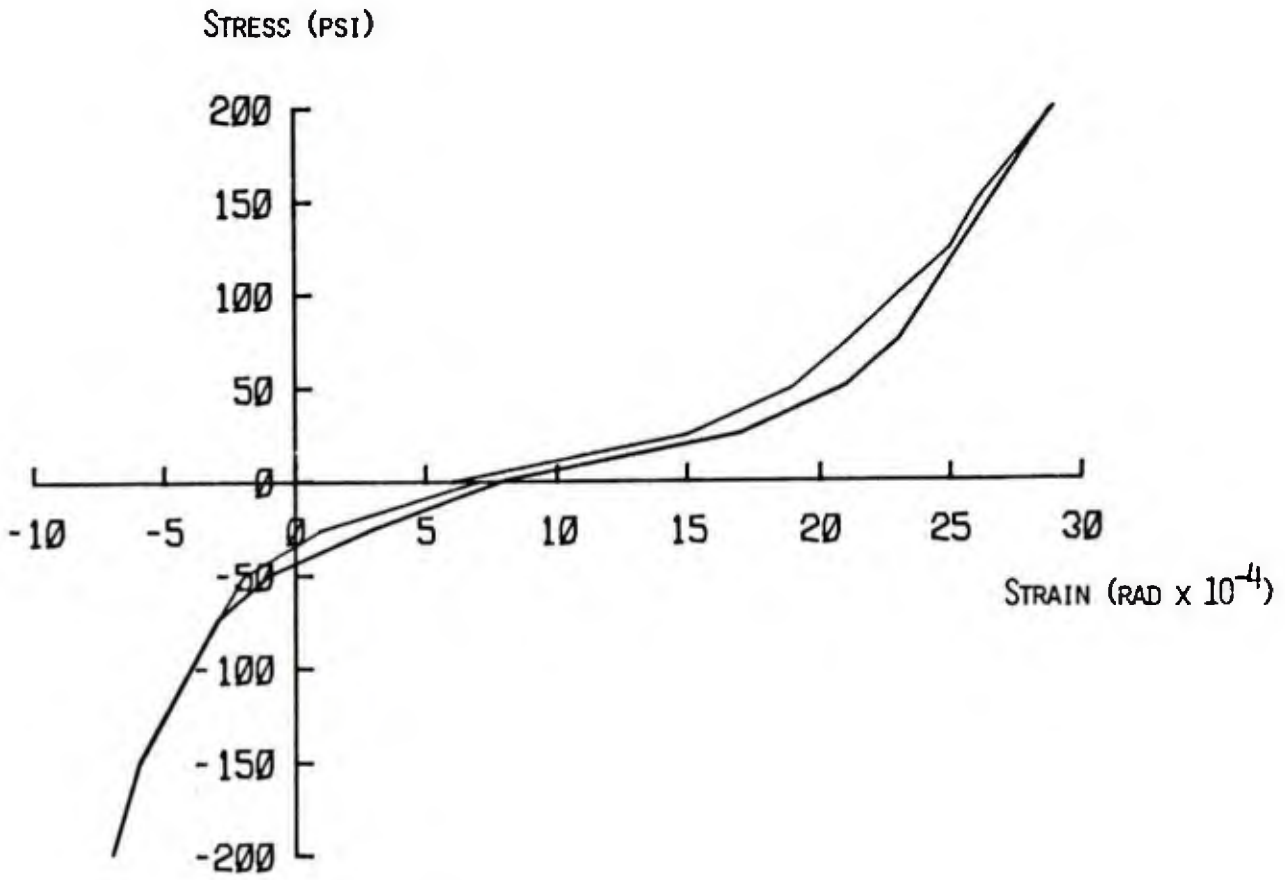

FIGURE B.7: CYCLE 11 STRESS-STRAIN HISOTRY FOR 4-0.6A SPECIMEN (2)

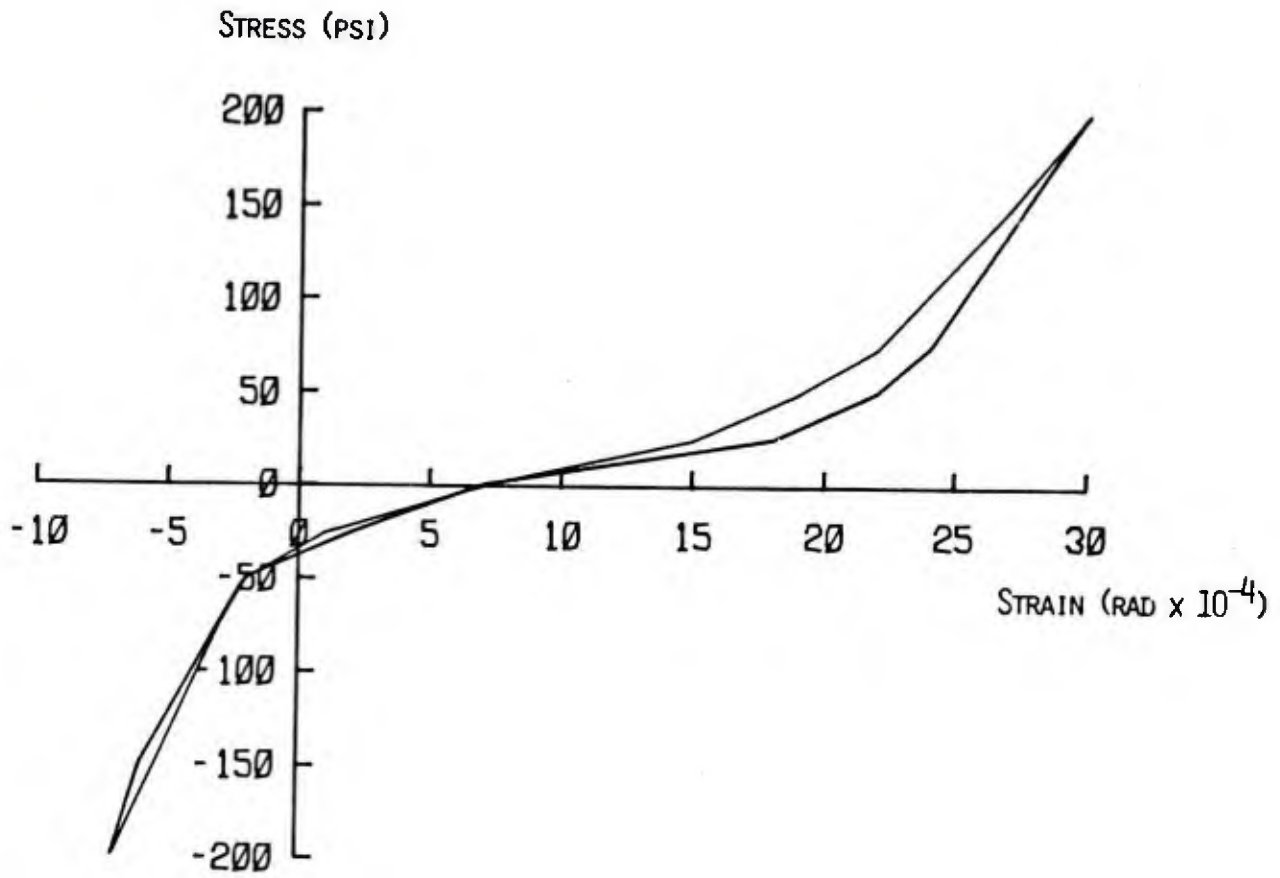

FIGURE B.8: CYCLE 12 STRESS-STRAIN CURVE FOR 4-0.6A SPECIMEN (2)

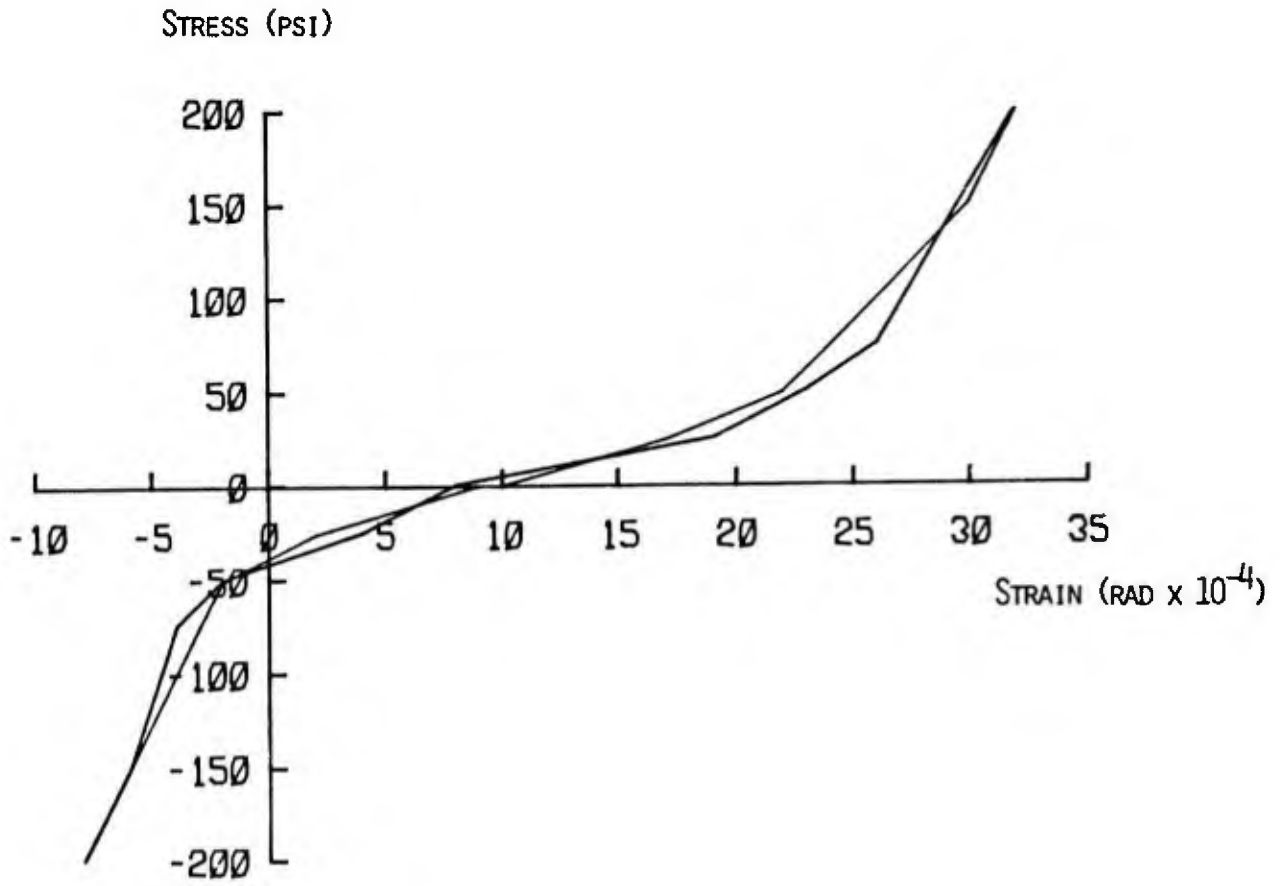

FIGURE B.9: CYCLE 20 STRESS-STRAIN CURVE FOR 4-0.6A SPECIMEN (2)

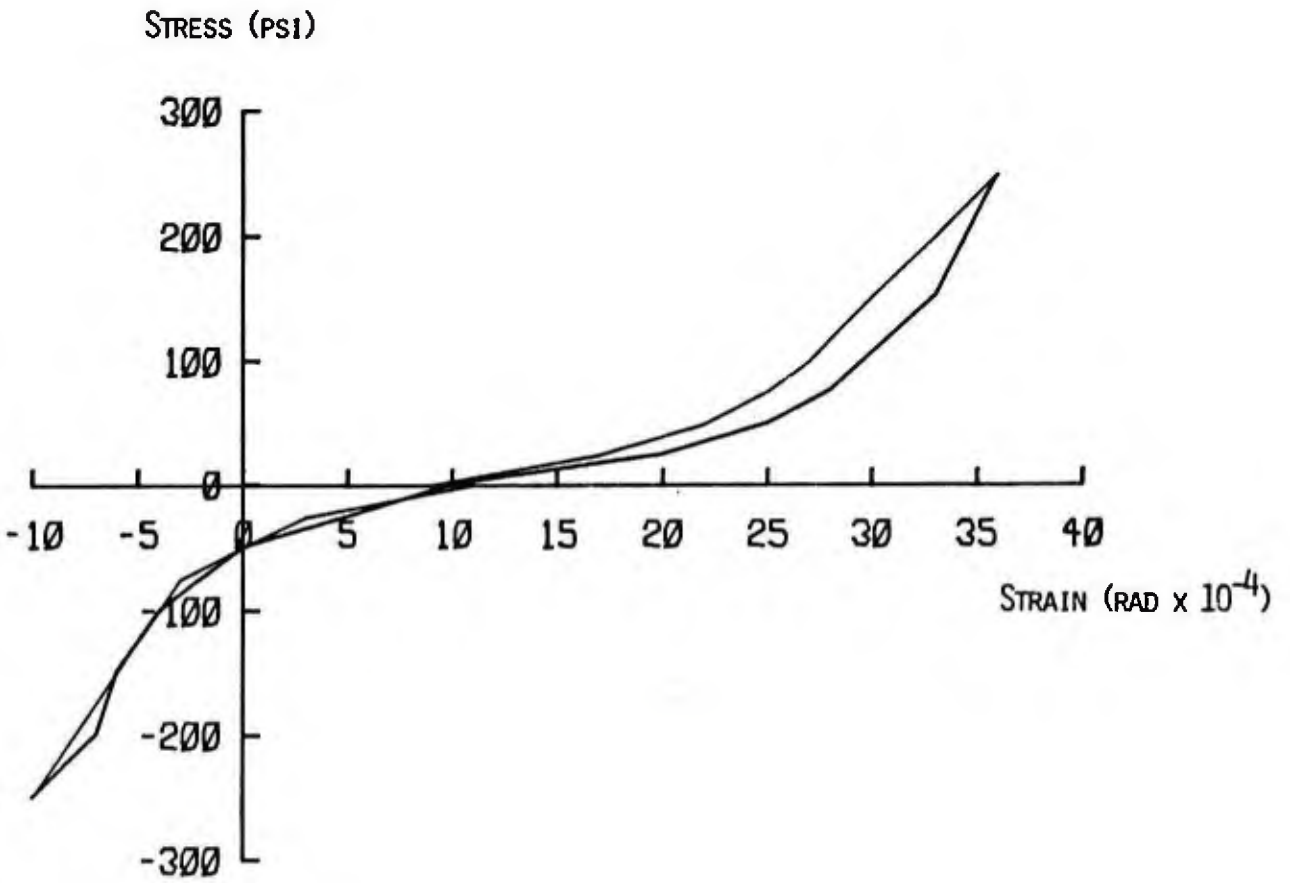

FIGURE B.10: CYCLE 21 STRESS-STRAIN HISTORY FOR 4-0.6A SPECIMEN (2)

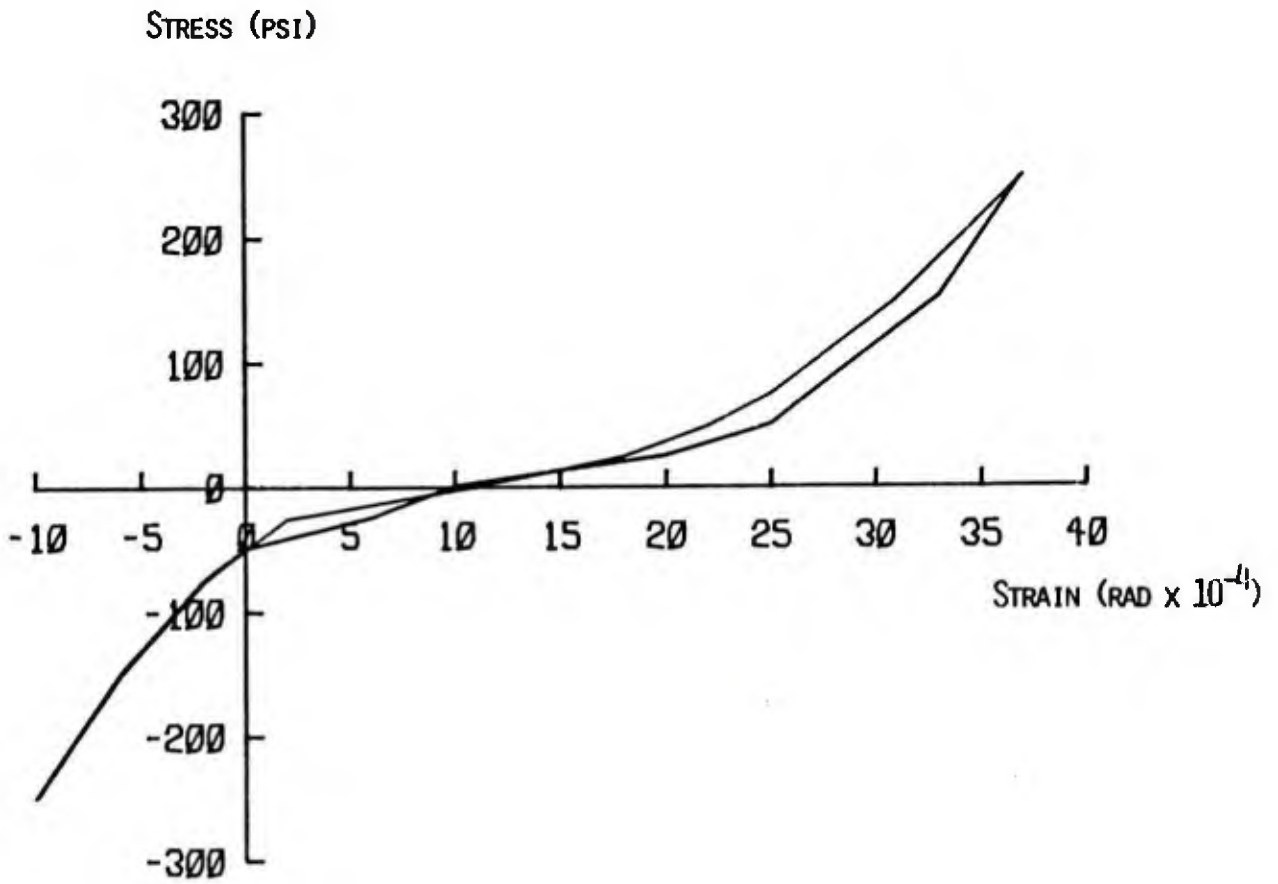

FIGURE B.11: CYCLE 22 STRESS-STRAIN HISTORY FOR SPECIMEN 4-0.6A (2)

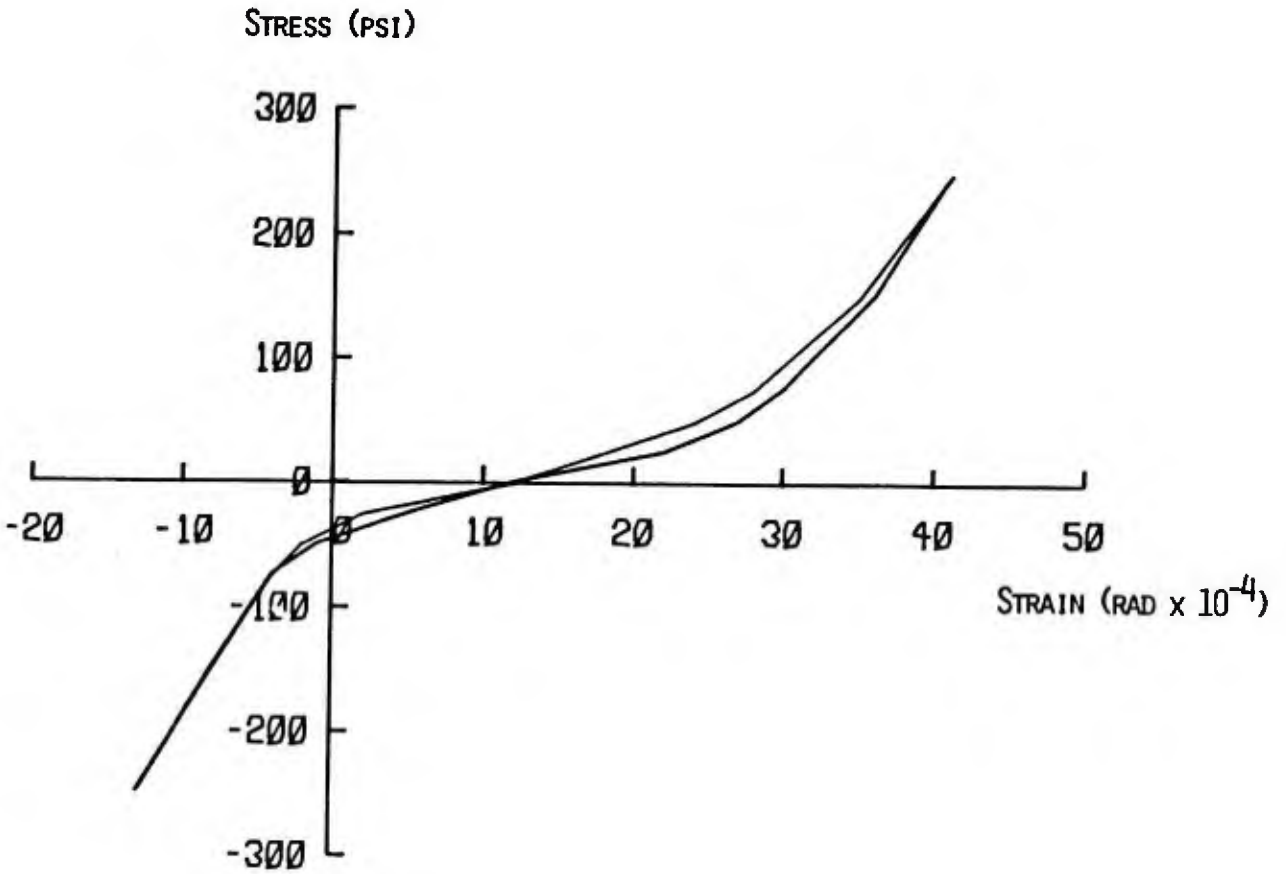

FIGURE B.12: CYCLE 30 STRESS-STRAIN HISTORY FOR 4-0.6A SPECIMEN (2)

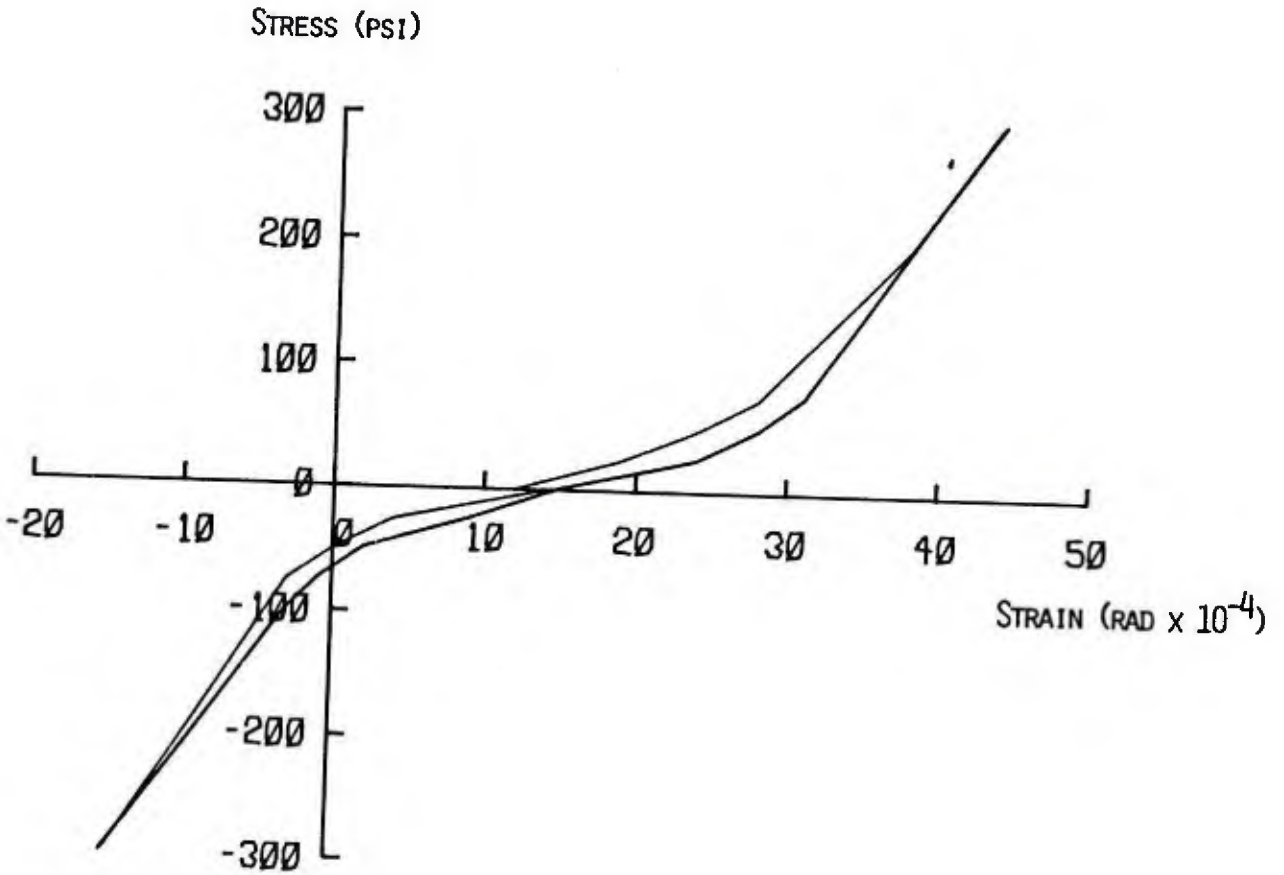

FIGURE B.13: CYCLE 31 STRESS-STRAIN HISTORY FOR 4-0.6A SPECIMEN (2)

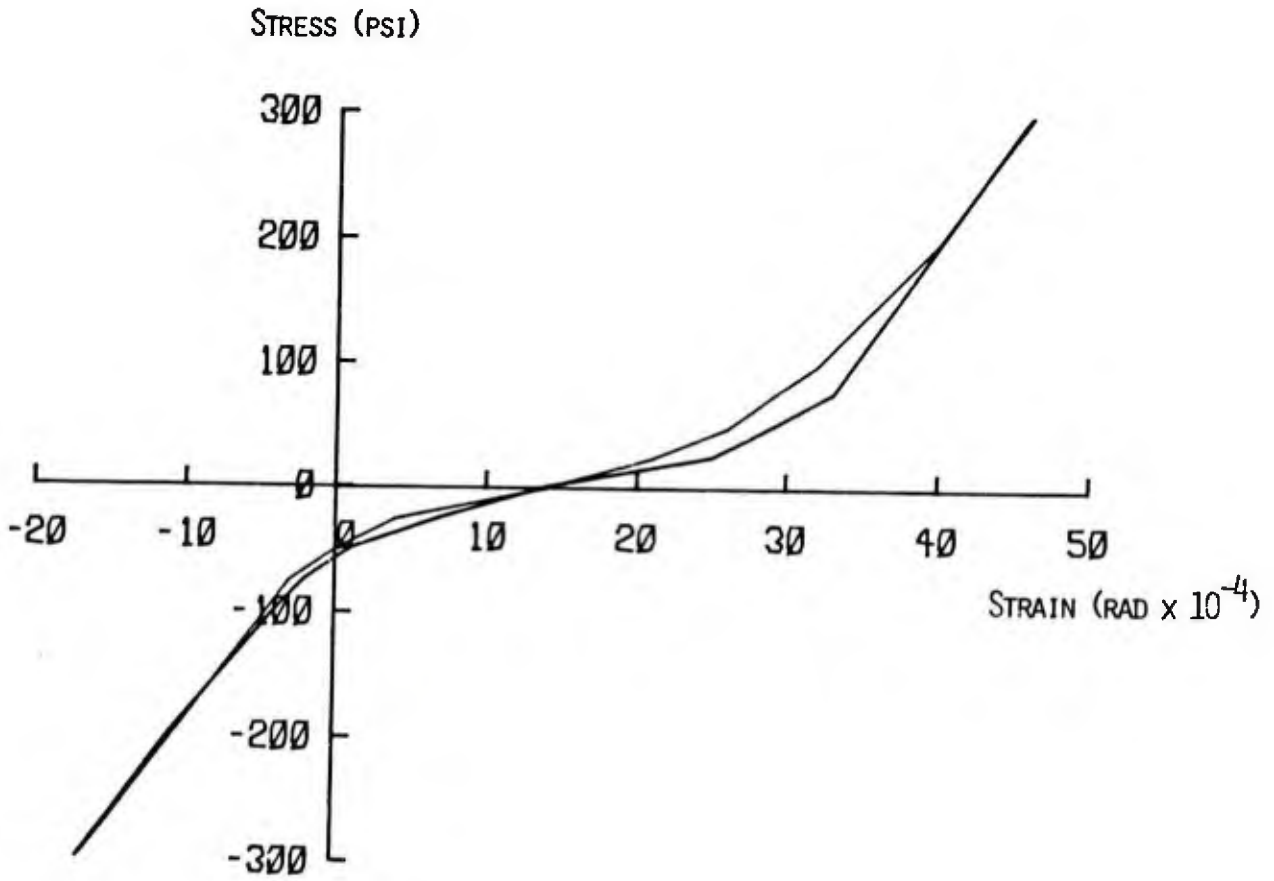

FIGURE B.14: CYCLE 32 STRESS-STRAIN HISTORY FOR 4-0.6M SPECIMEN (2)

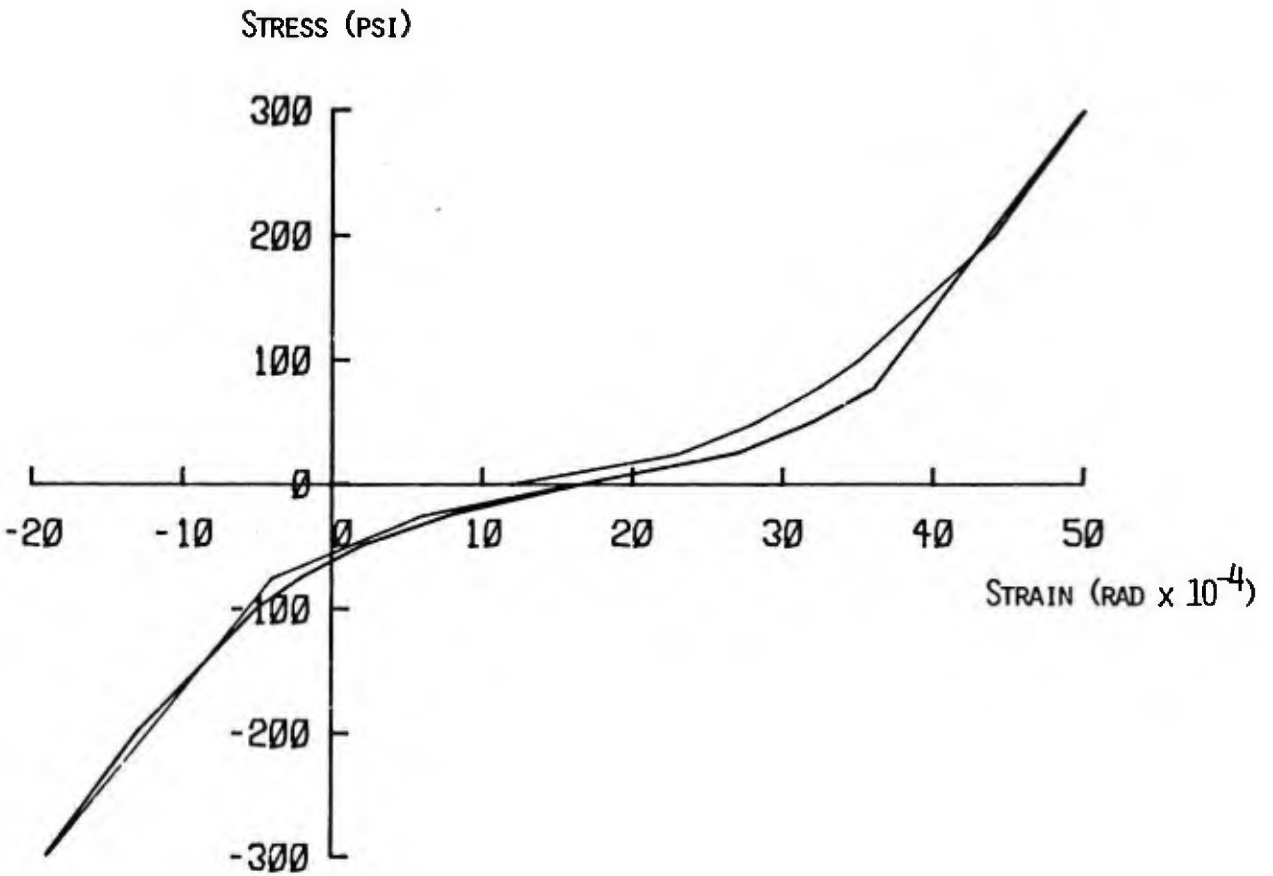

FIGURE B.15: CYCLE 40 STRESS-STRAIN HISTORY FOR 4-0.6A SPECIMEN (2)

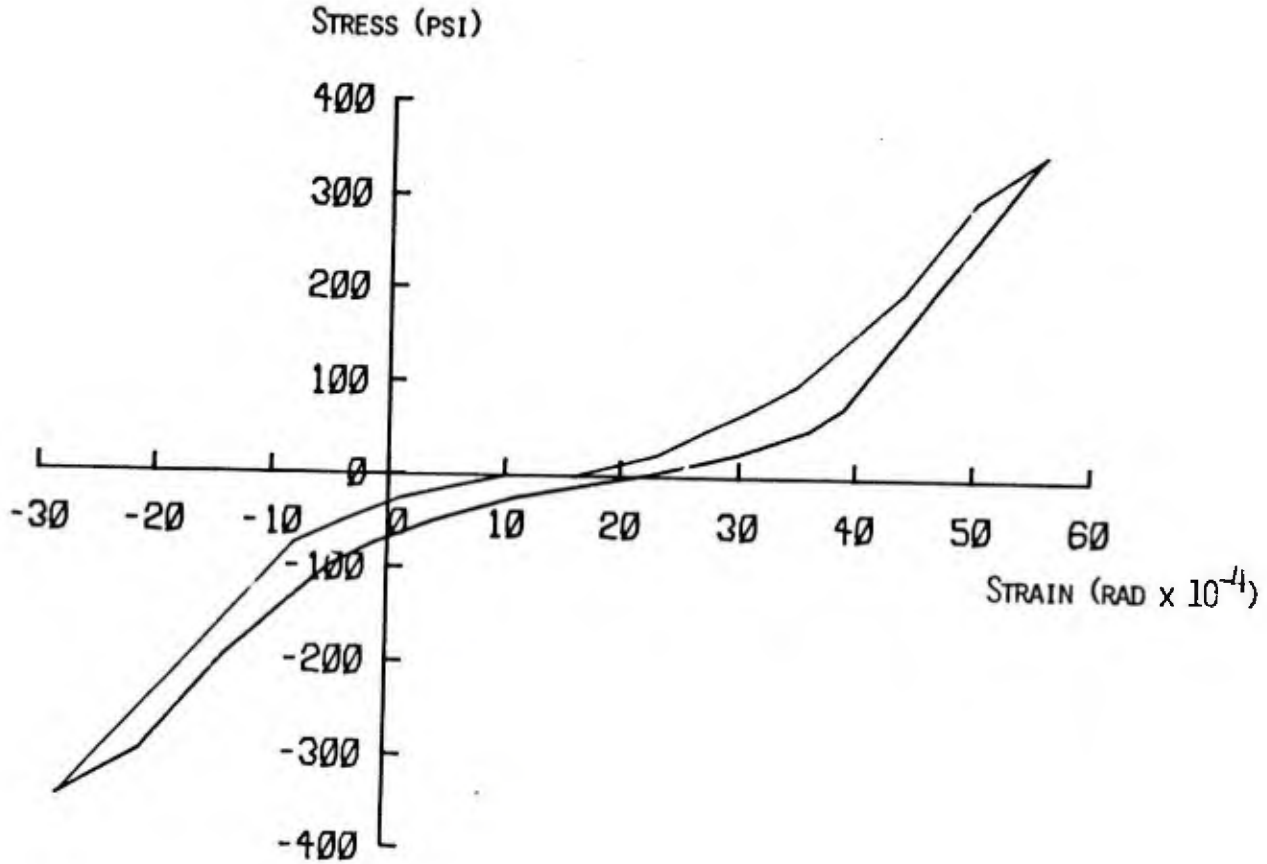

FIGURE B.16: CYCLE 41 STRESS-STRAIN HISTORY FOR 4-0.6A SPECIMEN (2)

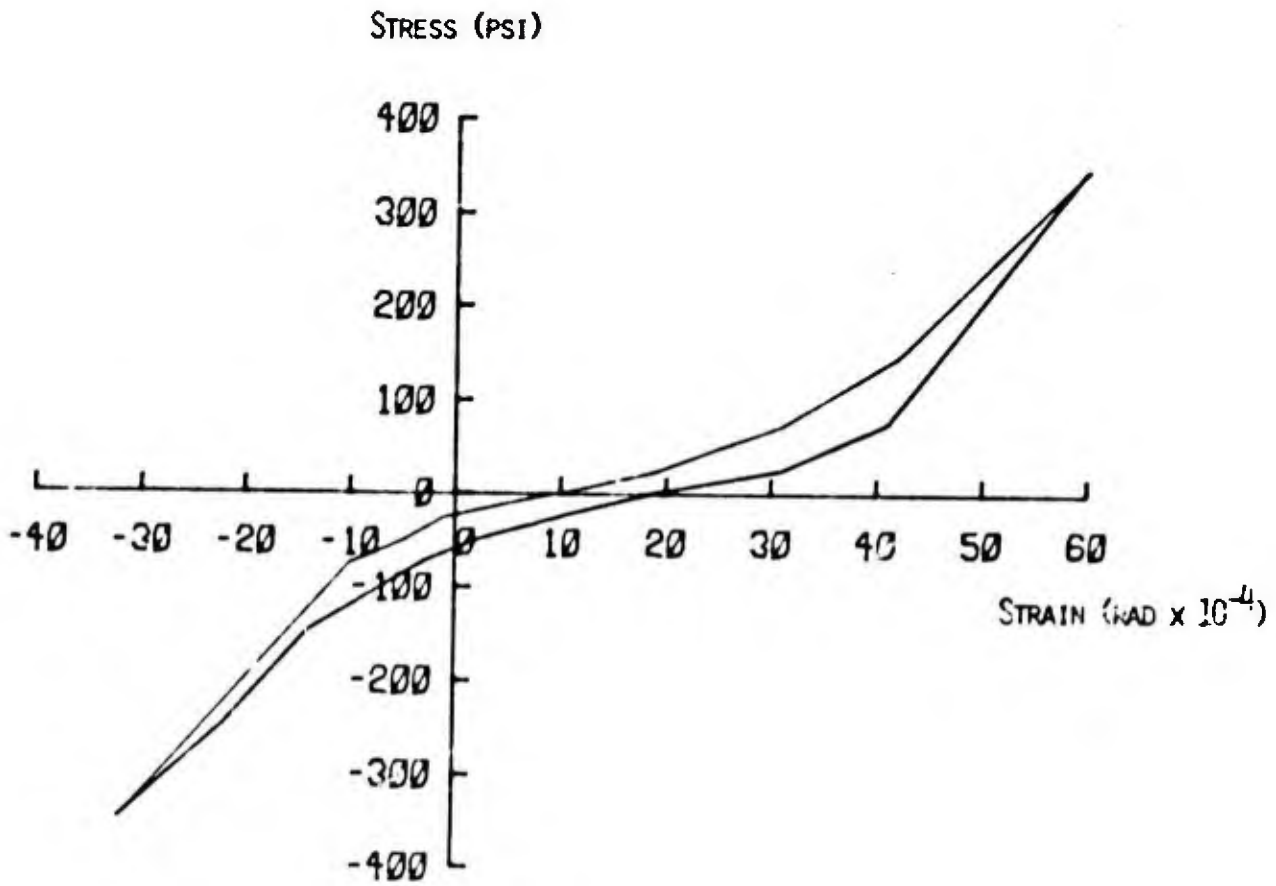

FIGURE P.17: CYCLE 42 STRESS-STRAIN HISTORY FOR 4-0.6A SPECIMEN (2)

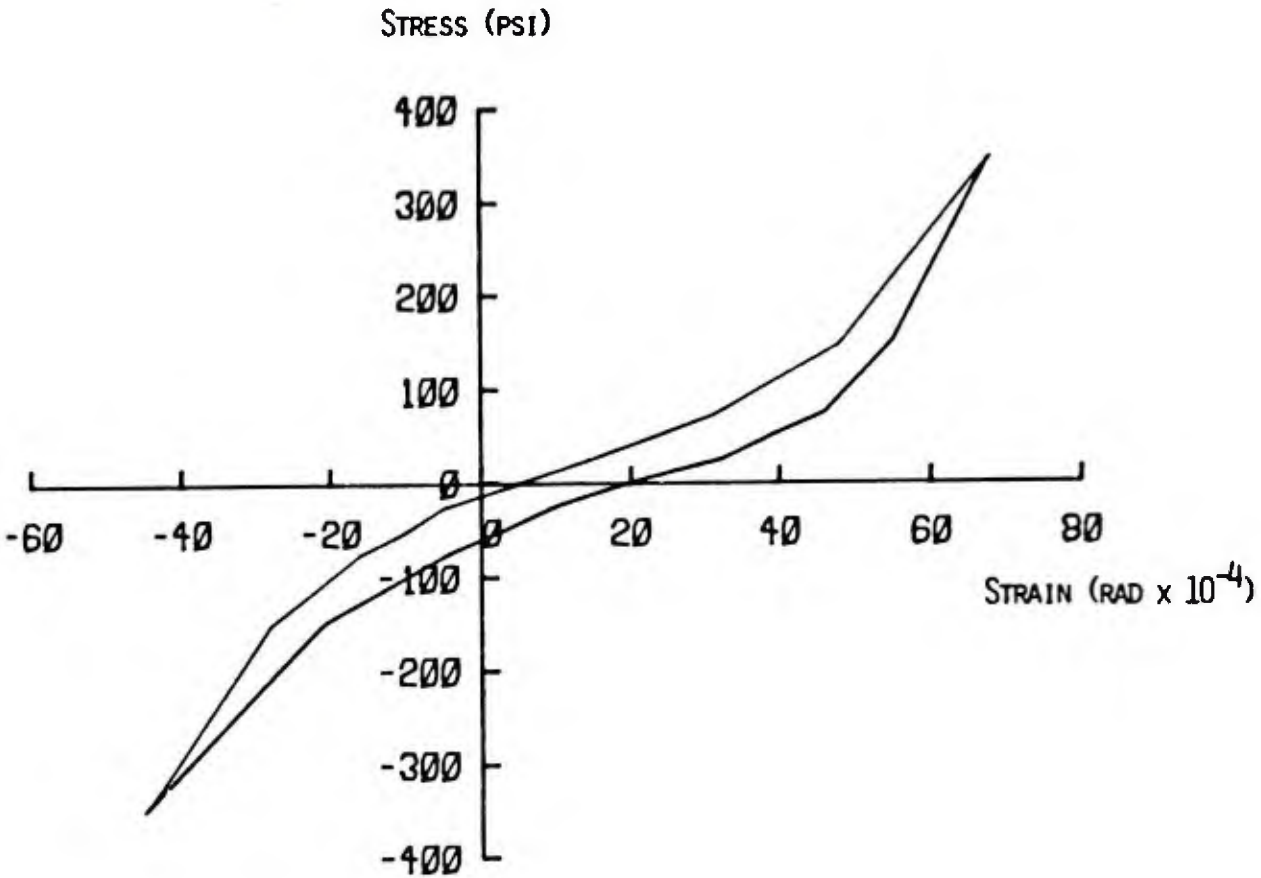

FIGURE B.18: CYCLE 50 STRESS-STRAIN HISTORY FOR 4-0.6A SPECIMEN (2)

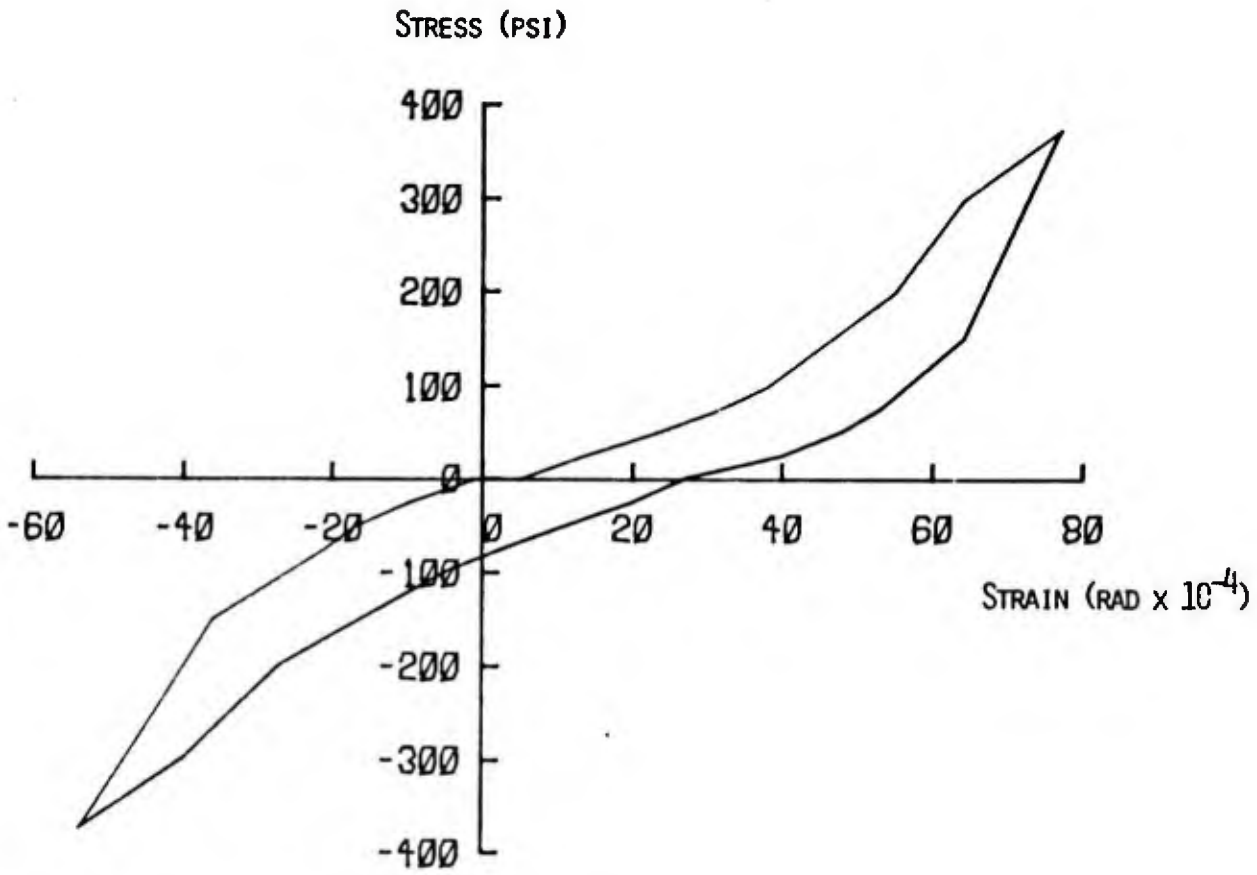

FIGURE B.19: CYCLE 51 STRESS-STRAIN HISTORY FOR 4-0.6A SPECIMEN (2)

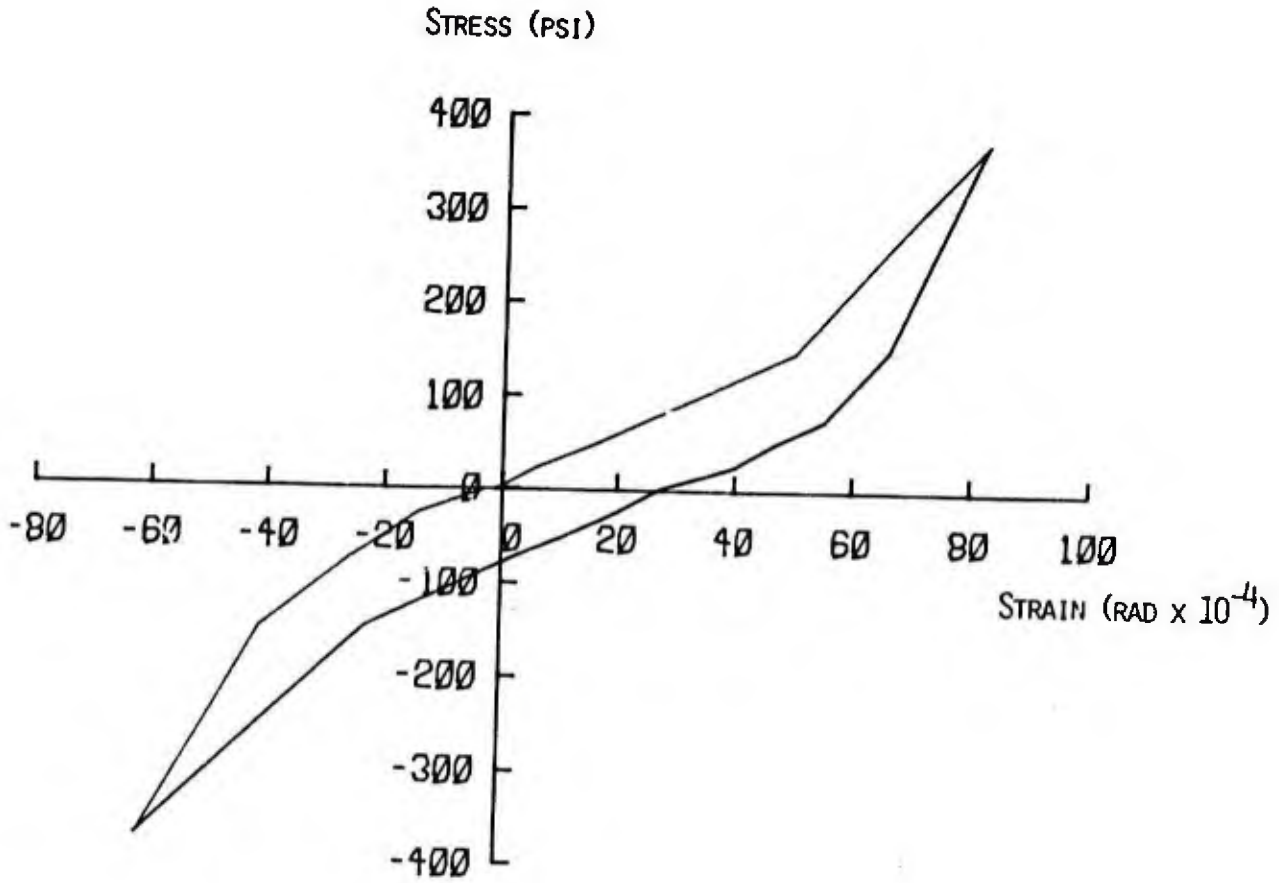

FIGURE B.20: CYCLE 52 STRESS-STRAIN HISTORY FOR 4-0.6A SPECIMEN (2)

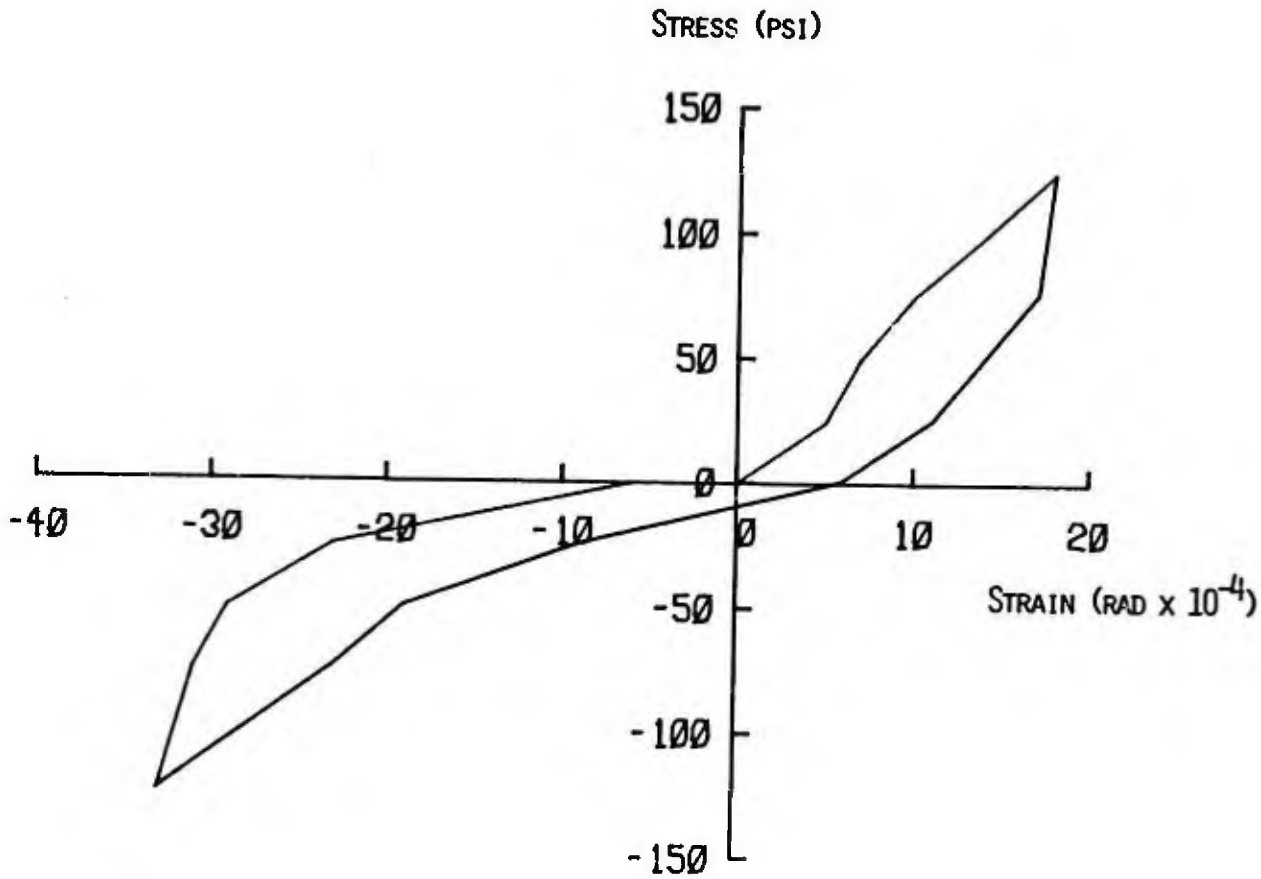

FIGURE B.21: CYCLE 1 STRESS-STRAIN HISTORY FOR 4-0.9A SPECIMEN (2)

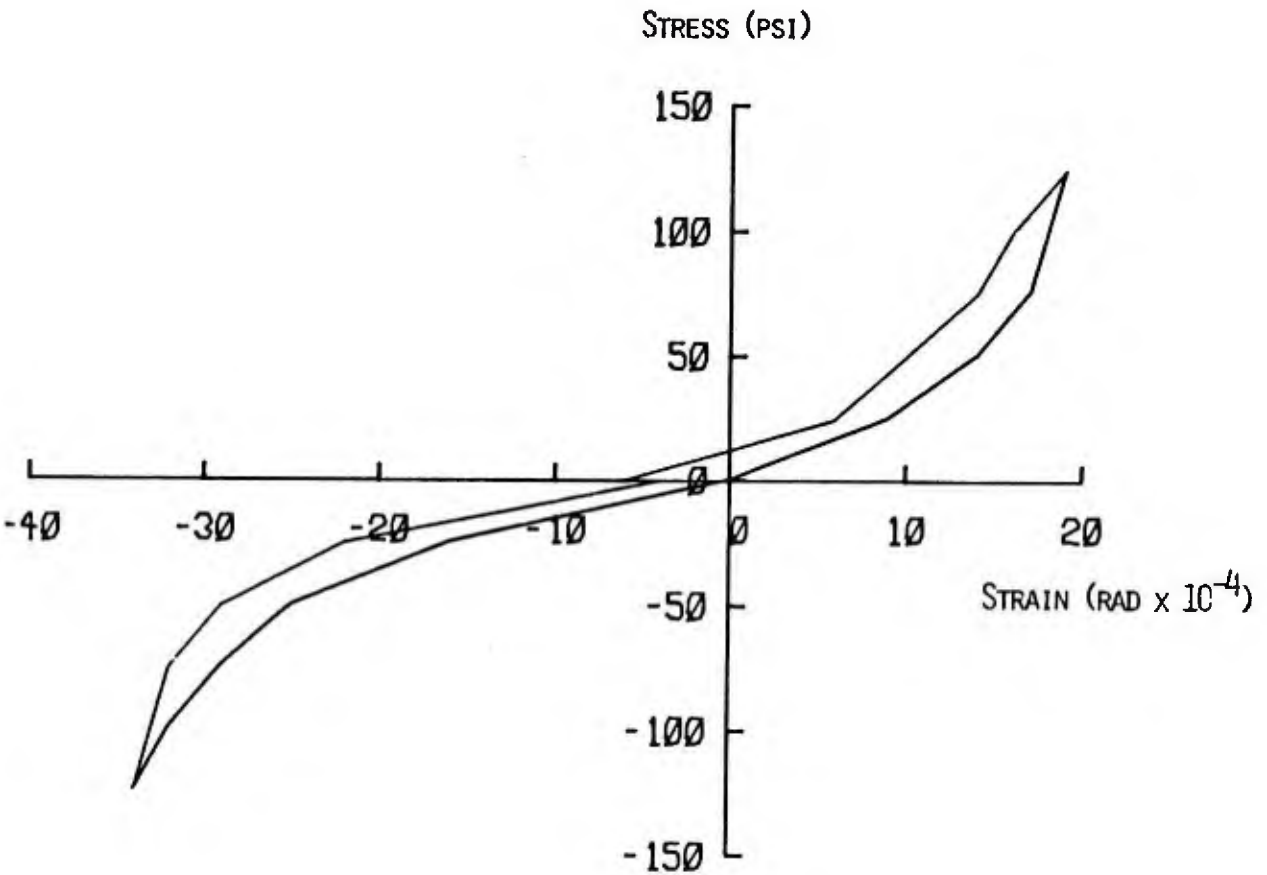

FIGURE B.22: CYCLE 2 STRESS-STRAIN HISTORY FOR 4-0.9A SPECIMEN (2)

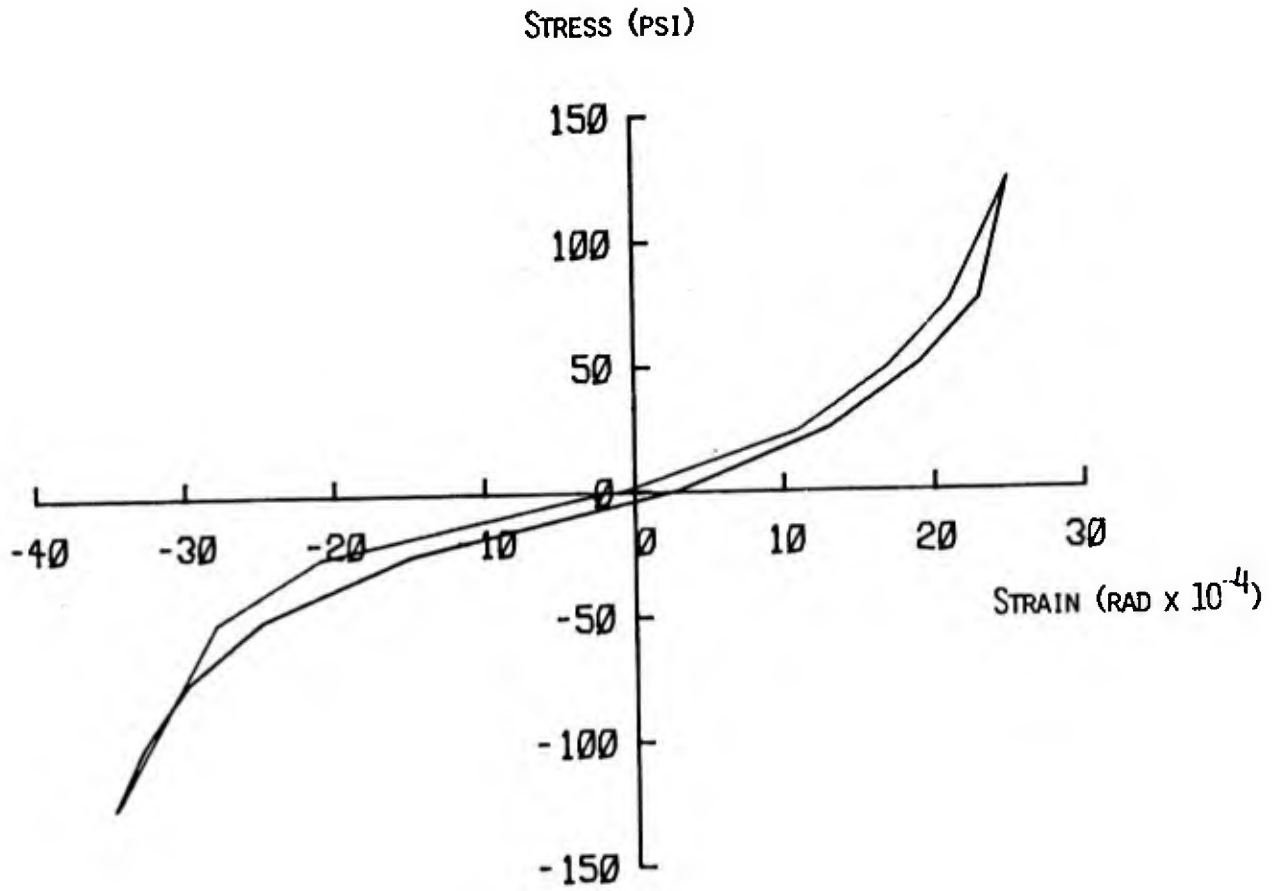

FIGURE B.23: CYCLE 10 STRESS-STRAIN HISTORY FOR 4-0.9A SPECIMEN (2)

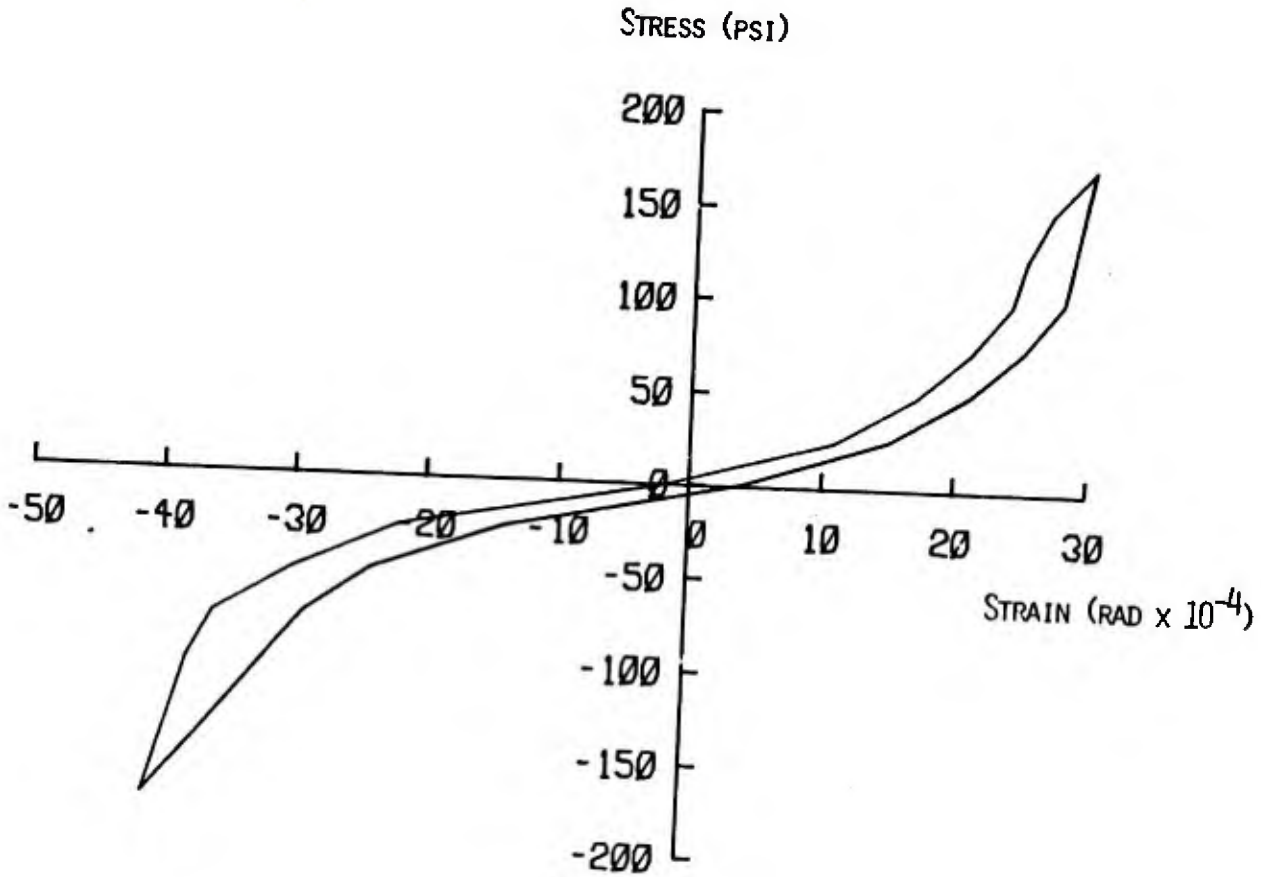

FIGURE B.24: CYCLE 11 STRESS-STRAIN HISTORY FOR 4-0.9A SPECIMEN (2)

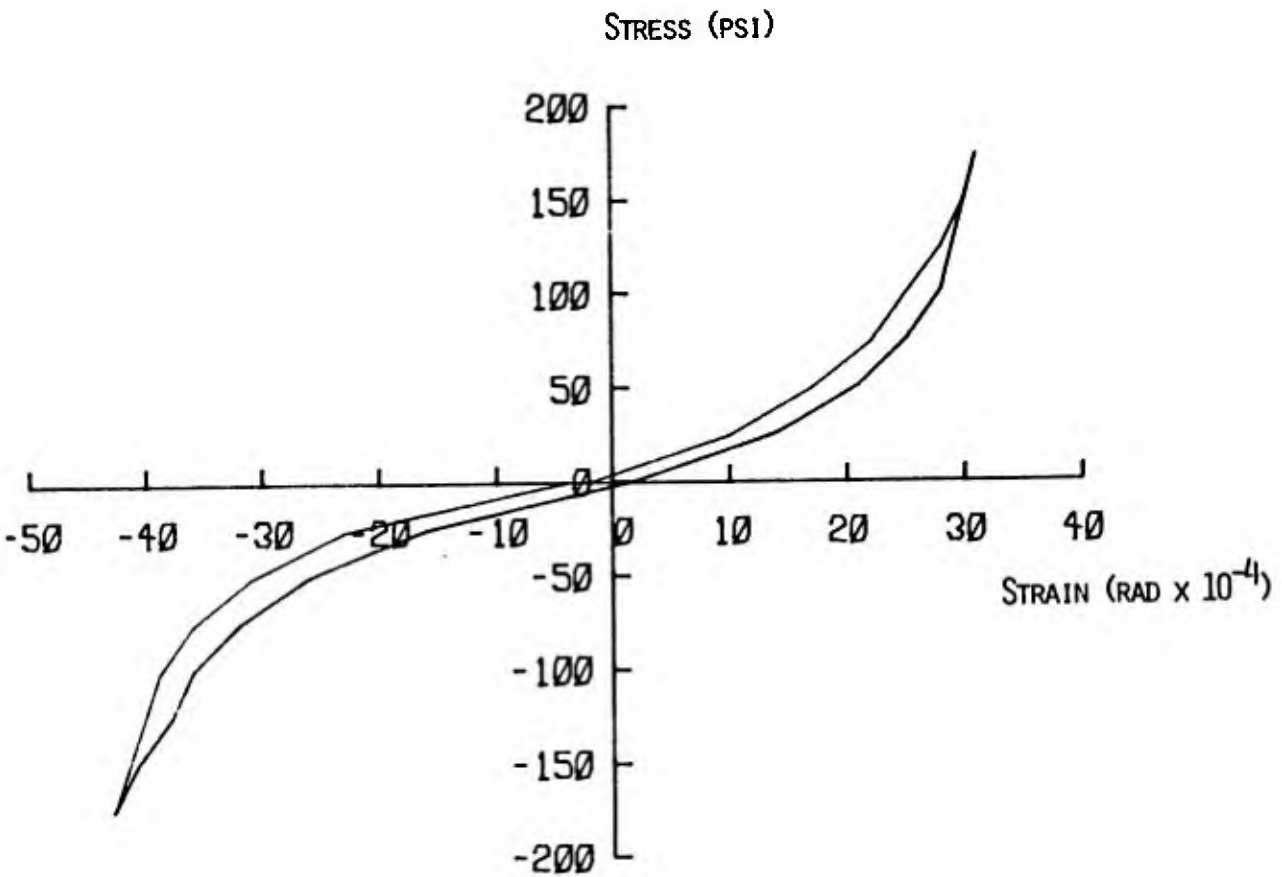

FIGURE B.25: CYCLE 12 STRESS-STRAIN HISTORY FOR 4-0,9A SPECIMEN (2)

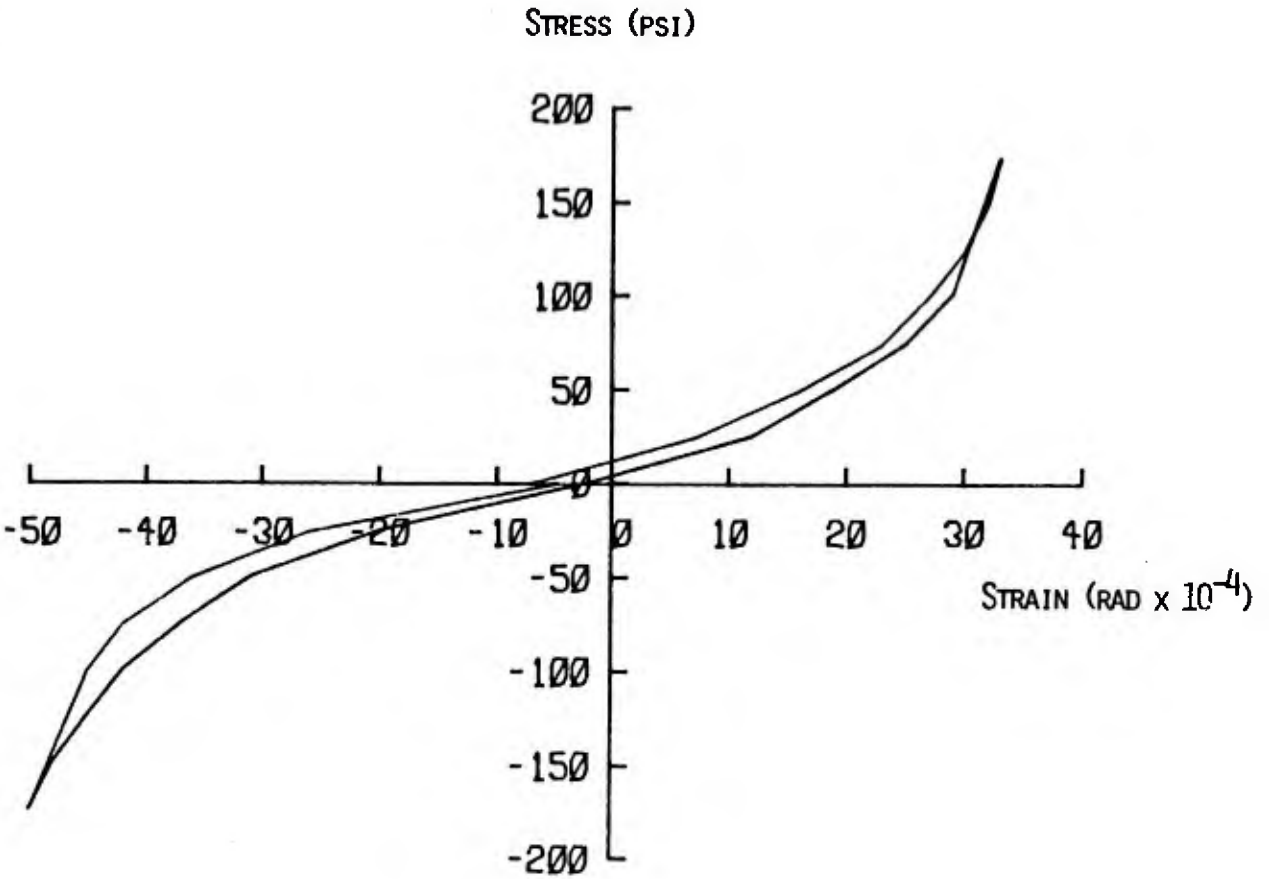

FIGURE B.26: CYCLE 20 STRESS-STRAIN HISTORY FOR 4-0.9A SPECIMEN (2)

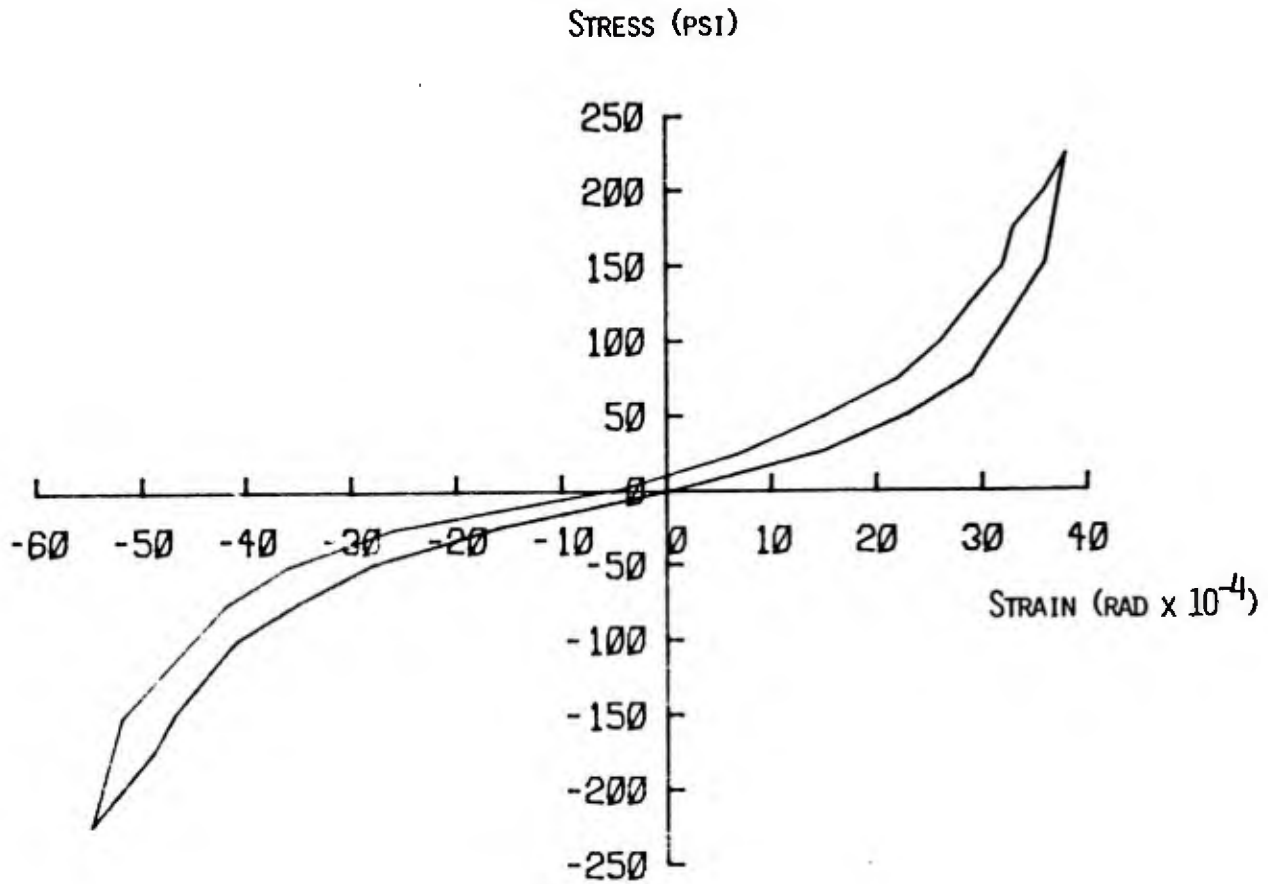

FIGURE B.27: CYCLE 21 STRESS-STRAIN HISTORY FOR 4-0.9A SPECIMEN (2)

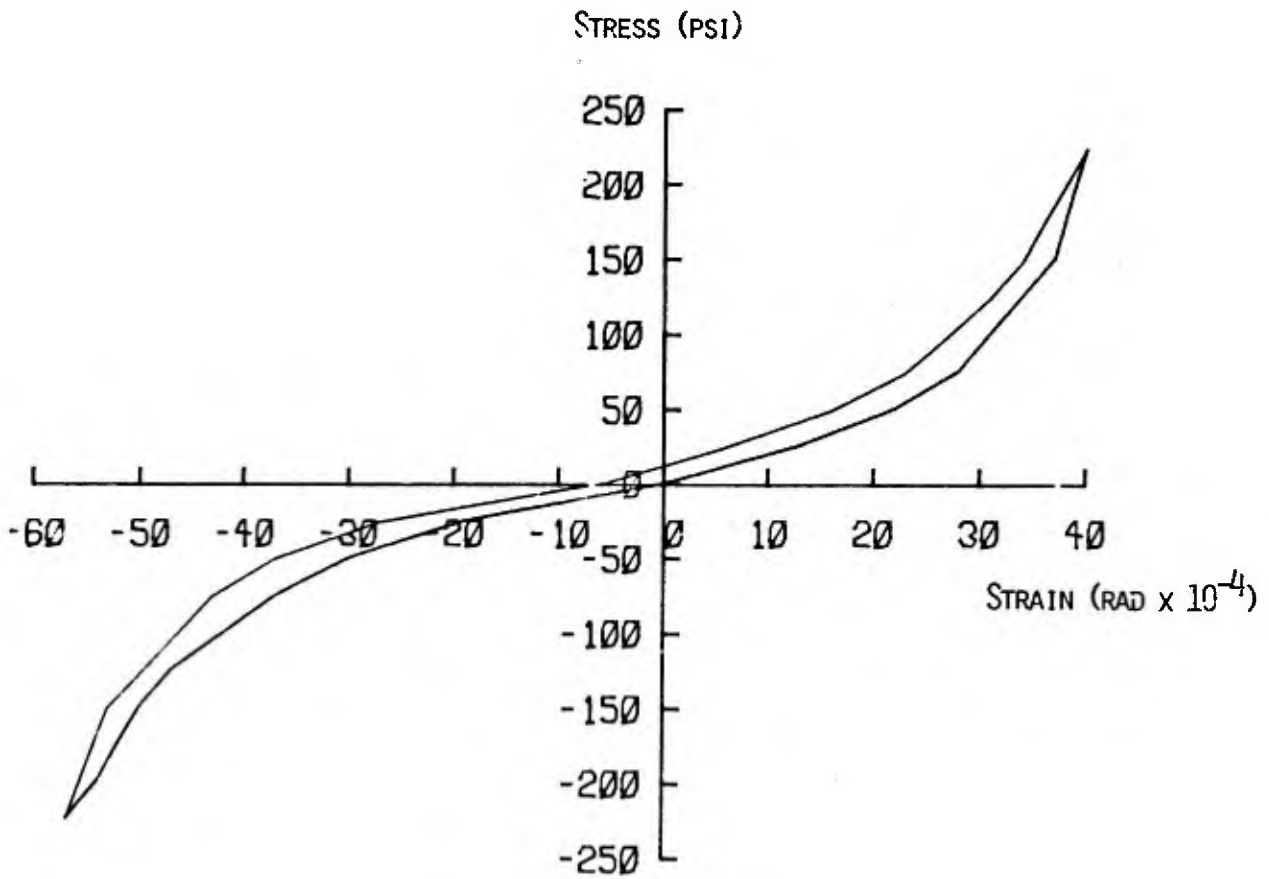

FIGURE B.28: CYCLE 22 STRESS-STRAIN HISTORY FOR ϵ=-0.9% HISTORY (2)

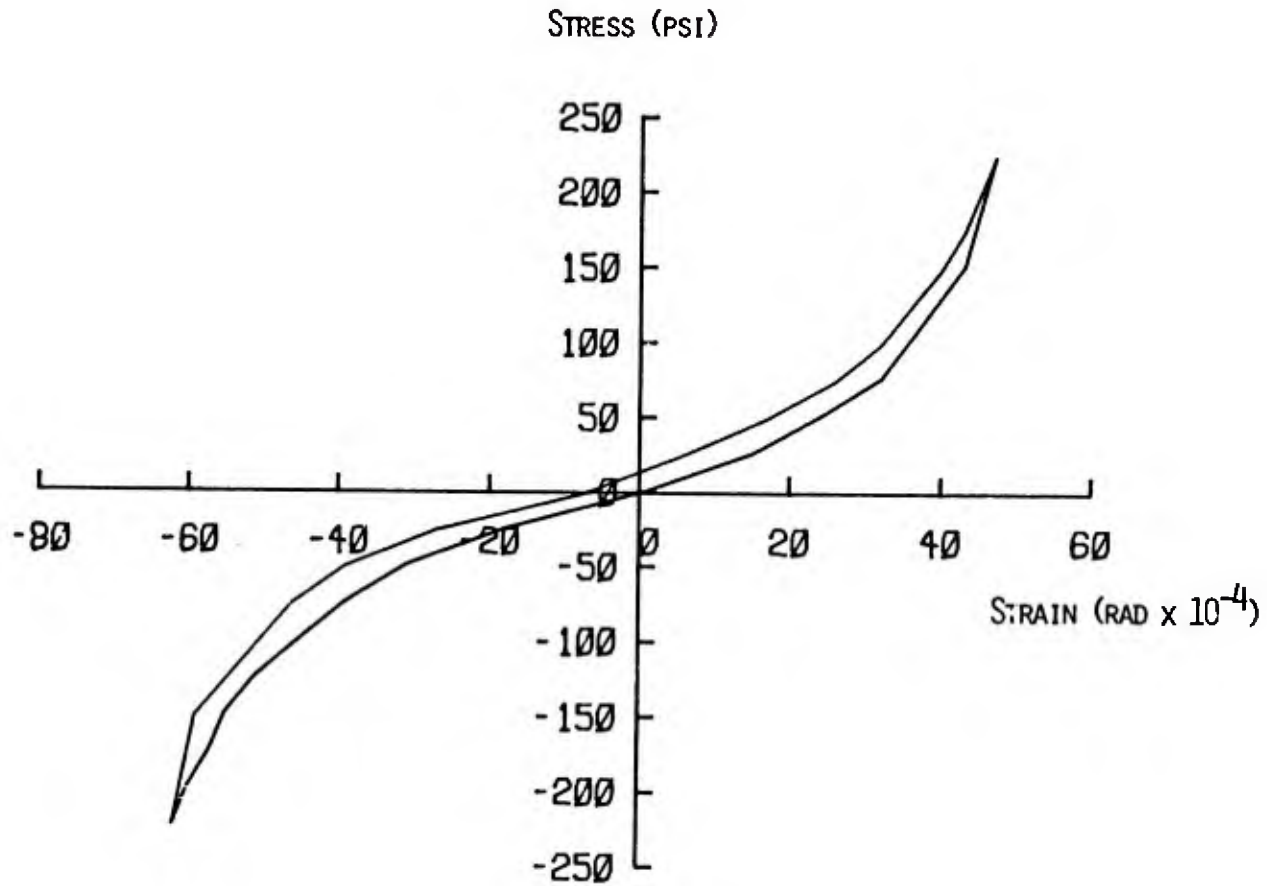

FIGURE B.29: CYCLE 30 STRESS-STRAIN HISTORY FOR 4-0.9A SPECIMEN (2)

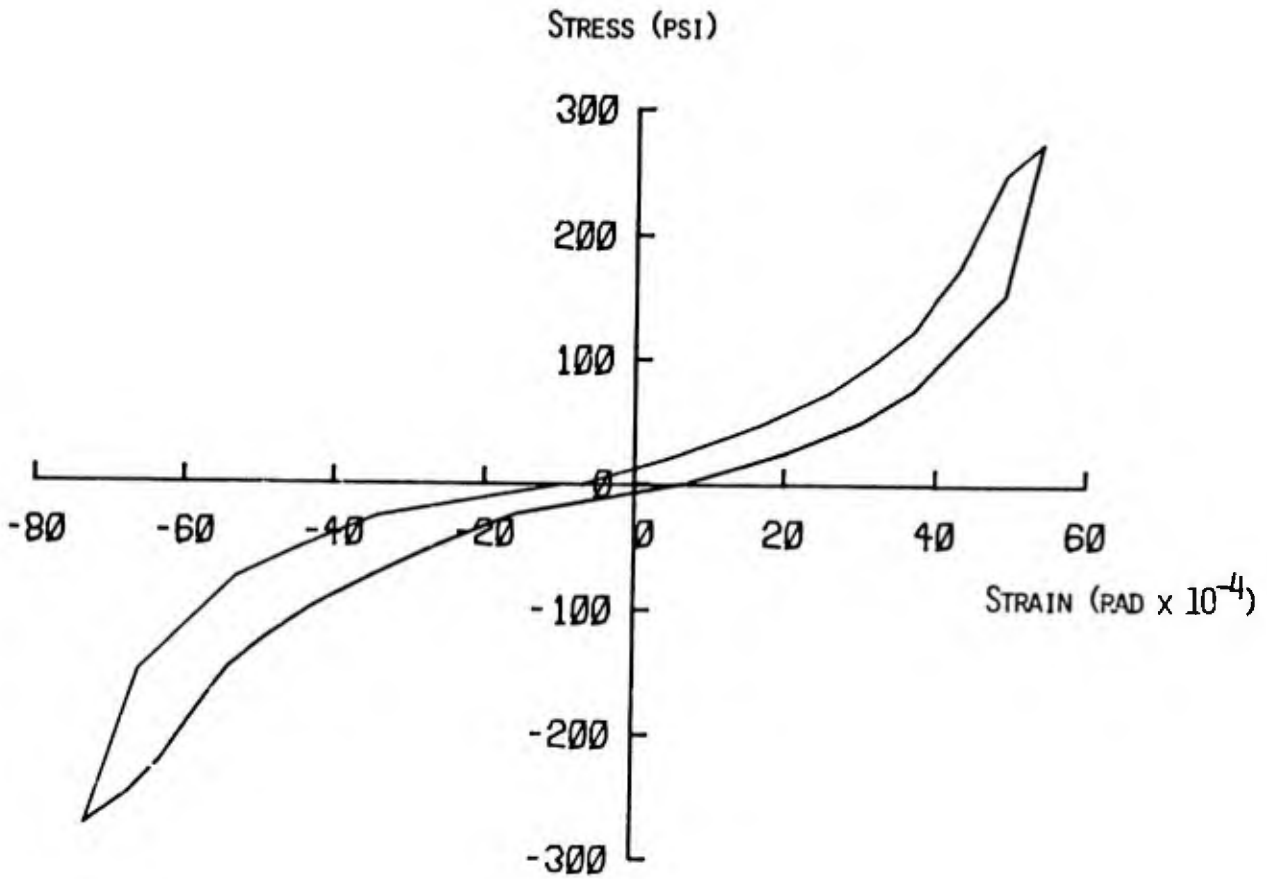

FIGURE B.30: CYCLE 31 STRESS-STRAIN HISTORY FOR 4-0.9A SPECIMEN (2)

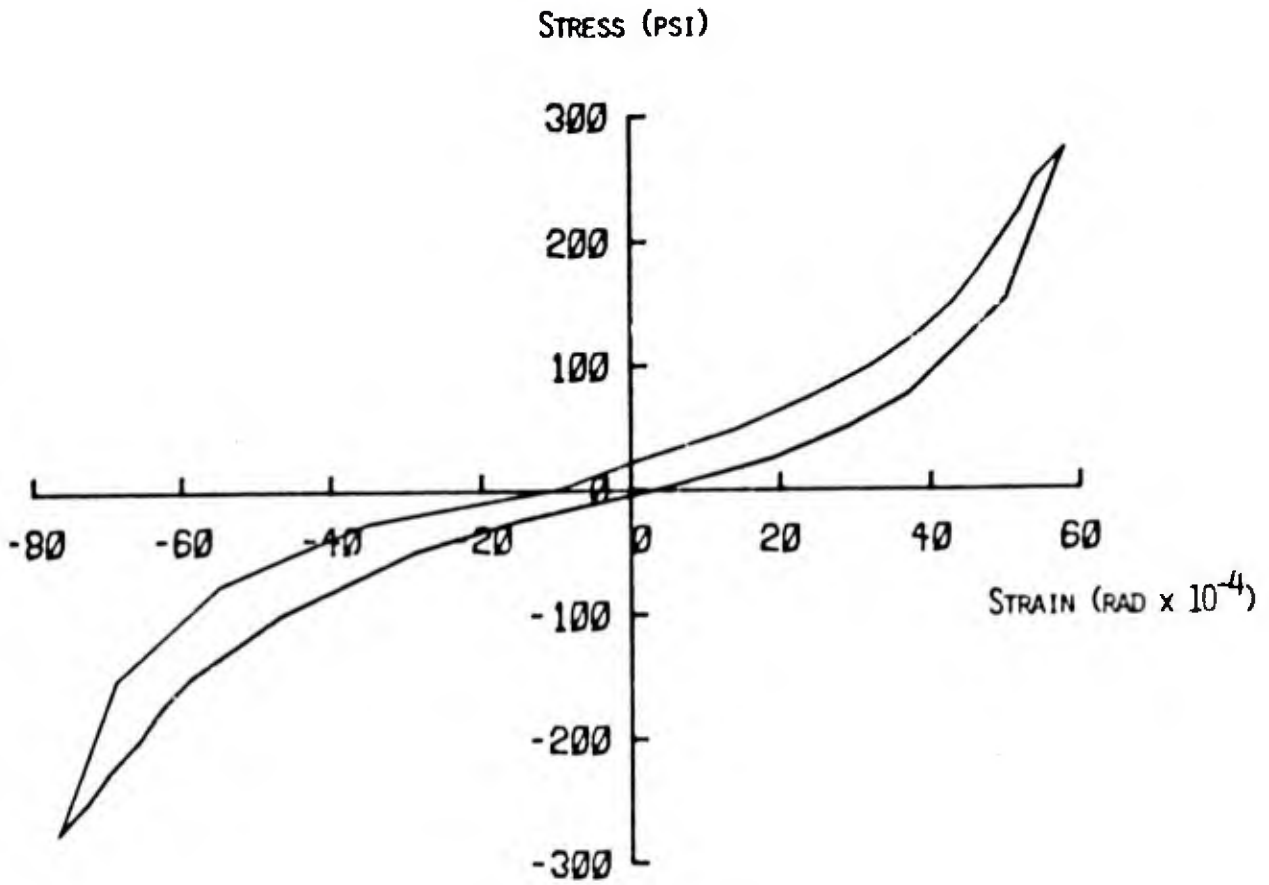

FIGURE B.31: CYCLE 32 STRESS-STRAIN HISTORY FOR 4-0.9A SPECIMEN (2)

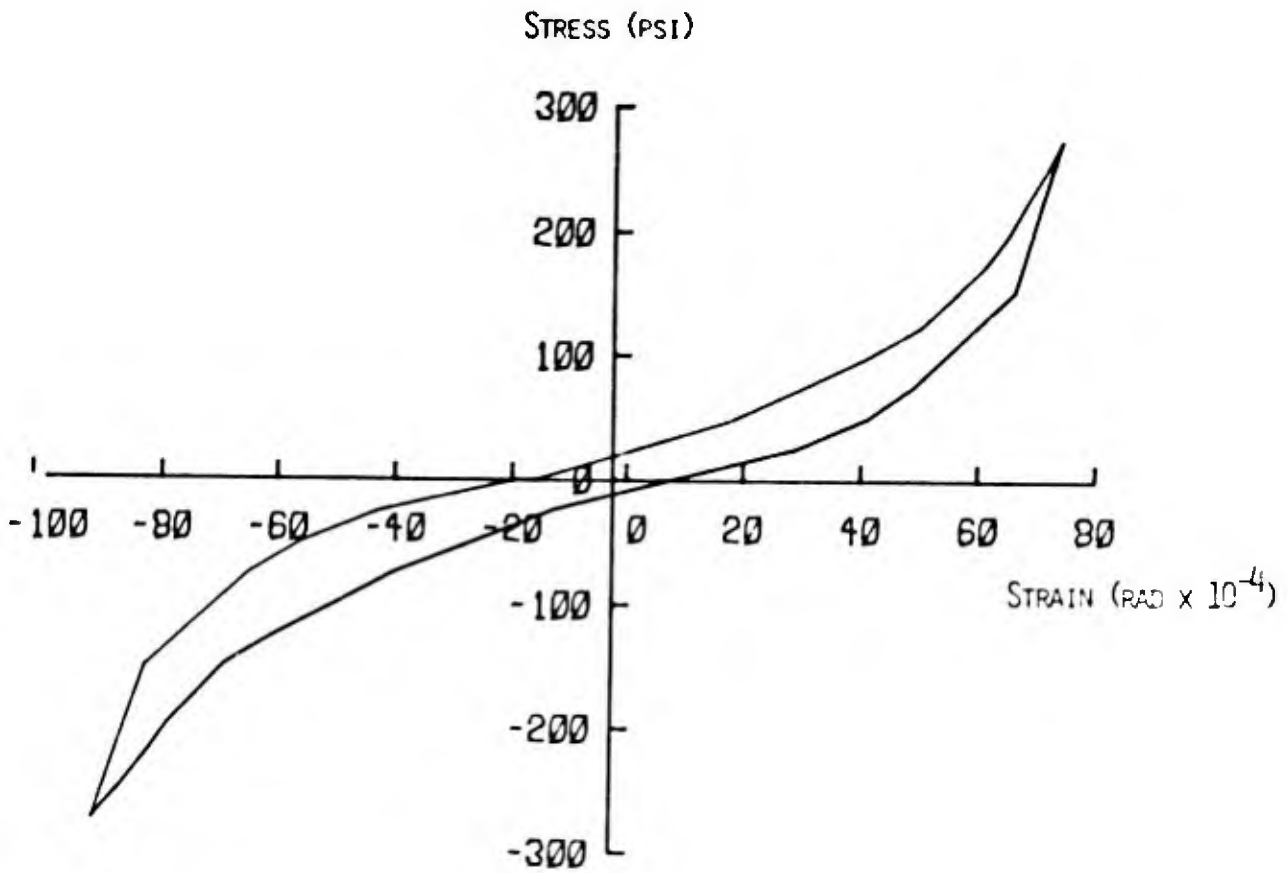

FIGURE B.32: CYCLE 40 STRESS-STRAIN HISTORY FOR 4-0.9A SPECIMEN (2)

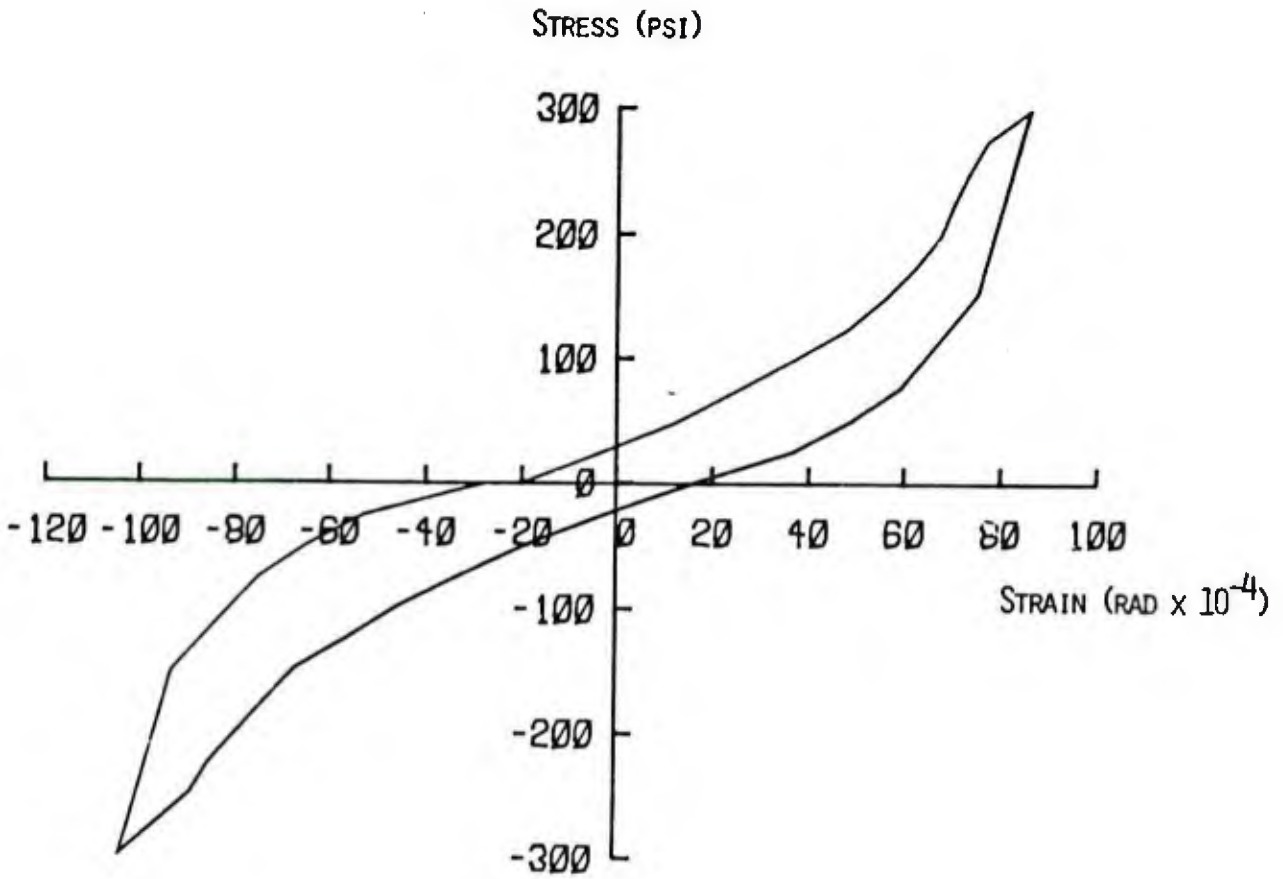

FIGURE B.33: CYCLE 41 STRESS-STRAIN HISTORY FOR 4-0.9A SPECIMEN (2)

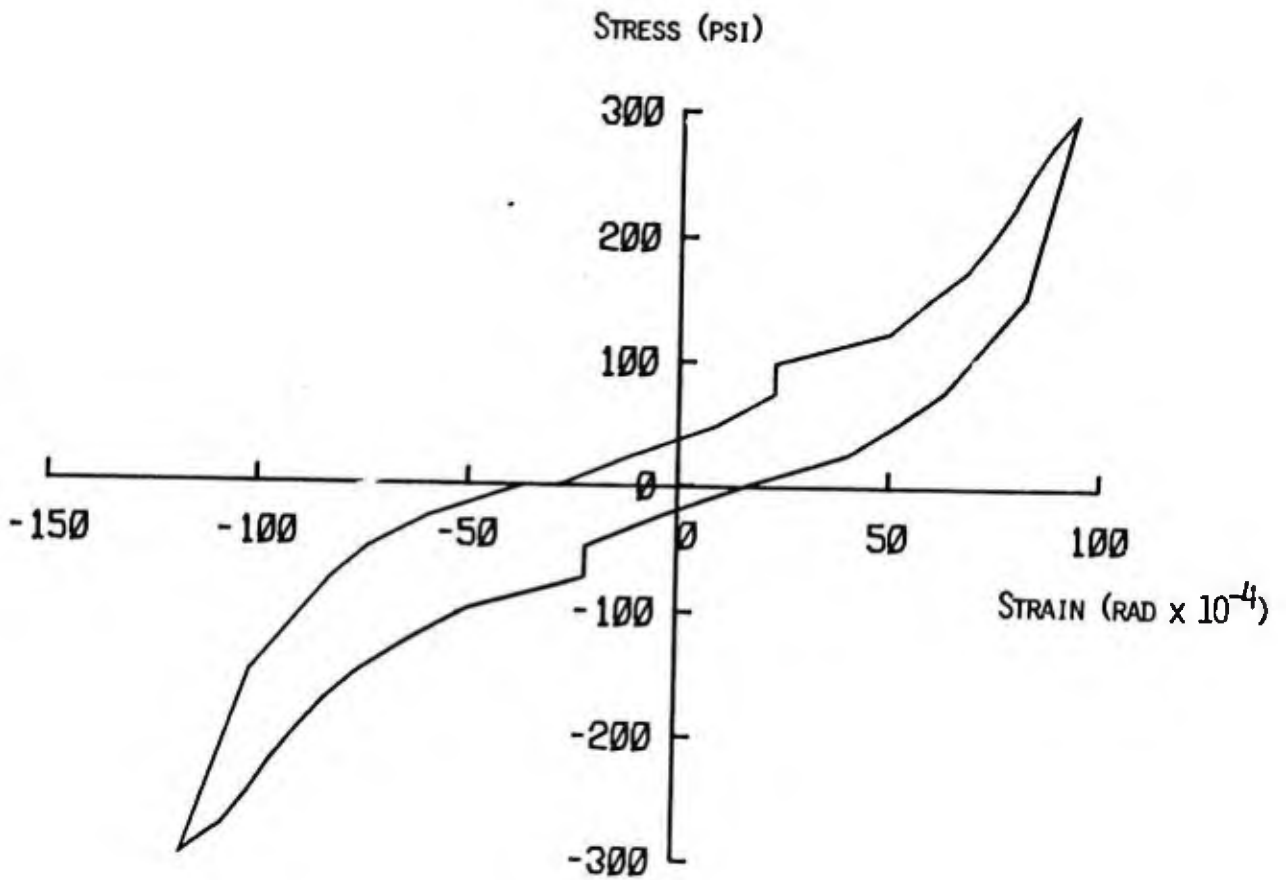

FIGURE B.34: CYCLE 42 STRESS-STRAIN HISTORY FOR 4-0.9A SPECIMEN (2)

APPENDIX C

Derivation of Equations (4.11) and (4.13)

Starting with Equation 4.7:

$$V_o = [0.063\rho_o(f_{yo} - f_s)]\sqrt{f'_c}$$

$$\text{for } 0 \leq \rho_o(f_{yo} - f_s) \leq 40 \text{ psi}$$

and noting that:

$$f_s = N/\rho_o \quad \text{where } N = N_h \text{ or } N_v$$

$$\rho_o = A_s/b_t \quad \text{where } A_s = A_{sh} \text{ or } A_{sv}$$

$$V_o = N_{hv}/b_t$$

substituting and setting the allowable steel stress to $0.9f_{yo}$ gives after simplifying

$$A_s = \left[\frac{N_h + (16/\sqrt{f'_c})N_{hv}}{0.9f_{yo}} \right]$$

$$\text{for } 0 \leq N_{hv}/b_t \leq 2.5\sqrt{f'_c}$$

Derivation of Equations (4.12) and (4.14)

$$V_o = [2.28 + 0.006\rho_o(f_{yo} - f_s)]\sqrt{f'_c}$$

$$\text{for } 740 \geq \rho_0(f_{yo}-f_s) > 40 \text{ psi}$$

and noting that:

$$f_s = N/\rho_o \quad \text{where } N = N_h \text{ or } N_v$$

$$\rho_o = A_s/b_t \quad \text{where } A_s = A_{sh} \text{ or } A_{sv}$$

$$V_o = N_{hv}/b_t$$

substituting and setting the allowable steel stress to $0.9f_{yo}$ gives after simplifying

$$A_s = \left[\frac{N_h \div (170/\sqrt{f'_c})N_{hv} - 380(b_t)}{0.9f_{yo}} \right]$$

for $2.5\sqrt{f'_c} < N_{hv}/b_t \leq 6.8\sqrt{f'_c}$

REFERENCES

1. Tseng, T.M., Calvo, J., Buyukozturk, O., Connor, J.J., "Behavioral Model for Reinforced Concrete Panels Under Cyclic Shear," Report MIT-CER-81-12, Department of Civil Engineering, Massachusetts Institute of Technology, November 1981.

2. Conley, C.H., White, R.N., and Gergely, P., "Strength and Stiffness of Reinforced Concrete Panels Subjected to Membrane Shear, Two-Way and Four-Way Reinforcing," Report prepared for the U.S. Nuclear Regulatory Commission, NUREG/CR-2049, April 1981.

3. Leombruni, P., Buyukozturk, O., and Connor, J.J., "Analysis of Shear Transfer in Reinforced Concrete with Application to Containment Wall Specimens," MIT-CE-R78-26, June 1979.

4. Oesterle, R.G., and Russell, H.G., "Shear Transfer in Large Scale Reinforced Concrete Containment Elements - Report No. 2," Construction Technology Laboratories, Portland Cement Association, Skokie, IL, September 1981.

5. "ASME Boiler and Pressure Vessel Code," Section III, Division 2, Code for Concrete Reactor Vessel and Containments, The American Society of Mechanical Engineers, New York, 1980.

6. Perdikaris, C., White, R.N., and Gergely, P., "Strength and Stiffness of Tensioned Reinforced Concrete Panels Subjected to Membrane Shear, Two-Way Reinforcing," Report prepared for the U.S. Nuclear Regulatory Commission, NUREG/CR-1602, July 1980.

7. Oesterle, R.G. and Russell, H.G., "Shear Transfer in Large Scale Reinforced Concrete Containment Elements - Report No. 1," Report prepared for the U.S. Nuclear Regulatory Commission, NUREG/CR-1374, April 1980.

8. Unpublished Results, "Experimental Study (Shear Tests on Reinforced Concrete Containment Element)," Kajima Institute of Construction Technology, Tokyo, Japan, Fall 1981.

9. White, R.N. and Holley, M.J., "Experimental Studies of Membrane Shear Transfer," ASCE, Journal of the Structural Division, Vol. 98, No. 3, August 1972, 1835-1852.

10. Umemura, H., Aoyama, H., Ito, M., and Hosokawa, Y., "Aseismic Characteristics of RC Box and Cylinder Walls," Preprints of Sixth World Conference on Earthquake Engineering, New Delhi, January 1977, Session 11.

11. Uchida, T., Ohmori, N., Takahashi, T., Watanabe, S., Abe, H., and Aoyagi, Y., "Behavior of Reinforced Concrete Containment Models Under the Combined Action of Internal Pressure and Lateral Force," Transactions of the 5th SMIRT, 1979, Berlin, Vol. J, J 4/4.

END

DATE

FILMED

6-1-83

NTIS